

Artificial Neural Network Model for Analysis of In-Plane Shear Strength of Partially
Grouted Masonry Shear Walls

by

Jeffrey Roy Hung

A thesis submitted in partial fulfillment of the requirements for the degree of

Master of Science

in

STRUCTURAL ENGINEERING

Department of Civil and Environmental Engineering
University of Alberta

© Jeffrey Roy Hung, 2018

ABSTRACT

The behaviour of partially grouted (PG) masonry shear walls is complex, due to the inherent anisotropic properties of masonry materials and nonlinear interactions between the mortar, blocks, grouted cells, ungrouted cells, and reinforcing steel. Since PG shear walls are often part of lateral force resisting systems in masonry structures, it is crucial that its shear behaviour is well understood, and its shear strength is accurately predicted.

This study presents the development of an artificial neural network (ANN) model for analyzing the shear strength of PG walls. ANNs have the unique ability to address highly complex problems and the potential to predict accurate results without a defined algorithmic solution. By providing an ANN with a dataset of multiple inputs and corresponding outputs, it can be trained to describe nonlinear relationships that may exist among the variables and provide insight into the influence of each input parameter.

An experimental dataset of PG shear walls is used as input for the ANN analysis model. It is necessary to assemble the dataset from multiple experimental studies using meta-analysis, given that no single experimental study contains enough information to build and validate a constitutive model for the shear strength and behaviour of PG walls. Finite element (FE) modelling is shown to be a viable option for addressing gaps in input values which exist in the dataset. The effect of previously unaccounted parameters in code-based approaches is discussed, as well as the influence of different types of ANN analysis options and input size on the model predictions. The ANN model results are compared against currently available design codes and equations to predict the in-plane shear strength of PG shear walls.

DEDICATION

*To my parents, Norman and Sarah Hung:
Thank you for your unconditional love and patience.*

*To my brother, Daniel:
Thank you for all the encouragement and reassurance.*

*To my best friend, Kebbin:
Thank you for putting up with my antics.*

To my Lord, my Saviour, and my King forever: Jesus Christ.

ACKNOWLEDGEMENTS

The pursuit of a graduate degree involves a multitude of people to guide, to encourage, and to graciously offer their assistance along the way. This thesis is a culmination of the love, support, and grace that has been poured into my life by those around me.

With that said, I would like to first and foremost thank my advisor, Dr. Carlos Cruz-Noguez, who provided invaluable guidance and patience throughout the course of this research project. Technical guidance and support was also provided by Dr. Mark Hagel of the Alberta Masonry Council. The financial and moral support of the Masonry Contractors Association of Alberta has been integral to the research performed.

My parents have been incredibly patient and encouraging throughout not only my graduate studies, but my education as a whole. Thank you for the home cooked meals, the car rides, the love, and the unconditional support for my passion. Words cannot capture the dedication that you have invested into my life, and though I may never fully understand it, I hope to one day give as generously as you have.

Thank you to my friends who reminded me of who I am when life was rough, and made time in their schedules to spend with me.

Funding for this research has been provided in part by the Natural Sciences and Engineering Research Council of Canada (NSERC), the Government of Alberta, the Masonry Contractors Association of Alberta (MCAA), Chris Ambrozic and Michelle Steele, Norman and Tess Reid, and the University of Alberta.

TABLE OF CONTENTS

1	INTRODUCTION	1
1.1	Background	1
1.2	Problem Statement	4
1.3	Objectives, Methods and Scope	4
1.4	Organization of Thesis	6
2	LITERATURE REVIEW	7
2.1	Introduction	7
2.2	Behaviour of Partially Grouted Masonry Walls	8
2.2.1	Failure Modes	8
2.2.1.1	Flexural Failure	8
2.2.1.2	Sliding Failure	8
2.2.1.3	Diagonal Tension Shear Failure	9
2.2.1.4	Masonry Compression Strut Shear Failure	11
2.2.2	Effect of Various Parameters on Shear Wall Behaviour	12
2.2.2.1	Effect of Masonry Compressive Strength ($f'm$).....	12
2.2.2.2	Effect of Wall Aspect Ratio H/L	13
2.2.2.3	Effect of Vertical Reinforcement	15
2.2.2.4	Effect of Horizontal (Shear) Reinforcement	17
2.2.2.5	Effect of Axial Stress	20
2.3	Design Expressions Predicting In-Plane Shear Strength of PG Walls.....	21
2.3.1	Matsumura (1987)	23
2.3.2	AIJ (1987).....	24

2.3.3	Shing et al. (1990).....	25
2.3.4	Anderson and Priestley (1992)	26
2.3.5	Fattal (1993).....	27
2.3.6	National Earthquake Hazards Reduction Program – NEHRP (1997)	29
2.3.7	UBC (1997)	29
2.3.8	NZS-4230 (2004).....	30
2.3.9	Eurocode 6 (2005)	33
2.3.10	Voon (2007).....	34
2.3.11	IMNC (2010)	36
2.3.12	CSA-S304.14 (2014)	37
2.3.13	Dillon (2015)	38
2.3.14	TMS 402/602 (2016)	39
2.3.15	Summary of Design Expressions.....	41
3	DATASET ASSEMBLY	43
3.1	Introduction.....	43
3.2	Experimental Studies on the Behaviour of Partially Grouted Masonry Shear Walls.....	45
3.2.1	Scrivener (1967)	45
3.2.2	Meli et al. (1968)	46
3.2.3	Meli and Salgado (1969)	47
3.2.4	Mayes et al. (1976)	48
3.2.5	Chen et al. (1978)	49
3.2.6	Thurstun and Hutchinson (1982).....	50
3.2.7	Matsumura (1987)	51

3.2.8	Tomažević and Lutman (1988).....	53
3.2.9	Johal and Anderson (1988).....	54
3.2.10	Yancey and Scribner (1989).....	55
3.2.11	Ghanem et al. (1992, 1993).....	56
3.2.12	Tomažević et al. (1996).....	58
3.2.13	Schultz (1996).....	59
3.2.14	Schultz et al. (1998).....	60
3.2.15	Voon and Ingham (2006) and Voon (2007).....	61
3.2.16	Haach et al. (2007).....	63
3.2.17	Maleki (2008) and Maleki et al. (2009).....	64
3.2.18	Elmapruk (2010).....	65
3.2.19	Minaie (2009) and Minaie et al. (2010).....	66
3.2.20	Baenziger and Porter (2011).....	67
3.2.21	Nolph (2010) and Nolph and Elgawady (2012).....	68
3.2.22	Oan (2013).....	69
3.2.23	Hoque (2013).....	71
3.2.24	Hamedzadeh (2013).....	72
3.2.25	Rizae (2015).....	73
3.2.26	Ramírez et al. (2016).....	75
3.2.27	Other Studies.....	76
3.3	Data Scrutinization.....	77
3.3.1	Failure Mode.....	77
3.3.2	Horizontal Reinforcement Pattern.....	78

3.3.3	Interior Vertical Reinforcement.....	81
3.3.4	ESECMaSE Test Setup.....	81
3.4	Data Synthesization.....	84
3.4.1	Prism Geometry	85
3.4.2	Prism Strength Estimation	85
3.4.3	Reported Shear Strength	86
3.4.4	Loading Pattern/Loading History	87
3.4.5	Loading Rate.....	88
3.4.6	Scaling	88
3.5	Dataset Summary	89
3.6	Distribution of Specimen Parameters	92
3.7	Evaluating the Performance of Existing Predictions	98
3.7.1	Mean	98
3.7.2	Standard Deviation	99
3.7.3	Mean Squared Error (MSE).....	99
3.7.4	Fifth Percentile.....	100
3.7.5	Residuals.....	100
3.7.6	Performance of Existing Predictions	102
4	ARTIFICIAL NEURAL NETWORK INVESTIGATION & RESULTS.....	118
4.1	Artificial Neural Network Fundamentals.....	118
4.1.1	Introduction.....	118
4.1.2	Hidden Layer and Hidden Neurons	120
4.1.3	Network Training, Validation and Testing	121

4.1.3.1	Training set.....	121
4.1.3.2	Validation set.....	121
4.1.3.3	Testing set.....	123
4.1.4	Iterative Approach to ANNs.....	123
4.1.5	ANN Performance Metrics and Model Selection.....	123
4.1.6	Structural Applications of Neural Networks.....	124
4.2	Previous Research Performed on PG Walls using Neural Networks.....	125
4.3	Neural Network Test Matrix.....	127
4.4	Results.....	129
4.5	Sensitivity Analysis.....	136
4.5.1	F-5-5-1 Neural Networks.....	138
4.5.2	F-7-5-1 Neural Networks.....	143
4.6	Summary of ANN Model Performance.....	147
4.7	Shear Expressions Based on ANN.....	151
4.7.1	General Formula.....	151
4.7.2	F-5-5-1 Neural Network Model.....	153
4.7.3	F-7-5-1 Neural Network Model.....	154
4.7.4	Sample Calculation.....	155
5	FINITE ELEMENT INVESTIGATION ON PARTIALLY GROUTED MASONRY SHEAR WALLS.....	157
5.1	Introduction.....	157
5.2	VecTor2 Background.....	159
5.3	VecTor2 Model Description.....	160
5.3.1	Material Properties.....	161

5.3.2	Boundary Conditions	163
5.3.3	Loading Conditions	163
5.4	VecTor2 Results and Discussion	166
5.5	Summary	168
6	CONCLUSIONS AND RECOMMENDATIONS	170
6.1	Summary	170
6.2	Conclusions	172
6.3	Recommendations & Future Research.....	174
	REFERENCES	176
	APPENDIX A: FULL DATASET	186
	APPENDIX B: MATLAB CODE.....	241
B.1	Neural Network MATLAB Function.....	241
B.2	Generate MATLAB Neural Network Function	244
B.3	Sensitivity Analysis MATLAB Function	246
	APPENDIX C: NOTES ON LINEAR REGRESSION	250
C.1	Linear Regression	250
C.2	Regression Through the Origin (RTO).....	252

LIST OF TABLES

Table 2.1 – Statistical comparison of test results with predicted values (<i>V_{exp}</i> / <i>V_{calc}</i>). (Hassanli et al. 2014)	22
Table 2.2 – In-plane shear strength equations for PG walls	41
Table 3.1 – PG dataset variations for neural network analysis.....	90
Table 3.2 – Summary of PG Wall Datasets.....	91
Table 3.3 – Performance metrics for existing models	102
Table 4.1 – ANN results from study performed by Aguilar et al. (2016)	126
Table 4.2 – Neural network test matrix used in this study	128
Table 4.3 – Range of input and output parameters developed by Aguilar et al. (2016) for (<i>x-5-n-1</i>) ANN analysis	128
Table 4.4 – Range of input and output parameters for (<i>x-7-n-1</i>) ANN analysis	129
Table 4.5 – ANN (<i>x-5-n-1</i>) and (<i>x-7-n-1</i>) performance.....	133
Table 4.6 – (<i>x-5-n-1</i>) ANN models compared with existing models’ performance	134
Table 4.7 – (<i>x-7-n-1</i>) ANN models compared with existing models’ performance	135
Table 4.8 – Sensitivity analysis input variables for “F-5-5-1” networks	139
Table 4.9 – Sensitivity analysis input variables for “F-7-5-1” networks	143
Table 4.10 – Summary of ANN model performance in comparison with existing PG shear wall models.....	147
Table 4.11 – Input minimum and maximum values for linear normalization.....	153
Table 4.12 – Input minimum and maximum values for linear normalization.....	154
Table 4.13 – Normalized input values for “PG254-48”	155
Table 5.1 – VecTor2 model properties	162
Table 5.2 – Comparison of experimental vs VecTor2 model.....	167

LIST OF FIGURES

Figure 2.1 – Typical reinforced concrete masonry block wall: (a) vertical reinforcement; (b) joint reinforcement; (c) bond beam reinforcement (Anderson and Brzev 2009).....	7
Figure 2.2 – Reinforced masonry shear wall failure modes: (a) flexural; (b) sliding, (c) shear (adapted from Voon 2007)	8
Figure 2.3 – Diagonal shear mode of failure: (a) step cracking at low axial compressive stress; (b) diagonal cracking across masonry (adapted from Voon 2007).....	9
Figure 2.4 – Shear Resistance Mechanism (Shing et al. 1990b)	10
Figure 2.5 – Modes of shear failure: (a) Brittle shear failure; (b) Ductile shear failure (adapted from Voon 2007).....	11
Figure 2.6 –Truss analogy for masonry shear wall (adapted from Oesterle et al. 1984)	11
Figure 2.7 – Effect of vertical reinforcement ratio, ρ_v , on the in-plane shear resistance provided by masonry (Adapted from Seif ELDin 2016)	13
Figure 2.8 – Walls tested by Maleki et al. (2009) with different aspect ratios (0.5, 1.0 and 1.5) and similar bar spacing.....	14
Figure 2.9 – Shear span ratio for (a) single curvature boundary condition and (b) double curvature boundary condition	15
Figure 2.10 – Effects of grout horizontal spacing on the shear strength of test specimens by Nolph and Elgawady (2012).....	16
Figure 2.11 – Effect of closely spaced vertical reinforcement explained with strut and tie models – (a) normal spaced and (b) closely spaced (adapted from Hassanli et al. 2014)	17
Figure 2.12 – Role of horizontal reinforcement in resisting masonry shear failure (adapted from Voon 2007)	18
Figure 2.13 – Effect of horizontal reinforcement ratio on shear strength for walls of varying height-to-length aspect ratios (Schultz et al. 1998).....	19

Figure 2.14 – Simple strut-and-tie models for (a) squat, (b) square, and (c) slender PG masonry walls (adapted from Hassanli et al. 2014).....	20
Figure 2.15 – Failure Criterion for Masonry Shear Walls (adapted from Page 1989) ...	21
Figure 2.16 – Contribution of axial load to wall shear strength by (Voon 2007).....	31
Figure 2.17 – Effective area for shear defined by NZS-4230 (2004).....	33
Figure 2.18 – Shear resisting mechanism versus masonry ductility (Voon 2007)	35
Figure 2.19 – Wall cross-sectional area (Seif EIDin 2016).....	38
Figure 3.1 – Test setup by Scrivener (1967).....	45
Figure 3.2 – Test setup by Meli et al. (1968).....	46
Figure 3.3 – Test setup by Meli and Salgado (1969).....	47
Figure 3.4 - Test setup by Mayes et al. (1976a)	48
Figure 3.5 – Test setup by Chen et al. (1978).....	49
Figure 3.6 – Test setup by Thurston and Hutchinson (1982)	50
Figure 3.7 – Test setup by Matsumura (1987).....	52
Figure 3.8 – Test setup by Johal and Anderson (1988)	54
Figure 3.9 – Test setup by Yancey and Scribner (1989)	55
Figure 3.10 – Test setup by Ghanem et al. (1992, 1993).....	56
Figure 3.11 – Displacement Time Histories used to Drive Actuator: (a) Monotonic; (b) Reverse Cyclic; (c) Phased-Sequential; (d) Simulated Earthquake Response (Tomazevic and Lutman 1996).....	59
Figure 3.12 – Test setup by Schultz (1996).....	60
Figure 3.13 – Test setup by Schultz et al. (1998)	61
Figure 3.14 – Test setup by Voon (2007)	62

Figure 3.15 – Force displacement envelopes in Voon and Ingham (2006) for FG and PG walls with no axial loading	62
Figure 3.16 – Test setup by Haach et al. (2007)	63
Figure 3.17 – Test setup by Maleki et al. (2009)	64
Figure 3.18 – Test setup by Elmapruk (2010)	65
Figure 3.19 – Test setup by Minaie (2009)	67
Figure 3.20 – Test setup by Baenziger and Porter (2011)	68
Figure 3.21 – Test setup by Nolph and Elgawady (2012)	69
Figure 3.22 – Test setup by Oan (2013)	70
Figure 3.23 – Mechanical fixation at the bottom of Oan’s walls (2013)	70
Figure 3.24 – Test setup by Hoque (2013)	72
Figure 3.25 – Test setup by Hamedzadeh (2013)	73
Figure 3.26 – Test setup by Rizaee (2015)	74
Figure 3.27 – Test setup by Ramírez et al. (2016)	76
Figure 3.28 – CSA S304.14 provision for horizontal reinforcement in PG walls (adapted from CSA 2014)	78
Figure 3.29 – Strut-and-tie model of PG masonry shear walls (Dillon 2015)	79
Figure 3.30 – Behaviour of horizontal reinforcement in a shear wall (Dillon 2015)	79
Figure 3.31 – Role of horizontal reinforcement in resisting masonry shear failure (Voon 2007)	80
Figure 3.32 – Crack pattern in PG wall tested by Minaie (2009)	80
Figure 3.33 – Maleki’s shear wall specimens (Maleki 2008)	80
Figure 3.34 – Footing details in Hoque’s experimental study (Hoque 2013)	83

Figure 3.35 – Application of horizontal load to the cap of the wall according to ESECMaSE (2005).....	83
Figure 3.36 – Interface between the specimen and loading beam by Hamedzadeh (2013)	83
Figure 3.37 – Histogram of average to ultimate strength ratios (Dillon 2015)	87
Figure 3.38 – Complete Model scaling vs. Simple Model scaling (Tomažević and Velechovsky 1992)	88
Figure 3.39 – Distribution of loading conditions for PG wall specimens	93
Figure 3.40 – Distribution of loading rates for PG wall specimens	94
Figure 3.41 – Distribution of wall areas for PG wall specimens.....	94
Figure 3.42 – Distribution of height-to-length ratios H/L for PG wall specimens.....	95
Figure 3.43 – Distribution of shear span ratios M/VL for PG wall specimens.....	95
Figure 3.44 – Distribution of corrected masonry strengths ($f'm$) for PG walls	96
Figure 3.45 – Distribution of vertical reinforcement (ρ_v) in PG wall specimens	96
Figure 3.46 – Distribution of horizontal reinforcement (ρ_h) in PG wall specimens.....	97
Figure 3.47 – Distribution of applied axial loads (σ_n) on PG wall specimens.....	97
Figure 3.48 – Distribution of peak shear stress (v_n, max) of PG wall specimens.....	98
Figure 3.49 – Hypothetical percentile distribution curve (5% of samples exhibit $V_{exp} < V_n$).....	100
Figure 3.50 – Plot of residuals, e_i , versus corresponding fitted values, y_i . Patterns for residual plots: (a) satisfactory (homoscedastic); (b) heteroscedastic; (c) double bow; (d) non-linear (Adapted from Mongometry et al. 2012)	101
Figure 3.51 – Matsumura (1987) model predictions; (a) Experimental strength vs. Predicted strength; (b) Experimental strength vs. Residuals	104

Figure 3.52 – AIJ (1987) model predictions; (a) Experimental strength vs. Predicted strength; (b) Experimental strength vs. Residuals	105
Figure 3.53 – Shing (1990) model predictions; (a) Experimental strength vs. Predicted strength; (b) Experimental strength vs. Residuals	106
Figure 3.54 – Anderson and Priestley (1992) model predictions; (a) Experimental strength vs. Predicted strength; (b) Experimental strength vs. Residuals	107
Figure 3.55 – Fattal (1993) model predictions; (a) Experimental strength vs. Predicted strength; (b) Experimental strength vs. Residuals	108
Figure 3.56 – NEHRP (1997) model predictions; (a) Experimental strength vs. Predicted strength; (b) Experimental strength vs. Residuals	109
Figure 3.57 – UBC (1997) model predictions; (a) Experimental strength vs. Predicted strength; (b) Experimental strength vs. Residuals	110
Figure 3.58 – NZS-4230 (2004) model predictions; (a) Experimental strength vs. Predicted strength; (b) Experimental strength vs. Residuals	111
Figure 3.59 – Eurocode 6 (2005) model predictions; (a) Experimental strength vs. Predicted strength; (b) Experimental strength vs. Residuals	112
Figure 3.60 – Voon (2007) model predictions; (a) Experimental strength vs. Predicted strength; (b) Experimental strength vs. Residuals	113
Figure 3.61 – IMNC (2010) model predictions; (a) Experimental strength vs. Predicted strength; (b) Experimental strength vs. Residuals	114
Figure 3.62 – CSA 304.14 (2014) model predictions; (a) Experimental strength vs. Predicted strength; (b) Experimental strength vs. Residuals	115
Figure 3.63 – Dillon (2015) model predictions; (a) Experimental strength vs. Predicted strength; (b) Experimental strength vs. Residuals	116
Figure 3.64 – TMS 402/602 (2016) model predictions; (a) Experimental strength vs. Predicted strength; (b) Experimental strength vs. Residuals	117

Figure 4.1 – Feedforward backpropagation neural network architecture (Adapted from Plevris and Asteris 2014).....	119
Figure 4.2 – Single neuron work (Garzón-Roca et al. 2013).....	119
Figure 4.3 – Effect of hidden layer size on network generalization (Basheer and Hajmeer 2000).....	120
Figure 4.4 – (a) An ANN predicting validation data with small errors is an indication of generalization; (b) an ANN predicting validation data with large errors is an indication of overfitting	122
Figure 4.5 – Illustration of the early-stopping rule based on cross-validation (Haykin 1994).....	122
Figure 4.6 – Identification tag for neural networks used in this study	127
Figure 4.7 – Sensitivity analysis demonstrating an ANN model predicting negative values of peak shear strength	137
Figure 4.8 – Sensitivity analysis suggestive of an ANN model overfitting data.....	137
Figure 4.9 – Sensitivity analysis for equations developed by trained 5-n-1 neural networks in Aguilar et al. (2016): (a) Concrete block (fully grouted) walls; (b) Ceramic brick (fully grouted) walls; (c) Ceramic brick (partially grouted) walls (adapted from Aguilar et al. (2016))	138
Figure 4.10 – Masonry compressive strength vs. experimental shear strength.....	140
Figure 4.11 – Sensitivity Analysis, “F-5-5-1” Network	142
Figure 4.12 - Sensitivity Analysis, “F-7-5-1” Network.....	146
Figure 4.13 – ANN “F-5-5-1” model predictions; (a) Experimental strength vs. Predicted strength; (b) Experimental strength vs. Residuals	149
Figure 4.14 – ANN “F-7-5-1” model predictions; (a) Experimental strength vs. Predicted strength; (b) Experimental strength vs. Residuals	150
Figure 4.15 – PG wall specimen “PG254-48” (adapted from Elmapruk (2010))	155

Figure 5.1 – Distribution of various parameters in dataset “F”	158
Figure 5.2 – Wall 1 (Maleki 2008)	160
Figure 5.3 – Wall 1 hysteresis loop with envelope outlined in green (adapted from Maleki (2008))	161
Figure 5.4 – VecTor2 model of Maleki (2008)’s PG specimen “Wall 1”	163
Figure 5.5 – Loading cycle used for “Wall 1” (Maleki 2008).....	164
Figure 5.6 – Loading cycle used for “Wall 1” in VecTor2	165
Figure 5.7 – VecTor2 define job dialog.....	165
Figure 5.8 – VecTor2 masonry structures default settings	166
Figure 5.9 – Wall 1 VecTor2 model hysteresis loop with envelope outlined in red	167
Figure 5.10 – Wall 1 experimental hysteresis loop envelope outlined in green with VecTor2 model hysteresis loop envelope outlined in red (adapted from Maleki (2008))	168

LIST OF SYMBOLS AND ABBREVIATIONS

A_h	Cross-sectional area of horizontal reinforcement (mm^2)
A_n	Net cross-sectional area of a member (mm^2)
A_{nv}	Net shear area (mm^2)
A_{scaled}	Area of wall (mm^2); $A = H \times L$
A_{sh}	Total horizontal steel area (mm^2)
A_{sv}	Total vertical steel area (mm^2)
A_v	Cross-sectional area of shear reinforcement (mm^2)
b_w	Overall web width, which does not include flanges or projections formed by intersecting walls when calculating factored shear resistance of walls (mm)
d	distance from compressive face of flexural member to centroid of longitudinal tensile reinforcement (mm)
d_v	Effective depth for shear calculations, taken as greater of $0.9d$ or $0.72h_b$ but need not be taken as less than $0.8l_w$ for walls (mm)
FG	Fully grouted
f'_m	Compressive strength of masonry (MPa)
f_{gr}	Compressive strength of grout (MPa)
f_{yh}	Yield strength of horizontal reinforcement (MPa)
f_{yv}	Yield strength of vertical reinforcement (MPa)
f_{yc}	Yield strength of confinement (interior) vertical reinforcement (MPa)
h	Height of wall (mm)
h_e	Effective height of wall, dependent on the support condition (mm)
IW	Input weights matrix
L	Length of masonry wall, in direction of applied shear force (mm)
LW	Output weights matrix
MSE	Mean-squared error
M_f	Factored maximum moment at the section under consideration ($\text{N}\cdot\text{mm}$)

P_d	Axial compressive load on the section under consideration (N)
PG	Partially grouted
s_{gh}	Horizontal grout spacing of partially grouted walls
s_{gv}	Vertical grout spacing of partially grouted walls
s_h	Spacing of shear reinforcement in direction parallel to longitudinal reinforcement (mm)
s_v	Spacing of vertical reinforcement in direction parallel to horizontal reinforcement (mm)
t	Wall thickness
V_n	Nominal shear strength of section (N)
V_f	Factored maximum shear at the section under consideration (N)
v_n	Predicted shear stress strength; $v_n = \frac{V_n}{A_T}$
v_m	Shear strength of masonry (MPa)
ϕ_m	Resistance factor for masonry
δ	Boundary condition factor; 1.0 for double bending and 0.6 for cantilever support condition
γ_g	Factor to account for partially grouted walls when calculating shear resistance, not greater than 0.5
ρ_c	Confinement (interior) vertical reinforcement ratio
ρ_h	Horizontal reinforcement ratio; $\rho_h = \frac{A_{sh}}{s_h t}$
ρ_v	Vertical reinforcement ratio; $\rho_v = \frac{2A_{ve} + \sum A_{sv}}{tL}$
σ	Acting vertical normal stress on the wall; $\sigma = \frac{P}{A_T} = \frac{P}{tL}$

1 INTRODUCTION

1.1 Background

Partially grouted (PG) concrete block shear walls are a common system to resist lateral forces in masonry structures. Unlike fully grouted (FG) masonry, PG walls are grouted only in locations where reinforcement bars are placed (vertically aligned cells with vertical flexural reinforcement and/or horizontal bond beams with shear reinforcement). As a result, they offer an economic advantage over FG walls due to reduced material and labour costs (Dhanasekar 2011; Minaie et al. 2010).

FG wall behaviour is often approximated by treating the masonry (block, grout and mortar) as an isotropic material, such as concrete. However, this approximation grows increasingly inaccurate for PG walls due to its inherent anisotropy and the nonlinear interactions that exist between mortar, blocks, grouted cells, ungrouted cells, and reinforcing steel. Unlike FG walls, the mechanical behavior of PG walls is analogous to infilled walls under lateral loading (Bolhassani et al. 2016; Minaie 2009).

The behaviour of PG walls under shear loading is not yet well understood. Despite fundamental differences in behaviour between FG and PG walls, currently available design equations are empirically formulated based on FG wall data and applies a reduction factor to PG walls to achieve safety levels comparable to FG walls (Dillon and Fonseca 2017). As a result, such equations often lack accuracy and consistency in shear strength predictions. Hassanli et al. (2014) compiled a dataset of 89 PG wall specimens and found the CSA S304.1-04 (2004) model to overestimate 24% of the specimens, with the experimental-to-predicted ratio (V_{test}/V_{calc}) ranging from 0.40 to 3.75. The same study found the MSJC-2011 (2011) model to overestimate 71% of the specimens, with the experimental-to-predicted ratio ranging from 0.35 to 1.65. Bolhassani et al. (2016) compiled a dataset of 42 PG wall specimens and found the TMS 402/602 (2016) model to overestimate 26% of the specimens. Minaie et al. (2010) compiled a dataset of 64 PG wall specimens and found the experimental-to-predicted ratio standard deviations of CSA

S304.1-04 (2004), MSJC (2011), and NZS 4230 (2004) of 0.72, 0.60, and 0.63, respectively.

The shear strength and behaviour of PG walls is dependent on variables such as the wall geometry, level of axial load (increasing interlocking between masonry units in diagonal cracks), ratio of net/gross area, and distribution of horizontal (increasing ductility and energy dissipation) and vertical reinforcement (resisting shear loading at crack openings) (Minaie et al. 2010; Voon and Ingham 2007). Various equations have been proposed by numerous researchers to predict the in-plane shear strength of PG walls by conducting regression analysis to determine the relative influence of these parameters. Matsumura (1987) conducted a regression analysis using his experimental study consisting of 57 concrete masonry walls and 23 brick masonry walls to formulate a shear strength equation as a sum of shear strength contributions from masonry, horizontal shear reinforcement, and applied normal force. Fattal (1993b) compiled 72 PG walls to perform a regression analysis and propose an improved version of Matsumura (1987)'s equation. Hassanli et al. (2014) compiled dataset of 89 PG wall specimens to perform both univariate and multivariate regression analysis and proposed an improved version of the MSJC (2011) equation by modifying the relative influence of shear strength contributions from masonry, horizontal shear reinforcement, and applied normal force. Dillon (2015) compiled a dataset of 182 PG walls to also perform a multivariate linear analysis and propose an improved version of the MSJC (2011) to include the influence of vertical steel reinforcement.

While regression analysis is relied upon extensively for formulating predictive models, the application of artificial neural networks (ANNs) for pattern recognition and model building has also demonstrated success in numerous structural engineering research studies. In comparison to regression analysis, ANNs are particularly useful for approximating nonlinear functions, and do not require any foreknowledge of any complex relationships which may exist between variables. In a literature review by Paliwal and Kumar (2009) consisting of 37 studies comparing ANN against regression analysis, 24 studies found equivalent or better predictive capacity using ANNs based on various

performance evaluation measures, such as the mean-squared error of predictions. However, the same study reported that determining the optimal architecture of the ANN models, such as the number of hidden neurons, was often complex and required extensive parametric analyses. Also, a disadvantage of ANNs compared to usual regression models is that the former does not provide an explicit interpretability of the relative importance of each input parameter. Therefore, the study suggested that ANNs and regression analysis should be considered not as competing methods, but as complimentary methods for model building.

The ability for ANNs to recognize patterns relies heavily on both the number of specimens and the quality of the input dataset for training the ANN. Since no single experimental study for PG walls contains enough information to build and validate a constitutive model for the shear strength and behaviour of this type of walls, it is necessary to assemble a dataset from multiple experimental studies using meta-analysis (Dillon and Fonseca 2014a). First, PG wall data from multiple experimental studies must be compiled, such as its geometric, material, and loading properties; then, a set of criteria is used to determine which PG walls are to be included or excluded from analysis; lastly, data must be converted or “synthesized” to minimize variation between studies and predict any missing information. This process is vital to ensure a consistent dataset for the ANN to perform pattern recognition.

Since ANN models rely heavily on the input dataset used, it is also necessary to consider and address gaps which may exist in the input dataset. In general, larger datasets are beneficial for training ANN models. While additional experimental studies can address such gaps and increase the dataset size, it is often time-consuming and costly. Alternatively, a finite-element (FE) model validated with experimental results can be used to generate hypothetical specimens and enlarge the dataset for ANN model development.

1.2 Problem Statement

Due to the inherent complex behaviour of PG walls and the lack of test data, many design codes have adopted a semi-empirical approach to predict shear strength of PG walls. Recent studies have shown that available design expressions currently used to predict the in-plane shear strength of PG walls are inconsistent and often non-conservative. An improved understanding of the behaviour of PG walls under lateral loading is required to address the limitations of current design expressions to predict the in-plane shear strength of PG shear walls.

1.3 Objectives, Methods and Scope

The main objective of this study is to develop an analysis model for the shear strength of PG walls using an ANN approach, with the purpose of generating an improved shear strength model, gaining further insight into the influence of each parameter, investigate the influence of unaccounted parameters, and improving understanding of interrelated variables. To achieve this main objective, the following specific objectives are identified. The methodology used to accomplish the objectives is also presented.

1. *Prepare a dataset through meta-analysis suitable for developing an ANN model:*
 - Dataset assembly: compiling PG concrete block masonry walls exhibiting in-plane diagonal tension shear failure from multiple experimental studies
 - Dataset scrutinization: selection/inclusion criteria are discussed and applied to determine which PG walls are to be included or excluded from analysis
 - Dataset synthesization: the data is collected in a consistent manner to ensure that the data is compatible for comparison and analysis
2. *Compare the performance of currently available equations with experimental results as a benchmark for ANN models:*
 - Shear strength expressions from various researchers and design codes are discussed
 - Statistical performance metrics for evaluating shear strength equations are discussed

- Using the compiled dataset, each design expression is evaluated to compare the experimental shear strengths with predicted shear strengths, and its performance metrics are compared and discussed
3. *Develop an ANN-based model to predict the in-plane shear strength of PG walls and compare its performance with currently available equations:*
 - The effects of varying neural network architecture parameters are investigated to produce an improved prediction output by a trained ANN
 - A comparison of performance metrics between the ANN model and currently available design expressions is discussed
 - ANN-based shear strength expressions are presented, and its performance is evaluated in the same manner as the design expressions in objective (2).
 4. *Perform sensitivity analyses on trained ANN models to gain insight and improve understanding of interrelated variables*
 - A sensitivity analysis is performed to gain further insight into the influence of each parameter on the shear strength of PG walls
 - Previously unaccounted parameters are investigated and discussed
 - Interrelationships between variables based on the sensitivity analysis is investigated
 5. *Demonstrate the potential of FE modelling for further ANN model development:*
 - Using the program VecTor2, develop and validate a preliminary finite-element (FE) model of a PG wall under in-plane shear loading

The scope of the thesis is to develop an ANN-based analysis model to investigate the in-plane shear strength and behaviour of PG concrete block masonry walls. FG walls are not considered in this study; no attempt has been made to generate a unified analysis model for PG and FG walls. Only PG walls governed by diagonal shear failure are considered; walls failing in flexure, sliding shear, or the crushing of the masonry compressive strut are not included in this study. Walls with openings are not included in the analysis. Both bond beam and joint reinforcement has been considered as “shear reinforcement;” no distinction has been made to study the influence of each type of

horizontal reinforcement separately. ANN-based models often produce equations that are challenging to distill; no attempt in this study has been made to generate simplified equations using techniques such as numerical methods. FE modelling is demonstrated as a viable option for increasing the training dataset for ANN modelling, but no expansion of the dataset is attempted in this study.

1.4 Organization of Thesis

The thesis is separated into six chapters:

- Chapter 1 introduces the research study and contains its objectives and scope
- Chapter 2 includes a comprehensive literature review of failure mechanisms, effect of various parameters on the in-plane shear strength of PG walls, and presents various design expressions currently available to predict the shear capacity of PG walls.
- Chapter 3 addresses objective (1) by presenting the meta-analysis involving dataset assembly, data scrutinization, and data synthesization. The dataset is compiled from 26 experimental studies, each of which are described briefly. Several variants of the dataset with varying levels of scrutinization and synthesization are generated for ANN analysis. The distribution of specimen parameters in each dataset are presented to provide a visual representation of potential gaps in experimental studies. Finally, objective (2) is addressed by evaluating and discussing the performance of the design expressions presented in Chapter 2.
- Chapter 4 introduces the fundamentals of ANNs and discusses the ANN type and architecture used in this study (i.e. the number of neurons in the hidden layer, transfer function, etc.). Objective (3) is addressed by presenting and discussing the results of trained ANNs. Objective (4) is addressed by performing a sensitivity analysis to select the optimum ANN model and gain further insight into the behaviour of PG walls.
- Chapter 5 addresses objective (5) by presenting a FE analysis model of a PG shear wall in the FE program VecTor2.
- Chapter 6 outlines the conclusions and recommendations based on Chapters 4 and 5.

2 LITERATURE REVIEW

2.1 Introduction

Reinforced concrete masonry block walls can be fully grouted (FG) or partially grouted (PG). FG masonry walls are characterized by grouting every cell, whereas PG masonry walls are characterized by having grout only in the cells containing vertical steel reinforcement. Horizontal reinforcement can be in the form of either joint reinforcement between courses, or bond beam reinforcement by using lintel blocks across the entire wall. Typical PG masonry shear walls with vertical and horizontal reinforcement details are illustrated in Fig. 2.1.

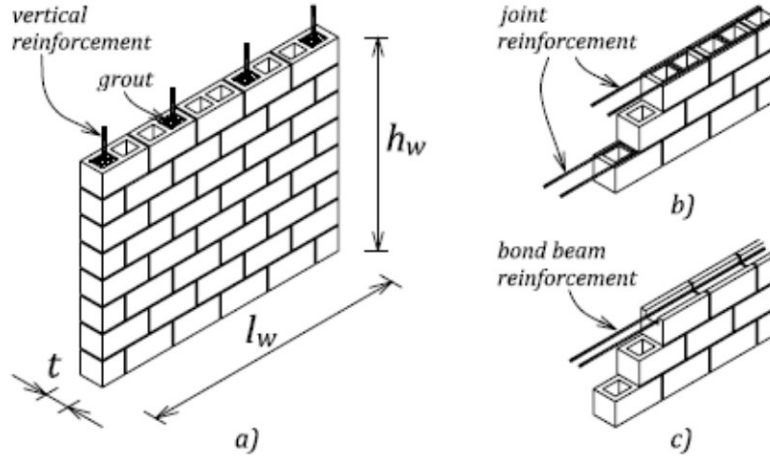


Figure 2.1 – Typical reinforced concrete masonry block wall: (a) vertical reinforcement; (b) joint reinforcement; (c) bond beam reinforcement (Anderson and Brzev 2009)

The purpose of this literature review is to provide a fundamental understanding of PG masonry walls subject to lateral loading as well as a description of the models and design expressions available for predicting its shear resistance.

2.2 Behaviour of Partially Grouted Masonry Walls

2.2.1 Failure Modes

Masonry shear walls are typically designed to resist both gravity and lateral loads. The mode of failure is dependent on a combination of variables, including material properties, geometric properties, boundary conditions, loading pattern, and relative magnitude of gravity and shear loads (Drysdale and Hamid 2005). PG masonry shear walls may fail in flexure, sliding shear, diagonal shear, or a combination of these failure mechanisms (i.e. flexural/shear failure). Each of the primary failure modes are illustrated by Fig. 2.2.

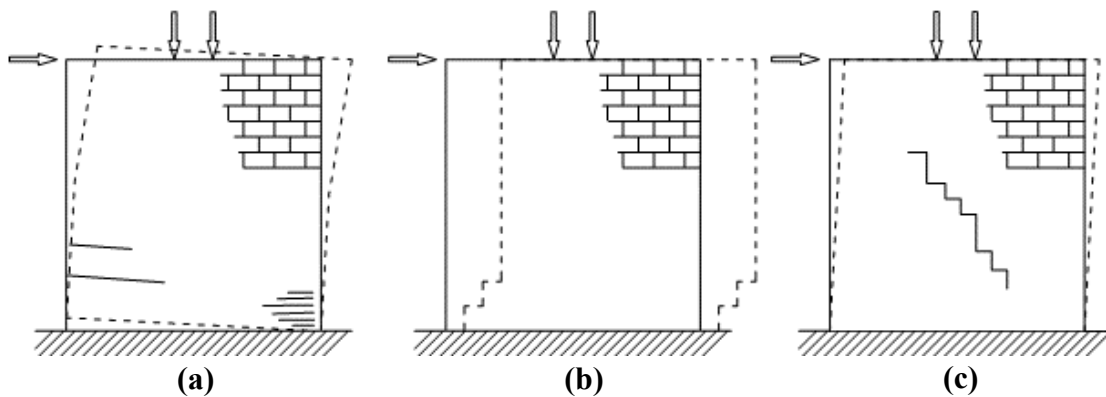


Figure 2.2 – Reinforced masonry shear wall failure modes: (a) flexural; (b) sliding, (c) shear (adapted from Voon 2007)

2.2.1.1 Flexural Failure

Flexural failure is characterized by crushing at the compression toe, yielding of the vertical reinforcement at the tension heel, and overturning of the wall. Walls failing in flexure exhibit higher ductility and energy dissipation largely due to the formation of a plastic hinge at the bottom of the wall and yielding of vertical reinforcement (Dillon 2015; Rizaei 2015). PG masonry walls are more likely to exhibit a flexural-shear failure or a flexural failure as the aspect ratio is increased (Haider 2007).

2.2.1.2 Sliding Failure

Sliding failure occurs when mortar joints along masonry courses fail. It is characterized by sliding of the wall along bed joints. Sliding failure in reinforced masonry walls is not common; typical axial loads and dowel action from vertical reinforcement prevent this

mode of failure (Oan 2013; Rizaee 2015). Localized sliding failure may increase the ductility of PG masonry shear walls with wide spaced vertical reinforcement, as long as the overall integrity of the wall remains (Hamedzadeh 2013).

2.2.1.3 Diagonal Tension Shear Failure

Diagonal tension failure is characterized by diagonal cracking along the shear wall. Depending on the level of axial stress, diagonal cracking can occur as either step cracking along mortar joints or diagonal cracking across masonry units (Oan 2013). Both are illustrated in Fig. 2.3.

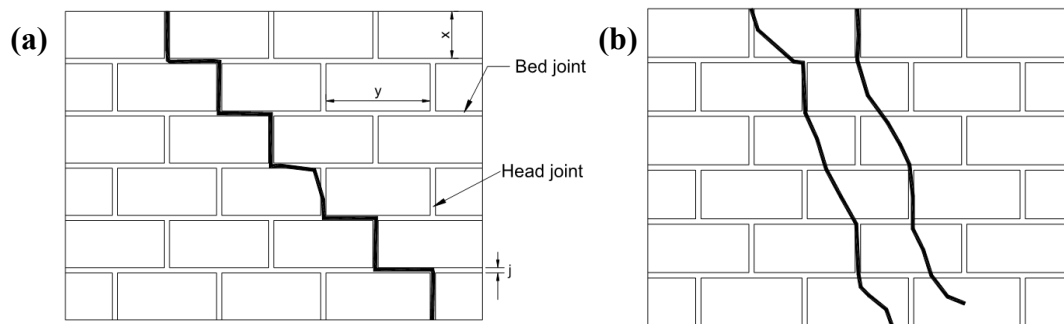


Figure 2.3 – Diagonal shear mode of failure: (a) step cracking at low axial compressive stress; (b) diagonal cracking across masonry (adapted from Voon 2007)

Once diagonal cracking occurs, the resisting mechanism is a combination of aggregate interlock of masonry units and grout as well as resistance provided by horizontal and vertical reinforcement (Shing et al. 1990b). A higher axial loading can minimize crack openings, thus increasing the contribution of aggregate interlocking to shear resistance. This shear resisting mechanism is illustrated by Fig. 2.4.

Since the horizontal and vertical reinforcing steel is not engaged until diagonal cracking occurs, the diagonal cracking load is independent of reinforcement ratios in either direction (Ghanem et al. 1992; Haach et al. 2010; Matsumura 1987; Schultz et al. 1998).

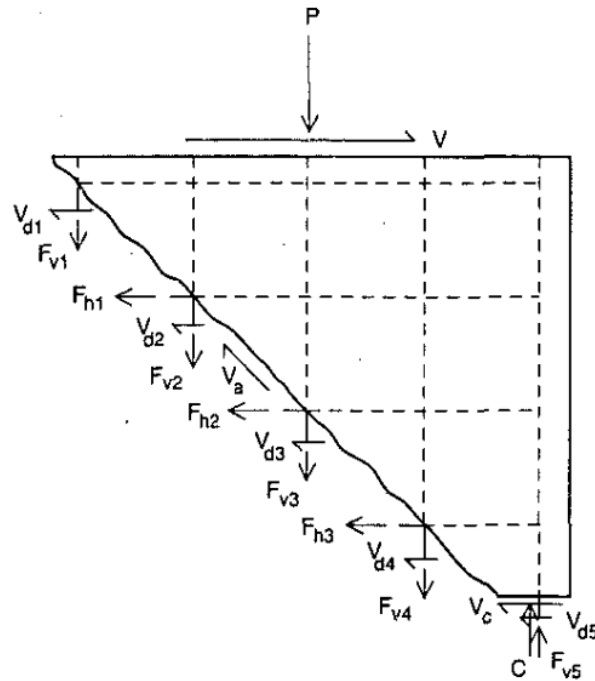


Figure 2.4 – Shear Resistance Mechanism (Shing et al. 1990b)

Two types of diagonal tension failure for PG masonry walls have been documented: a “brittle” shear failure and a “ductile” shear failure (Dillon 2015; Ghanem et al. 1992; Sveinsson et al. 1985). A “brittle” failure is characterized by a single, wide crack at approximately 45 degrees across the entire wall. “Brittle” shear failures are characteristic of walls with widely spaced reinforcement and high axial stresses (Nolph 2010). However, it is possible to design PG masonry shear walls with greater ductility and energy dissipation. A “ductile” shear failure is achieved by using narrow spacing between reinforcing bars, and ensuring an axial load-to-masonry compressive strength ratio of less than 0.05 (Ghanem et al. 1992). Distributed vertical reinforcement minimizes crack openings, allowing new cracks to form throughout the wall, while preserving the aggregate interlocking of masonry blocks that provides shear resistance. This results in a “ductile” diagonal shear failure governed by widening of cracks and localized crushing of the masonry (Dillon 2015; Rizaee 2015). Typical cracking patterns of “brittle” and “ductile” shear failures are illustrated by Fig. 2.5.

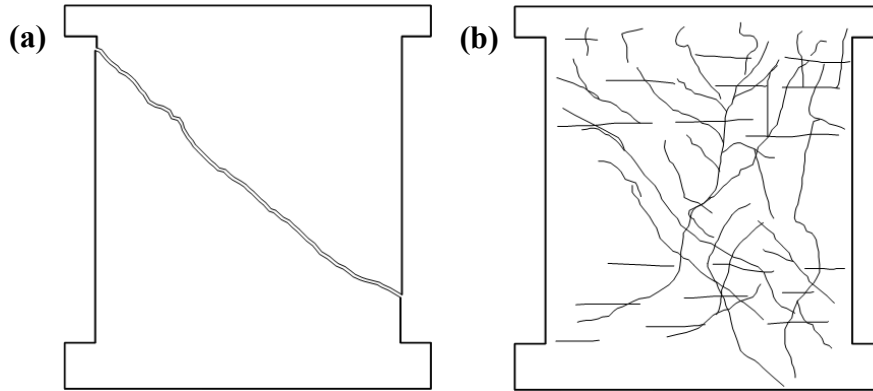


Figure 2.5 – Modes of shear failure: (a) Brittle shear failure; (b) Ductile shear failure (adapted from Voon 2007)

2.2.1.4 Masonry Compression Strut Shear Failure

The shear failure of PG masonry walls may also be governed by the crushing of the masonry compressive strut. Typically, shear walls heavily reinforced with horizontal steel are susceptible to this type of shear failure. Using a truss analogy, horizontal shear reinforcement form tension ties, while masonry compressive struts form diagonally between cracks, as illustrated in Fig. 2.6.

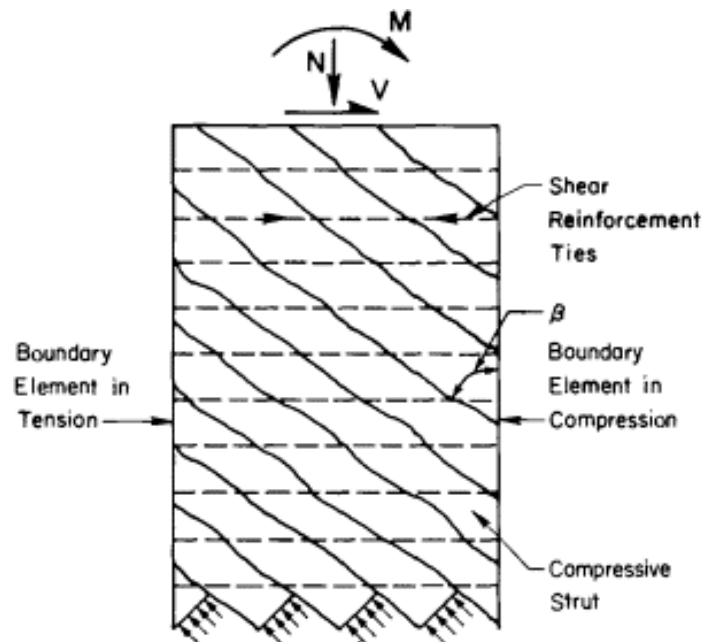


Figure 2.6 –Truss analogy for masonry shear wall (adapted from Oesterle et al. 1984)

Some code equations, such as the CSA S304.14 (2014), imposes an upper limit on the maximum amount of shear that stirrups can resist and limits the shear capacity of PG shear walls. The upper limit prevents crushing of the masonry strut by placing a limit on the amount of horizontal reinforcement to be used in the wall, so that the mode of failure does not shift from a flexural-shear type to a strut-crushing one.

2.2.2 Effect of Various Parameters on Shear Wall Behaviour

2.2.2.1 Effect of Masonry Compressive Strength (f'_m)

Past studies have suggested that the shear strength of PG walls increases approximately in proportion to the square root of the masonry compressive strength (Matsumura 1987; Voon and Ingham 2006). However, more recent studies suggest that the square root relationship loses accuracy with extremely high or low masonry compressive strength values due its empirical derivation (Dillon 2015). It has been suggested by Morrison (2013) that Matsumura (1987)'s study does not contain sufficient data points to conclude a strong correlation between masonry compressive strength and PG shear strength.

The shear strength equation proposed by Shing et al. (1990) combines the vertical reinforcement ratio with the compressive strength of masonry in a single term, and suggests that the residual strength of masonry after cracking is influenced by the dowel action provided by vertical reinforcement. An increase in vertical reinforcement would enhance aggregate-interlock forces by reducing the width of crack openings, resulting in an increase of the ultimate shear strength. Seif ElDin (2016) explains the indirect influence of vertical reinforcement on shear strength by using the shear strength envelope illustrated by Fig. 2.7.

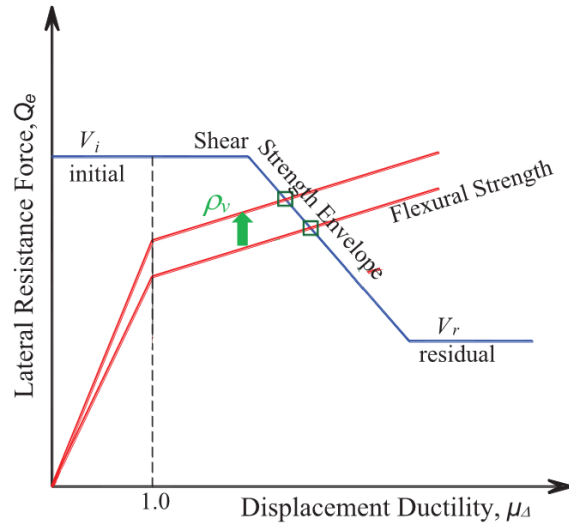


Figure 2.7 – Effect of vertical reinforcement ratio, ρ_v , on the in-plane shear resistance provided by masonry (Adapted from Seif EIDin 2016)

2.2.2.2 Effect of Wall Aspect Ratio $\left(\frac{H}{L}\right)$

Several studies have reported that a decrease in the height-to-length aspect ratio of a PG wall increases its shear strength (Matsumura 1988; Ramírez et al. 2015; Voon and Ingham 2006). However, most experimental studies have focused solely on aspect ratios of 1 or less. This is in part due to the increased likelihood of PG walls to exhibit flexural-shear failure or flexural failure as the aspect ratio is increased (Haider 2007). This is consistent with the study by Maleki et al. (2009), which found walls with aspect ratios equal to or less than 1.0 failed primarily in shear, while the wall tested with an aspect ratio equal to 1.5 exhibited a shear-flexure failure mode. The reduced stiffness and ultimate shear capacity of Maleki’s walls as the aspect ratio is increased is illustrated by Fig. 2.8.

Schultz et al. (1998) also tested walls with varying height-to-length aspect ratios (0.5, 0.7 and 1.0) and found that increasing the aspect ratio increased the ultimate shear strength, while the deformation and energy dissipation capacity of the wall decreased. A study by Ramírez et al. (2016) also found the energy dissipation capacity to be inversely related to the height-to-length aspect ratio.

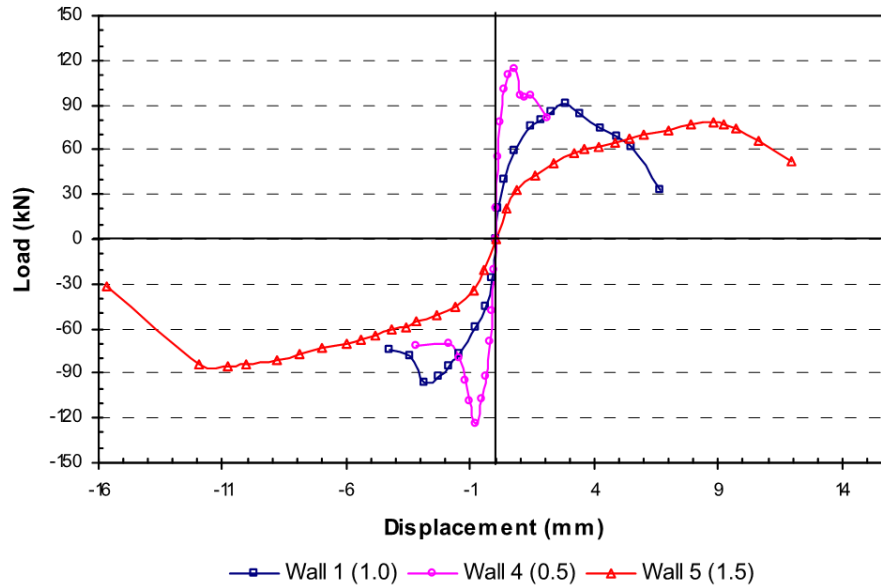


Figure 2.8 – Walls tested by Maleki et al. (2009) with different aspect ratios (0.5, 1.0 and 1.5) and similar bar spacing

Some design expressions include the shear span ratio instead of the height-to-length aspect ratio. In doing so, the boundary conditions of the wall are considered without having to include another constant to separate single curvature and double curvature walls. The shear span ratio is typically expressed as either $\frac{M}{VL}$ (moment divided by length and applied shear force), or $\frac{M}{d_v V}$ (moment divided by the effective depth and applied shear force). Figure 2.9 illustrates how the shear span ratio accounts for both the height-to-length ratio and boundary condition simultaneously.

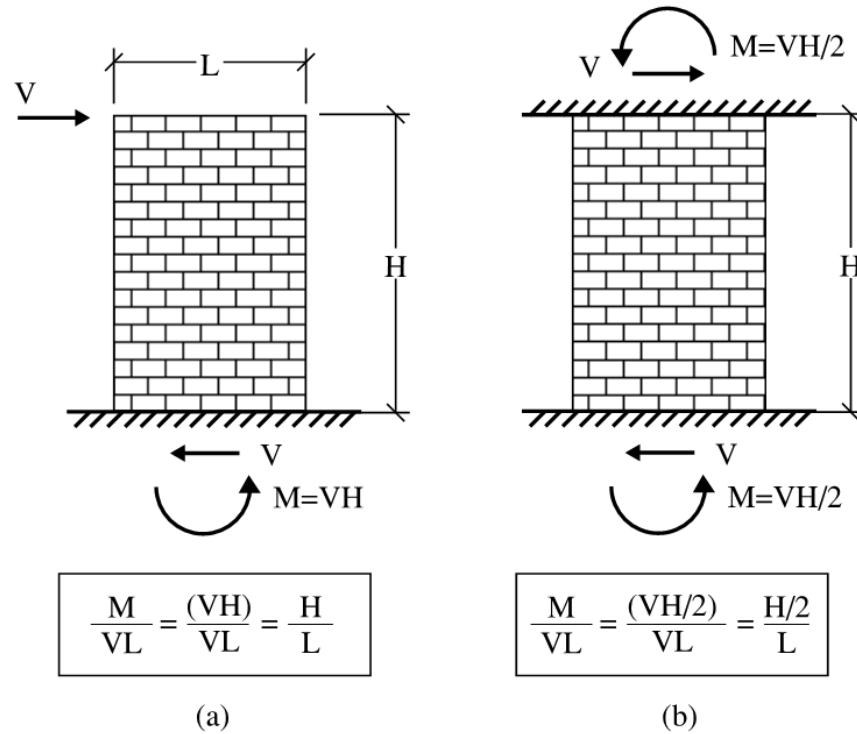


Figure 2.9 – Shear span ratio for (a) single curvature boundary condition and (b) double curvature boundary condition

2.2.2.3 Effect of Vertical Reinforcement

While vertical reinforcement is typically used to increase the flexural resistance of walls, the effect of vertical reinforcement on shear strength has not been considered in most design equations. However, vertical reinforcement is theorized to contribute the shear strength of PG walls through vertical confinement and dowel action (Dillon 2015). The shear strength equation proposed by Shing et al. (1990) includes a term that accounts for the vertical reinforcement, which was subsequently adopted in the NZS-4230 (2004) design equation and the equation proposed by Voon and Ingham (2007). Ghanem et al. (1992) suggested that only interior reinforcing bars should be considered for shear resistance, since boundary bars are considered to carry the tension forces due to flexural loads.

According to Thurston and Hutchinson (1982), vertical reinforcing steel provides shear resistance as cracking occurs. Thus, it has been suggested that the spacing of vertical

reinforcement is more critical than the ratio of vertical reinforcement in allowing a more even distribution of cracks. Distributed vertical reinforcement can minimize these crack openings, allowing the aggregate interlocking of masonry blocks to continue providing shear resistance (Ghanem et al. 1992). Dhanasekar and Haider (2011) found that shear walls under cyclic loading containing vertical reinforcement spaced greater than 2000 mm apart led to significant damage, whereas a spacing of less than 2000 mm resulted in localized diagonal cracking. Conversely, an investigation by Nolph and Elgawady (2012) found that an increase of grout horizontal spacing linearly decreased the shear strength, as shown in Fig. 2.10.

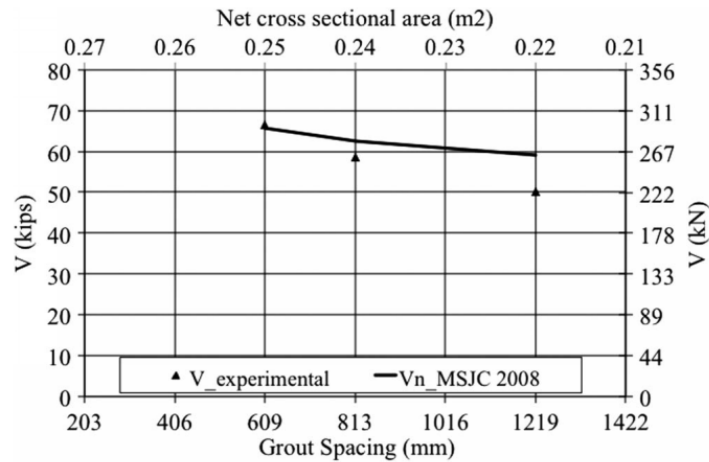


Figure 2.10 – Effects of grout horizontal spacing on the shear strength of test specimens by Nolph and Elgawady (2012)

Using a strut-and-tie model, it appears that beyond a certain threshold, decreasing the spacing of vertical reinforcement does not necessarily increase the shear capacity of a wall (Hassanli et al. 2014). As illustrated by Fig. 2.11, an additional steel tie in (b) compared to (a) may not increase the ultimate strength, due to the maximum number and width of struts that have already been developed.

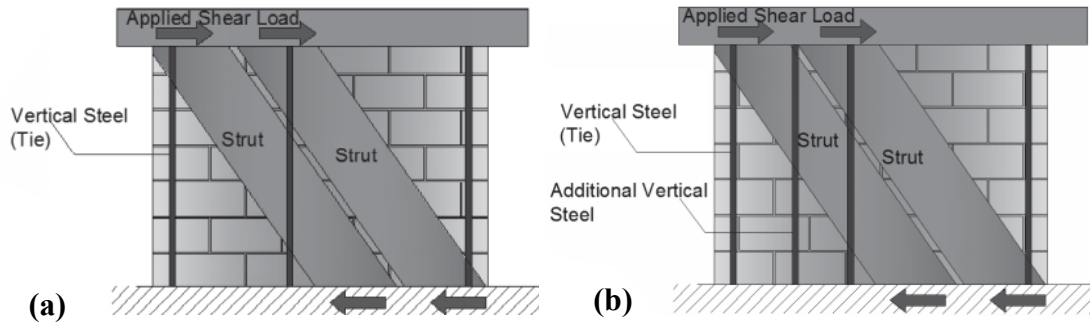


Figure 2.11 – Effect of closely spaced vertical reinforcement explained with strut and tie models – (a) normal spaced and (b) closely spaced (adapted from Hassanli et al. 2014)

This strut-and-tie model assumes that the shear strength is controlled by the capacity of the masonry strut, such that any increment in tie area or number of ties cannot lead to more shear strength. However, if the limiting element is the yielding of the tensile bar (i.e. the shear strength is controlled by the capacity of the ties), an increased area of steel would still be expected to increase the overall shear capacity.

2.2.2.4 Effect of Horizontal (Shear) Reinforcement

Although horizontal reinforcement can be in the form of joint reinforcement or bond beam reinforcement, current design equations do not differentiate between them. A few research studies have investigated the difference in horizontal reinforcement and demonstrates that the behaviour of PG walls is dependent on which type of horizontal reinforcement is used (Baenziger and Porter 2011; Hoque 2013; Schultz 1996; Schultz et al. 1998; Yancey and Scribner 1989). It has been suggested by Dillon (2015) that additional research is necessary to investigate the influence of bond beams on the shear strength of PG walls.

Anderson and Priestley (1992) suggested that prior to diagonal cracking of a PG masonry shear wall, the shear load is resisted entirely by masonry blocks (i.e. horizontal reinforcement remains unstressed). Once diagonal cracking has occurred, horizontal reinforcement is engaged as the shear capacity of the masonry decreases. The role of horizontal reinforcement in PG shear walls is illustrated in Fig. 2.12.

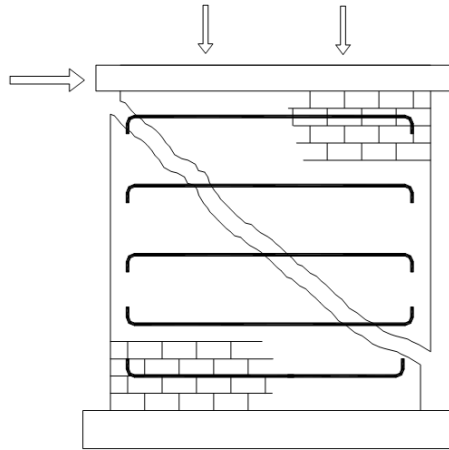


Figure 2.12 – Role of horizontal reinforcement in resisting masonry shear failure (adapted from Voon 2007)

Compared with concrete, masonry is made up of finer aggregates, and therefore, it is expected that the shear capacity of masonry begins to decrease with relatively smaller crack openings. As a result, the horizontal reinforcement steel has likely not begun yielding when the wall has reached its maximum shear capacity. Additionally, a weaker bond exists between masonry and steel compared to concrete and steel. This phenomenon is reflected in many design expressions limiting the efficiency of horizontal reinforcement to about 50-60%; these expressions are discussed in further detail in the following section of this chapter. Janaraj and Dhanasekar (2016a) have gone further to say that the inclusion of horizontal reinforcement ratio in calculating shear strength is unjustified due to the lack of yielding.

Schultz et al. (1998) tested PG walls containing joint reinforcement with 0.056% and 0.11% horizontal reinforcement ratios. Overall, Schultz et al. concluded that the horizontal reinforcement ratio has a marginal influence on the ultimate shear strength. However, the increased horizontal reinforcement had a greater benefit on shear strength for walls with a higher height-to-length aspect ratio, as illustrated in Fig. 2.13.

Both Shing et al. (1990) and Tomažević and Lutman (1988) have suggested that increasing the horizontal reinforcement also improves the post-cracking ductility of PG masonry shear walls.

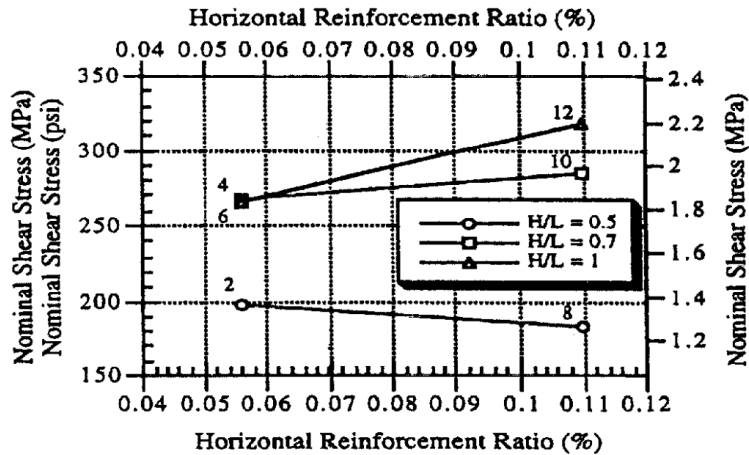


Figure 2.13 – Effect of horizontal reinforcement ratio on shear strength for walls of varying height-to-length aspect ratios (Schultz et al. 1998)

Using a simple strut-and-tie model, Hassanli et al. (2014) also comments on the interaction of height-to-length aspect ratio and horizontal reinforcement on the shear strength of a PG masonry shear wall. As illustrated in Fig. 2.14, horizontal reinforcement is expected to carry a much greater proportion of the lateral load via truss action in slender walls than in squat walls.

Although much of the experiments conducted involve a horizontal reinforcement ratio of 0-0.2%, it has been reported by several authors that horizontal reinforcement ratios above 0.2% lead to a negligible increase in ultimate strength and deformation (Elmapruk 2010; Fattal 1993b; Haach et al. 2012; Hamid and Moon 2005; Shing et al. 1990b).

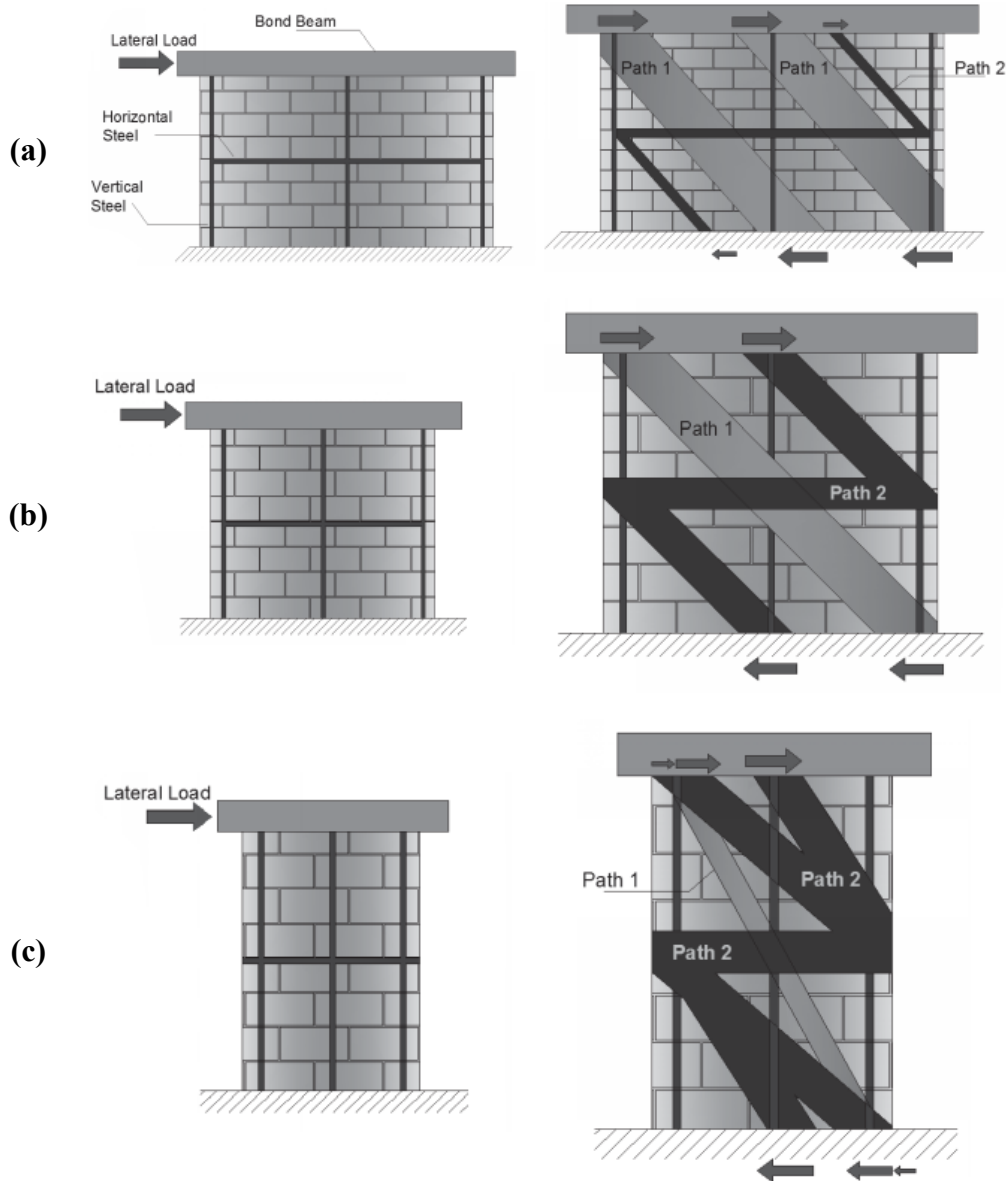


Figure 2.14 – Simple strut-and-tie models for (a) squat, (b) square, and (c) slender PG masonry walls (adapted from Hassanli et al. 2014)

2.2.2.5 Effect of Axial Stress

Multiple studies have found that an increase of axial load increases the ultimate shear resistance of PG shear walls (Haach 2009; Matsumura 1988; Ramírez et al. 2015; Voon and Ingham 2006). The cracking capacity of shear walls under lateral loading increases with greater axial loading due to the increased compressive field that must be overcome (Oan 2013; Voon 2007). After cracking, the resistance mechanism of PG shear walls

includes the aggregate interlock of masonry units; thus, higher axial stresses can minimize crack openings and increase the contribution of aggregate interlocking on shear resistance. A strut-and-tie model by Dillon (2015) predicts that the relationship between axial load and shear resistance is nonlinear.

However, there is a maximum amount of axial stress that will increase the shear strength of masonry walls. Higher levels of axial stress tends to limit ductility by reducing yielding of vertical reinforcing bars, and can lead to more severe diagonal cracking and brittle failures (Haach et al. 2007; Tomazevic and Lutman 1996; Voon and Ingham 2006). Such failures also tend to dissipate less energy (Haach et al. 2010). It was recommended by Ghanem et al. (1993) that the axial load to masonry compressive strength ratio should be less than 0.05 to prevent brittle shear failure. Beyond a certain threshold, the failure mode of the wall becomes a “compression” failure (Page 1989). This relationship is illustrated by Fig. 2.15.

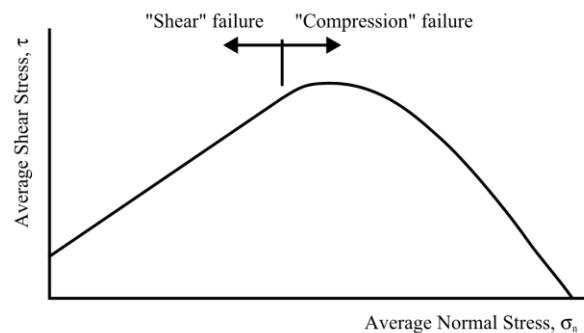


Figure 2.15 – Failure Criterion for Masonry Shear Walls (adapted from Page 1989)

2.3 Design Expressions Predicting In-Plane Shear Strength of PG Walls

Many design codes have adopted a semi-empirical approach to predict shear strength of PG walls, due to the inherent complex behaviour of PG walls and the lack of test data. Therefore, currently available design equations predicting the shear strength of PG walls often rely on overly conservative reduction factors to achieve safety levels comparable to those used in the better-understood FG walls. Currently available design equations also

neglect the decrease of masonry shear strength in plastic hinge regions, limiting their application to describe flexural-shear failure mechanisms (Voon and Ingham 2007).

Recent studies have shown that available design expressions currently used around the world to predict the in-plane shear strength of PG walls are inconsistent and may be non-conservative, and in some cases, overestimate the lateral load capacities of PG walls by as much as three to four times (Haider 2007; Hassanli et al. 2014; Hassanli and Elgawady 2013; Janaraj and Dhanasekar 2016b; Minaie et al. 2010; Nolph and Elgawady 2012).

In one evaluation of several design expressions by Hassanli et al. (2014), a set of 89 experimental specimens were compared with the shear strength predictions of 4 different codes: the MSJC-2011, AS 3700-2011, NZS 4230-2004 and CSA S304.1-04. The study reveals the extent of non-conservatism that exists in these design codes and is summarized in Table 2.1. Notably, some design expressions have underestimated the shear strength of PG walls as frequently as 70% of the time.

**Table 2.1 – Statistical comparison of test results with predicted values ($\frac{V_{exp}}{V_{calc}}$).
(Hassanli et al. 2014)**

	MSJC-2011	AS 3700-2011	NZS 4230-2004	CSA S304.1-04
Minimum	0.35	0.28	0.50	0.40
Maximum	1.65	1.83	3.25	3.75
Average	0.86	0.79	1.49	1.36
Standard deviation	0.25	0.30	0.54	0.55
Percentage of over-predicted specimens	71%	76%	17%	24%

Despite parametric analyses performed on various design expressions, the revision of these expressions is often challenging. Studies have reported parameter coupling: modifying the weight of one parameter affects the weight of other parameters simultaneously. For example, Fattal (1993b) suggests that the effectiveness of vertical reinforcement decreases with increasing aspect ratio. Empirical formulas require

extensive calibration to ensure adequacy in predicting the in-plane shear strength of PG walls (Hassanli et al. 2014).

The remainder of this chapter will present various models for predicting the in-plane shear strength of PG walls. All equations have been converted to SI units where necessary (i.e. force in N, dimensions in mm, stress in MPa). Similar notations have been substituted where appropriate to maintain consistency between equations. Only the nominal predictions are considered, and thus any safety factors that may exist (e.g. ϕ_m and ϕ_s in the Canadian CSA Standard S304.14 (2014)) have been omitted. Equations are presented in chronological order. A summary of all design expressions comparing each term is compiled in Section 2.3.15.

2.3.1 Matsumura (1987)

Matsumura (1987) conducted a regression analysis using his experimental study consisting of 57 concrete masonry walls and 23 brick masonry walls to obtain the predicted shear strength, expressed as a sum of shear stress from masonry, steel reinforcement, and applied normal force as given in Eq. (2.1).

$$v_n = v_m + v_s + v_p \quad (2.1)$$

The shear stress from the masonry, v_m , is given by Eq. (2.2), which is influenced by both the effective flexural depth ratio, $\frac{h}{d}$, and compressive strength of masonry.

$$v_m = 0.875 \cdot k_u k_p \left(\frac{0.76}{\frac{h}{d} + 0.7} + 0.012 \right) \sqrt{f'_{m(g)}} \quad (2.2)$$

where $k_p = 1.16(\rho_{ve})^{0.3}$

$k_u = 1.0$ for FG walls, 0.64 for PG concrete masonry walls

$\rho_{ve} =$ ratio of outermost wall vertical reinforcing steel

$$= \frac{A_{ve}}{b_w d} \times 100$$

A_{ve} = cross-sectional area of vertical reinforcing bar(s) in one side (mm²)

The shear stress from the steel shear reinforcement, v_s , given by Eq. (2.3), includes a relationship between horizontal reinforcement and the compressive strength of masonry.

$$v_s = 0.1575 \cdot \gamma \delta \sqrt{\rho_h f_y h f'_m} \quad (2.3)$$

where γ = factor concerning the type of reinforcement used to confine grout: 1.0 for hoop-type reinforcement in FG masonry, 0.8 for single reinforcing bar with semi-circular hooks at the ends (180° standard hook) in FG masonry, and 0.6 for PG masonry, regardless of reinforcement type

δ = numerical coefficient to account for the effect of boundary conditions in prediction of shear strength: 1.0 for double curvature (inflection point at mid-height), and 0.6 for single curvature

The shear stress from an applied normal stress, v_p , is given by Eq. (2.4).

$$v_p = 0.175\sigma \quad (2.4)$$

By multiplying td to each term, the original form of Matsumura's proposed equation to predict shear strength given by Eq. (2.5).

$$V_n = \left\{ k_u k_p \left(\frac{0.76}{\frac{h}{d} + 0.7} + 0.012 \right) \sqrt{f'_m} + 0.18\gamma\delta\sqrt{\rho_h f_y h f'_m} + 0.2\sigma \right\} \times (0.875td) \quad (2.5)$$

2.3.2 AIJ (1987)

The Architectural Institute of Japan developed an equation to evaluate the shear strength of masonry walls, and appears in Okamoto et al. (1987) as Eq. (2.6):

$$\tau_{su} = \left[0.053\rho_{te}^{0.23} \frac{f'_m + 180}{\frac{M}{Vl_w} + 0.12} + 2.7\sqrt{\sigma_{wh}\rho_{we}} + 0.1\sigma_{0e} \right] \frac{b_e j}{b_w d} \quad (2.6)$$

where $j = 0.875d$

$b_e =$ equivalent wall width

$\rho_{te} =$ flexural reinforcement ratio

$\rho_{we} =$ shear reinforcement ratio

$\sigma_{wh} =$ yield strength of shear reinforcement

$\sigma_{0e} =$ vertical axial stress

Rearranged, the shear stress of masonry walls can be evaluated using Eq. (2.7).

$$v_n = 0.0464\rho_{te}^{0.23} \frac{f'_m + 17.7}{\frac{M}{Vl} + 0.12} + 0.0875\sigma + 0.740\sqrt{\rho_h f_{yh}} \quad (2.7)$$

Limited information has been retrieved in English regarding the derivation process for the formula provided by the AIJ. Nonetheless, Eq. 2.7 is evaluated in Chapter 3 of this thesis for its performance.

2.3.3 Shing et al. (1990)

Based on an experimental program consisting of 22 FG walls, Shing et al. (1990b) proposed Eq. (2.8).

$$V_n = (0.166 + 0.0217\rho_v f_{yv})A_n\sqrt{f'_m} + 0.0217\sigma_n A_n\sqrt{f'_m} + \left(\frac{L - 2d'}{s_h}\right)A_h f_{yh} \quad (2.8)$$

where $d' =$ distance between wall edge and outermost wall vertical reinforcing steel (mm)

Shing et al. (1990b) predicts the in-plane shear strength as a combination of masonry compressive strength, horizontal steel reinforcement, vertical steel reinforcement, as well

as axial compression. The horizontal reinforcement term excludes the reinforcing bars at the top and the bottom of the wall, based on the assumption that there is an insufficient development length to yield. The equation does not consider the shear span to depth ratio, $\frac{M}{Vd_v}$, nor the wall aspect ratio, $\frac{h}{L}$.

Unlike other equations, Shing et al. (1990b) couples the axial compressive stress with the compressive strength of masonry in the same term. Through a least-squares fit, Shing et al. (1990b) found an increase in normalized masonry strength was with respect to the axial compression. Also, the entire vertical steel reinforcement yield strength is considered in contributing to the in-plane shear strength.

Since this equation was originally developed for predicting the shear strength of FG walls and makes no distinction for PG walls, Schultz (1994) recommends that caution should be exercised when using this formula, and suggests that the net area of PG walls should be used for the variable A_n when used to predict the shear strength of PG walls.

2.3.4 Anderson and Priestley (1992)

Using three experimental studies on PG walls [Sveinsson et al. (1985), Matsumura (1987) and Shing et al. (1990)], Anderson and Priestley (1992) assembled the test data and performed a regression analysis. The empirical equation predicts the in-plane shear strength of reinforced masonry walls as the sum of the contribution of masonry, horizontal reinforcement, and axial compression, given by Eq. (2.9).

$$V_n = C_{ap}A_nk\sqrt{f'_m} + 0.5A_{sh}f_{yh}\frac{d}{s_h} + 0.25\sigma_nA_n \quad (2.9)$$

where k = ductility coefficient factor:

$$= 1 - \frac{\mu_\Delta - 2}{2}, 0 \leq k \leq 1$$

μ_Δ = displacement ductility ratio

C_{ap} = 0.24 for concrete masonry

The equation proposed by Anderson and Priestley (1992) takes the degradation and fatigue associated with cyclic loading into account by including the ductility coefficient factor, k . The equation also assumes that 50% of the yield capacity of horizontal reinforcement contributes to the shear strength of the wall.

Additionally, Anderson and Priestley (1992) found that the vertical reinforcing steel did not have a significant influence on the shear strength. Similar to the equation proposed by Shing et al. (1990), this equation also does not consider the shear span to depth ratio, $\frac{M}{Vd_v}$, nor the wall aspect ratio, $\frac{h}{L}$, and makes no distinction between PG and FG walls. Overall, this equation was found to be non-conservative by Voon and Ingham (2007).

2.3.5 Fattal (1993)

In a study performed by Fattal (1993b), 72 PG masonry wall specimens were compiled from three experimental programs (51 tests by Matsumura (1987), 11 tests by from Chen et al. (1978) and 10 tests by Yancey and Scribner (1989)) to evaluate the performance of the equation proposed by Matsumura (1987) for predicting the shear strength of masonry walls. All the walls in his analysis had double curvature boundary conditions and were tested under displacement controlled, reverse cyclic loading.

The analysis performed by Fattal found that the lateral strength predicted by Matsumura's equation (Eq. (2.8)) varied from 23% to 180% of the test specimens' measured strengths with a coefficient of variation of 0.31. Fattal noted that Matsumura's equation was especially inaccurate in predicting shear strength for walls without vertical reinforcement. Fattal found that Matsumura's equation underestimates effect of horizontal reinforcement and overestimates the effect of v_m when no vertical reinforcement is used and suggests that the relative weights given to the v_m and v_s terms require adjustment.

The following equations for predicting the shear strength of masonry shear walls are from a linear regression model proposed by Fattal (Fattal 1993a; b) as an improvement of the equation proposed by Matsumura (1987). Using the same dataset, Fattal's equation varied from 41-146% of the test specimens' measured strengths with a coefficient of variation

of 0.21, demonstrating a statistical improvement compared to Matsumura's equation. The predicted shear strength is a sum of shear stress from masonry, steel shear reinforcement and applied normal force, given by Eq. (2.10).

$$V_n = (v_m + v_s + v_p)bd \quad (2.10)$$

The shear stress from the masonry, v_m , is given by Eq. (2.11).

$$v_m = k_o k_u \left[\left(\frac{0.5}{\left(\frac{H}{L}\right) + 0.8} \right) + 0.18 \right] \sqrt{f'_m f_{yv}} \cdot (\rho_v)^{0.7} \quad (2.11)$$

The shear stress from the steel shear reinforcement, v_s , is given by Eq. (2.12).

$$v_s = k_o \cdot 0.011 \gamma_F \delta_F f_{yh} (\rho_h)^{0.31} \quad (2.12)$$

The shear stress from an applied normal force, v_p , is given by Eq. (2.13).

$$v_p = k_o \cdot 0.012 f'_m + 0.20 \sigma_n \quad (2.13)$$

The notation used in Equations (2.10) to (2.13) is as follows:

- k_o = 0.8 for PG walls, and 1.0 for FG walls (unitless)
- k_u = numerical coefficient specified according to type of masonry and type of grouting (unitless): 1.0 for FG masonry, 0.8 for PG brick masonry, and 0.64 for PG concrete masonry
- δ_F = numerical coefficient to account for the effect of boundary conditions in prediction of shear strength (unitless): 1.0 for fixed-fixed (double bending) type loading, and 0.6 for cantilever (single bending) type loading
- γ_F = numerical coefficient specified according to type of masonry and type of grouting (unitless): 1.0 for FG masonry, and 0.6 for PG masonry

2.3.6 National Earthquake Hazards Reduction Program – NEHRP (1997)

The NEHRP adopted an equation similar to the one proposed by Anderson and Priestley (1992); however, the NEHRP equation replaces the ductility factor with the effect of shear span to depth ratio, $\frac{M}{VL}$, on masonry shear strength. The predicted shear strength is a sum of shear stress from masonry, steel shear reinforcement and applied normal force, given by Eq. (2.14).

$$V_n = 0.083 \left[4.0 - 1.75 \left(\frac{M}{VL} \right) \right] A_n \sqrt{f'_m} + 0.5 A_{sh} f_{yh} \frac{L}{S_h} + 0.25 \sigma_n A_n \quad (2.14)$$

where V_n is limited to

$$V_{n(\max)} = \begin{cases} 0.5 A_n \sqrt{f'_m} & \text{for } \frac{M}{VL} \leq 0.25 \\ 0.33 A_n \sqrt{f'_m} & \text{for } \frac{M}{VL} \geq 1.00 \end{cases} \quad (2.15)$$

with linear interpolation for $0.25 \leq \frac{M}{VL} \leq 1.00$, and $\frac{M}{VL}$ need not be taken greater than 1.0.

2.3.7 UBC (1997)

The Uniform Building Code (UBC) (1997) uses an empirically derived formula for predicting the in-plane shear strength of masonry walls. The nominal shear strength is calculated as the shear strength provided by masonry combined with the shear strength provided by horizontal reinforcement, given by Eq. (2.16).

$$V_n = 0.083 C_d A_n \sqrt{f'_m} + A_{sh} f_{yh} \leq 0.33 A_n \sqrt{f'_m} \quad (2.16)$$

$$C_d = \begin{cases} 2.4 & \text{for } \frac{M}{VL} \leq 0.25 \\ 2.8 - 1.6 \left(\frac{M}{VL} \right) & \text{for } 0.25 < \frac{M}{VL} < 1.0 \\ 1.2 \sqrt{f'_m} & \text{for } \frac{M}{VL} \geq 1.00 \end{cases} \quad (2.17)$$

Unlike most other design codes, UBC (1997) does not account for axial compression. Additionally, UBC (1997) considers 100% yield strength of horizontal reinforcement, whereas the CSA S304.14 (2014) considers 60% of the yield strength and 50% in the TMS402/602 (2016). Similar to the equation given by NEHRP (1997), the shear span to depth ratio, $\frac{M}{VL}$ is bound between 0.25 and 1. No distinction is made between PG and FG walls.

The UBC (1997) has since been superseded by the International Building Code (IBC) in 2000. Nonetheless, the equation presented in UBC (1997) is evaluated in Chapter 3 of this thesis for its performance.

2.3.8 NZS-4230 (2004)

The New Zealand standard for PG masonry shear walls is found in NZS-4230:2004 Section 10.3. It was formulated primarily on the research by Voon and Ingham (2001, 2002). The equation for predicting the shear strength of a wall is based on strength provided by masonry, axial load, and reinforcing steel, and is given by Eq. (2.18).

$$V_n = v_n b_{w,NZS} d = (v_m + v_p + v_s) b_{w,NZS} d \quad (2.18)$$

$$v_n \leq 0.45 \sqrt{f'_m} \quad (2.19)$$

The shear stress provided by masonry, v_m , is given by Eq. (2.20).

$$v_m = (C_1 + C_2) \cdot 0.2k \sqrt{f'_m} \quad (2.20)$$

The coefficient C_1 , given by Eq. (2.21) accounts for the dowel action of vertical reinforcement.

$$C_1 = 33 \rho_v \frac{f_y}{300} \quad (2.21)$$

The coefficient C_2 , given by Eq. (2.22) accounts for the shear span ratio, $\frac{M}{VL}$.

$$C_2 = \begin{cases} 1.5 & \text{if } \frac{M}{VL} < 0.25 \\ 0.42 \left[4 - 1.75 \frac{M}{VL} \right] & \text{if } 0.25 \leq \frac{M}{VL} \leq 1 \\ 1 & \text{if } \frac{M}{VL} > 1 \end{cases} \quad (2.22)$$

The shear stress provided by the axial compression stress, v_p , is given by Eq. (2.23).

$$v_p = 0.9 \frac{N^*}{b_w N_Z S d} \tan \alpha \leq 0.1 f'_m \quad (2.23)$$

The effect of axial compression is dependent on the angle α , which is based on the theoretical location of the compression strut. The compression strut location will vary depending on whether single bending or double bending boundary conditions exist, as shown in Fig. 2.16.

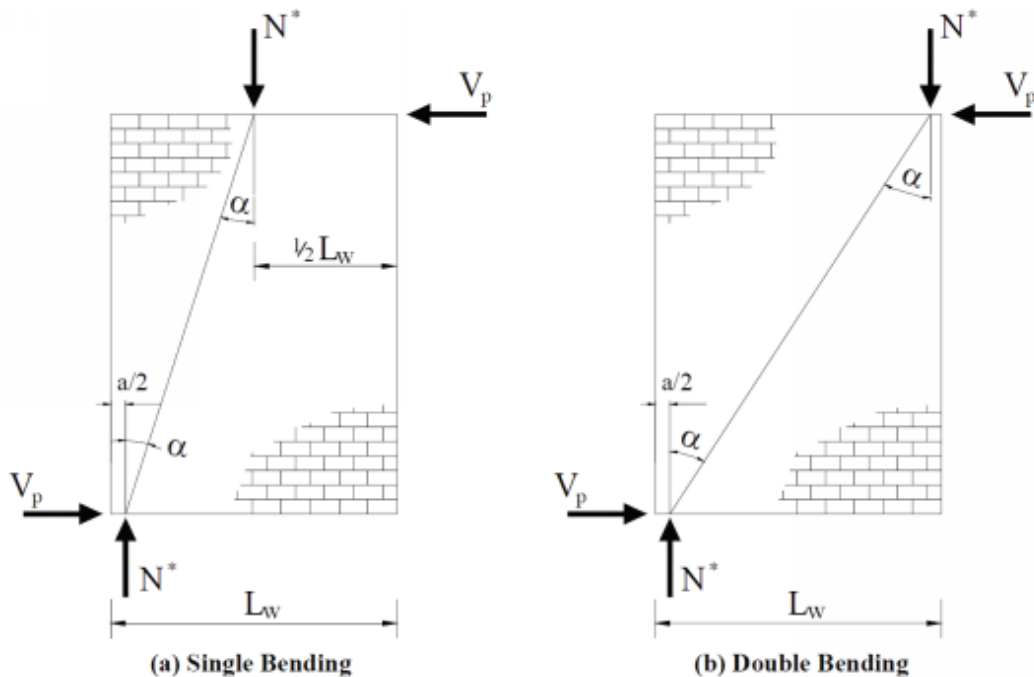


Figure 2.16 – Contribution of axial load to wall shear strength by (Voon 2007)

The shear stress provided by the shear reinforcement, v_s , is given by Eq. (2.24).

$$v_s = C_3 \frac{A_h f_{yh}}{b_{w,NZS} s_h} \quad (2.24)$$

The notation used in Equations (2.18) to (2.24) is as follows:

- $b_{w,NZS}$ = effective width of the wall, defined by NZS-4230 (see Fig. 2.17)
- $= t - b_f$
- k = ductility reduction factor (unitless)
- N^* = factored axial load on wall, no greater than $0.1 \cdot f'_m A_g$, limited to prevent brittle shear failure (N)
- α = angle to account for effects of double bending in walls; constant determined from experimental testing for the stiffness degradation (see Fig. 2.16)
- $\rho_v = \frac{\sum A_v}{b_{w,NZS} d} = \frac{A_s + A_{ps}}{b_{w,NZS} d}$
- $C_3 = 0.8$ for masonry walls

While codes such as the TMS 402/602 consider the net cross-sectional area as the gross cross-sectional area minus the area of any ungrouted cells, NZS-4230 considers only the face shells as the net cross-sectional area to account for shear flow continuity requirements, as shown in Fig. 2.17.

Further insight regarding the masonry shear equation in the NZS-4230 standard can be found in Voon and Ingham (2007) and Nolph and Elgawady (2012).

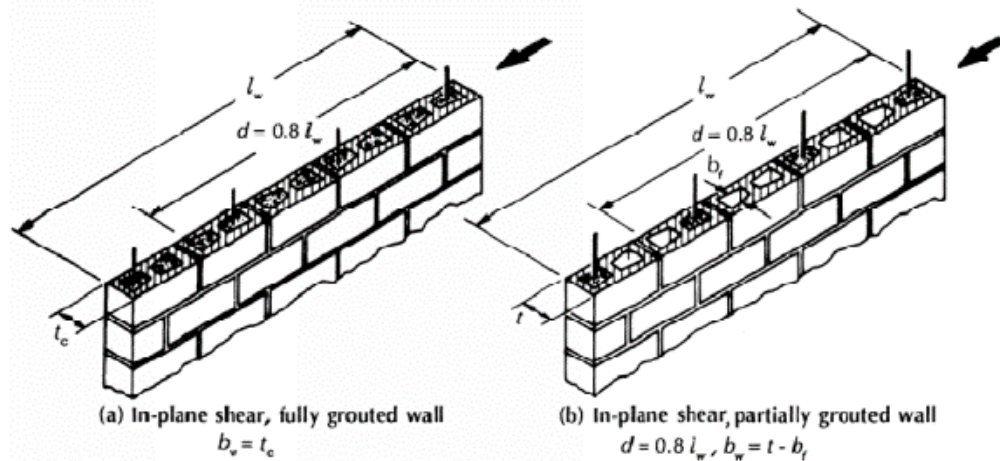


Figure 2.17 – Effective area for shear defined by NZS-4230 (2004)

2.3.9 Eurocode 6 (2005)

Eurocode 6 (Design of masonry structures), also known as the BS EN 1996 or EC6, is part of the set of European Standards developed by the European Committee for Standardization. Eurocode 6 is based on two design philosophies: a “no collapse” requirement and a “damage limitation” requirement (Tomažević 1997).

The equation used to determine the shear strength of reinforced masonry walls is outlined in BS EN 1996-1.1-2005 Section 6.7.2 as a combination of horizontal shear reinforcement and masonry shear strength influenced by compressive axial loading:

$$V_n = v_m t L + 0.9 d_v \frac{A_{sh} f_{yh}}{s_h} \leq 2.0 t L \quad (2.25)$$

$$v_m = \left(0.3 + 0.4 \frac{P_d}{t L} \right) \quad (2.26)$$

Notably, the shear strength of masonry is limited to 0.3 MPa by Eurocode 6. As a result of this arbitrary value, Eurocode 6 predicts overly conservative values of shear strength (El-Dakhkhni et al. 2013). In addition, the use of partially grouted masonry is relatively uncommon in Europe; hence, the Eurocode 6 does not distinguish between FG and PG walls (Oan 2013).

2.3.10 Voon (2007)

The equation developed by Voon (2007) is based on a combination of equations by Shing et al. (1990), Matsumura (1987), Anderson and Priestley (1992), NEHRP (1997), and NZS 4230-1990 (1990). Voon's equation predicts the in-plane shear strength of PG masonry walls as a combination of masonry shear strength, axial compression, and horizontal reinforcement:

$$V_n = V_m + V_p + V_s \quad (2.27)$$

The shear strength provided by masonry, V_m , is given by Eq. (2.28):

$$V_m = k(C_a + C_b)\sqrt{f'_m}b_wd \quad (2.28)$$

where k = ductility reduction factor associated with increasing ductility displacement of the wall (refer to Fig. 2.18)

$$\begin{aligned} C_a &= \text{coefficient to account for vertical reinforcement} \\ &= 0.022\rho_v f_{yv} \end{aligned}$$

$$\begin{aligned} C_b &= \text{coefficient to account for the wall aspect ratio} \\ &= 0.083 \left[4 - 1.75 \frac{M}{VL} \right] \end{aligned}$$

The ductility reduction factor, k , predicts the decrease of shear strength provided by the masonry as the displacement ductility is increased as represented in Fig. 2.18. A similar factor is utilized in the equation proposed by Anderson and Priestley (1992). However, Anderson and Priestley consider a reduction in strength at a displacement ductility of greater than 2, while Voon's ductility reduction factor applies at values of displacement ductility greater than 1.25. In both cases, the ductility reduction factor reduces to zero when the displacement ductility is greater than or equal to 4.

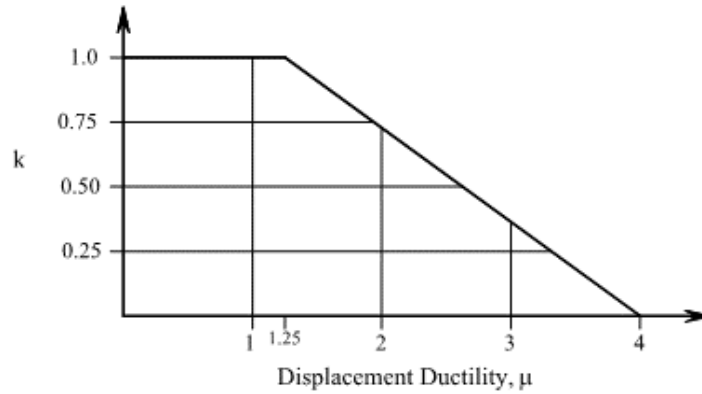


Figure 2.18 – Shear resisting mechanism versus masonry ductility (Voon 2007)

The coefficient to account for the influence of vertical reinforcement on the shear strength provided by masonry, C_a , is also found in the equation by Shing et al. (1990). The coefficient to account for the influence of the shear span to depth ratio, C_b , is adopted from the expression found in NEHRP (1997), where the shear span to depth ratio, $\frac{M}{VL}$, is also bound between 0.25 and 1. However, where the NEHRP equation considers the net area (A_n), Voon's equation uses the total area ($b_w d$) in predicting the shear strength provided by masonry.

The shear strength provided by the axial compression stress, V_p , is given by Eq. (2.29):

$$V_p = 0.9N^* \tan \alpha \quad (2.29)$$

where N^* = factored axial load on wall, no greater than $0.1 \cdot f'_m A_g$, limited to prevent brittle shear failure (N)

α = angle formed between centers of load application and reaction (refer to Fig. 2.16)

This term is a modification of the shear strength prediction of a diagonal compression strut proposed by Priestley et al. (1994), with the addition of the factor 0.9 to ensure a degree of conservatism.

The shear strength provided by the shear reinforcement, V_s , is given by Eq. (2.30):

$$V_s = A_h f_{yh} \frac{d_{eff}}{s_h} \quad (2.30)$$

where d_{eff} = effective depth of the section
 $= L - 2d' - l_{dh}$
 d' = distance between wall edge and outermost wall vertical reinforcing steel
 l_{dh} = development length of shear reinforcement, and shall be taken as $20d_b$ and $35d_b$ for reinforcement with f_y of 300 and 500 MPa, respectively

In this term, Voon predicts a reduced efficiency of horizontal shear reinforcement within the development length at each end of the wall where up to 50% of the reinforcement yield strength can be developed. Therefore, the development length of reinforcing steel, l_{dh} , is considered when calculating the shear strength contribution of shear reinforcement.

Combining V_m , V_p and V_s together results in the following shear strength prediction:

$$V_n = 0.8k(C_a + C_b)A_n\sqrt{f'_m} + 0.9N^* \tan \alpha + A_h f_{yh} \frac{d_{eff}}{s_h} \leq 0.33A_n\sqrt{f'_m} \quad (2.31)$$

The predicted shear strength is limited to a maximum of $0.33A_n\sqrt{f'_m}$ to prevent the proposed equation from being less conservative than the NEHRP (1997) equation.

2.3.11 IMNC (2010)

The IMNC is the Mexican code for masonry structures. The equation provided for calculating the shear resistance of masonry walls. No distinction is made between FG and PG walls. The wall typology that is common in Mexico, however, consists of solid masonry blocks that are bound by reinforced concrete frames (the so-called confined masonry). Hence, the capacity predicted by this code may be better suited to fully grouted walls. The shear resistance is predicted to be the contribution of shear strength of masonry units, axial compression, and horizontal steel reinforcement.

$$V_n = F_R(.5v_m^*A_T + .3P) + F_R\eta\rho_h f_{yh}A_T \leq 1.5F_Rv_m^*A_T \quad (2.32)$$

$$\eta = \begin{cases} .6 & \text{if } \rho_h f_{yh} \leq .6 \\ .2 & \text{if } \rho_h f_{yh} \geq .9 \end{cases} \quad (2.33)$$

where v_m^* = diagonal shear resistance
 $= 0.25\sqrt{f'_m}$
 F_R = resistance factor ($F_R = 0.7$)
 A_T = total cross-sectional area of the wall
 η = efficiency factor for horizontal reinforcement

Limited information has been retrieved in English regarding the formula provided by the IMNC. Nonetheless, the equation presented in is evaluated in Chapter 3 of this thesis for its performance.

2.3.12 CSA-S304.14 (2014)

CSA-S304 is the Canadian code for masonry structures. The equation provided for calculating the shear resistance of PG masonry shear walls is described in CSA-S304.14 Section 10.10.2.1 and predicts the in-plane shear strength of partially grouted masonry walls as a combination of masonry shear strength, axial compression, and horizontal reinforcement given by Eq. (2.34).

$$V_n = (v_m b_w d_v + 0.25P_d)\gamma_g + \left(0.6A_{sh}f_{yh} \frac{d_v}{s_h}\right) \leq 0.4\sqrt{f'_m}b_w d_v \gamma_g \quad (2.34)$$

where γ_g = factor to account for partially grouted walls when calculating shear resistance
 $= \frac{A_e}{A_g}$, but not greater than 0.5 (refer to Fig. 2.19)

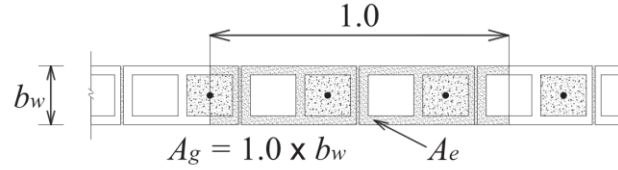


Figure 2.19 – Wall cross-sectional area (Seif EIDin 2016)

The shear strength of masonry, v_m , is given by Eq. (2.35).

$$v_m = 0.16 \left(2 - \frac{M_f}{V_f d_v} \right) \sqrt{f'_m} \quad (2.35)$$

where $\frac{M_f}{V_f d_v}$ = shear span to depth ratio; the value shall not be more than 1 nor less than 0.25 for the concurrent factored moment and factored shear at section under consideration

The equation provided in CSA-S304.14 (2014) is similar to the equation provided by NEHRP (1997). Where the CSA-S304.14 equation considers 60% of the yield strength of the horizontal reinforcement, only 50% is considered in NEHRP. The $\sqrt{f'_m}$ term is bound between $0.16\sqrt{f'_m}$ and $0.28\sqrt{f'_m}$ corresponding to the limits of the shear span to depth ratio, $\frac{M_f}{V_f d_v}$, between 0.25 and 1. CSA-S304.14 also limits the spacing of horizontal reinforcement to a maximum of 2400 mm.

2.3.13 Dillon (2015)

In an statistical analysis of data collected for both FG and PG walls, Dillon (2015) determined best-fit parameters to perform a stepwise regression to select the best parameters for developing a unified model for predicting the shear strength of both FG and PG masonry walls. In analyzing the performance of several models, Dillon found that most existing models predicting masonry wall shear strength was underfitted (i.e. models with non-optimum values for parameter coefficients and/or omit parameters that contribute to shear strength, such as vertical reinforcement).

Using a multivariate linear regression of parameters identified using stepwise regression, Dillon found that boundary vertical reinforcement does not contribute to the shear strength of PG walls, and only confinement (interior) vertical reinforcement should be considered. Dillon also suggested that horizontal reinforcement and confinement (interior) vertical reinforcement are equally effective in contributing to shear strength by resisting crack openings. The model proposed by Dillon using optimized the numerical coefficients for the contribution of masonry units, axial compression, confinement (interior) vertical reinforcement and shear reinforcement is given by Eq. (2.36).

$$v_n = 0.083 \left(1.1 + 0.9 \frac{V S_{gh}}{M} \right) \sqrt{f'_m} + 0.15 \sigma_o + 0.12 [\rho_c f_{yc} + \rho_h f_{yh}] \quad (2.36)$$

where ρ_c = confinement reinforcement (interior vertical reinforcement) ratio
 f_{yc} = tensile strength of confinement reinforcement

2.3.14 TMS 402/602 (2016)

TMS 402/602 is the American code for masonry structures, formerly known as ACI 530, and provides the equation for calculating the allowable shear stress of PG masonry shear walls in Section 8.3.5.1.2. The TMS 402/602 predicts the allowable shear strength as a combination of the strength of masonry, axial compression, and horizontal reinforcement, given by Eq. (2.37).

$$V_n = \left\{ 0.083 \left[\left(4.0 - 1.75 \left(\frac{M_f}{V_f d_v} \right) \right) \sqrt{f'_m} \right] + 0.25 \sigma_n + 0.5 \left(\frac{A_{sh} f_{yh} d_v}{A_{nv} s_h} \right) \right\} A_n \gamma_g, \quad (2.37)$$

where $\gamma_{g,US} = 0.75$ for partially grouted shear walls and 1.0 otherwise

where V_n is limited to

$$V_{n(\max)} = \begin{cases} 0.5\gamma_{g,US}A_n\sqrt{f'_m} & \text{for } \frac{M}{VL} \leq 0.25 \\ \left(0.56 - 0.22\frac{M}{VL}\right)A_n\sqrt{f'_m} & \text{for } 0.25 < \frac{M}{VL} < 1.0 \\ 0.33\gamma_{g,US}A_n\sqrt{f'_m} & \text{for } \frac{M}{VL} \geq 1.00 \end{cases} \quad (2.38)$$

Similar to NEHRP (1997), only 50% of the yield strength of the horizontal reinforcement is considered, compared with 60% considered by the CSA S304.14 (2014). Notably, the TMS 402/602 partial grouting factor, denoted as $\gamma_{g,US}$ in this thesis, is not equivalent to the CSA S304 partial grouting factor, γ_g . Instead, the net shear area, A_{nv} , used in TMS 402/602 is analogous to γ_g in CSA S304.14 (2014), the commentary in TMS 402/602 (2016) describes “the grouted shear wall factor, $[\gamma_{g,US}]$, [as an additional factor] used to compensate for [the] reduced capacity [of PG walls] until methods can be developed to more accurately predict the performance of these elements.”

2.3.15 Summary of Design Expressions

Table 2.2 – In-plane shear strength equations for PG walls

Code / Author	Equation Reference	Shear Strength Equation			
		Masonry (V_m)	Axial Stress (V_p)	Horizontal Steel (V_s)	Vertical Steel
Matsumura (1987)	(2.4)	$\left\{ 0.875 \cdot k_u k_p \left(\frac{0.76}{\frac{H}{d} + 0.7} + 0.012 \right) \sqrt{f'_m(g)} \right\} (b_w d)$	$0.175 \sigma (b_w d)$	$\left(0.1575 \cdot \gamma \delta \sqrt{\rho_h f_{yh} f'_m} \right) (b_w d)$	-
AIJ (1987)	(2.6)	$0.0464 \rho_{te}^{0.23} \frac{f'_m + 17.7}{\frac{M}{VL} + 0.12}$	$0.0875 \sigma_o$	$0.740 \sqrt{\rho_h f_{yh}}$	-
Shing et al. (1990)	(2.8)	$0.0217 \sigma_n A_n \sqrt{f'_m}$		$\left(\frac{L - 2d'}{s_h} \right) A_{sh} f_{yh}$	$(0.166 + 0.0217 \rho_v f_{yv}) A_n \sqrt{f'_m}$
Anderson and Priestley (1992)	(2.9)	$C_{ap} A_n k \sqrt{f'_m}$	$0.25 \sigma_n A_n$	$0.5 A_{sh} f_{yh} \frac{d}{s_h}$	-
Fattal (1993)	(2.10)	$k_o k_u \left[\left(\frac{0.5}{\left(\frac{H}{L} \right) + 0.8} \right) + 0.18 \right] \sqrt{f'_m f_{yv}} \cdot (\rho_v)^{0.7} (b_w d)$	$k_o \cdot 0.012 f'_m + 0.20 \sigma_n$	$k_o \cdot 0.011 \gamma_F \delta_F f_{yh} (\rho_h)^{0.31}$	-
NEHRP (1997)	(2.14)	$0.083 \left[4.0 - 1.75 \left(\frac{M_f}{V_f L} \right) \right] A_n \sqrt{f'_m}$	$0.25 \sigma_n A_n$	$0.5 A_{sh} f_{yh} \frac{L}{s_h}$	-
UBC (1997)	(2.16)	$0.083 \left[2.8 - 1.6 \left(\frac{M_f}{V_f d_v} \right) \right]$	$A_n \sqrt{f'_m}$	$A_{sh} f_{yh}$	-

Code / Author	Equation Reference	Shear Strength Equation			
		Masonry (V_m)	Axial Stress (V_p)	Horizontal Steel (V_s)	Vertical Steel
NZS-4230 (2004)	(2.18)	$[(C_2) \cdot 0.2k\sqrt{f'_m}]b_{w,NZS}d$	$0.9N^* \tan \alpha$	$\left(C_3 \frac{A_v f_y}{b_w s_h}\right)b_{w,NZS}d$	$[(C_1) \cdot 0.2k\sqrt{f'_m}]b_{w,NZS}d$
Eurocode 6 (2005)	(2.25)	$0.3b_w L + 0.4P_d$	-	$0.9A_{sh}f_{yh} \frac{d_v}{s_h}$	-
Voon (2007)	(2.27)	$k \left(0.083 \left[4 - 1.75 \frac{M}{VL}\right]\right) \sqrt{f'_m} b_w d$	$0.9N^* \tan \alpha$	$A_h f_{yh} \frac{d_{eff}}{s_h}$	$k(0.022\rho_v f_{yv})\sqrt{f'_m} b_w d$
IMNC (2010)	(2.32)	$F_R(0.5v_m A_T)$	$F_R(0.3P)$	$F_r \eta \rho_h f_{yh} A_T$	-
CSA-S304.14 (2014)	(2.34)	$\left[0.16 \left(2 - \frac{M_f}{V_f d_v}\right) \sqrt{f'_m} b_w d_v\right] \gamma_g$	$0.25P_d \gamma_g$	$0.6A_{sh}f_{yh} \frac{d_v}{s_h}$	-
Dillon (2015)	(2.36)	$0.083 \left(1.1 + 0.9 \frac{V S_{gh}}{M}\right) \sqrt{f'_m} A_{nv}$	$0.15P$	$0.12 \left(\frac{A_h f_{yh}}{s_h} + \frac{A_j f_{yj}}{s_j}\right) h_g$	$0.12 \left(\frac{A_c f_{yc}}{s_c}\right) l_w$
TMS 402/602 (2016)	(2.37)	$0.083 \left[\left(4.0 - 1.75 \left(\frac{M_f}{V_f d_v}\right)\right) \sqrt{f'_m}\right] A_n \gamma_{g,US}$	$0.25\sigma_n A_n \gamma_{g,US}$	$0.5 \left(\frac{A_{sh} f_{yh} d_v}{A_{nv} s_h}\right) A_n \gamma_{g,US}$	-

3 DATASET ASSEMBLY

3.1 Introduction

Prior to performing a regression analysis to investigate the influence of various parameters on the behaviour of PG walls, a dataset must first be assembled. However, given that experimental research programmes are often expensive and time-consuming, no single experimental study for PG walls contains enough information to build and validate a constitutive model for the shear strength and behaviour of these structural elements (Dillon and Fonseca 2014a). Therefore, it becomes necessary to assemble a dataset from multiple experimental studies.

Meta-analysis is defined as “a quantitative, formal, epidemiological study design used to systematically assess previous research studies to derive conclusions about that body of research” (Haidich 2010). It can be considered “a form of survey research, in which research reports, rather than people, are surveyed” (Lipsey and Wilson 2001).

In this study, meta-analysis is performed in three parts:

- 1) Dataset assembly: compiling a dataset of PG walls from experimental studies;
- 2) Data scrutinization: using a set of selection/inclusion criteria to determine which parts PG walls are to be included or excluded from analysis;
- 3) Data synthesization: converting data to minimize variation between studies and synthesizing or predicting missing information. The purpose of data synthesization is to eliminate inconsistencies where possible.

Data synthesization is necessary due to differences in testing methodology, such as boundary conditions, strain rate, loading patterns, and size effects, there is a lack of consistency in reporting the shear strength of PG walls (Dillon and Fonseca 2014a). Gaps of information also exist in some studies, such as testing apparatus details, compressive strength of grouted and/or ungrouted masonry prisms, reinforcing steel yield strength, or reinforcement spacings.

Several authors such as Oan (2013) and Hassanli et al. (2014) compiled experimental datasets to evaluate the performance of existing design equations to predict the in-plane shear strength of PG masonry walls. Dillon (2015) compiled a dataset of FG and PG masonry walls to perform meta-analysis. Aguilar (2013) compiled a dataset of PG wall specimens primarily for artificial neural network analysis. While Aguilar (2013), Oan (2013), Hassanli et al. (2014) reported to have used only engineering judgement to assume values for missing parameters, Dillon (2015) used statistical analysis to achieve the same goal.

The following section provides brief summaries of each experimental study that has been used to compile the PG masonry wall dataset used in this study, highlighting the methodology, setup, design details and material properties used in each experimental programme. It is presented in chronological order – such that the progression of research throughout the past several decades is documented. Then, a description of the twofold dataset assembly process of data scrutinization and data synthesization used in this study is discussed. A summary of the dataset is presented, along with subsets of the complete dataset that will be used for neural network analysis in Chapter 4.

The performance of each existing design expression discussed in Chapter 2 is investigated at the end of this chapter, providing a benchmark of existing models for comparison with neural network based models in Chapter 4.

3.2 Experimental Studies on the Behaviour of Partially Grouted Masonry Shear Walls

3.2.1 Scrivener (1967)

Total Number of PG Walls in Study: 12			
Loading Type:	Monotonic	f'_m :	<i>Varied</i> (12.0-13.6)
Loading Rate:	Quasi-Static	A_{net}/A_{gross} :	<i>Varied</i> (0.36-0.61)
Support Type:	Cantilever	Axial Stress:	<i>Varied</i> (0.60-2.40)
Height:	2642 mm	Flexural Reinf.:	<i>Varied*</i>
Length:	2438 mm	Vertical (Interior) Reinf.:	<i>Varied*</i>
Thickness:	143 mm	Bond Beam Reinf.:	<i>Varied*</i>
H/L:	1.08	Joint Reinf.:	None*
<i>*Varied reinforcement indicates varied bar sizes used for reinforcement</i>			

Scrivener tested a total of 12 PG masonry shear walls to investigate the effect of reinforcement ratio, relative effectiveness of horizontal and vertical reinforcing, and distribution of vertical reinforcement. The cantilever racking test used in this study is illustrated in Fig. 3.1.

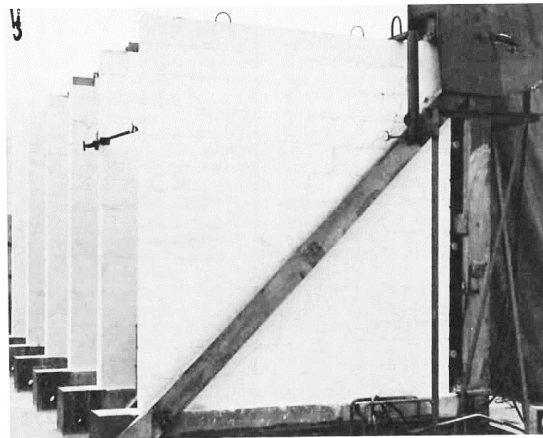


Figure 3.1 – Test setup by Scrivener (1967)

Scrivener concluded that both horizontal and vertical reinforcement provided PG shear walls with more lateral resistance after cracking. Furthermore, evenly distributed reinforcement patterns were found to reduce the severity of cracking in walls. However, a limit to the influence of increased reinforcement ratio was observed; a combined

(horizontal and vertical) reinforcement ratio of greater than 0.3% resulted only in a marginal increase in the ultimate shear strength of PG walls.

3.2.2 Meli et al. (1968)

Total Number of PG Walls in Study: 16			
Loading Type:	Reverse Cyclic	f'_m :	9.66 MPa
Loading Rate:	Quasi-Static	A_{net}/A_{gross} :	<i>Varied</i> (0.68-0.72)
Support Type:	Cantilever	Axial Stress:	<i>Varied</i> (0-0.41)
Height:	2650 mm	Flexural Reinf.:	<i>Varied</i>
Length:	3200 mm	Vertical (Interior) Reinf.:	<i>Varied</i>
Thickness:	150 mm	Bond Beam Reinf.:	None
H/L:	0.83	Joint Reinf.:	<i>Varied</i>

Meli et al. tested a total of 18 PG shear walls. Sixteen walls were built with concrete masonry units and 2 of which were built with hollow clay bricks. Eight specimens were subject to diagonal compression tests, while the other 8 specimens were cantilevered and subject to lateral loading. This experimental study investigated the effect of vertical reinforcement ratios and axial stresses on the behaviour of PG shear walls. The cantilever test configuration used in this study is illustrated in Fig. 3.2.

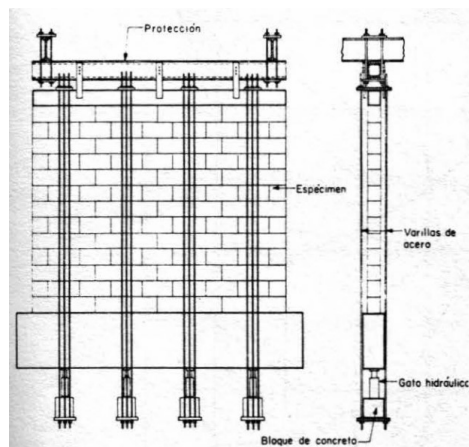


Figure 3.2 – Test setup by Meli et al. (1968)

Meli et al. observed that the cracking strength of walls was independent of both horizontal and vertical reinforcement, while increased axial stresses led to higher cracking strength and improved the behaviour of walls subject to reverse cyclic loading. The amount of of

vertical reinforcement was found to have a negligible influence on the shear strength of PG walls. Additionally, Meli et al. proposed an empirical equation predicting the flexural and shear capacity of masonry walls based on this experimental study.

3.2.3 Meli and Salgado (1969)

Total Number of PG Walls in Study: 11			
Loading Type:	Monotonic	f_m :	<i>Varied</i> (9.66-13.5)
Loading Rate:	Quasi-Static	A_{net}/A_{gross} :	<i>Varied</i> (0.47-0.60)
Support Type:	Cantilever	Axial Stress:	<i>Varied</i> (0-0.98)
Height:	2000 mm	Flexural Reinf.:	<i>Varied</i>
Length:	2000 mm	Vertical (Interior) Reinf.:	<i>Varied</i>
Thickness:	150 mm	Bond Beam Reinf.:	None
H/L:	1.0	Joint Reinf.:	None

Meli and Salgado tested a total of 46 reinforced masonry walls, 11 of which were PG walls subject to monotonic loading. The purpose of this experimental study was to investigate the effect of axial stress and quantity of interior vertical reinforcement on the behaviour of masonry walls subject to lateral loading. No horizontal reinforcement was used in any specimens. The cantilever test configuration used in this study is illustrated in Fig. 3.3.

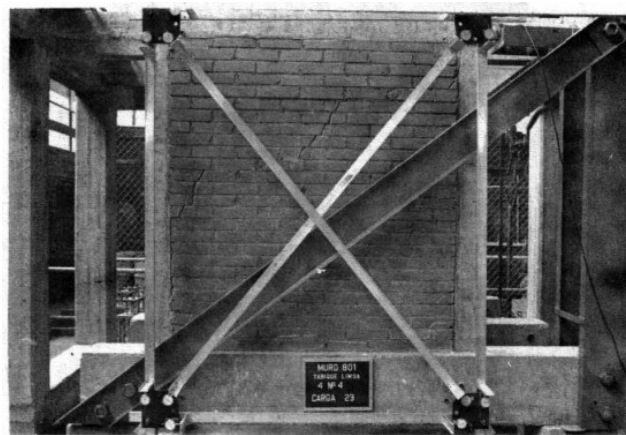


Figure 3.3 – Test setup by Meli and Salgado (1969)

Meli and Salgado observed that the amount of vertical reinforcement influenced the failure mode of masonry walls; walls with more interior reinforcement tended to fail in

diagonal shear, whereas walls with less interior reinforcement were more likely to fail in flexure. The cracking capacity was not influenced by the amount of reinforcement. Axial stresses up to 20% of wall compressive strength was observed to increase the shear strength by a factor of half the ratio of applied axial stresses to wall compressive strength.

3.2.4 Mayes et al. (1976)

Total Number of PG Walls in Study: 2			
Loading Type:	Reverse Cyclic	f'_m :	16.7 MPa
Loading Rate:	Quasi-Static	A_{net}/A_{gross} :	0.72
Support Type:	Double Curvature	Axial Stress:	1.72 MPa
Height:	1626 mm	Flexural Reinf.:	2#6
Length:	813 mm	Vertical (Interior) Reinf.:	None
Thickness:	143 mm	Bond Beam Reinf.:	None
H/L:	2.0	Joint Reinf.:	None

Mayes et al. built 8 pairs of masonry double-pier specimens and a single unreinforced specimen to investigate the effect of axial stress, loading rate, quantity and distribution of reinforcement, and effect of partial grouting on the lateral behaviour of masonry piers. However, only one pair of identical double-piers was partially-grouted. The double-curvature pier test configuration used in this study is intended to replicate the boundary conditions of piers in real structures, illustrated in Fig. 3.4.

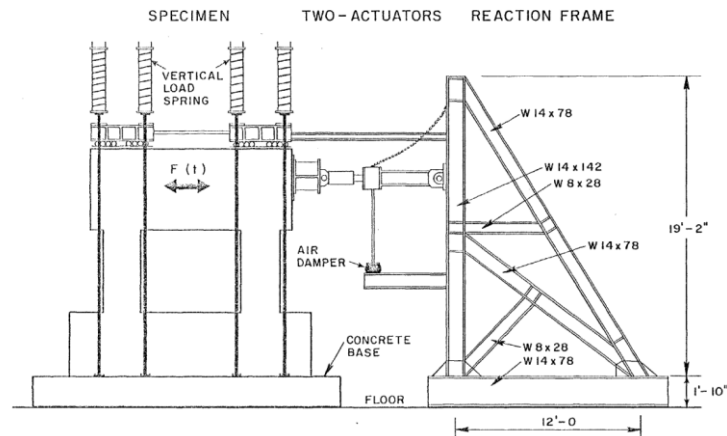


Figure 3.4 - Test setup by Mayes et al. (1976a)

Mayes et al. compared the behaviour of PG masonry piers with FG masonry piers, and noted that the net ultimate shear strength is similar. The PG masonry piers were also found to have less load degradation in comparison to its FG counterparts. The remaining conclusions from this experimental study are drawn mostly on FG masonry piers, and thus are not summarized here.

3.2.5 Chen et al. (1978)

Total Number of PG Walls in Study: 4			
Loading Type:	Reverse Cyclic	f'_m :	11.8 MPa
Loading Rate:	Dynamic	A_{net}/A_{gross} :	0.60
Support Type:	Double Curvature	Axial Stress:	<i>Varied</i> (0.55-0.80)
Height:	1422 mm	Flexural Reinf.:	<i>Varied</i>
Length:	1219 mm	Vertical (Interior) Reinf.:	None
Thickness:	193 mm	Bond Beam Reinf.:	<i>Varied</i>
H/L:	1.17	Joint Reinf.:	None

Chen et al. tested a total of 31 concrete block masonry piers, 4 of which were partially-grouted. The objective of this study was to investigate the effect of reinforcement ratio and partial grouting on the performance of masonry piers. Gr. 40 and 60 steels were used for vertical and horizontal reinforcement. The double-curvature test configuration used in this study is illustrated in Fig. 3.5.

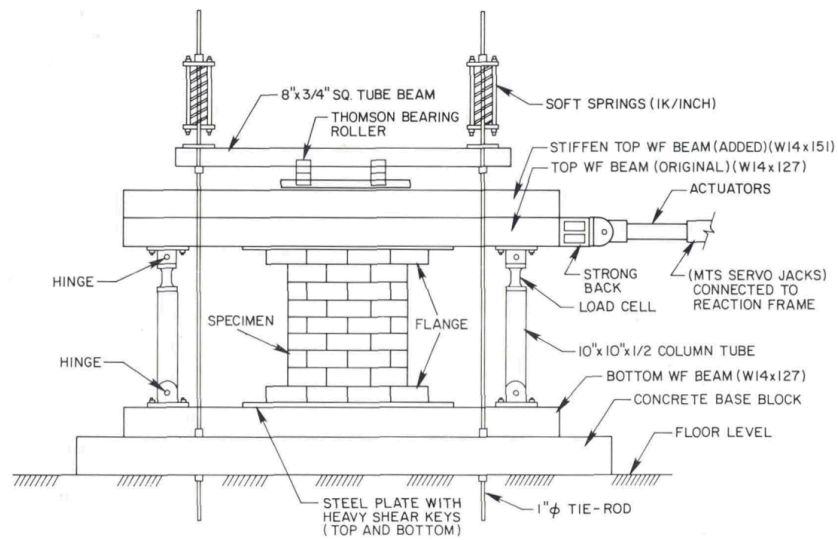


Figure 3.5 – Test setup by Chen et al. (1978)

Chen et al. observed a 22% increase in shear strength calculated using net area of FG piers compared with PG piers. However, the hysteresis curves suggested similar stiffness degradation behaviour between of FG and PG piers. It was also concluded that the amount of vertical reinforcement did not significantly increase the shear strength of masonry piers.

3.2.6 Thurston and Hutchinson (1982)

Total Number of PG Walls in Study: 3			
Loading Type:	Reverse Cyclic	f'_m :	14.2 MPa
Loading Rate:	Quasi-Static	A_{net}/A_{gross} :	0.71
Support Type:	Double Curvature	Axial Stress:	0 MPa
Height:	2400 mm	Flexural Reinf.:	<i>Varied</i>
Length:	1600 mm	Vertical (Interior) Reinf.:	<i>Varied</i>
Thickness:	140 mm	Bond Beam Reinf.:	<i>Varied</i>
H/L:	1.5	Joint Reinf.:	None

Thurston and Hutchinson tested a total of 9 masonry shear walls, 3 of which were PG walls. The objective of this study was to investigate the effect of axial loading and distribution of reinforcement on the performance of shear walls under inelastic loading conditions. Notably, no axial stresses were applied to any of the PG wall specimens. The double-curvature test configuration used in this study is illustrated in Fig. 3.6.

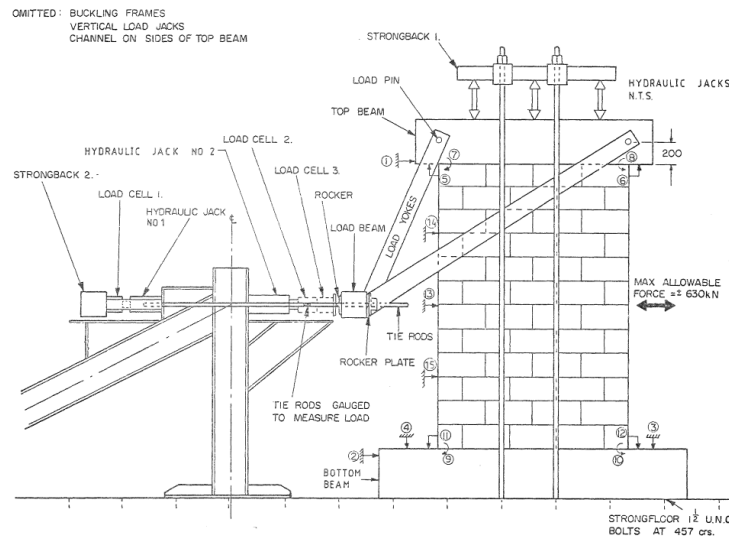


Figure 3.6 – Test setup by Thurston and Hutchinson (1982)

Thurston and Hutchinson observed better inelastic performance (characterized by gradual strength degradation) in both PG and FG shear walls reinforced with smaller bars and closer spacing compared with walls with the same reinforcement ratio but using larger bars spaced further apart. It was also concluded that PG walls exhibited similar ductility but lower stiffness and strength compared with FG walls.

3.2.7 Matsumura (1987)

Total Number of PG Walls in Study: 29			
Loading Type:	Reverse Cyclic	f'_m :	<i>Varied</i>
Loading Rate:	Quasi-Static	A_{net}/A_{gross} :	0.71
Support Type:	Double Curvature	Axial Stress:	<i>Varied</i> (0-1.47)
Height:	1800 mm	Flexural Reinf.:	<i>Varied</i>
Length:	<i>Varied</i> (920-1720)	Vertical (Interior) Reinf.:	<i>Varied</i>
Thickness:	150 mm	Bond Beam Reinf.:	<i>Varied</i>
H/L:	<i>Varied</i> (1.05-1.96)	Joint Reinf.:	None

Matsumura tested a total of 80 full-scale masonry walls in this study to investigate the influence of vertical and horizontal reinforcement ratio, shear span ratio, axial stress, material strength, and grouting type. Twenty-nine of the specimens were PG concrete block masonry walls. Two test configurations were used by Matsumura: a “wall type” loading, and a “beam type” loading, both designed to provide specimens with double-curvature boundary conditions. The “wall type” loading had specimens subject to horizontal shear loads, whereas the “beam type” loading had specimens laid horizontally and subject to vertical shear loads designed for smaller specimens as supplementary tests. Both configurations are illustrated in Fig. 3.7.

Matsumura observed the following relationships:

- v_n increases approximately in proportion to the square root of masonry compressive strength, $\sqrt{f'_m}$
- $\frac{v_n}{\sqrt{f'_m}}$ increases in relation to the increase of the horizontal reinforcement ratio
- $\frac{v_n}{\sqrt{f'_m}}$ decreases inversely in relation to the increase of shear span ratio, $\frac{M}{Vd}$.

- v_n increases by applying axial stress

Matsumura also concluded that horizontal reinforcement improved the shear strength of FG walls more than PG walls.

Matsumura performed a regression analysis based on his experimental study to formulate an equation to predict the shear strength of masonry walls, as explained in Section 2.3.1.

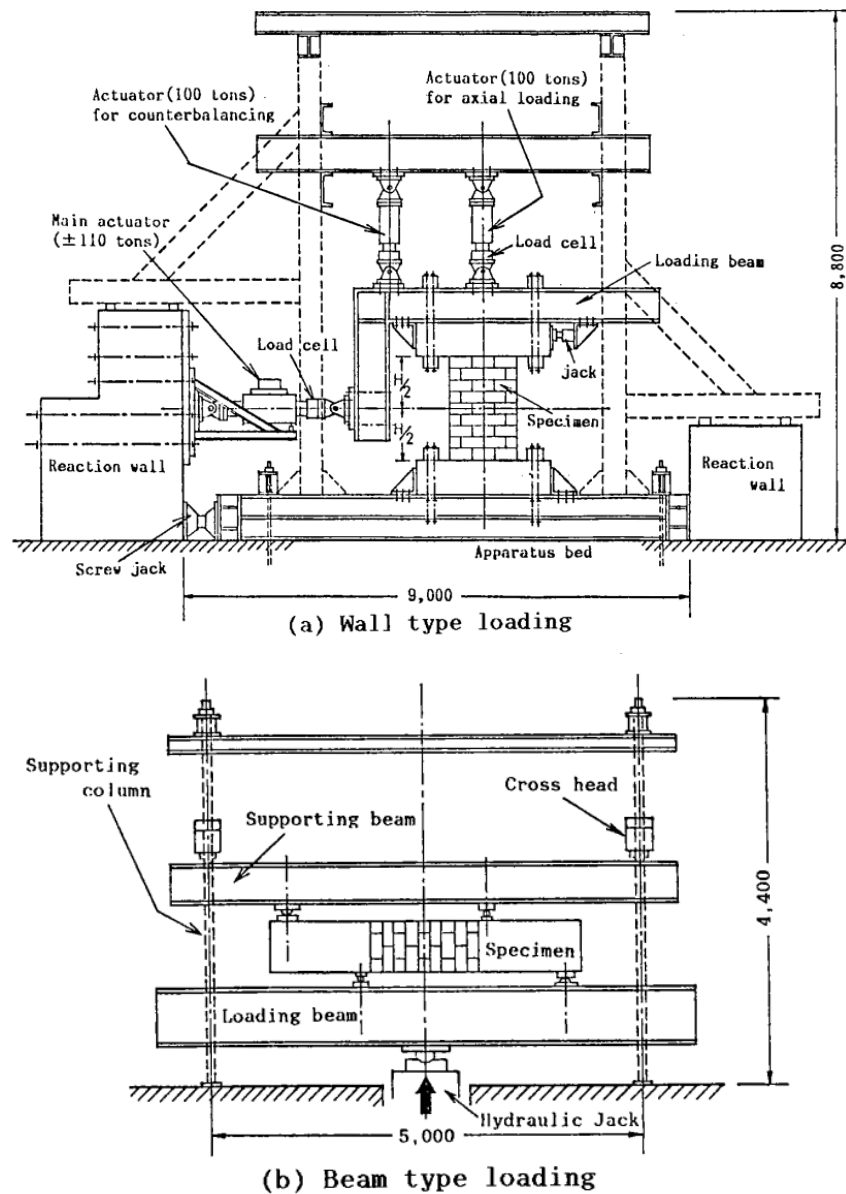


Figure 3.7 – Test setup by Matsumura (1987)

3.2.8 Tomažević and Lutman (1988)

Total Number of PG Walls in Study: 10			
Loading Type:	Reverse Cyclic	f'_m :	<i>Varied</i>
Loading Rate:	Quasi-Static	A_{net}/A_{gross} :	0.60
Support Type:	Cantilever	Axial Stress:	0.98 MPa
Height:	<i>Varied</i> (760-1400)	Flexural Reinf.:	<i>Varied</i>
Length:	610 mm	Vertical (Interior) Reinf.:	None
Thickness:	100 mm	Bond Beam Reinf.:	None
H/L:	<i>Varied</i> (1.25-2.30)	Joint Reinf.:	<i>Varied</i>

Tomažević and Lutman tested two series of 8 1/2-scale concrete block masonry walls each, totalling 16 masonry wall specimens to investigate the effect of flexural and joint reinforcement on the seismic performance of masonry shear walls. Each series contained identical walls with exception to the flexural reinforcement at each end of the walls; the “C” series used (1)10 mm bar as flexural reinforcement ($\rho_v = 0.26\%$), where the “D” series used (2)10 mm bars ($\rho_v = 0.52\%$). Within each series, the joint reinforcement was varied as well as the height-to-length ratio. 10 of 16 masonry walls tested were PG specimens.

Tomažević and Lutman observed that the joint horizontal reinforcement did not engage until diagonal cracking occurred under shear loads, and found that the reinforcement did not yield before each specimen failed. The effectiveness of horizontal reinforcement at shear failure ranged from 41-66% at the ultimate shear load, and 61-83% at maximum displacement/failure load. Nonetheless, it was concluded that wall specimens containing horizontal joint reinforcement improved both shear capacity and ductility under seismic conditions.

3.2.9 Johal and Anderson (1988)

Total Number of PG Walls in Study: 16			
Loading Type:	Reverse Cyclic	f'_m :	<i>Varied</i> (7.56-9.84)
Loading Rate:	Quasi-Static	A_{net}/A_{gross} :	0.64
Support Type:	Double Curvature	Axial Stress:	None
Height:	813 mm	Flexural Reinf.:	#5
Length:	813 mm	Vertical (Interior) Reinf.:	None
Thickness:	200 mm	Bond Beam Reinf.:	None
H/L:	1.0	Joint Reinf.:	None

Johal and Anderson tested a total of 14 specimens to investigate the effect of different mortar types on the behaviour of PG shear walls under seismic loading. Four different mortars were used: masonry cement (“Type M”), blended Portland cement and lime (“Type M”), masonry cement (“Type S”), and blended Portland cement and lime (“Type S”). The double-curvature test configuration used in this study is illustrated in Fig. 3.8.

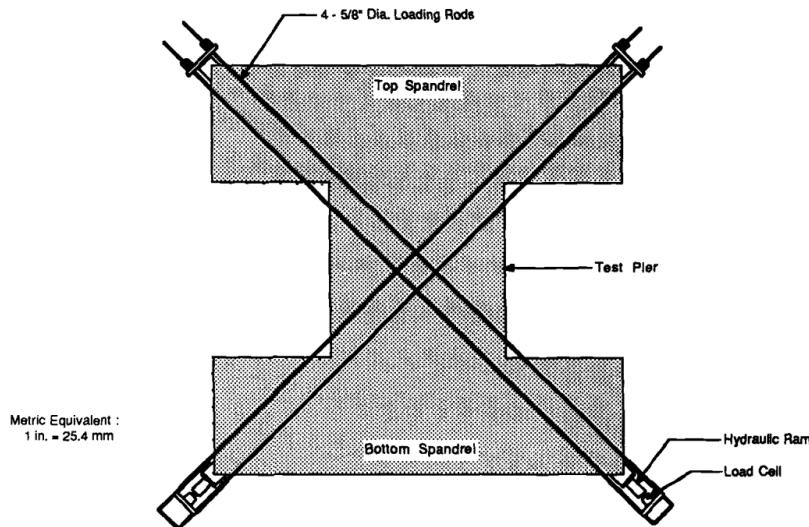


Figure 3.8 – Test setup by Johal and Anderson (1988)

Johal and Anderson concluded that PG masonry walls constructed with masonry cement-based mortars performed better than PG walls constructed with Portland cement-based mortars. The use of “Type M” or “Type S” mortars did not exhibit a significant difference in shear strength.

3.2.10 Yancey and Scribner (1989)

Total Number of PG Walls in Study: 13			
Loading Type:	Reverse Cyclic	f'_m :	10.1 MPa
Loading Rate:	Phased Sequential	A_{net}/A_{gross} :	0.54
Support Type:	Double Curvature	Axial Stress:	0.74 MPa
Height:	1422 mm	Flexural Reinf.:	None
Length:	1219 mm	Vertical (Interior) Reinf.:	None
Thickness:	194 mm	Bond Beam Reinf.:	<i>Varied</i>
H/L:	1.16	Joint Reinf.:	<i>Varied</i>

Yancey and Scribner tested a total of 13 PG walls to investigate the effect of varying the amount and distribution of joint and bond beam horizontal reinforcement on the behaviour of PG shear walls. 10 of the 13 walls exhibited shear failure, with the remaining 3 failing in flexure due to the large aspect ratio of 2.17. One specimen remained unreinforced, two specimens were reinforced exclusively with joint reinforcement, five specimens were reinforced exclusively with one or two bond beams, and the remaining two specimens were reinforced with both joint and bond beam reinforcements. The double-curvature test configuration used in this study is illustrated in Fig. 3.9.

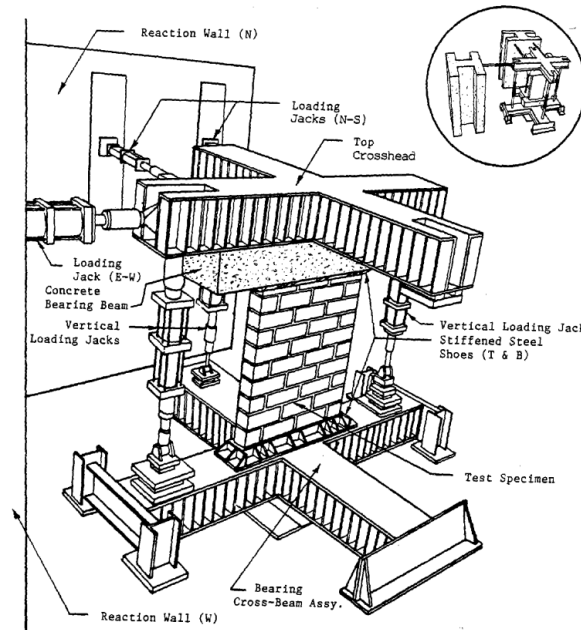
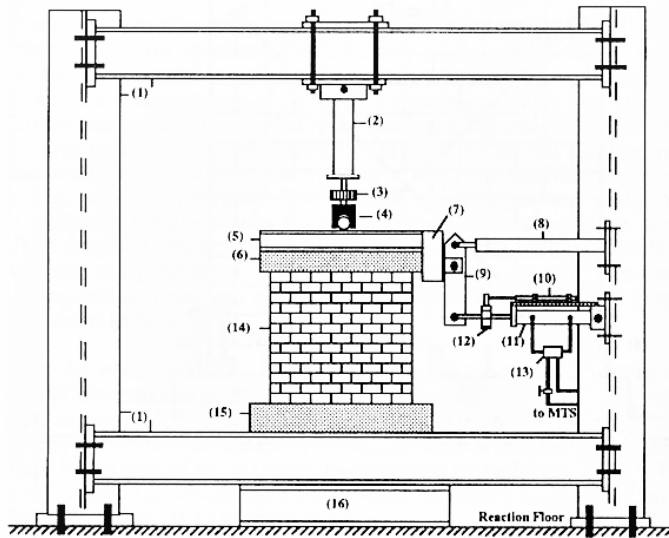


Figure 3.9 – Test setup by Yancey and Scribner (1989)

Yancey and Scribner observed that PG shear walls with joint reinforcement at every course failed at similar loads as those with joint reinforcement at every second course. It was also observed that PG shear walls reinforced with both joint reinforcement and a bond beam at mid-height exhibited higher drift capacities. Overall, Yancey and Scribner concluded that an increasing the horizontal reinforcement increased the shear capacity of PG walls, though the relationship was not linear.

3.2.11 Ghanem et al. (1992, 1993)

Ghanem et al. tested a total of 14 1/3-scale PG walls in this study to investigate the effect of five parameters: axial stress, block strength, lateral load, and the amount and distribution of vertical and horizontal steel. The cantilever test configuration used in this study is illustrated in Fig. 3.10. Two papers (Ghanem et al. 1992, 1993) were published from the total study, each presenting a set of three walls to discuss the effect of different parameters.



1-Testing Frame, 2-Jack for Axial Load, 3-Load Cell, 4-Roller Allowing Horizontal Displacement of the Wall, 5-Load Distributing Beam, 6-Reinforced Concrete Top Beam, 7-Bracket for Lateral Load, 8-Lateral Support for Lever Arm, 9-Lever Arm (Magnification of Lateral Load), 10-Controlled LVDT, 11-Jack for Lateral Load, 12-Load Cell, 13-Servo-Valve, 14-Shear Wall Specimen, 15-Reinforced Concrete Base Beam, 16-Steel Beam

Figure 3.10 – Test setup by Ghanem et al. (1992, 1993)

Ghanem et al. (1992) presents the results of three walls investigating the effect of vertical and horizontal steel reinforcement distribution on the behaviour of PG walls. Ghanem et al. (1993) presents the results of three walls investigating the effect of axial stress on the behaviour of PG walls.

Ghanem et al. (1992)

Total Number of PG Walls in Study: 3			
Loading Type:	Monotonic	f'_m :	15.37 MPa
Loading Rate:	Quasi-Static	A_{net}/A_{gross} :	0.54
Support Type:	Cantilever	Axial Stress:	0.69 MPa
Height:	920 mm	Flexural Reinf.:	<i>Varied</i>
Length:	939 mm	Vertical (Interior) Reinf.:	<i>Varied</i>
Thickness:	48 mm	Bond Beam Reinf.:	<i>Varied</i>
H/L:	0.98	Joint Reinf.:	None

One of the three walls discussed in Ghanem et al. (1992) failed in flexure and was not included in the PG shear wall dataset. Ghanem et al. (1992) concluded that increasing the distribution of reinforcement increased the shear strength of PG walls. Additionally, flexural vertical reinforcement (i.e. bars located in the outermost cells), while effective in increasing the flexural strength, did not significantly increase the shear strength.

Ghanem et al. (1993)

Total Number of PG Walls in Study: 3			
Loading Type:	Monotonic	f'_m :	15.37 MPa
Loading Rate:	Quasi-Static	A_{net}/A_{gross} :	0.54
Support Type:	Cantilever	Axial Stress:	<i>Varied</i> (0.69-1.38)
Height:	940 mm	Flexural Reinf.:	#5/3
Length:	940 mm	Vertical (Interior) Reinf.:	#5/3
Thickness:	48 mm	Bond Beam Reinf.:	(3)#5/3
H/L:	1.00	Joint Reinf.:	None

One of the three walls discussed in Ghanem et al. (1993) failed in flexure and thus was not included in the PG shear wall dataset. The three walls were tested under axial loadings of 0 MPa, 0.69 MPa and 1.38 MPa. Ghanem et al. concluded that higher levels of axial

pre-compression resulted in higher stiffness and strength, as well as a greater tendency to exhibit shear failure in PG walls.

An increased shear cracking strength of PG walls was also attributed to higher axial stresses, largely due to the higher shear load required to exceed the tensile cracking capacity of masonry blocks. Ghanem et al. (1993) recommended that axial stresses on PG walls do not exceed 5% of masonry compressive strength to avoid brittle failure.

3.2.12 Tomažević et al. (1996)

Total Number of PG Walls in Study: 32			
Loading Type:	<i>Varied</i>	f'_m :	5.20 MPa
Loading Rate:	<i>Varied</i>	A_{net}/A_{gross} :	0.43
Support Type:	Cantilever	Axial Stress:	0.67 MPa
Height:	760 mm	Flexural Reinf.:	D10
Length:	1800 mm	Vertical (Interior) Reinf.:	None
Thickness:	100 mm	Bond Beam Reinf.:	None
H/L:	0.42	Joint Reinf.:	6 mm ladder

Tomažević et al. built 16 pairs (total of 32) identical 1/2-scale PG masonry walls and varied the loading type (monotonic, reverse cyclic, phased-sequential, and simulated seismic loading) and loading rate (static, dynamic) to investigate the effect of different loading conditions on the lateral response of masonry walls. The test configuration used in this study was not provided in the original paper. However, Tomažević et al. provided the four displacement time histories used to drive the actuator, illustrated in Fig. 3.11.

Tomažević et al. concluded that the loading type and rate had a significant impact on both the strength and stiffness degradation of PG walls. Dynamically loaded specimens had higher lateral resistances than quasi-statically loaded specimens. Specimens subject to monotonic loading had higher lateral resistances than reverse cyclic loading. The reverse cyclic and phased-sequential cyclic loading were considered to be more representative of actual loading conditions experienced by masonry walls. Additionally, Tomažević et al. observed the horizontal reinforcement had stresses ranging from 30 to

50% of the yield stress at the cracking displacement, and between 55-80% of the yield stress at peak load.

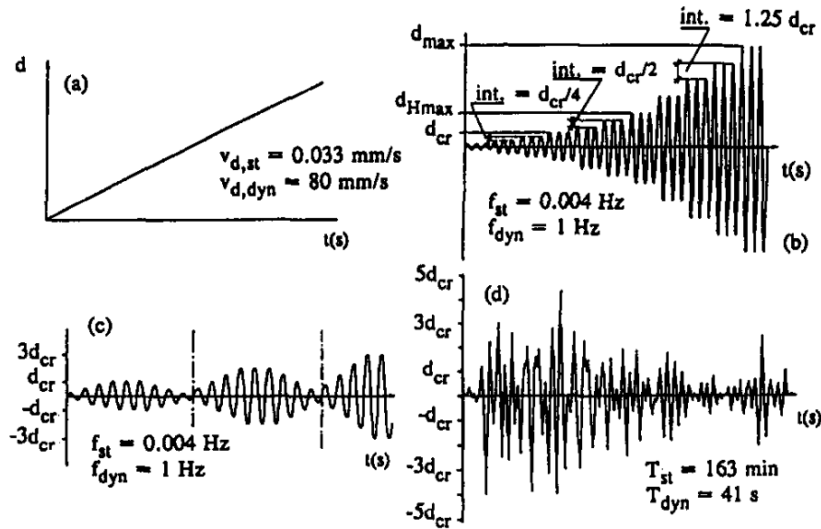


Figure 3.11 – Displacement Time Histories used to Drive Actuator: (a) Monotonic; (b) Reverse Cyclic; (c) Phased-Sequential; (d) Simulated Earthquake Response (Tomazevic and Lutman 1996)

3.2.13 Schultz (1996)

Total Number of PG Walls in Study: 6			
Loading Type:	Phased-Sequential	f'_m :	13.89 MPa
Loading Rate:	Quasi-static	A_{net}/A_{gross} :	<i>Varied</i> (0.44-0.53)
Support Type:	Double curvature	Axial Stress:	0.48 MPa
Height:	1422 mm	Flexural Reinf.:	2#6
Length:	<i>Varied</i> (1422-2845)	Vertical (Interior) Reinf.:	None
Thickness:	195 mm	Bond Beam Reinf.:	<i>Varied</i>
H/L:	<i>Varied</i> (0.5-1.0)	Joint Reinf.:	None

Schultz built 6 full-scale PG masonry walls to investigate the effect of horizontal reinforcement ratio, type of horizontal reinforcement, and height-to-length aspect ratio on the shear strength of PG shear walls. Each wall was vertically reinforced with 2#6 (19 mm) bars in each exterior vertical cell. The horizontal reinforcement ratio was varied by changing the bond beam reinforcement located mid-height using either 2#3 (9.5 mm) bars or 1#4 (13 mm) bar and 1#5 (16 mm) bar ($\rho_h = 0.051\%$ or 0.119% , respectively). The double-curvature test configuration used in this study is illustrated in Fig. 3.12.

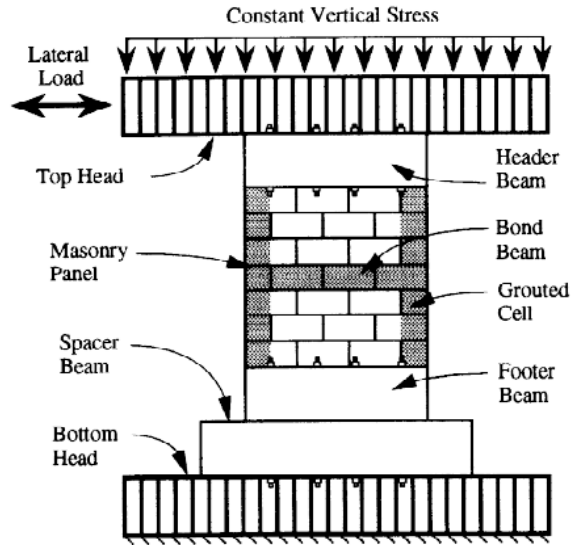


Figure 3.12 – Test setup by Schultz (1996)

Schultz concluded based on this experimental study that a decreased height-to-length aspect ratio increased shear capacity. An increase in bond beam horizontal reinforcement ratio was found to marginally increase shear strength.

3.2.14 Schultz et al. (1998)

Total Number of PG Walls in Study: 6			
Loading Type:	Phased-Sequential	f'_m :	11.78 MPa
Loading Rate:	Quasi-static	A_{net}/A_{gross} :	<i>Varied</i> (0.44-0.53)
Support Type:	Double curvature	Axial Stress:	0.48 MPa
Height:	1422 mm	Flexural Reinf.:	2#6
Length:	<i>Varied</i> (1422-2845)	Vertical (Interior) Reinf.:	None
Thickness:	195 mm	Bond Beam Reinf.:	None
H/L:	<i>Varied</i> (0.5-1.0)	Joint Reinf.:	<i>Varied</i>

Schultz et al. built 6 full-scale PG masonry walls to investigate the effect of horizontal reinforcement ratio, type of horizontal reinforcement, and height-to-length aspect ratio on the shear strength of PG shear walls. Each wall was vertically reinforced with 2#6 bars in each exterior vertical cell. The horizontal reinforcement ratio was varied by using either 9-ga (2.91 mm) ladder joint reinforcement or 5-ga (4.62 mm) ladder joint reinforcement located in all bed joints. The double-curvature test configuration used in this study is illustrated in Fig. 3.13.

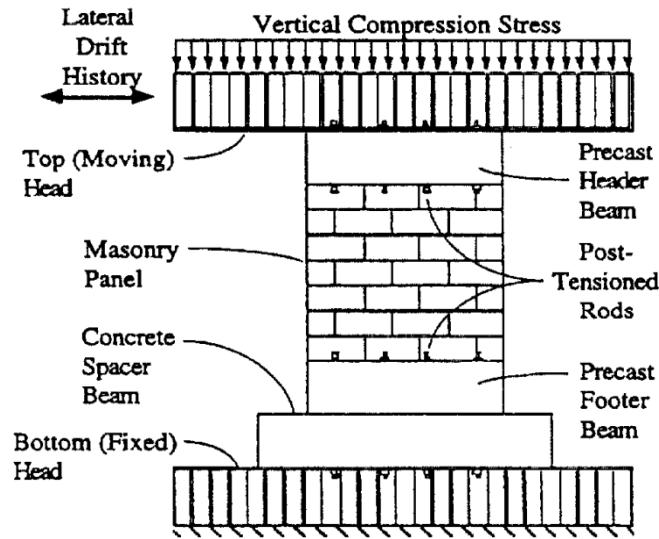


Figure 3.13 – Test setup by Schultz et al. (1998)

Schultz et al. (1998) concluded based on this experimental study that a decreased height-to-length aspect ratio increased the ultimate shear stress. In comparison to the previous study by Schultz (1996), PG walls were observed to have better stability and energy dissipation when joint reinforcement in each bed joint is used instead of a single bond beam located mid-height.

3.2.15 Voon and Ingham (2006) and Voon (2007)

Total Number of PG Walls in Study: 2			
Loading Type:	Reverse Cyclic	f'_m :	17.7 MPa
Loading Rate:	Quasi-static	A_{net}/A_{gross} :	0.74
Support Type:	Cantilever	Axial Stress:	0 MPa
Height:	1800 mm	Flexural Reinf.:	D20
Length:	1800 mm	Vertical (Interior) Reinf.:	<i>Varied</i>
Thickness:	140 mm	Bond Beam Reinf.:	None
H/L:	1.0	Joint Reinf.:	None

Voon and Ingham tested a total of 10 masonry walls, 2 of which were PG walls. The PG walls had no horizontal reinforcement. The vertical reinforcement spacing was varied; while one specimen had a spacing of 400 mm (5 grouted cells), the other specimen had a spacing of 800 mm (3 grouted cells). The objective of Voon and Ingham's study was to

investigate the performance of the NZS 4230-2004 (2004) equation predicting the shear strength of masonry walls. The cantilever test configuration used in this study is illustrated in Fig. 3.14.

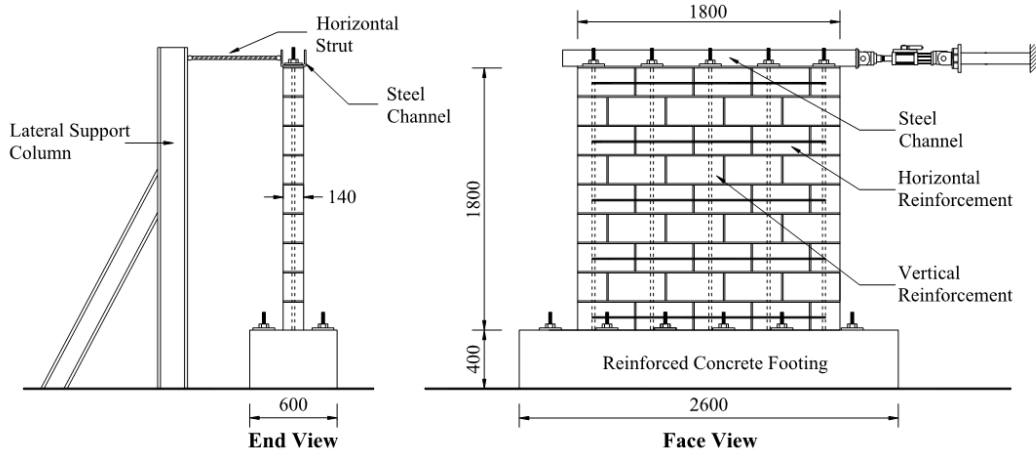


Figure 3.14 – Test setup by Voon (2007)

Voon and Ingham observed that a smaller spacings for vertical reinforcement significantly increased the shear strength of the wall. It was also observed that the PG walls had significantly less shear strength than FG walls, but only when the gross shear strength was considered. The net shear strength and force-displacement envelopes of PG walls was found to be comparable with the FG walls when no axial load was applied to either set of specimens, as shown in Fig. 3.15.

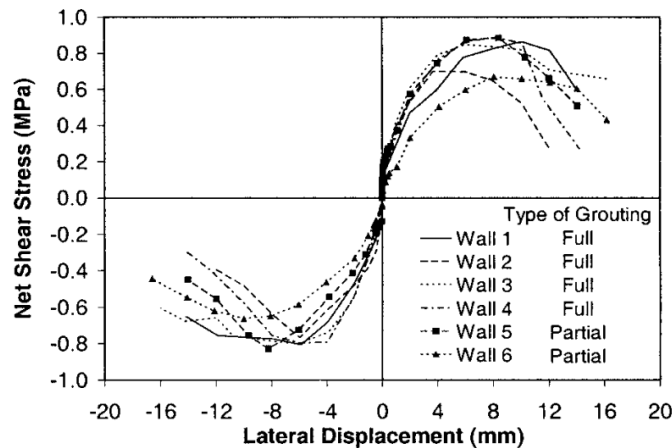


Figure 3.15 – Force displacement envelopes in Voon and Ingham (2006) for FG and PG walls with no axial loading

3.2.16 Haach et al. (2007)

Total Number of PG Walls in Study: 4			
Loading Type:	Reverse Cyclic	f'_m :	5.27 MPa
Loading Rate:	Quasi-static	A_{net}/A_{gross} :	<i>Varied</i> (0.48-0.70)
Support Type:	Cantilever	Axial Stress:	<i>Varied</i> (0.5-1.25)
Height:	808 mm	Flexural Reinf.:	Ø5mm truss
Length:	1200 mm	Vertical (Interior) Reinf.:	Ø5mm truss
Thickness:	100 mm	Bond Beam Reinf.:	None
H/L:	0.67	Joint Reinf.:	Ø4mm truss

Haach tested a total of 5 1/2-scale masonry walls, 4 of which were reinforced PG walls. The objective of Haach's study was to investigate the influence of the horizontal and vertical reinforcement and axial stress on the behaviour of PG shear walls. Truss reinforcement was used in both horizontal and vertical directions. Since truss reinforcement could be placed either within cells or between mortar joints, two different masonry bond patterns were also studied. The cantilever test configuration used in this study is illustrated in Fig. 3.16.

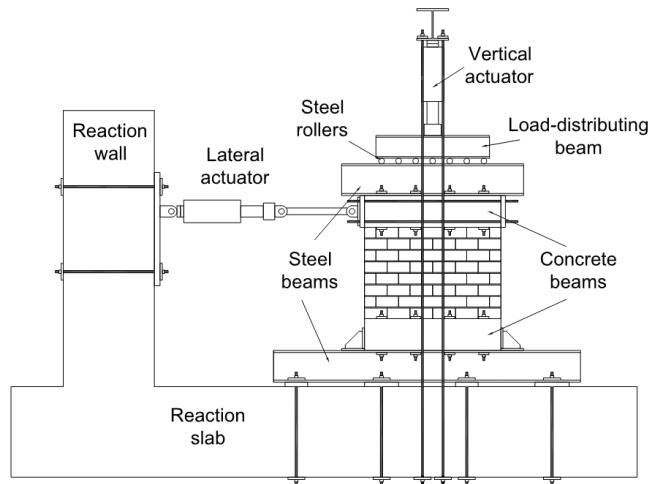


Figure 3.16 – Test setup by Haach et al. (2007)

Haach concluded that higher reinforcement ratios in both horizontal and vertical directions increase the lateral strength, energy dissipation and lateral drift of PG walls. Increased axial stresses also increased the shear strength of PG walls but led a greater

likelihood of brittle failure. It was found that the mortar bond type had no influence on the shear behaviour of PG walls.

3.2.17 Maleki (2008) and Maleki et al. (2009)

Total Number of PG Walls in Study: 5			
Loading Type:	Reverse Cyclic	f'_m :	11.93 MPa
Loading Rate:	Quasi-static	A_{net}/A_{gross} :	<i>Varied</i> (0.66-0.75)
Support Type:	Double curvature	Axial Stress:	0.75 MPa
Height:	<i>Varied</i> (900-1800)	Flexural Reinf.:	<i>Varied</i>
Length:	1800 mm	Vertical (Interior) Reinf.:	<i>Varied</i>
Thickness:	90 mm	Bond Beam Reinf.:	<i>Varied</i>
H/L:	<i>Varied</i> (0.5-1.0)	Joint Reinf.:	None

Maleki built 5 half-scale PG masonry walls to investigate the performance of PG walls with vertical reinforcement spacing beyond the maximum spacing limitation imposed by CSA Standard S304.1 (2004). The horizontal reinforcement ratio for each wall was 0.05%, while the vertical reinforcement ratio was 0.18%. The effect of aspect ratio was also considered. The double-curvature test configuration used in this study is illustrated in Fig. 3.17.

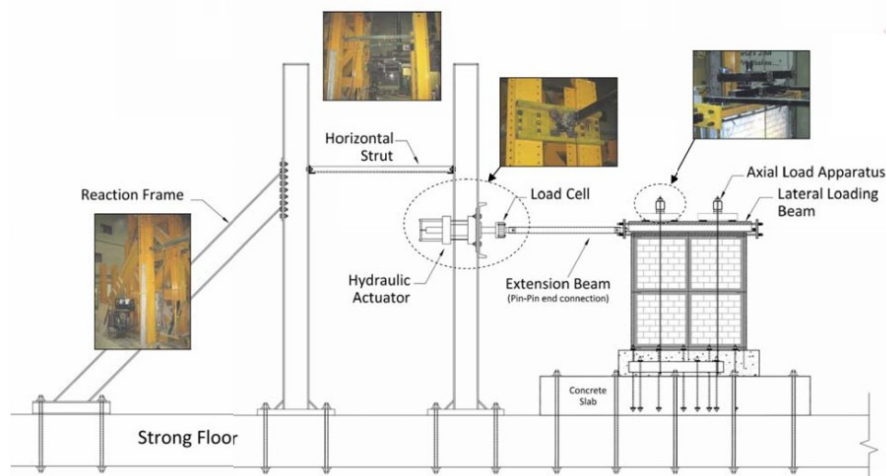


Figure 3.17 – Test setup by Maleki et al. (2009)

Maleki observed that the spacing of vertical reinforcement had no significant influence on the shear strength of the wall. However, it was observed that a decrease in aspect ratio

of the wall greatly increased its shear strength and wall stiffness. Maleki observed walls with aspect ratios equal to or less than 1.0 failed primarily in shear, while the wall tested with an aspect ratio equal to 1.5 exhibited a shear-flexure failure mode.

3.2.18 Elmapruk (2010)

Total Number of PG Walls in Study: 6			
Loading Type:	Reverse Cyclic	f'_m :	14.11 MPa
Loading Rate:	Quasi-Static	A_{net}/A_{gross} :	<i>Varied</i> (0.45-0.53)
Support Type:	Double curvature	Axial Stress:	0.10 MPa
Height:	1524 mm	Flexural Reinf.:	2#6
Length:	2642 mm	Vertical (Interior) Reinf.:	<i>Varied</i>
Thickness:	193 mm	Bond Beam Reinf.:	<i>Varied</i>
H/L:	0.58	Joint Reinf.:	None

Elmapruk built 6 full-scale PG masonry walls to investigate the effect of spacing between vertical grouted cells on the strength and failure mechanism of PG shear walls. The vertical reinforcement spacings used were 24, 32 or 48 inches. The horizontal reinforcement ratio was varied by changing the bond beam reinforcement located mid-height using (1)#5 bar, (1)#6 bar, or (2)#5 bars ($\rho_h = 0.085\%$, 0.120% or 0.169% , respectively). The double-curvature test configuration used in this study is illustrated in Fig. 3.18.

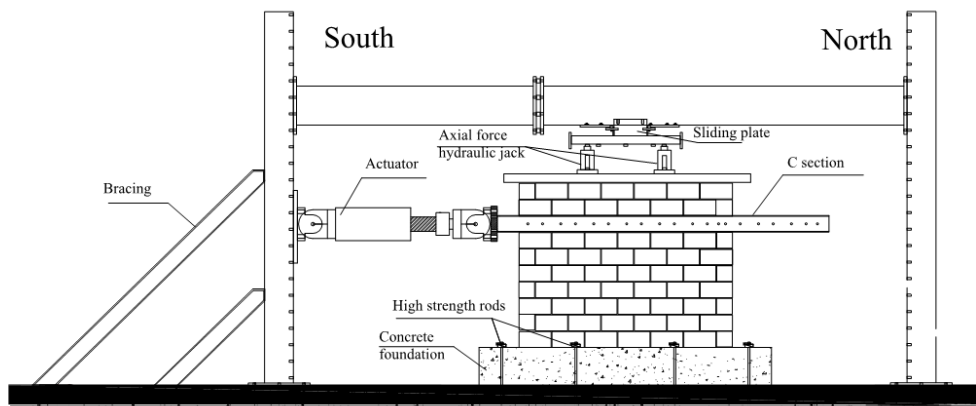


Figure 3.18 – Test setup by Elmapruk (2010)

Elmapruk observed that a decrease in grout horizontal spacing significantly increased the shear strength of the wall. It was also observed that that horizontal reinforcement ratios past a certain threshold led to a negligible increase in ultimate shear strength. Lastly, Elmapruk found the MSJC (2008) design shear equation overestimated the shear strength of PG walls by 60-91%.

3.2.19 Minaie (2009) and Minaie et al. (2010)

Total Number of PG Walls in Study: 4			
Loading Type:	Reverse Cyclic	f'_m :	11.37 MPa
Loading Rate:	Quasi-static	A_{net}/A_{gross} :	0.40
Support Type:	<i>Varied</i>	Axial Stress:	<i>Varied</i> (0-0.28)
Height:	2640 mm	Flexural Reinf.:	#6
Length:	3860 mm	Vertical (Interior) Reinf.:	(2)#6
Thickness:	200 mm	Bond Beam Reinf.:	(3)#6
H/L:	0.68	Joint Reinf.:	None

Minaie built 4 full-scale PG masonry walls with identical geometric properties and reinforcement pattern. The type of mortar, level of axial stress, and boundary conditions were varied in this experimental study. Either Portland cement/line-based mortar or masonry cement-based mortar was used. Two walls were tested with cantilever support conditions, while the remaining two walls were restrained against rotation at the top. The primary objective of this study was to determine the accuracy of MSJC (2008) in predicting the shear strength of PG walls. The test configuration used in this study is illustrated in Fig. 3.19.

Minaie concluded that PG masonry shear walls with vertical reinforcement behaved more similarly to infilled masonry walls rather than FG masonry walls. He also concluded that MSJC (2008) was non-conservative for predicting the shear strength of PG walls due to the empirical development of the formula, which was based on results obtained for FG walls.

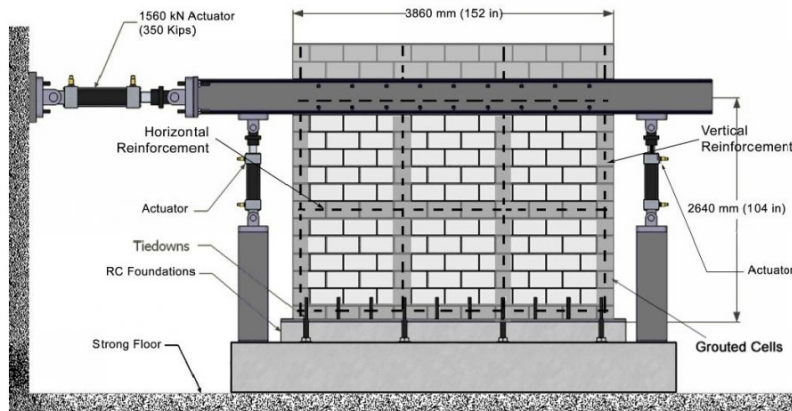


Figure 3.19 – Test setup by Minaie (2009)

3.2.20 Baenziger and Porter (2011)

Total Number of PG Walls in Study: 10			
Loading Type:	Reverse Cyclic	f'_m :	<i>Varied</i> (15.2-19.8)
Loading Rate:	Quasi-static	A_{net}/A_{gross} :	<i>Varied</i> (0.61-0.69)
Support Type:	Cantilever	Axial Stress:	0 MPa
Height:	2640 mm	Flexural Reinf.:	<i>Varied</i>
Length:	<i>Varied</i> (2850-4270)	Vertical (Interior) Reinf.:	<i>Varied</i>
Thickness:	193 mm	Bond Beam Reinf.:	<i>Varied</i>
H/L:	<i>Varied</i> (0.62-0.93)	Joint Reinf.:	<i>Varied</i>

Baenziger and Porter tested 4 sets of walls (totalling 10 walls) to investigate the effect of varying the type of horizontal reinforcement on the lateral response of masonry walls. Single ladder style joint reinforcement, double seismic style joint reinforcement, or bond beam reinforcement was used in each wall. 3 sets of walls (totalling 8 walls) were PG masonry shear walls. The cantilever test configuration used in this study is illustrated in Fig. 3.20.

Baenziger and Porter concluded that joint reinforcement was a viable option for horizontal reinforcement in masonry shear walls. Furthermore, horizontal reinforcement distributed evenly through the wall through joint reinforcement was found to provide better ductility and crack control than concentrated horizontal reinforcement in bond beams.

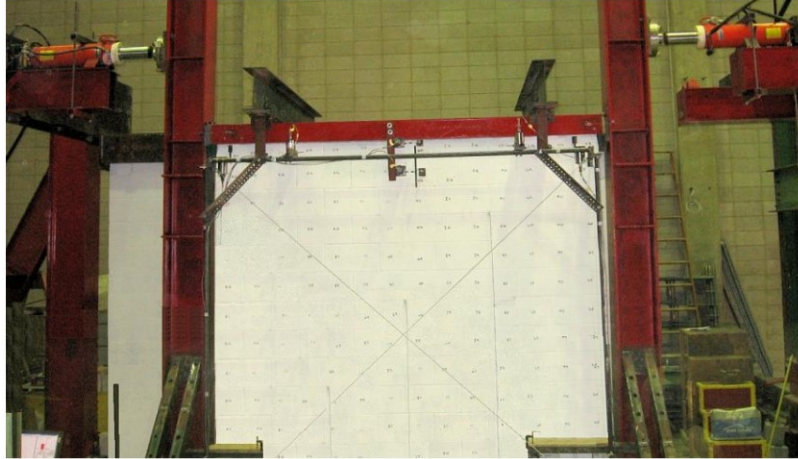


Figure 3.20 – Test setup by Baenziger and Porter (2011)

3.2.21 Nolph (2010) and Nolph and Elgawady (2012)

Total Number of PG Walls in Study: 5			
Loading Type:	Reverse Cyclic	f'_m :	9.95 MPa
Loading Rate:	Quasi-Static	A_{net}/A_{gross} :	0.45
Support Type:	Cantilever	Axial Stress:	0.10 MPa
Height:	2337 mm	Flexural Reinf.:	<i>Varied</i>
Length:	2631 mm	Vertical (Interior) Reinf.:	<i>Varied</i>
Thickness:	194 mm	Bond Beam Reinf.:	<i>Varied</i>
H/L:	0.89	Joint Reinf.:	None

Nolph and Elgawady built 5 PG wall specimens to investigate the influence of vertical reinforcement spacing and horizontal reinforcement ratio on the shear strength of PG walls. The vertical reinforcement spacings used were 24, 32 or 48 inches. The horizontal reinforcement ratio was varied by changing the reinforcement in the bond beam located mid-height using (1)#5 bar, (1) #6 bar, or (2)#5 bars ($\rho_h = 0.085\%$, 0.120% or 0.169% , respectively). The cantilever test configuration used in this study is illustrated in Fig. 3.21.

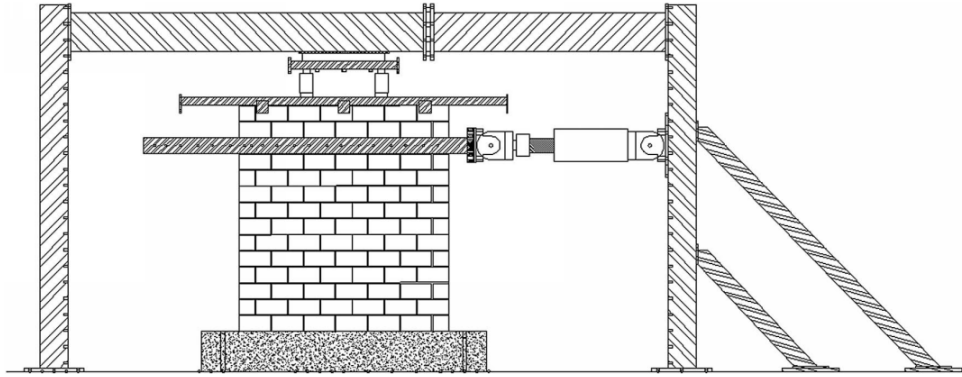


Figure 3.21 – Test setup by Nolph and Elgawady (2012)

Nolph observed that horizontal reinforcement ratios above approximately 0.085-0.1% led to a negligible increase in ultimate strength for PG walls with a grout horizontal spacing of 48 in. (1219 mm). Additionally, it was observed that the MSJC (2011) equation overestimated the strength of specimens built with 48 in. grout horizontal spacing due to the overestimation of horizontal reinforcement contribution.

3.2.22 Oan (2013)

Total Number of PG Walls in Study: 66			
Loading Type:	Monotonic	f'_m :	<i>Varied</i> (11.0-17.3)
Loading Rate:	Quasi-static	A_{net}/A_{gross} :	0.68
Support Type:	Cantilever	Axial Stress:	<i>Varied</i> (1.04-2.78)
Height:	1200 mm	Flexural Reinf.:	<i>Varied</i>
Length:	1590 mm	Vertical (Interior) Reinf.:	<i>Varied</i>
Thickness:	190 mm	Bond Beam Reinf.:	None
H/L:	0.75	Joint Reinf.:	<i>Varied</i>

Oan tested a total of 66 PG walls to investigate the influence of horizontal reinforcement, vertical reinforcement, axial stress, and methods of construction on the behaviour of PG shear walls. Duplicate specimens for each parameter combination were tested. Specimens were loaded monotonically at a displacement rate of 0.1 mm/s. The cantilever test configuration used in this study is based on ESECMaSE guidelines and is illustrated in Fig. 3.22.

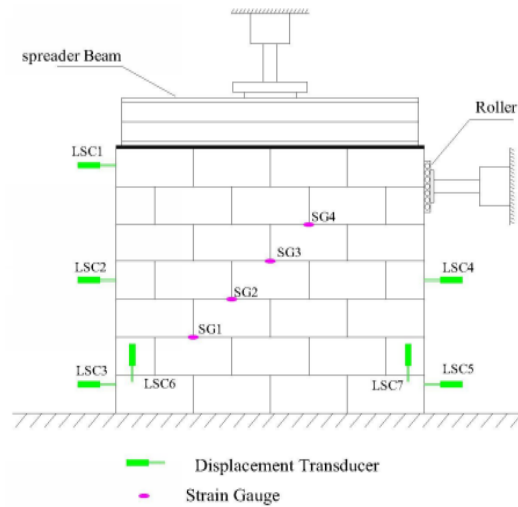


Figure 3.22 – Test setup by Oan (2013)

Vertical reinforcing bars were not anchored to a concrete base beam. Reportedly, this was done with the intention of isolating the effect of vertical reinforcement from anchorage effects. In the absence of vertical reinforcement anchorage, two struts and two plates were installed on each side of the wall to restrain the wall from sliding, as illustrated in Fig. 3.23.



Figure 3.23 – Mechanical fixation at the bottom of Oan's walls (2013)

Oan concluded that axial stress had a significant impact on the shear strength of PG walls. An increase of axial stress from 2 MPa to 3 MPa and 4 MPa led to an average 33% and 55% increase in shear strength, respectively. Horizontal reinforcement was found to improve ductility of the wall, although it did not improve shear strength.

3.2.23 Hoque (2013)

Total Number of PG Walls in Study: 18			
Loading Type:	<i>Varied</i>	f'_m :	16.5 MPa
Loading Rate:	Quasi-static	A_{net}/A_{gross} :	0.55
Support Type:	Double Curvature	Axial Stress:	2 MPa
Height:	1800 mm	Flexural Reinf.:	15M
Length:	1800 mm	Vertical (Interior) Reinf.:	15M
Thickness:	190 mm	Bond Beam Reinf.:	<i>Varied</i>
H/L:	1.0	Joint Reinf.:	<i>Varied</i>

Hoque tested a total of 18 PG walls to investigate the effect of the position of bond beam, reinforcement anchorage type in the bond beam, dowel and splice position, and variation in load history on the behaviour of PG shear walls. The bond beam anchorage was varied using straight ends, 90° hooks, 180° hooks, or using circular discs welded to the bar ends. The vertical reinforcement splices were placed at the top, the bottom, or both the top and the bottom of the wall. A total of eight different wall configurations were tested. The vertical reinforcement pattern remained constant in all specimens.

The experimental setup is based on the ESECMaSE (2005) guidelines. Specimens were built on steel channel sections with flexural reinforcement welded at the bottom. Vertical loads were applied using hydraulic actuators placed on roller bearings. Horizontal loads were applied using an I-beam placed on a cement-mortar bed at the top of the wall. The double-curvature test configuration used in this study is illustrated in Fig. 3.24.

Hoque observed little difference in shear strength despite varying the horizontal reinforcement. However, the cracking pattern was more distributed over the surface of the specimens containing a bond beam, while cracks concentrated into a large X-pattern in specimens containing joint reinforcement. It was also observed that the difference in splice patterns did not significantly affect the shear behaviour of PG walls.

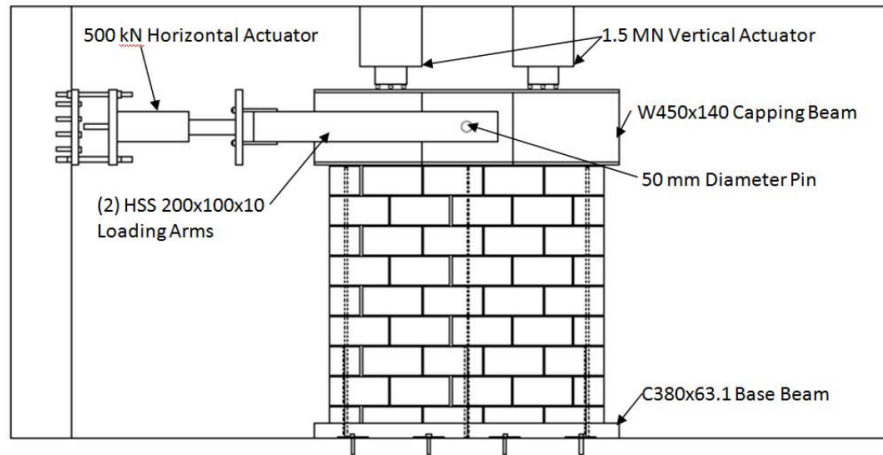


Figure 3.24 – Test setup by Hoque (2013)

3.2.24 Hamedzadeh (2013)

Total Number of PG Walls in Study: 21			
Loading Type:	Monotonic	f'_m :	<i>Varied</i> (7.3-7.9)
Loading Rate:	Quasi-static	A_{net}/A_{gross} :	<i>Varied</i> (0.45-0.67)
Support Type:	Double Curvature	Axial Stress:	<i>Varied</i> (0.5-2)
Height:	1800 mm	Flexural Reinf.:	10M
Length:	1800 mm	Vertical (Interior) Reinf.:	<i>Varied</i>
Thickness:	90.7 mm	Bond Beam Reinf.:	10M
H/L:	<i>Varied</i> (1.0-3.1)	Joint Reinf.:	None

Hamedzadeh built 21 1/2-scale widely reinforced squat masonry walls to investigate the effect of different methods of load application, initial axial stresses and specimens size on the strength and behaviour of PG shear walls. The specimens were laterally loaded with either concentrated load or distributed load. Three aspect ratios were tested; panel walls with a height-to-length aspect ratio of 1 were assembled as either single-, double- or triple-panel walls. A total of eight different wall configurations were tested. The vertical reinforcement pattern remained constant in all specimens.

The experimental setup is based on the ESECMaSE (2005) guidelines, and is similar to the setup used by Hoque (2013). The double-curvature configuration used in this study is illustrated in Fig. 3.25.



Figure 3.25 – Test setup by Hamedzadeh (2013)

Hamedzadeh observed no significant difference in shear strength whether the specimens were subject to a concentrated or distributed lateral load. The observed crack pattern suggested that shear loads were mainly transferred through the grouted core at the midspan of walls. The aspect ratio was found to have a significant effect on shear strength; shear strength increased by 132% when the aspect ratio was decreased from 1.0 to 0.5, and increased by 70% when the aspect ratio was decreased from 0.5 to 0.33.

3.2.25 Rizaee (2015)

Total Number of PG Walls in Study: 14			
Loading Type:	Reverse Cyclic	f'_m :	<i>Varied</i> (11.9-17.9)
Loading Rate:	Quasi-static	A_{net}/A_{gross} :	0.48
Support Type:	Double Curvature	Axial Stress:	2 MPa
Height:	1790 mm	Flexural Reinf.:	15M
Length:	1790 mm	Vertical (Interior) Reinf.:	None
Thickness:	190 mm	Bond Beam Reinf.:	<i>Varied</i>
H/L:	1.0	Joint Reinf.:	None

Rizae built 14 full-scale specimens to investigate the influence of bond beam reinforcement on the shear strength and behaviour of PG walls. The bond beam reinforcement diameter, location of bond beam, and bond beam anchorage type were varied. A total of seven different wall configurations were tested.

The experimental setup is based on the ESECMaSE (2005) guidelines, and is similar to setups by Hoque (2013) and Hamedzadeh (2013). The double-curvature configuration used in this study is illustrated in Fig. 3.26.

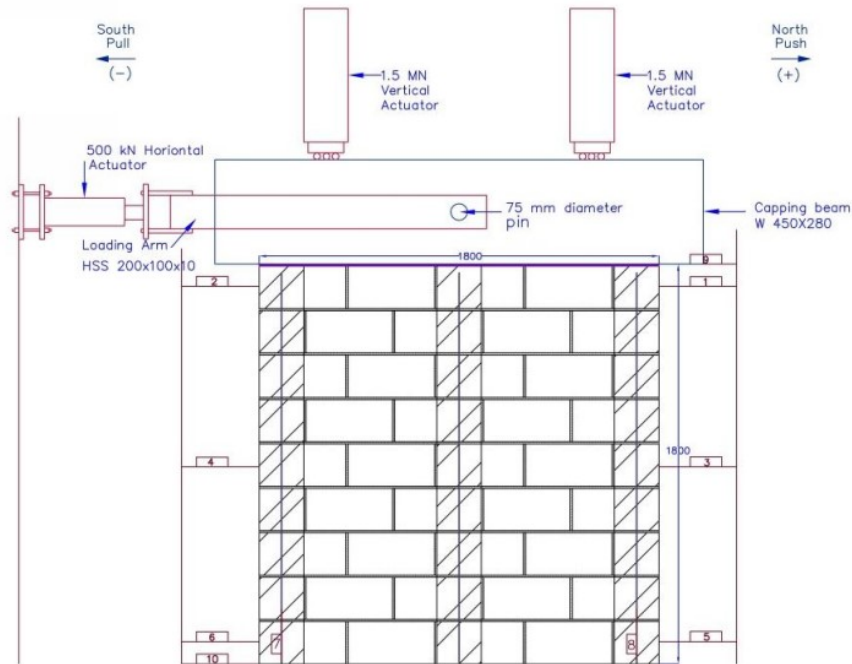


Figure 3.26 – Test setup by Rizae (2015)

Rizae observed that the different anchorage conditions did not have a significant effect on shear strength and behaviour. However, using a 15M reinforcing bar in the horizontal bond beam resulted in better stiffness and energy dissipation than using a 10M bar.

3.2.26 Ramírez et al. (2016)

Total Number of PG Walls in Study: 10			
Loading Type:	Reverse Cyclic	f'_m :	4.12 MPa
Loading Rate:	Quasi-static	A_{net}/A_{gross} :	<i>Varied</i> (0.60-0.74)
Support Type:	Cantilever	Axial Stress:	<i>Varied</i> (0-0.56)
Height:	<i>Varied</i> (1130-1930)	Flexural Reinf.:	<i>Varied</i>
Length:	<i>Varied</i> (990-2590)	Vertical (Interior) Reinf.:	<i>Varied</i>
Thickness:	140 mm	Bond Beam Reinf.:	None
H/L:	<i>Varied</i> (0.44-1.95)	Joint Reinf.:	<i>Varied</i>

Ramirez et al. tested 10 PG masonry shear walls to investigate the effect of aspect ratio, horizontal reinforcement ratio, and axial stress on the behaviour of PG shear walls. Three height-to-length aspect ratios were tested in this study ($\frac{h}{L} = 0.44, 0.97, 1.95$). Horizontal reinforcement was exclusively in the form of 4.2 mm diameter ladder joint reinforcement built into mortar joints either at each course ($s_v = 200$ mm) or every other course ($s_v = 400$ mm). A net axial precompression of 0.56 MPa was applied to 8 walls, while the remaining 2 had no axial precompression. The cantilever test configuration used in this study is illustrated in Fig. 3.27.

Ramirez et al. concluded that the height-to-length aspect ratio of the wall had the greatest influence on the shear strength and behaviour of PG walls; a higher aspect ratio was found to decrease shear strength. Also, horizontal reinforcement improved the shear strength of PG walls, although it had a greater benefit to slender walls compared with squat walls. Increasing the axial stress on PG walls also increased its shear strength, although its effect was more pronounced on squat walls compared with slender walls.

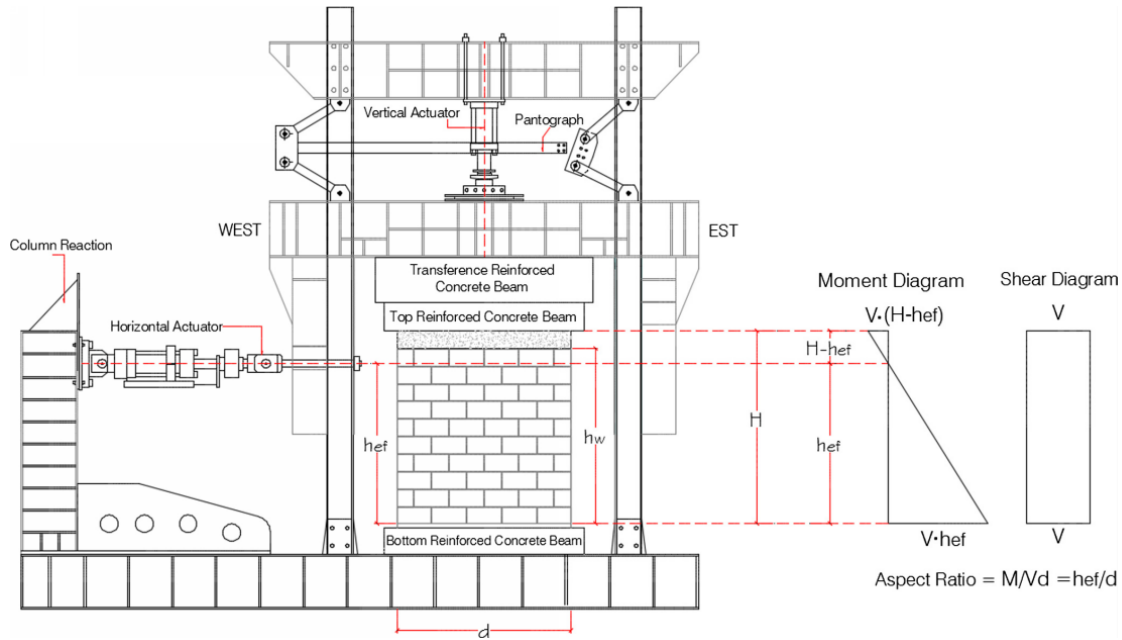


Figure 3.27 – Test setup by Ramírez et al. (2016)

3.2.27 Other Studies

Several other experimental studies which have tested PG masonry shear walls have not been included in the dataset due to the unavailability of the conference paper, journal paper, and/or thesis corresponding to the study. They have been referenced by other researchers who have built similar datasets, and are listed below in chronological order:

- Igarashi, I. and Matsumura, A. (1984). “Effects of height-to-length ratio on shear strength of reinforced hollow concrete block loadbearing walls.” *Transactions, Architectural Institute of Japan*, 59(10), 1783–1784. (in Japanese).
- Lüders, C., Hidalgo, P., & Gavilán, C. (1985). *Comportamiento Sísmico de Muros de Albañilería Armada*. (Proyecto No. 70/83). Santiago: Departamento de Ingeniería Estructural. Pontificia Universidad Católica de Chile. (in Spanish).
- Lüders, C., & Hidalgo, P. (1986). *Influencia del Refuerzo Horizontal en el Comportamiento sísmico de muros de albañilería Armada* [Influence of horizontal reinforcement on seismic behaviour of reinforced masonry walls]. In IV Jornadas Chilenas de Sismología e Ingeniería Antisísmica. Viña del Mar, Chile. (in Spanish).

- Muñoz, W. E. (1992). *Estudio experimental del comportamiento de muros de albañilería de bloques de hormigón sometidos a carga lateral alternada* [Experimental study on in-plane cyclic behaviour of reinforced concrete masonry walls]. Memoria de Ingeniero Civil. Santiago: Universidad de Chile. (in Spanish).
- Brammer, D. R. (1995). *The lateral force-deflection behaviour of nominally reinforced concrete masonry walls*. Master's thesis, University of Auckland, Auckland.
- Sierra, G. A. (2002). *Estudio experimental de la influencia del refuerzo vertical en muros de albañilería armada sometidos a carga lateral alternada* [Influence of vertical reinforcement on reinforced masonry walls under cyclic lateral loading. An experimental study]. Memoria de Ingeniero Civil. Santiago: Universidad de Chile. (in Spanish).
- Dickie, J. and Lissel, S. (2011), "In-Plane Shear Test Method for Reinforced Concrete Masonry and Comparison of Test Results", 9th Australasian Masonry Conference, Queenstown, New Zealand , 15 – 18 February , 543-552.
- DICTUC (2014). *Ensayo de dos muros de albañilería armada de ladrillo cerámico perforado* [Testing of two reinforced masonry walls made of hollow clay bricks]. Informe Técnico: Pontificia Universidad Católica de Chile. (in Spanish).

3.3 Data Scrutinization

3.3.1 Failure Mode

The current study investigates the strength and behaviour of PG masonry shear walls. Although each experimental study in this section is focused on the shear behaviour of PG walls, some walls were observed to fail in flexure instead of shear. Flexural failure is characterized by higher ductility and fail at loads lower than the ultimate shear capacity. In most cases, flexural failures were the result of a high height-to-length aspect ratio. Walls exhibiting flexural failure were not included in the dataset.

3.3.2 Horizontal Reinforcement Pattern

In CSA S304.14, Section 10.15.1.4(d), it states that horizontal reinforcement is required "where the wall is connected to roof and floor assemblies." This may be interpreted as a requirement to provide horizontal bond beams in the bottom and top course of each wall specimen.

10.15.1.4

Where horizontal reinforcement is required to resist in-plane shear forces, it shall be

- (a) continuous along the wall length;
- (b) spaced at not more than the lesser of 2400 mm or $0.5\ell_w$ for bond beams, and 600 mm for joint reinforcement;
- (c) provided above and below each opening over 1200 mm high; and
- (d) provided at the top of the wall and where the wall is connected to roof and floor assemblies.

Figure 3.28 – CSA S304.14 provision for horizontal reinforcement in PG walls (adapted from CSA 2014)

However, strut-and-tie models predict that a horizontal tension tie at the bottom of the wall would not necessarily benefit the shear strength of the wall, especially if a concrete grade beam or concrete element exists at the base of the wall. A typical strut and tie model of a PG shear wall is illustrated in Fig. 3.29.

Additionally, the amount of load carried by horizontal reinforcing steel is dependent on the crack width, assuming the reinforcement has not yet reached yielding stress at the ultimate shear capacity of the wall. The diagonal shear crack is assumed to be larger at the top of the wall compared to the bottom in cantilevered boundary conditions (Fig. 3.30). In this case, horizontal reinforcing bars would be expected to carry significantly less load near the bottom of the shear wall.

When the boundary conditions restrain the top of the wall from rotation, the shear crack is assumed to be the same along the height of the wall, as illustrated in Fig. 3.31. However, experimental results have shown that the cracks are typically located at the bottom corners of the wall, such as the ones obtained by Minaie (2009) illustrated in Fig. 3.32. Since horizontal bars are expected to have very little anchorage at its ends—especially given the severity of the cracking at these locations—they would not be expected to carry a significant amount of loading.

A horizontal bond beam at the bottom course exists in the design of PG walls by several researchers (Ghanem et al. 1992, 1993; Maleki 2008; Minaie 2009), while others did not (Elmapruk and Elgawady 2009; Nolph and Elgawady 2012; Ramírez et al. 2016; Schultz 1996; Scrivener 1967; Thurston and Hutchinson 1982; Yancey and Scribner 1989). Maleki's (2008) wall specimens are illustrated in Fig. 3.33 as an example.

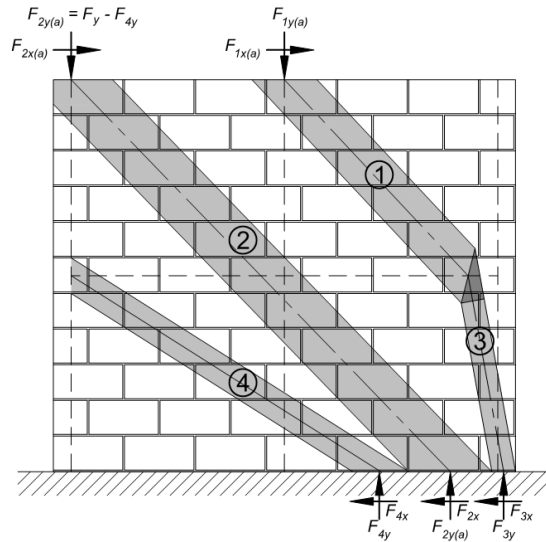


Figure 3.29 – Strut-and-tie model of PG masonry shear walls (Dillon 2015)

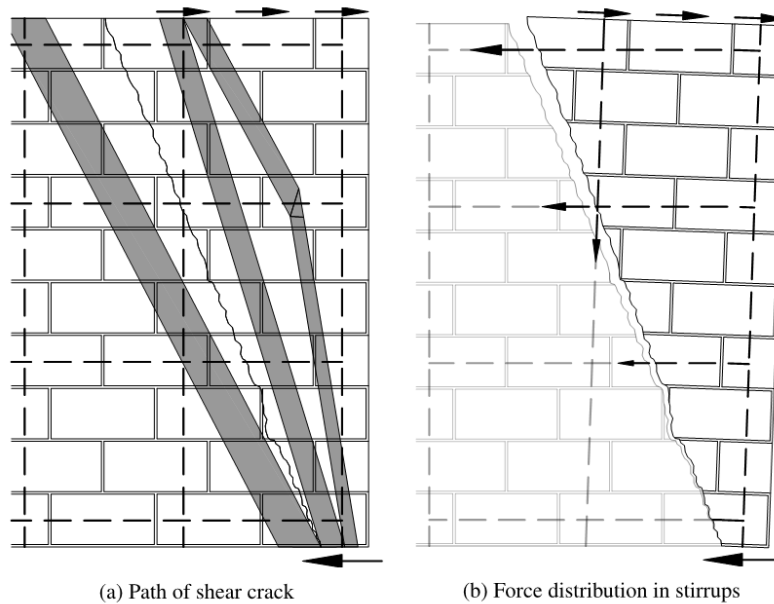


Figure 3.30 – Behaviour of horizontal reinforcement in a shear wall (Dillon 2015)

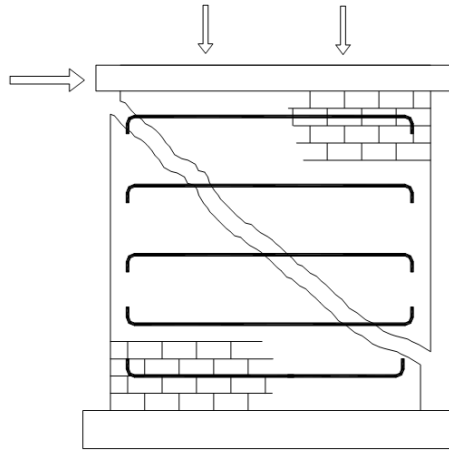


Figure 3.31 – Role of horizontal reinforcement in resisting masonry shear failure (Voon 2007)

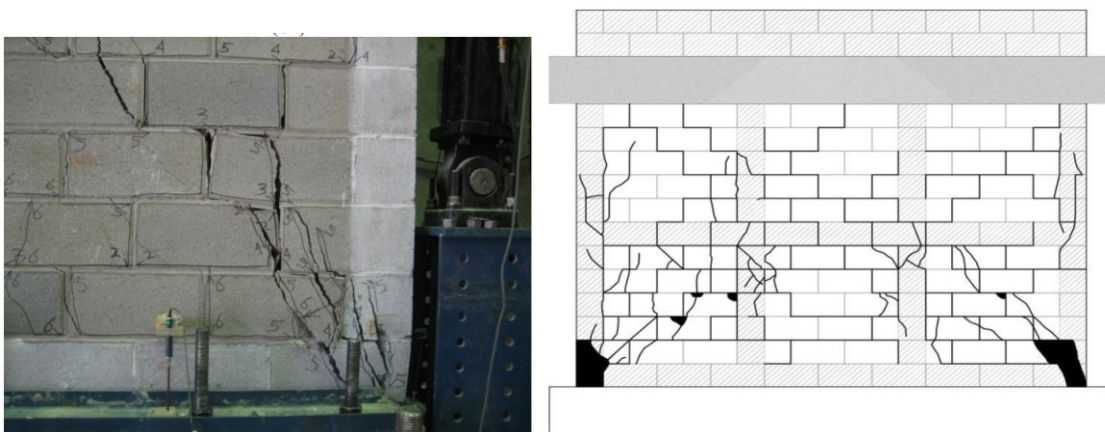


Figure 3.32 – Crack pattern in PG wall tested by Minaie (2009)

Specimen Label	Wall 1	Wall 2	Wall 3	Wall 4	Wall 5
Reinforcing Pattern					
	Wall 1	Wall 2	Wall 3	Wall 4	Wall 5

Figure 3.33 – Maleki’s shear wall specimens (Maleki 2008)

3.3.3 Interior Vertical Reinforcement

Only a few design expressions (Dillon 2015; Shing et al. 1990b; Standards New Zealand 2004; Voon 2007) consider the contribution of vertical reinforcement on the in-plane shear strength of PG walls. However, Thurston and Hutchinson (1982) suggest that vertical reinforcing steel provides shear resistance as cracking occurs. Distributed vertical reinforcement minimizes crack openings, allowing the aggregate interlocking of masonry blocks to continue providing shear resistance (Ghanem et al. 1992).

Ghanem et al. (1992) suggested that only interior reinforcing bars should be considered for shear resistance, since boundary bars were considered to carry the tension forces due to flexural loads. Dillon (2015) refers to the interior vertical reinforcing bars as “confinement” reinforcement due to its role in minimizing diagonal cracking in masonry walls which maintain the friction and shear transfer across cracks.

The multiple linear regression performed by Dillon (2015) found that interior vertical reinforcement should be equally effective in resisting diagonal crack openings as horizontal reinforcement, and neglects the influence of boundary vertical reinforcement. As a result, the equation proposed by Dillon applies the same numerical coefficient for predicting the influence of both horizontal and interior vertical reinforcement on the in-plane shear strength for PG walls.

$$v_n = 0.083 \left(1.1 + 0.9 \frac{V S_{gh}}{M} \right) \sqrt{f'_m} + 0.15 \sigma_o + 0.12 [\rho_c f_{yc} + \rho_h f_{yh}] \quad (3.1)$$

3.3.4 ESECMaSE Test Setup

The Enhanced Safety and Efficient Construction of Masonry Structures in Europe (ESECMaSE) developed a method for testing unreinforced masonry walls, with its latest standard released in 2005. However, this standard does not provide any detailing requirements for reinforced masonry walls, and thus is not directly applicable to develop experimental programs testing reinforced PG shear walls.

Comprehensive studies on the structural performance of shear-critical walls made of reinforced-concrete, such as the MCEER-09-0010 (Gulec and Whittaker 2009), and FEMA P695 (Applied Technology Council 2009), have provided recommendations to develop reliable testing programs. These studies have emphasized the importance of accounting for cumulative damage effects (i.e. monotonic loading is not representative of the cumulative damage produced by cyclic loading), the use of full-size specimens (unless it can be shown by theory and experiment that testing of reduced-scale specimens will not significantly affect the behavior), and the use of realistic construction details.

The experimental programme studying the behaviour of PG shear walls conducted by Oan (2013), Hoque (2013), Hamedzadeh (2013), and Rizaee (2015) have adopted the ESECMaSE standard, despite differences between unreinforced masonry and reinforced masonry in both detailing and behaviour under lateral loading.

One of the biggest shortcomings of these is the loading mechanism used. The base of the walls is mortared to a steel channel rigidly fixed to the laboratory strong floor, illustrated by Fig. 3.34. The top of the wall is mortared to a stiff beam according to ESECMaSE, illustrated by Figs 3.35 and 3.36. Dowels are welded to the base channel to connect the vertical reinforcement through splices, but it is unclear how the reinforcement is not connected to the top element. This setup was used to simulate walls in double curvature.

However, since the bars are not connected at the top, and the welded bottom dowels do not provide a realistic development at the bottom, this setup does not capture the bar development mechanisms found in shear walls under double curvature accurately. Rather, such a setup appears to mimic partition walls that are rigidly connected at the top to the slab, a form of construction not typical in Canada, where partition walls are isolated from the floor slab.



Figure 3.34 – Footing details in Hoque’s experimental study (Hoque 2013)

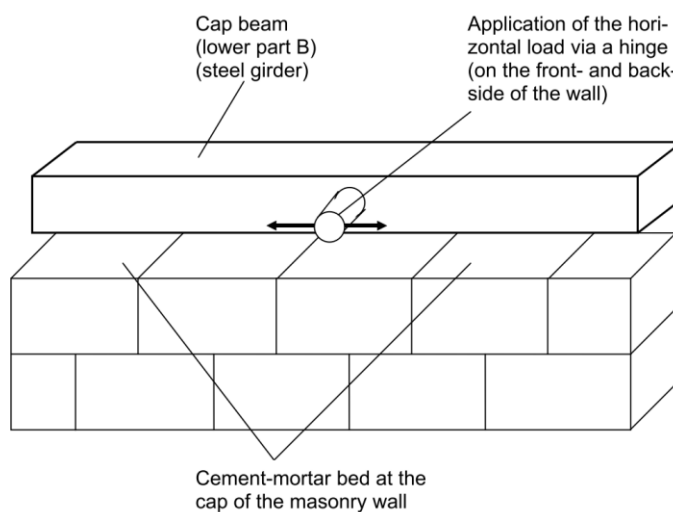


Figure 3.35 – Application of horizontal load to the cap of the wall according to ESECMaSE (2005)

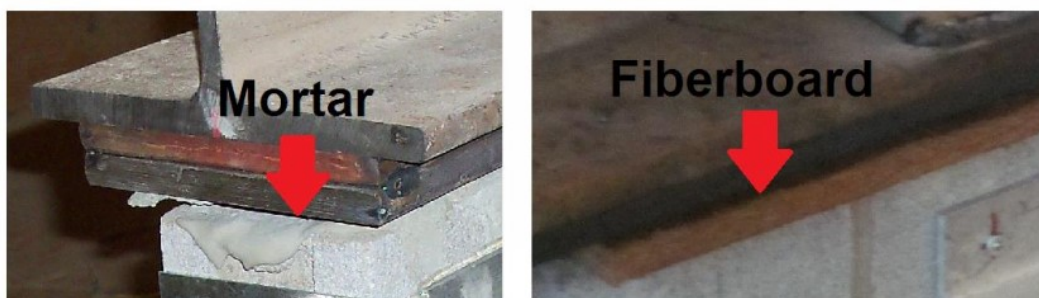


Figure 3.36 – Interface between the specimen and loading beam by Hamedzadeh (2013)

Furthermore, the lack of anchorage in vertical reinforcement into a base beam does not reflect common practice of loadbearing masonry, especially in seismic regions. The transmission of loads to the shear wall is achieved through concrete foundation blocks

and concrete cap beams in milestone studies [Matsumura (1987, 1988); Minaie et al. (2010); Schultz (1994, 1996); Schultz et al. (1998); Shing et al. (1990a)]. The use of concrete foundation blocks and cap beams is recommended by the MCEER-09-0010 (Gulec and Whittaker 2009) and FEMA P695 (Applied Technology Council 2009) reports as well. The ESECMaSE setup lacks these elements. As a result, specimens tested using the ESECMaSE setup showed unusual or atypical cracking patterns, not observed in other testing programs.

In addition, the foundation system used in the ESECMaSE setup, in which the walls are mounted in channels that confine the wall panel, do not reflect usual construction practices in which the blocks are mortared on a grade beam or slab which allows for some sliding occurs under the application of loads. The response of a wall must include the sliding mechanism as it is present in the response of real walls, but it is artificially prevented when using the ESECMaSE setup.

Summarizing, the limitations in the test setup (unrealistic details, concerns about the suitability of the loading protocol and testing methods, varying block sizes/strength/scale, etc.) prevents drawing conclusions about the usefulness or significance of the results.

3.4 Data Synthesization

Data synthesization is defined as compiling experimental data from multiple researchers using different methods in a consistent manner, ensuring that the data is compatible for comparison and analysis (Dillon 2015). A consistent dataset is vital for using neural networks to predict the shear strength of PG walls.

The most basic synthesization process is maintaining consistent units throughout the dataset. Beyond unit conversion, methodologies were proposed by Dillon (2015) for prism strength estimation, inflection height, net shear area, prism aspect ratio, shear reinforcement, loading patterns, loading rates, and experimental shear strength reporting.

3.4.1 Prism Geometry

Although most researchers take the average compressive strength measured from several masonry prism tests as f'_m , there is significant variability among how many blocks are in the prism and how many tests are performed. This variation in measurement exists even among international codes; while CSA Standard S304.14 (2014), BS 5628 (2005) and AS 3700 (2011) specify a standard aspect ratio of 5-to-1, the TMS 402/602-16 (2016) specifies a standard aspect ratio of 2. In cases where the aspect ratio of tested prisms is not 5-1, the CSA Standard S304.14 (2014) applies a corrective factor.

A regression model was proposed by Dillon (2015) to predict the mean prism strength correction factor k in cases where the prism geometry had an aspect ratio other than 5 (fewer than 5 blocks) by combining four design codes. The corrective factor proposed by Dillon for these prisms is given in Eq. (3.2):

$$k = 1 - 0.058 \left(5 - \frac{h}{t} \right)^{1.07} \quad (3.2)$$

where h/t = aspect ratio of the prism

3.4.2 Prism Strength Estimation

The compressive strength of masonry typically exhibits a high variation relative to other building materials; a variation of 10% from measured to predicted values is considered reasonable (Blume and Proulx 1968). This is consistent with CSA Standard S304.14, which limits the coefficient of variation of tested compressive strengths to a maximum of 10% if less than ten masonry prisms are tested.

Dillon (2015) suggested using a regression model to predict the compressive strength of masonry prisms would not likely exceed the variation that would exist in measured prism tests. Thus, in a statistical analysis performed by Dillon (2015) of 593 individual prism tests, a model was proposed for predicting the compressive strength of hollow masonry prisms (Eq. (3.3)) and for predicting the compressive strength of grouted masonry prisms (Eq. (3.4)).

$$f'_m = v^{0.636} f_b^{0.688} f_j^{0.317} \quad (3.3)$$

$$f'_m = t^{-0.221} (1 - v)^{0.0818} f_b^{-0.425} (f_j + f_b)^{1.01} (f_g + f_b)^{0.312} \quad (3.4)$$

- where
- v = ratio of net to gross area
 - f_b = compressive strength of the brick or block
 - f_j = compressive strength of the mortar
 - t = thickness of the prism in the smallest dimension
 - f_g = compressive strength of the grout

In cases where the compressive strength of masonry prisms was not available from the reference, but the constituent material strengths (compressive strength of concrete block, mortar, and grout) were available (Haach et al. 2007; Johal and Anderson 1988; Minaie et al. 2010; Scrivener 1967; Tomaževič and Lutman 1988), the model proposed by Dillon (2015) (Eq. 3.3 and 3.4) is used to predict both the hollow and grouted masonry prism strength. However, where data was unavailable, the model could not be applied and the reference was not used (Meli et al. 1968; Meli and Salgado 1969; Tomaževič et al. 1996; Yancey and Scribner 1989).

3.4.3 Reported Shear Strength

While experimental studies using monotonic loading consistently documented the peak shear strength, the experimental studies using reverse cyclic loading were less consistent in reporting the shear strength. Some studies reported the average peak shear strength, some reported the peak shear strength in each loading direction, and others reported only the maximum shear strength obtained in one direction.

With a dataset of 176 specimens tested cyclically, Dillon (2015) generated a histogram of average to ultimate strength ratios and calculated an mean (expected) ratio of 0.94, illustrated in Fig. 3.37. Therefore, for studies that reported peak shear strength, a correction factor of 0.94 was applied to the ultimate shear strength and taken as the average shear strength of the wall.

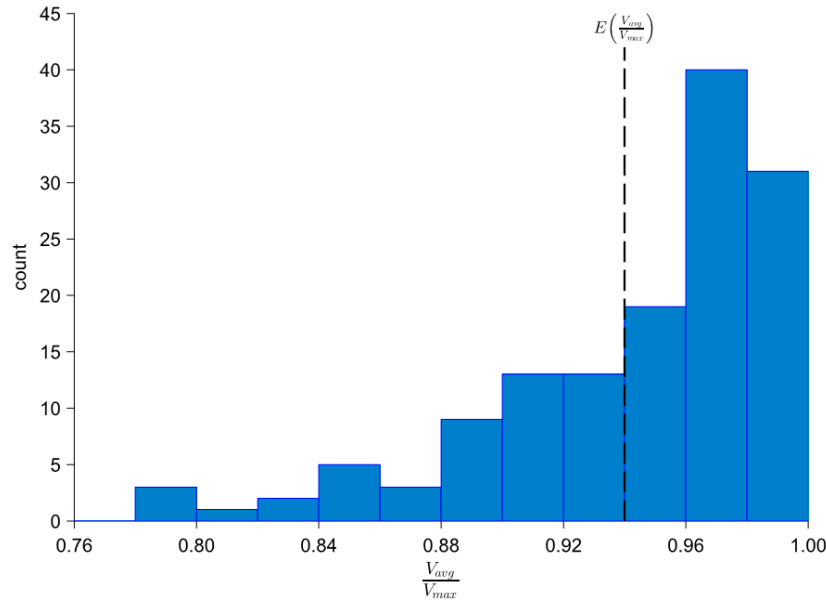


Figure 3.37 – Histogram of average to ultimate strength ratios (Dillon 2015)

3.4.4 Loading Pattern/Loading History

Various loading histories have been used in masonry research: monotonic, incrementally-increasing cyclic (reverse cyclic), sequential-phased displacement, and simulated seismic. Cyclic testing allows for the quantification of strength degradation, an important parameter to assess structural performance, which cannot be observed through monotonic loading. More cracks form from the repeated cycles of shear load, resulting in a lower shear capacity compared to monotonic loading (Dillon 2015). Dhanasekar and Haider (2011) concluded that ductility for PG masonry shear walls must be measured during cyclic load testing to understand its seismic response.

While an analysis by Dillon and Fonseca (2014b) found no significant statistical difference in shear strength among periodic and harmonic loading histories, the same study reported that walls tested monotonically had higher strength (by 19%, in average) compared to walls loaded periodically or harmonically. An earlier study by Tomažević et al. (1996) had confirmed a cyclic-to-monotonic strength ratio of 0.81, with a 95% confidence interval bounded between 0.72 and 0.91.

In this study, a correction factor of 0.81 is applied to monotonically loaded specimens in this study to transform the strength into that of an equivalent, cyclically tested wall.

3.4.5 Loading Rate

Dynamic loading produces a higher strain rate than monotonic loading, which results in a greater shear capacity than that obtained through quasi-static loading. A total of twelve pairs of specimens over three studies comparing the effect of dynamic loading vs. quasi-static loading on the shear strength of masonry walls [Williams (1971), Mayes et al. (1976b), and Tomažević et al. (1996)] was used by Dillon (2015) to suggest a correction factor of 0.9 applied to monotonically loaded specimens to transform the strength into that of an equivalent, dynamic loading tested wall.

3.4.6 Scaling

Some experimental studies have tested walls at 1/2-scale or 1/3-scale, due to the high cost of full-scale testing. There are two main techniques to account for scaling: the Simple Model and the Complete Model. Whereas the Complete Model includes the scaling of all geometric, material and loading properties, the Simple Model does not scale the strength, stress, strain, Young's modulus, and loading rate/velocity. A comparison of the two models is summarized in Fig. 3.38.

Quantity	General equation	Complete model	Simple model
Length (L)	$S_L = L_P/L_M$	S_L	S_L
Strain (ϵ)	$S_\epsilon = \epsilon_P/\epsilon_M$	1	1
Strength (f)	$S_f = f_P/f_M$	S_L	1
Stress (σ)	$S_\sigma = \sigma_P/\sigma_M$	S_L	1
Young's modulus (E)	$S_E = E_P/E_M$	S_L	1
Sp. weight (Γ)	$S_\Gamma = \Gamma_P/\Gamma_M$	1	1
Force (F)	$S_F = S_L^2 S_f$	S_L^3	S_L^2
Time (t)	$S_t = S_L \sqrt{S_\Gamma S_\epsilon / S_f}$	$\sqrt{S_L}$	S_L
Frequency (Ω)	$S_\Omega = 1/S_t$	$1/\sqrt{S_L}$	$1/S_L$
Displacement (d)	$S_d = S_L S_\epsilon$	S_L	S_L
Velocity (v)	$S_v = S_\epsilon \sqrt{S_f / S_\Gamma}$	$\sqrt{S_L}$	1
Acceleration (a)	$S_a = S_f / S_L S_\Gamma$	1	$1/S_L$

Figure 3.38 – Complete Model scaling vs. Simple Model scaling (Tomažević and Velechovsky 1992)

In each study testing scaled specimens, the Simple Model scaling has been used over Complete Model scaling due to difficulty in scaling material properties such as Young's modulus. However, based on a study by Abrams and Kreger (1982) consisting of eighteen 1/12th scale specimens investigating the effect of scaling in reinforced concrete elements, it was found that the strength and stiffness behaviour and energy dissipation are modeled correctly at small scales. Though the study was not performed on masonry elements, the similarity in material suggest that the results from the study are likely valid for masonry. Additionally, it is argued by Dillon and Fonseca (2014a) that most size effects are taken into account by testing reduced-scale masonry prisms. Research performed by Bažant (1997) and Bažant and Yu (2009) on quasi-brittle materials such as concrete and masonry suggests that the scaling factor for strength and other material properties is approximately a function of the scale and largest aggregate size. Resultingly, no correction factors are applied to scaled walls; rather, the equivalent full-scale form of each wall is used for analysis.

3.5 Dataset Summary

An experimental dataset totaling 292 PG masonry shear walls was compiled from 27 independent studies. This dataset is termed “Complete” (Table 3.1) and is presented in its entirety in Appendix A.

Five subsets of the dataset have been generated for neural network analysis, to account for the effects of major variables. The five subsets possess generally increasing levels of data scrutinization and synthesization as described in Section 3.3 and Section 3.4. Dataset “A” excludes all studies in which the compressive strength of the masonry could not be calculated, while dataset “B” excludes those specimens that were tested under monotonic loading. Dataset “C” is a variant of dataset “B”, where the horizontal reinforcement considered for analysis is modified based on the assumption that any bond beams at the bottom course do not provide additional shear resistance. Dataset “D” is the same as dataset “C” but excludes also the specimens tested using the ESECMaSE setup. Dataset “E” is a variant of dataset “D”, in the same sense that dataset “C” is a variant of dataset “B”. Finally, Dataset “F” is a variant of dataset “E,” where only the interior (web)

reinforcement is considered as vertical reinforcement contributing to the shear strength of PG walls. The dataset variations are summarized in Table 3.1, and the summary of which studies are included in each dataset are is summarized in Table 3.2.

Table 3.1 – PG dataset variations for neural network analysis

Description	Dataset						
	Complete	A	B	C	D	E	F
Number of specimens	292	255	150	150	120	120	120
Data synthesization	✓	✓	✓	✓	✓	✓	✓
Specimens without sufficient information to predict $f'_{m,eff}$ removed		✓	✓	✓	✓	✓	✓
Monotonic specimens removed			✓	✓	✓	✓	✓
ESECMaSE specimens removed					✓	✓	✓
Horizontal reinforcement modified				✓		✓	✓
Boundary vertical reinforcement neglected; only interior vertical bars considered							✓

Table 3.2 – Summary of PG Wall Datasets

Source	Dataset			
	Complete	A	B, C	D, E, F
Scrivener (1967)	12	12	-	-
Meli et al. (1968)	10	-	-	-
Meli and Salgado (1969)	11	-	-	-
Mayes et al. (1976)	2	2	2	2
Chen et al. (1978)	4	4	4	4
Thurston and Hutchinson (1982)	3	3	3	3
Matsumura (1987)	29	29	29	29
Tomažević and Lutman (1988)	10	10	10	10
Johal and Anderson (1988)	16	16	16	16
Yancey and Scribner (1989)	10	-	-	-
Ghanem et al. (1992)	2	2	-	-
Ghanem et al. (1993)	2	2	-	-
Tomažević et al. (1996)	6	-	-	-
Schultz (1996)	6	6	6	6
Schultz et al. (1998)	6	6	6	6
Voon and Ingham (2006)	2	2	2	2
Haach et al. (2007)	4	4	4	4
Maleki et al. (2009)	5	5	5	5
Elmapruk (2010)	6	6	6	6
Minaie et al. (2010)	4	4	4	4
Baenziger and Porter (2011)	8	8	8	8
Nolph and Elgawady (2012)	5	5	5	5
Oan (2013)	66	66	-	-
Hoque (2013)	18	18	16	-
Hamedzadeh (2013)	21	21	-	-
Rizaei (2015)	14	14	14	-
Ramírez et al. (2016)	10	10	10	10
# of specimens in dataset	292	255	150	120

3.6 Distribution of Specimen Parameters

The distribution of specimen parameters is presented in Figs. 3.39 to 3.48. The purpose of this is to present the range of data studied, as well as provide insight into the gaps which exist within each dataset.

Some observations can be made from the distributions presented:

- Almost all the samples are tested under a quasi-static loading rate; only 7 samples from three PG wall studies (Chen et al. 1978; Tomazevic and Lutman 1996) use dynamic loading rates, suggesting a gap in understanding the behaviour of PG walls under dynamic loads.
- The majority of walls have an area ($H \times L$) of 5 m² or less. Although there are currently no studies that have investigated the size effect of PG shear walls, a study by Sarhat and Sherwood (2015) on reinforced masonry beams observed smaller shear stress capacities and more brittle behaviour was in larger specimens due to larger crack spacing and crack width as the effective depth of the beam is increased. In a literature review by Minaie (2009), it was found that most experimental programs tested walls that were smaller than masonry shear walls found in typical buildings.
- Most experimental studies have focused solely on aspect ratios of 1 or less. This is explained in part due to the increased likelihood of PGM walls to exhibit flexural-shear failure or flexural failure as the aspect ratio is increased (Haider 2007).
- Recent studies suggest that the square root relationship loses accuracy in extremely high or low masonry compressive strength values (Dillon 2015). Most experimental studies have built PGM walls with masonry blocks with typical strengths, but little experimental investigation has been performed for PGM walls using high strength masonry.
- Although the majority of experiments conducted involve a horizontal reinforcement ratio of 0-0.2%, it has been reported by several authors that horizontal reinforcement ratios above 0.2% lead to a negligible increase in ultimate strength and deformation

(Elmapruk 2010; Fattal 1993b; Haach et al. 2012; Hamid and Moon 2005; Shing et al. 1990b).

- The range of axial load is less when comparing dataset “A” with datasets “D”, “E” and “F,” revealing a gap in walls tested under reverse cyclic loading with a realistic test set-up.
- Many wall specimens are exclusively reinforced in the vertical direction with boundary vertical reinforcement, revealing a gap in walls tested with distributed and/or interior vertical reinforcement as shown in Fig. 3.45.
- The range of gross shear strength is significantly less when comparing dataset “A” with datasets “D”, “E”, and “F”, revealing a gap in high-strength PG shear walls ($v_n > 1.2$ MPa) tested under reverse cyclic loading and with a realistic test set-up.

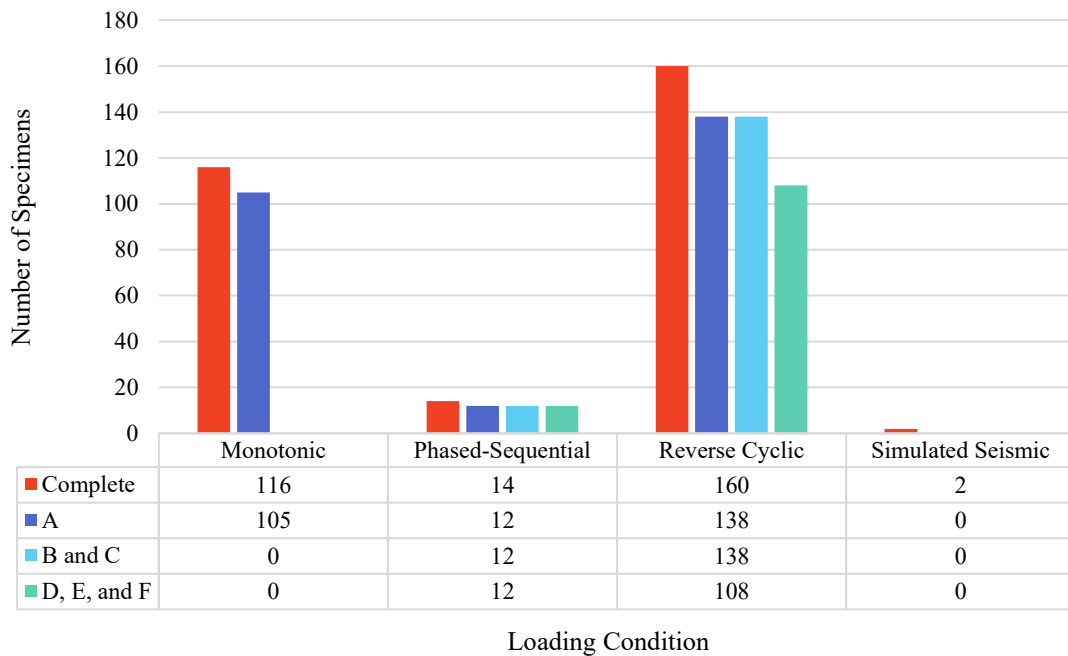


Figure 3.39 – Distribution of loading conditions for PG wall specimens

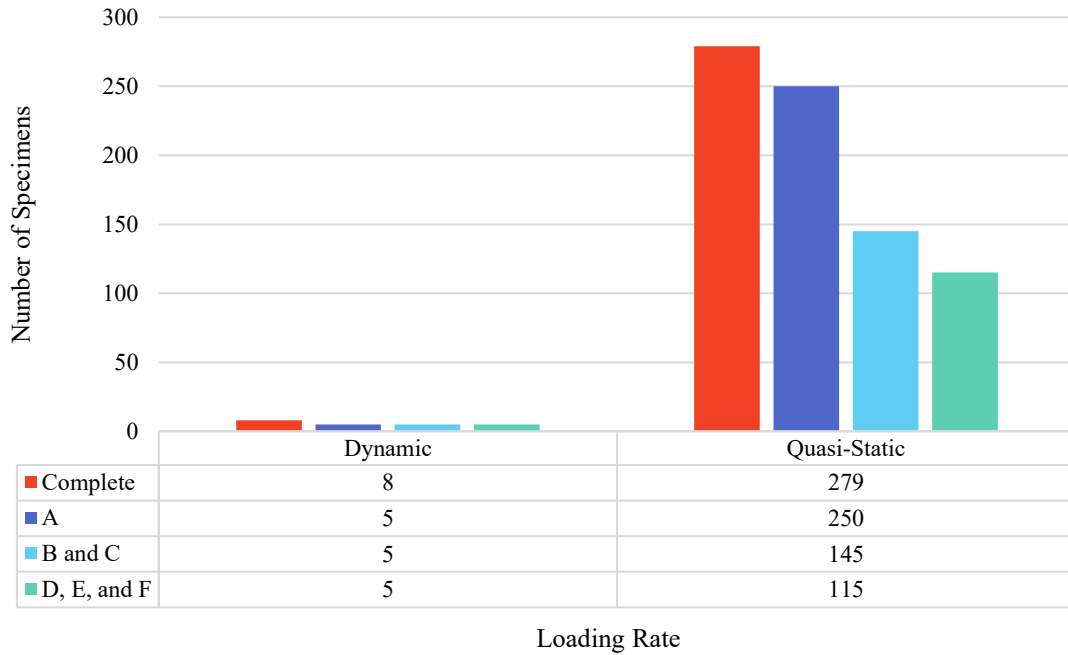


Figure 3.40 – Distribution of loading rates for PG wall specimens

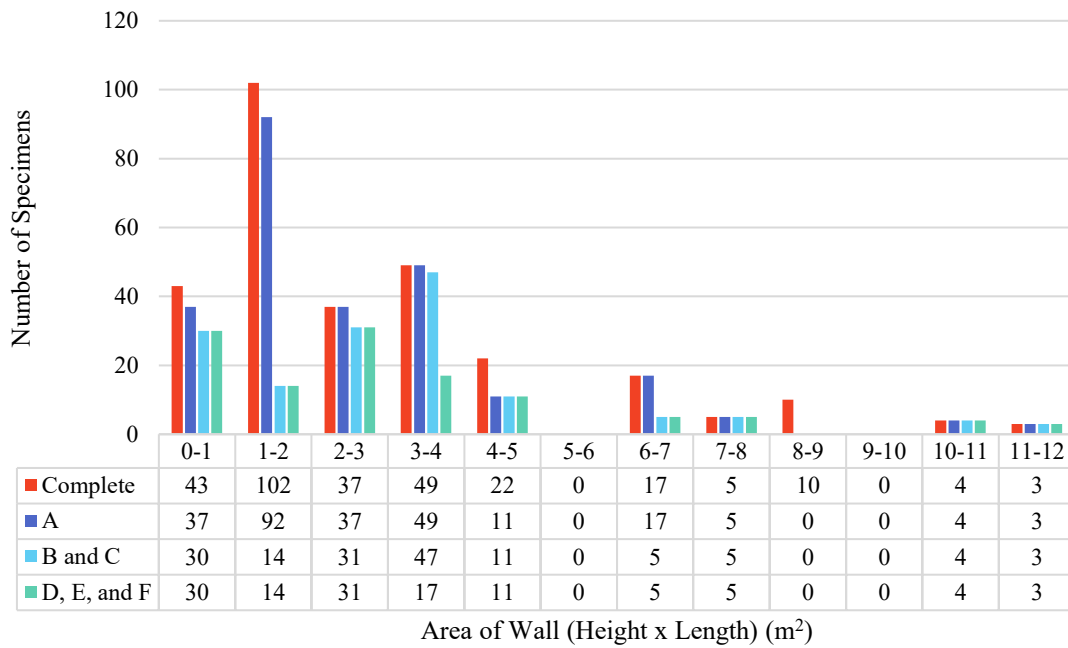


Figure 3.41 – Distribution of wall areas for PG wall specimens

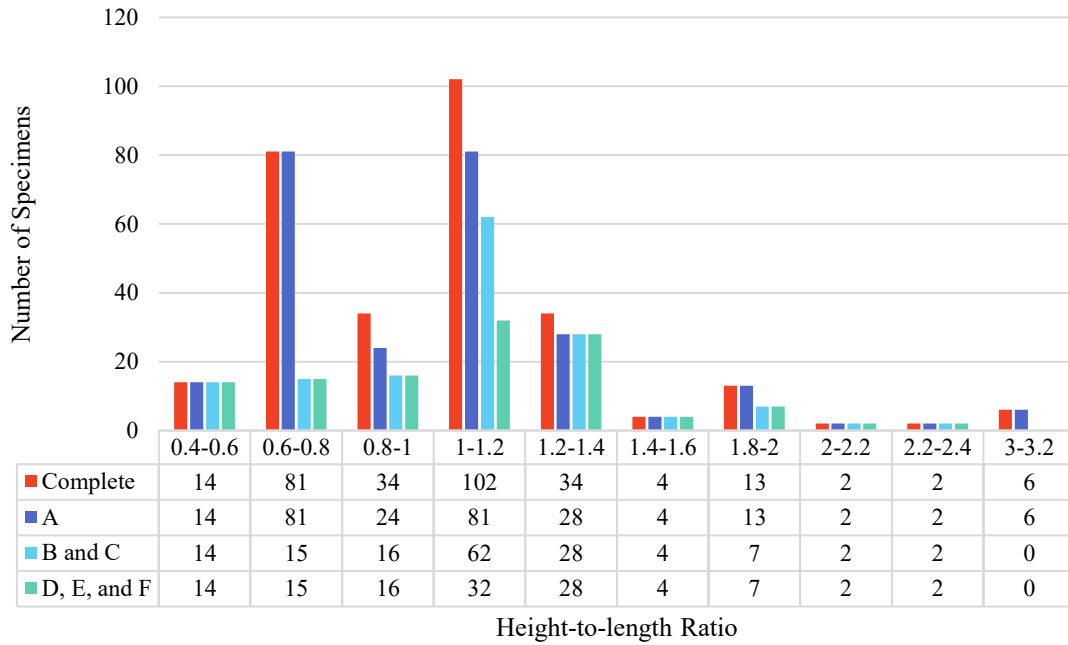


Figure 3.42 – Distribution of height-to-length ratios $\left(\frac{H}{L}\right)$ for PG wall specimens

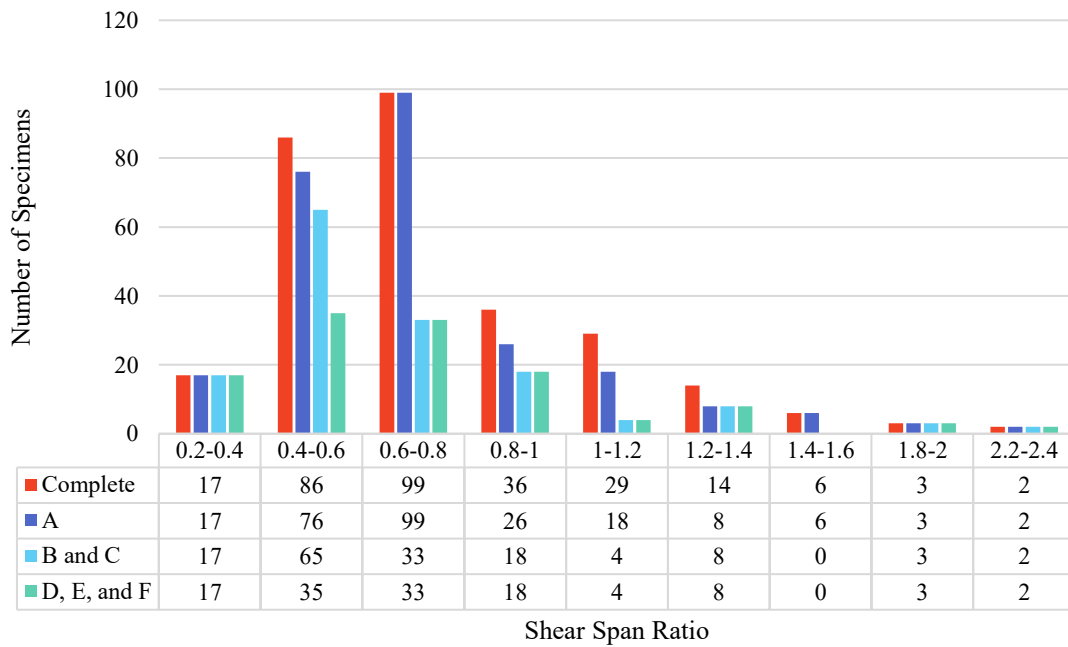


Figure 3.43 – Distribution of shear span ratios $\left(\frac{M}{VL}\right)$ for PG wall specimens

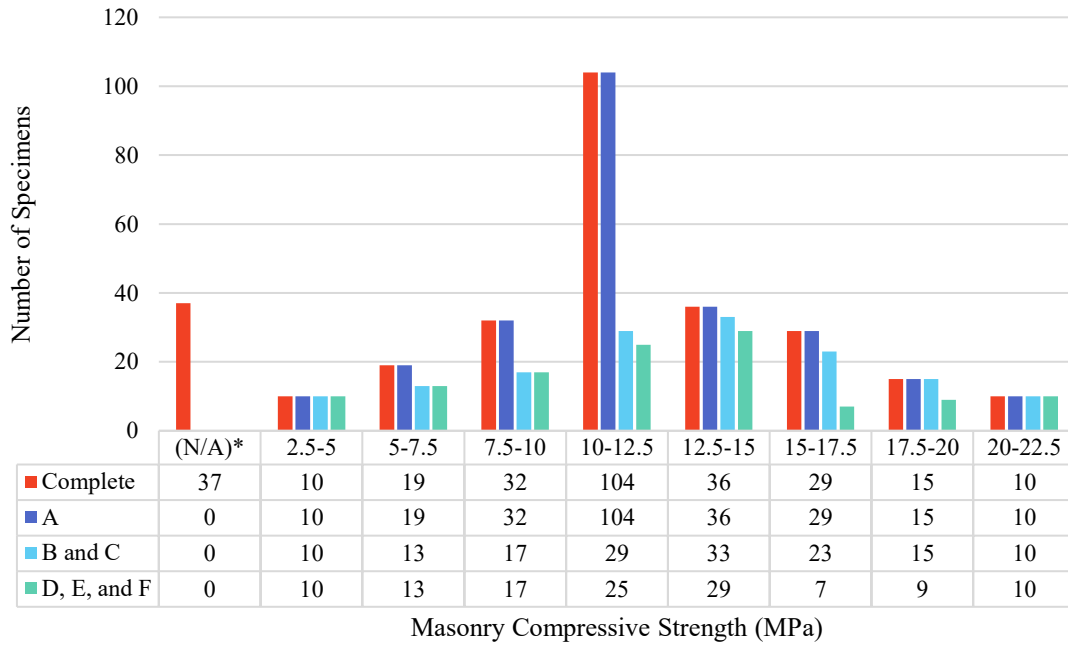


Figure 3.44 – Distribution of corrected masonry strengths (f'_m) for PG walls

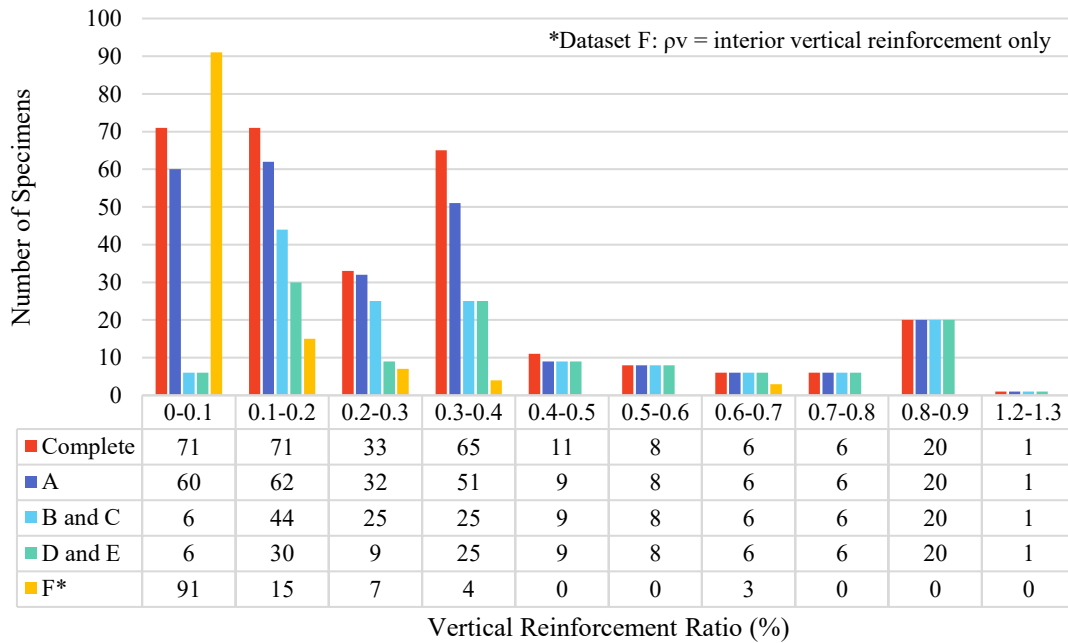


Figure 3.45 – Distribution of vertical reinforcement (ρ_v) in PG wall specimens

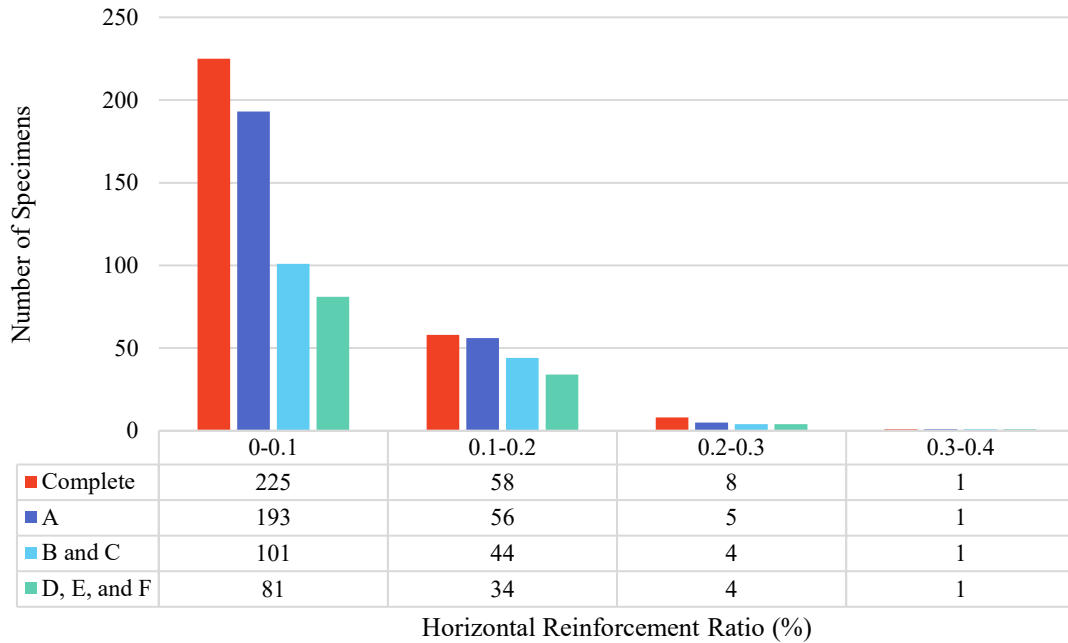


Figure 3.46 – Distribution of horizontal reinforcement (ρ_h) in PG wall specimens

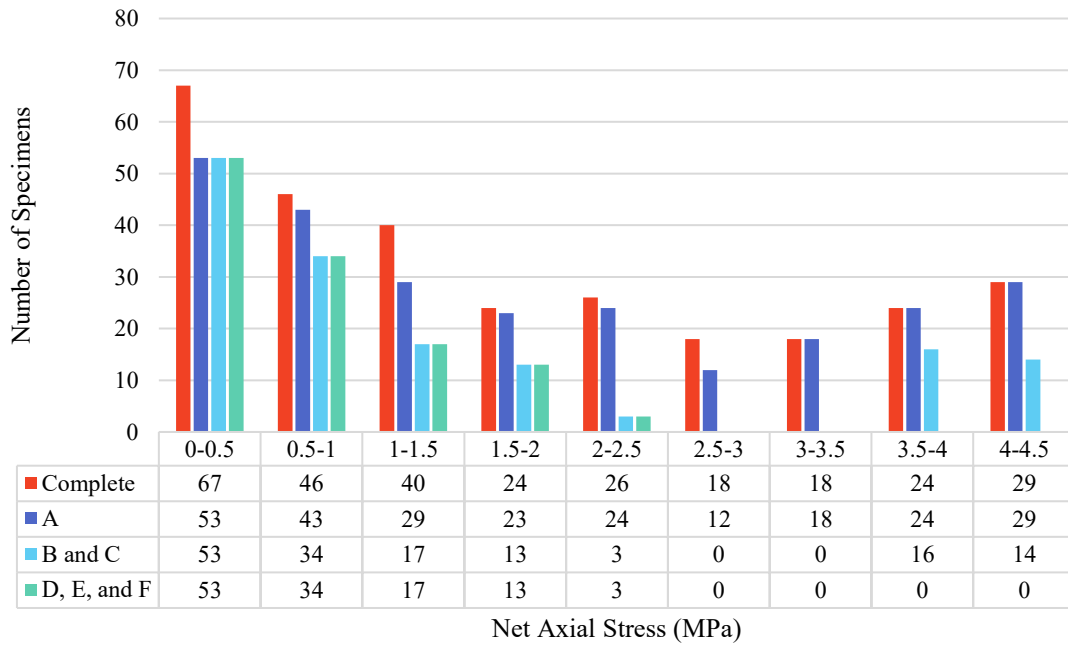


Figure 3.47 – Distribution of applied axial loads (σ_n) on PG wall specimens

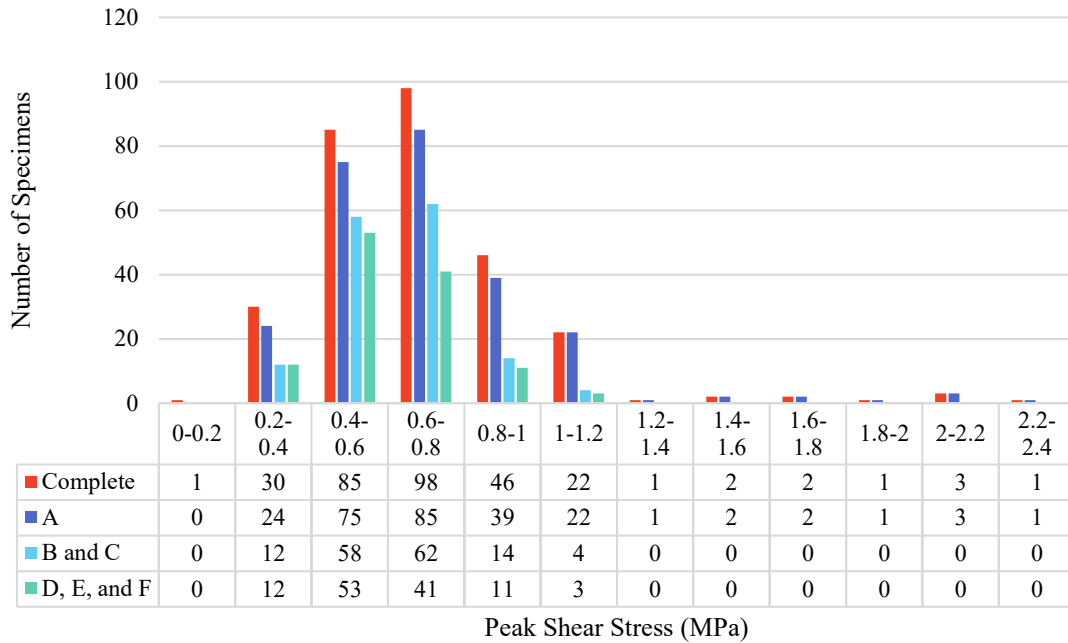


Figure 3.48 – Distribution of peak shear stress ($v_{n,max}$) of PG wall specimens

3.7 Evaluating the Performance of Existing Predictions

To provide a benchmark and statistical comparisons of model performance, each design expression explained in Chapter 2 is used to predict the shear strength of PG walls in the complete dataset. First, a brief description of the statistical performance metrics used are presented, followed by a statistical evaluation of existing models. Further details regarding statistical metrics can be found in Casella (1983), Chatterjee and Hadi (2006), Dillon (2015), Eisenhauer (2003), Frost (2012), Kozak and Kozak (1995), and Montgomery et al. (2012).

3.7.1 Mean

A mean value for the V_{exp}/V_n ratio greater than one indicates that the predictive model tends to overpredict the shear capacity, whereas a ratio less than one indicates the tendency to predict non-conservative shear strengths. The sample mean formula is given by Eq. (3.5).

$$\text{Mean} = \frac{\overline{V_{exp}}}{V_n} = \frac{\sum \frac{V_{exp}}{V_n}}{N} \quad (3.5)$$

3.7.2 Standard Deviation

The standard deviation represents the extent of dispersion of the V_{exp}/V_n ratio from its mean value. A mean value close to one combined with lower standard deviation values is desirable, indicating more accurate predictions. The sample standard deviation formula is given by Eq. (3.6).

$$\text{Standard Deviation} = \sqrt{\frac{\sum \left(\frac{V_{exp}}{V_n} - \frac{\overline{V_{exp}}}{V_n} \right)^2}{N - 1}} \quad (3.6)$$

3.7.3 Mean Squared Error (MSE)

The mean squared error is a measurement of the average of the squares of the errors or residuals between the predicted and experimental values. It is often used as a performance metric to provide an indication of both the accuracy and precision of an estimator. The formula for mean squared error is given by Eq. (3.7).

$$\text{MSE} = \sum_{i=1}^N \frac{(y_i - \hat{y}_i)^2}{N} \quad (3.7)$$

where N = number of samples
 \hat{y}_i = predicted (model) output
 y_i = experimental (observed) output

3.7.4 Fifth Percentile

The fifth percentile of the V_{exp}/V_n ratio represents the V_{exp}/V_n ratio exceeded by 95% of the walls in the dataset. A high value of the fifth percentile of the V_{exp}/V_n ratio indicates a more conservative prediction model.

For instance, a fifth percentile of $V_{exp}/V_n = 1.00$ indicates that 95% of shear walls in the dataset failed at loads equal to, or higher than, the predicted shear load. A hypothetical percentile distribution curve has been generated to illustrate this example in Fig. 3.49.

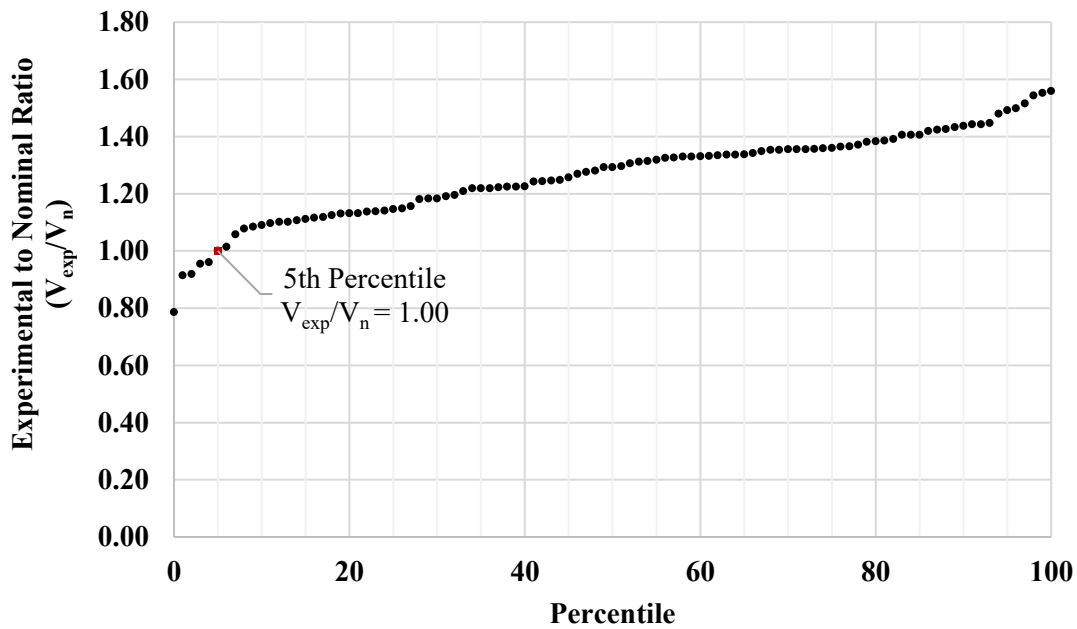


**Figure 3.49 – Hypothetical percentile distribution curve
(5% of samples exhibit $V_{exp} < V_n$)**

3.7.5 Residuals

Residuals are defined as the difference between the experimental (observation) value and the corresponding prediction (model) value, given by Eq. (3.8).

$$e_i = y_i - \hat{y}_i \quad (3.8)$$

where e_i = residual between an observation and its predicted value

A plot of the residuals offers a visual representation of whether the model exhibits homoscedasticity; a homoscedastic plot will exhibit minimal variation in its residuals regardless of the magnitude of predicted value, shown in Fig. 3.50(a). Conversely, a heteroscedastic plot of residuals exhibits non-uniform variance across the range of predicted values. In Fig. 3.50(b), for example, the residuals plot indicates that the predictive model is more accurate when predicting low values but becomes highly inconsistent when predicting higher values. It is most desirable for a model to exhibit homoscedasticity (Mongometry et al. 2012).

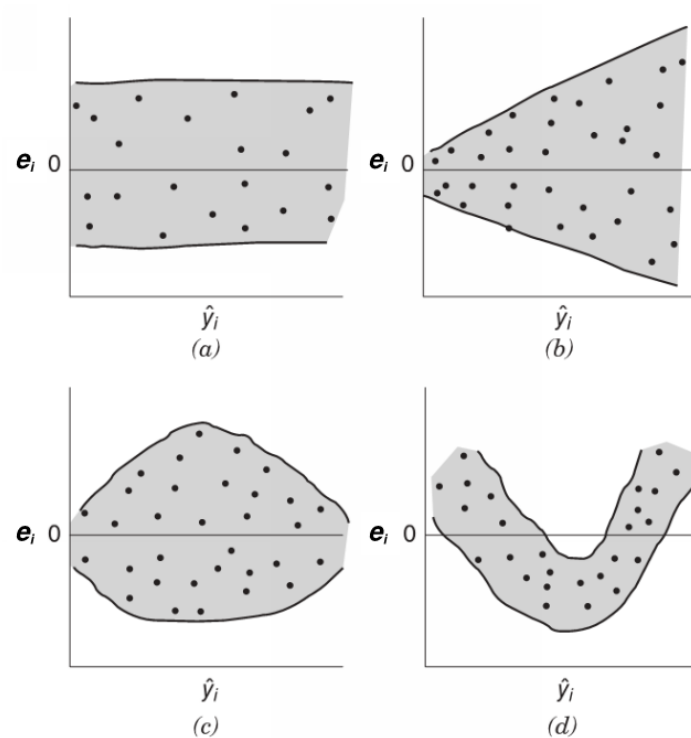


Figure 3.50 – Plot of residuals, e_i , versus corresponding fitted values, \hat{y}_i . Patterns for residual plots: (a) satisfactory (homoscedastic); (b) heteroscedastic; (c) double bow; (d) non-linear (Adapted from Mongometry et al. 2012)

3.7.6 Performance of Existing Predictions

Table 3.3 summarizes the performance metrics for the existing models. The performance of trained neural network models is evaluated and presented in the same way in Chapter 4 for comparison.

Table 3.3 – Performance metrics for existing models

Model	MSE (MPa)	Mean $\frac{V_{exp}}{V_n}$	Std Dev $\frac{V_{exp}}{V_n}$	Fifth Percentile $\frac{V_{exp}}{V_n}$
Matsumura (1987)	0.163	2.263	1.855	0.369
AIJ (1987)	0.242	1.299	1.320	0.325
Shing et al. (1990)	0.199	0.916	0.489	0.334
Anderson and Priestley (1992)	0.139	0.782	0.316	0.469
Fattal (1993)	0.181	0.993	0.776	0.162
NEHRP (1997)	0.168	0.921	0.524	0.419
UBC (1997)	0.114	1.051	0.526	0.505
NZS-4230 (2004)	0.450	1.917	1.077	0.375
Eurocode 6 (2005)	1.218	0.972	0.896	0.191
Voon (2007)	0.113	1.073	0.531	0.527
IMNC (2010)	0.090	1.164	0.561	0.617
CSA-S304.14 (2014)	0.170	1.338	0.666	0.453
Dillon (2015)	0.110	1.505	0.684	0.793
TMS 402/602 (2016)	0.111	1.223	0.691	0.678

A plot of experimental strength vs. predicted strengths, and a plot of its residuals follows to illustrate the predictive capacity of each model. A few observations are made from the performance metrics and plots presented:

- The residual plots of each model reveal varying degrees of heteroscedasticity; all models tend to over-predict walls with lower shear strength, and significantly over-

predict walls with higher shear strength, although it is noted that there are relatively fewer samples with higher shear strength for evaluating the models.

- The model given by Eurocode 6 (2005) appears to be the worst performing model based on both the plots and the performance metrics. This is largely due to the code equation limiting the shear strength of masonry is limited to 0.3 MPa. It also does not distinguish between FG and PG walls.
- Although the model proposed by Matsumura (1987) has a reasonable mean-squared error in comparison to the other models, it has a high mean V_{exp}/V_n while having a low fifth percentile V_{exp}/V_n . This is non-ideal, indicating a tendency to severely overpredict shear strength, yet simultaneously being relatively under-conservative, suggesting a large spread in V_{exp}/V_n also reflected in the high standard deviation.
- The NZS-4230 (2004) has a relatively low fifth percentile, indicating a high likelihood for it to predict unconservative shear strengths. Notably, Voon (2007)'s study proposes an improved model based on the NZS-4230 (2004) model and exhibits significant improvement in performance metrics.
- Interestingly, the IMNC (2010) makes no distinction between FG and PG walls yet exhibits the lowest mean-squared error out of all the models.
- The model proposed by Dillon (2015) exhibits the lowest mean-squared error. Its performance metrics and plots are very similar to those for CSA-S304.14 (2014) and TMS 402/602 (2016), which is expected due to the similarity in the form of these equations but with different coefficients. Notably, Dillon (2015) achieves a slightly better prediction, perhaps due to the inclusion of vertical reinforcement contribution to PG wall shear strength.
- Overall, there is certainly room for improvement; an improved model would exhibit lower mean-squared errors, a mean V_{exp}/V_n closer to 1, lower V_{exp}/V_n standard deviation, higher fifth percentile V_{exp}/V_n . It would also exhibit homoscedasticity in its residual plots.

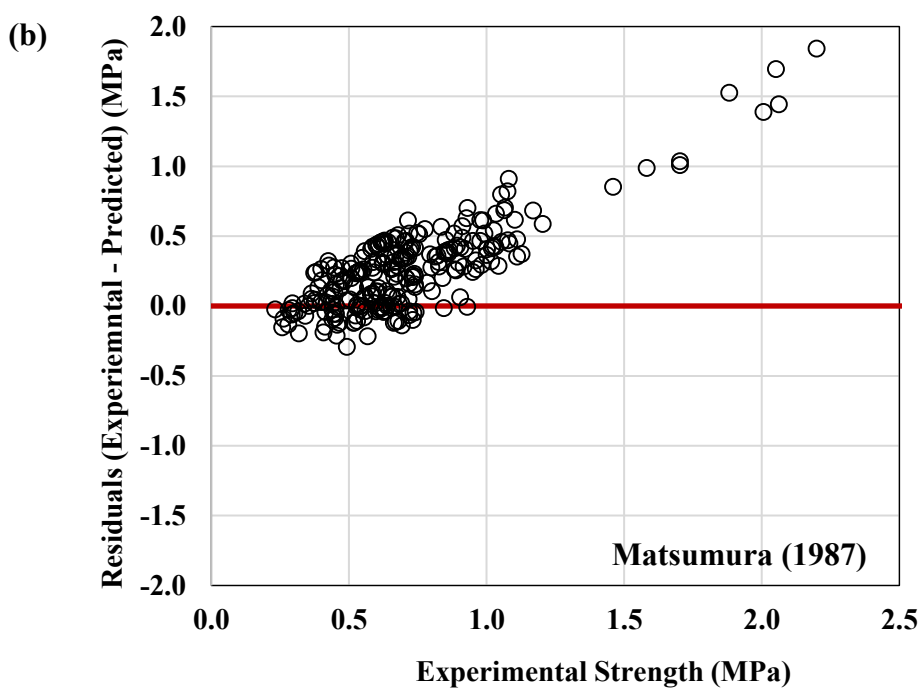
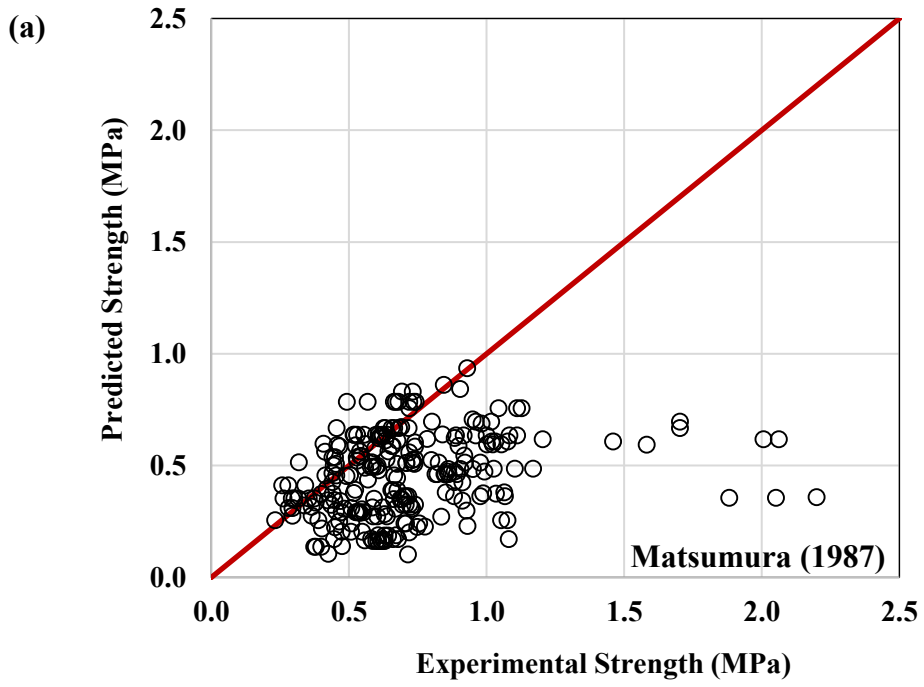


Figure 3.51 – Matsumura (1987) model predictions; (a) Experimental strength vs. Predicted strength; (b) Experimental strength vs. Residuals

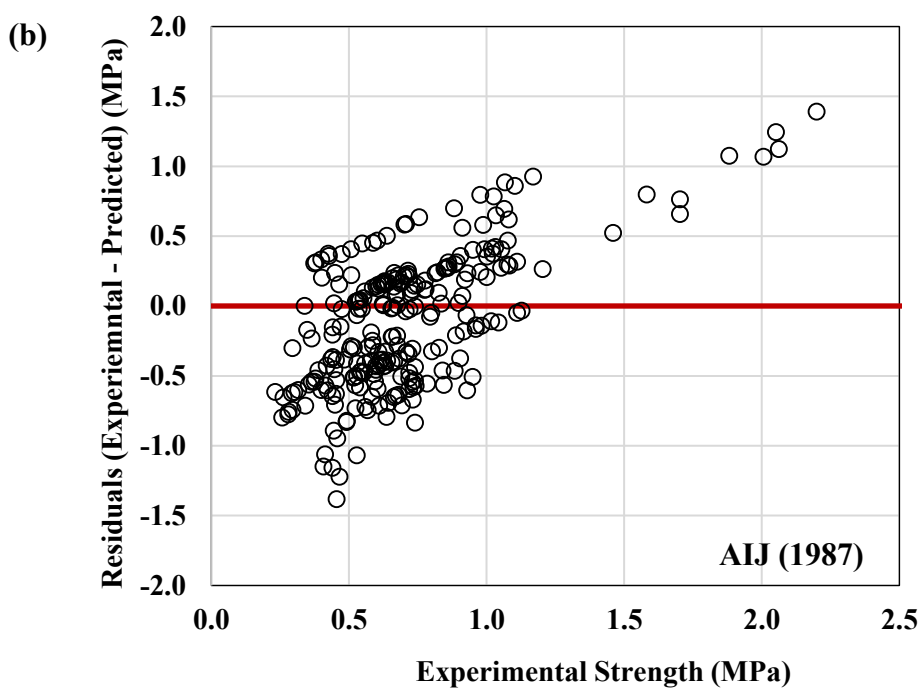
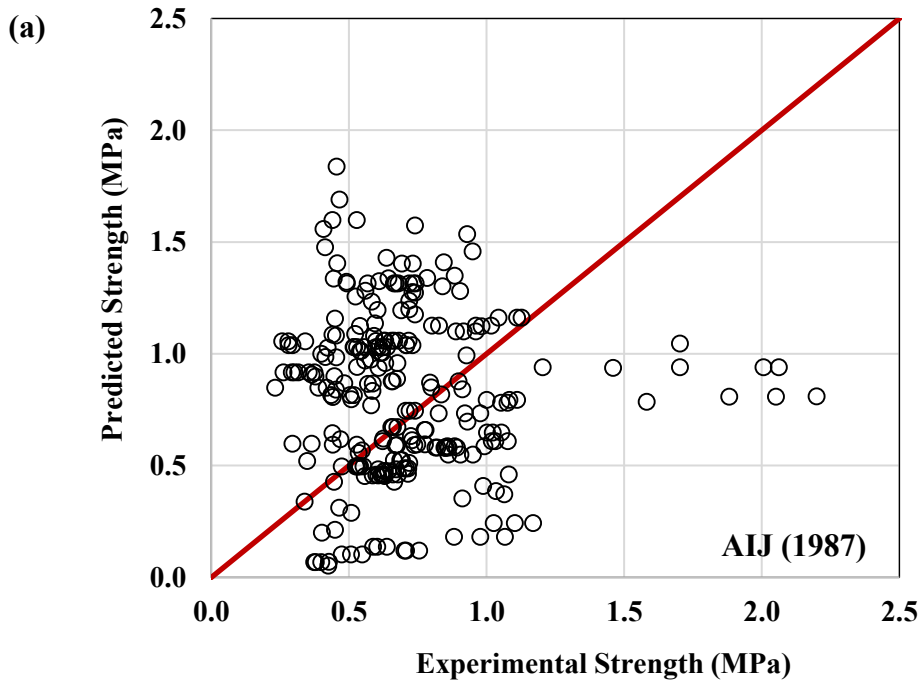


Figure 3.52 – AIJ (1987) model predictions; (a) Experimental strength vs. Predicted strength; (b) Experimental strength vs. Residuals

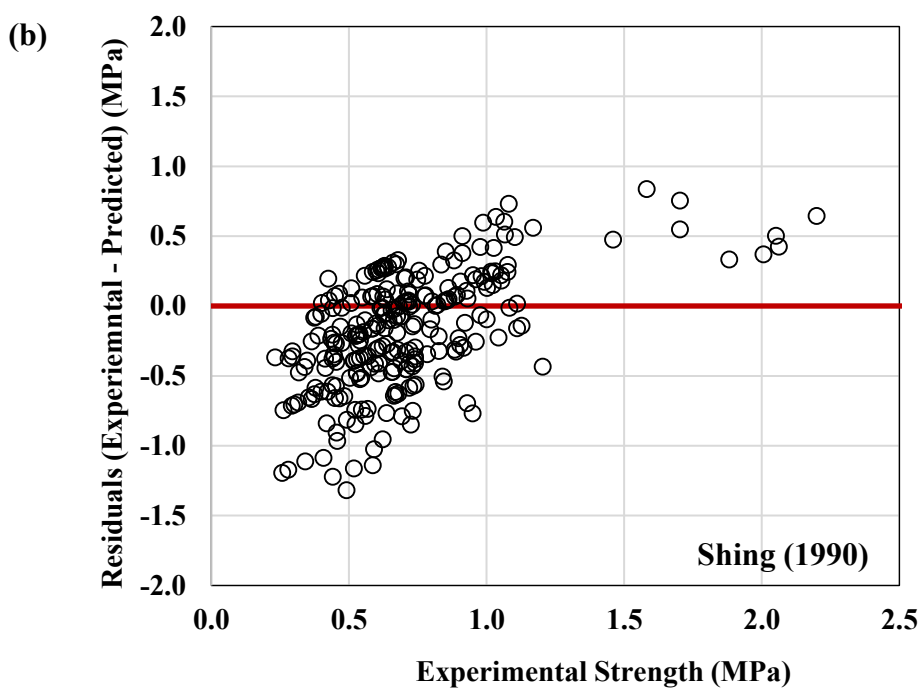
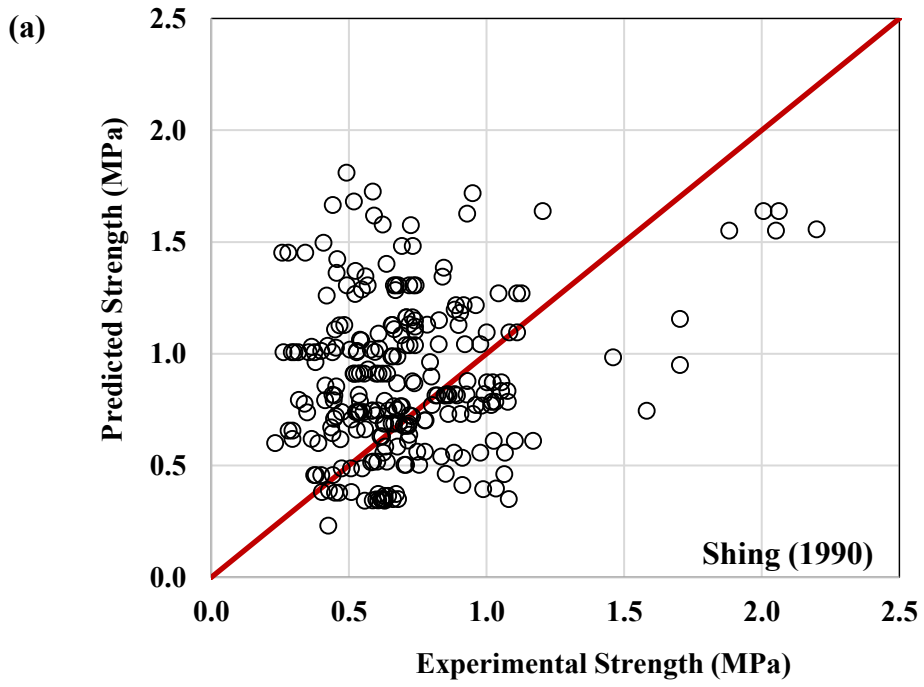


Figure 3.53 – Shing (1990) model predictions; (a) Experimental strength vs. Predicted strength; (b) Experimental strength vs. Residuals

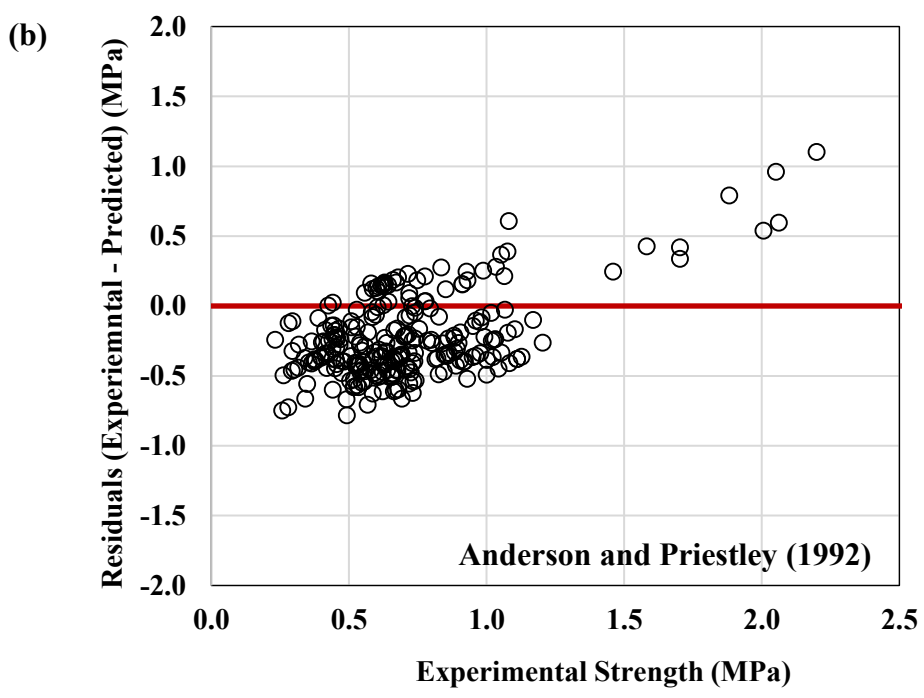
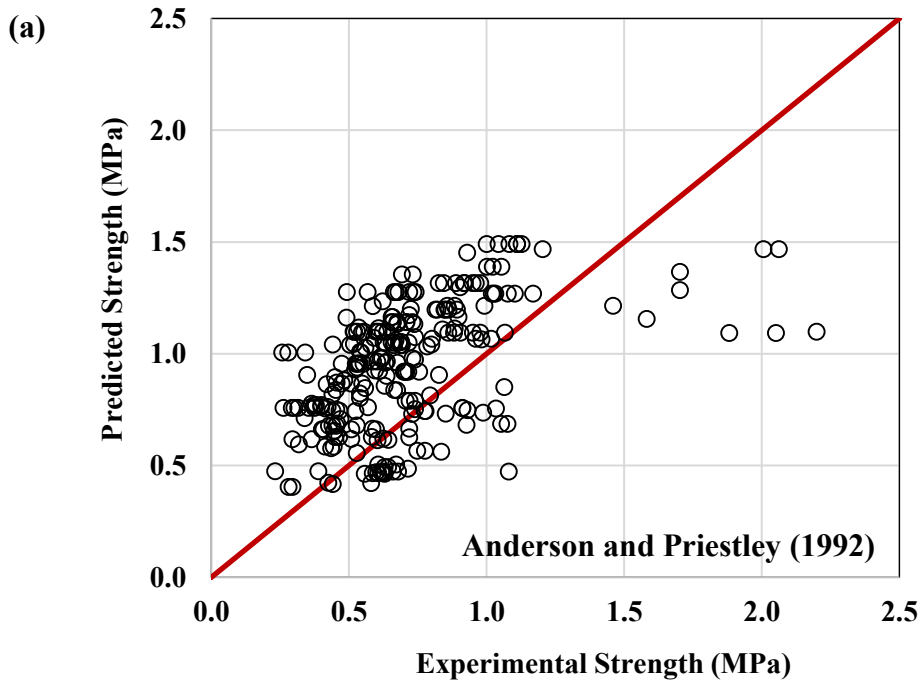


Figure 3.54 – Anderson and Priestley (1992) model predictions; (a) Experimental strength vs. Predicted strength; (b) Experimental strength vs. Residuals

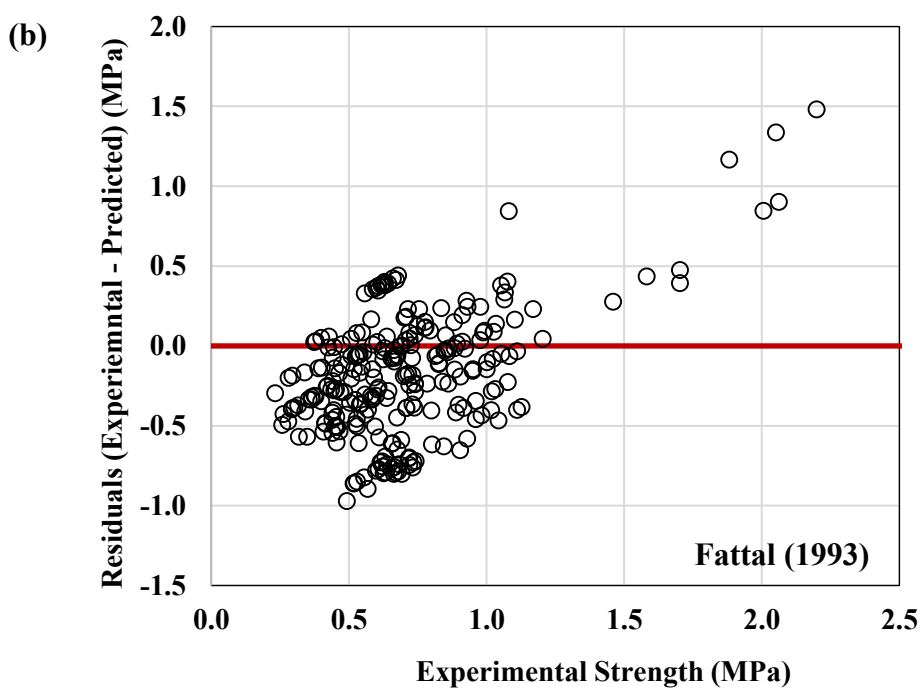
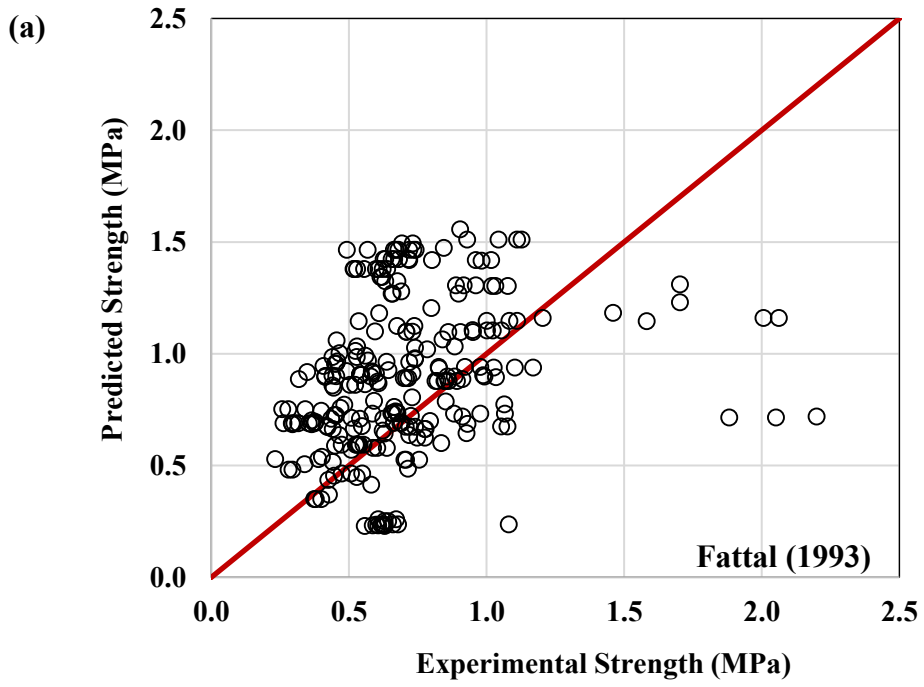


Figure 3.55 – Fattal (1993) model predictions; (a) Experimental strength vs. Predicted strength; (b) Experimental strength vs. Residuals

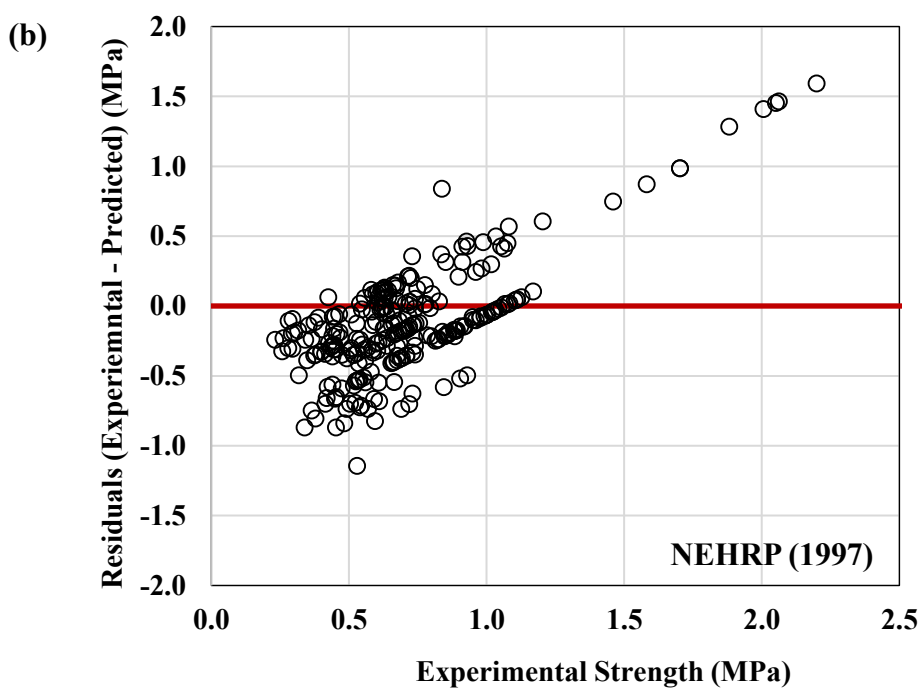
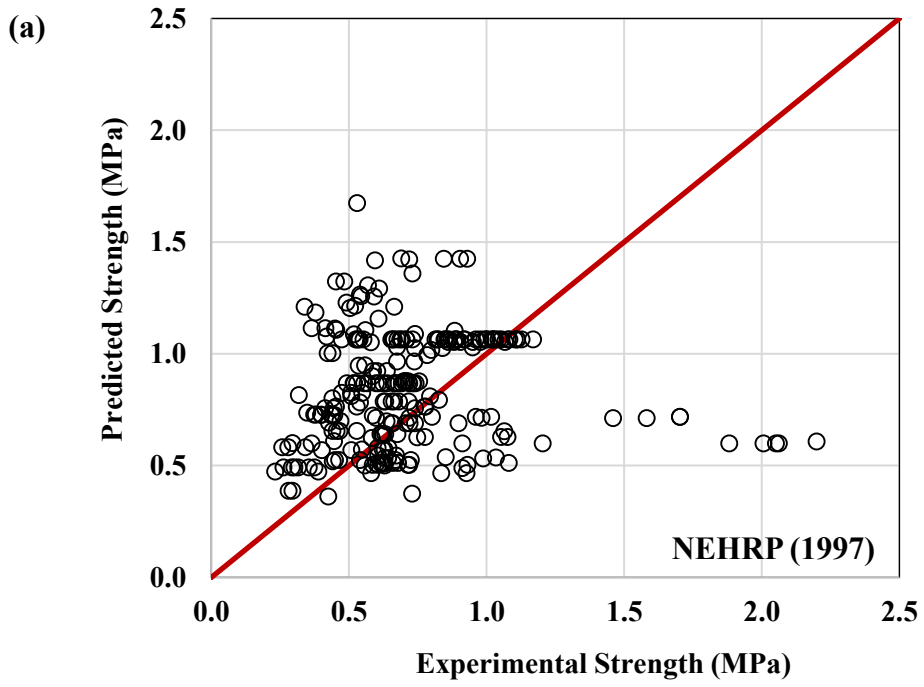


Figure 3.56 – NEHRP (1997) model predictions; (a) Experimental strength vs. Predicted strength; (b) Experimental strength vs. Residuals

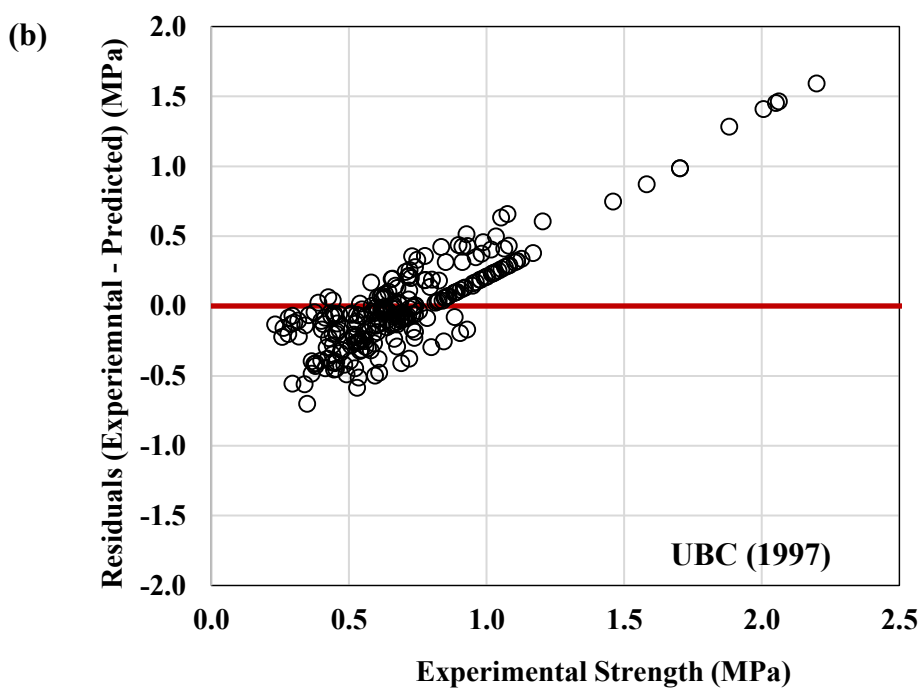
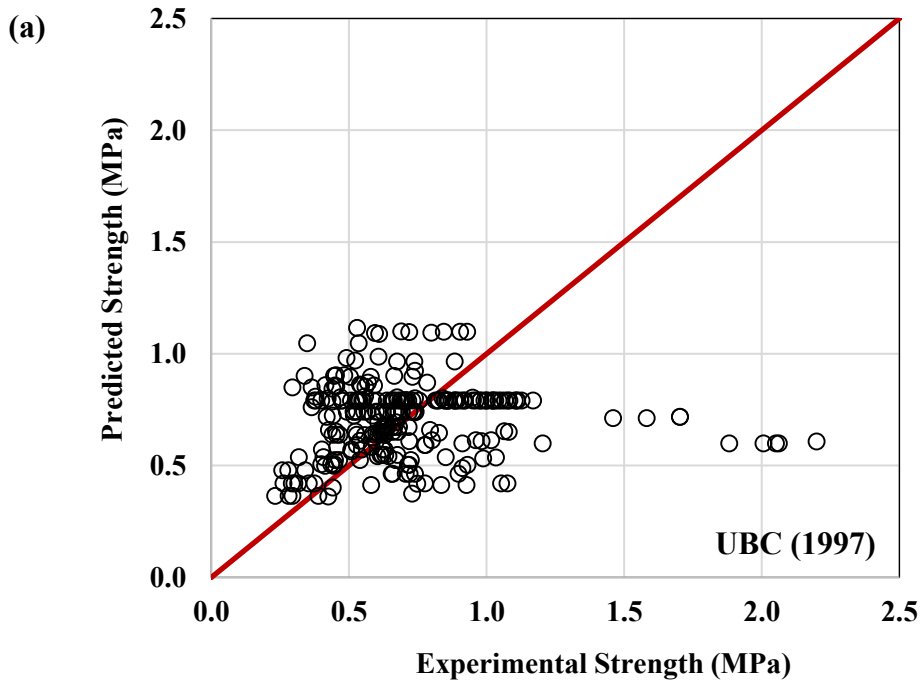


Figure 3.57 – UBC (1997) model predictions; (a) Experimental strength vs. Predicted strength; (b) Experimental strength vs. Residuals

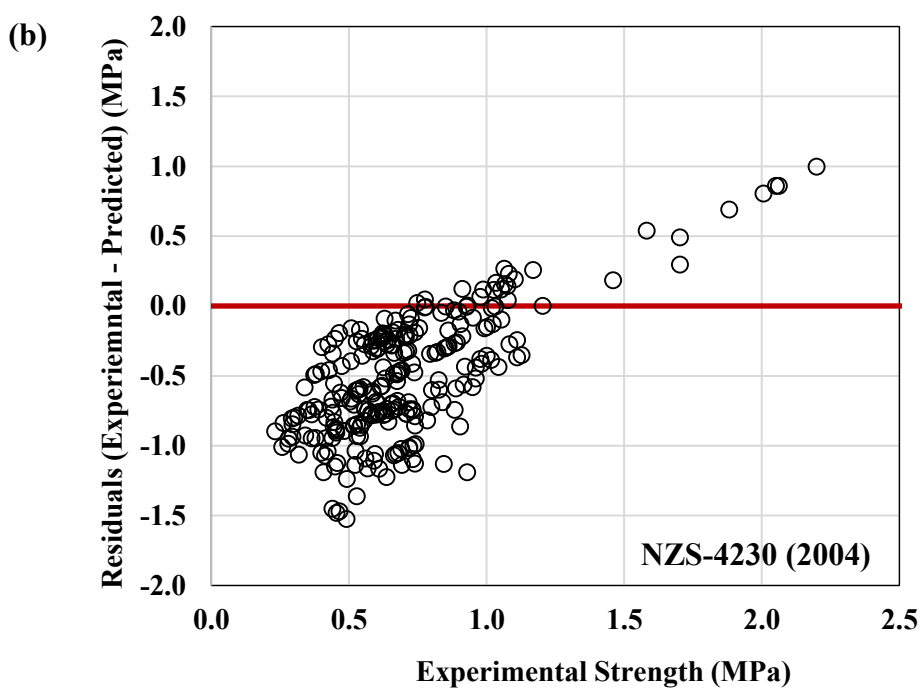
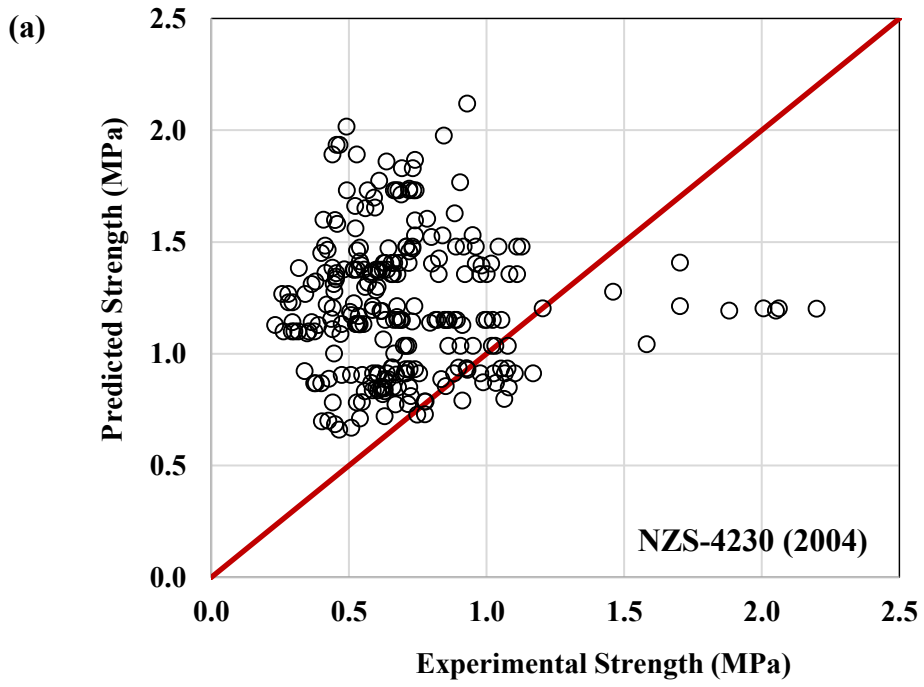


Figure 3.58 – NZS-4230 (2004) model predictions; (a) Experimental strength vs. Predicted strength; (b) Experimental strength vs. Residuals

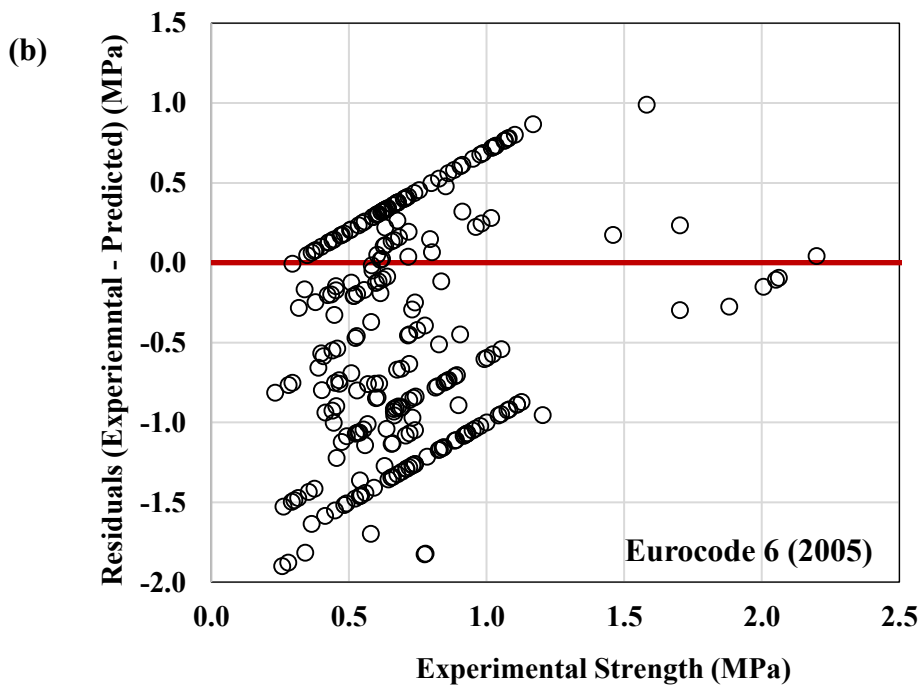
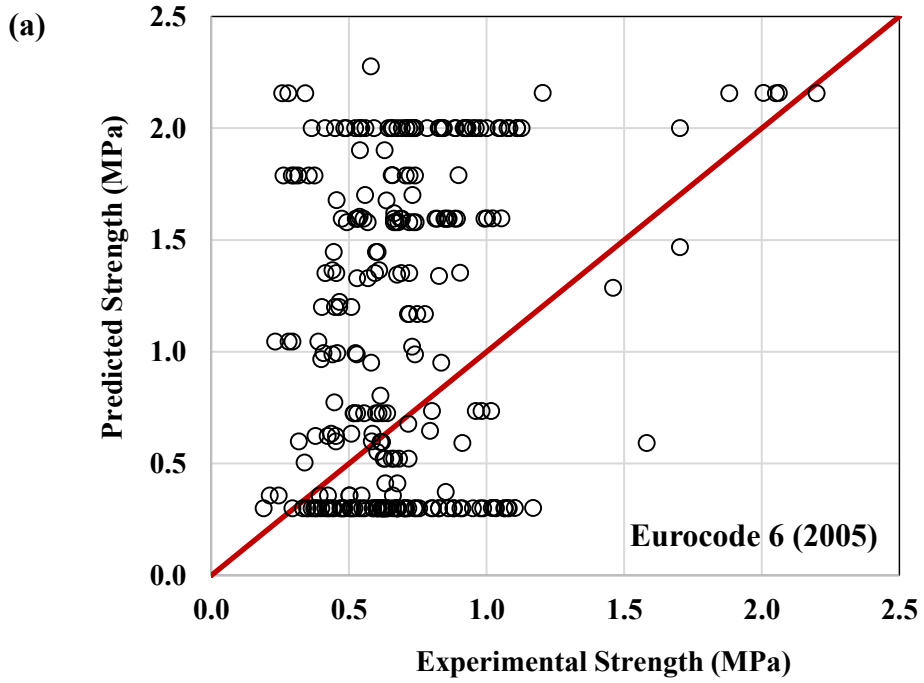


Figure 3.59 – Eurocode 6 (2005) model predictions; (a) Experimental strength vs. Predicted strength; (b) Experimental strength vs. Residuals

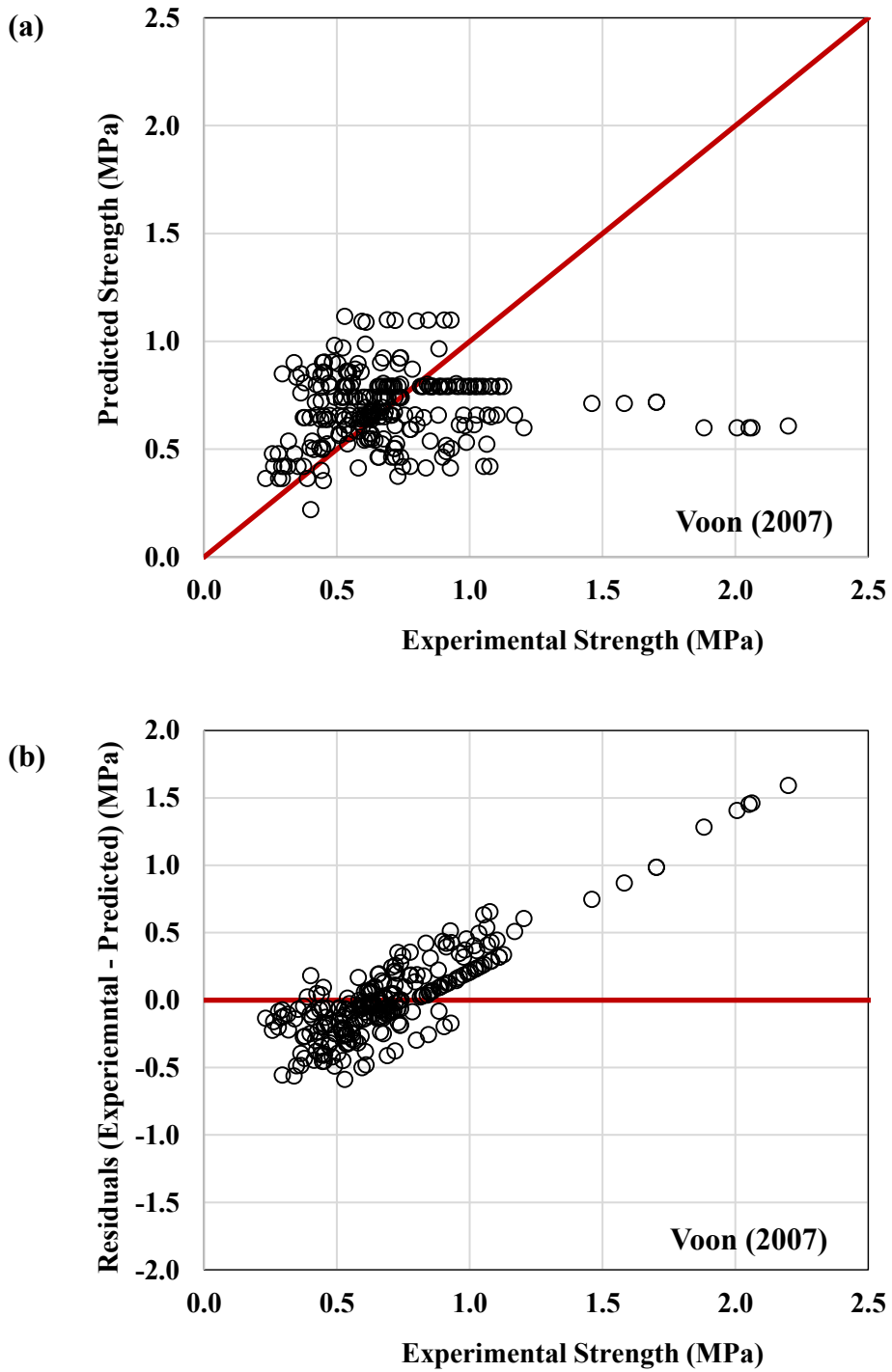


Figure 3.60 – Voon (2007) model predictions; (a) Experimental strength vs. Predicted strength; (b) Experimental strength vs. Residuals

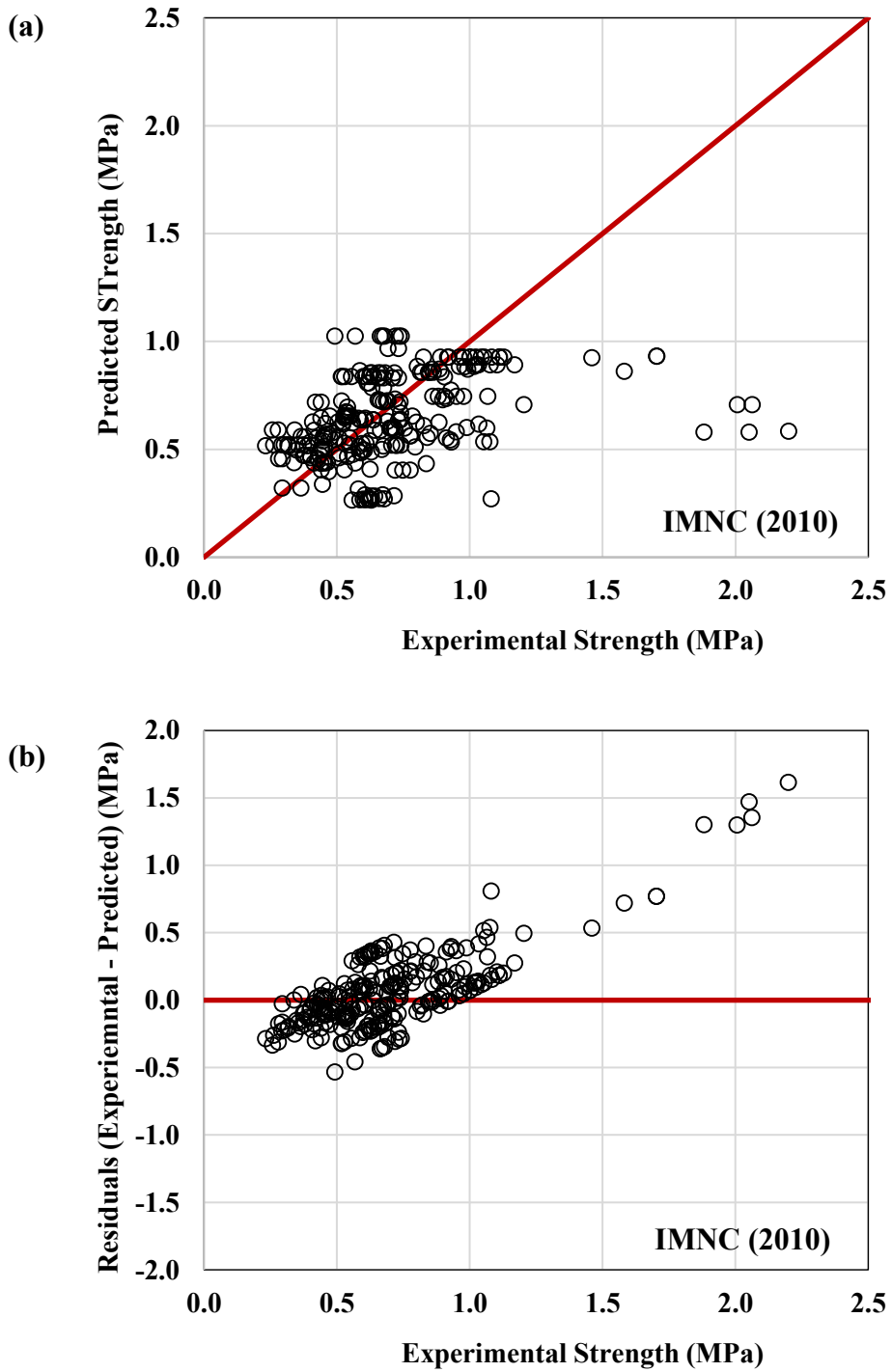


Figure 3.61 – IMNC (2010) model predictions; (a) Experimental strength vs. Predicted strength; (b) Experimental strength vs. Residuals

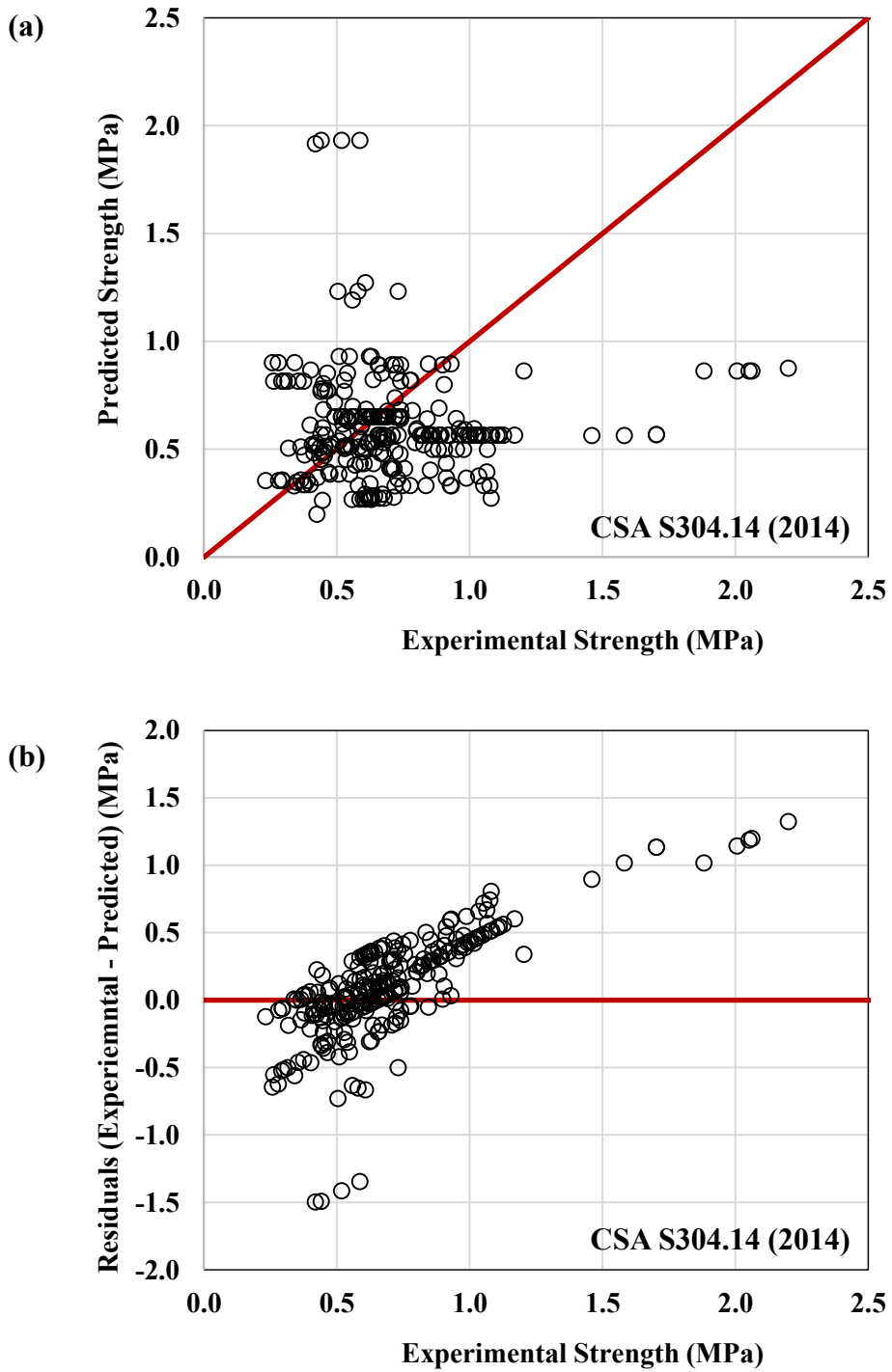


Figure 3.62 – CSA 304.14 (2014) model predictions; (a) Experimental strength vs. Predicted strength; (b) Experimental strength vs. Residuals

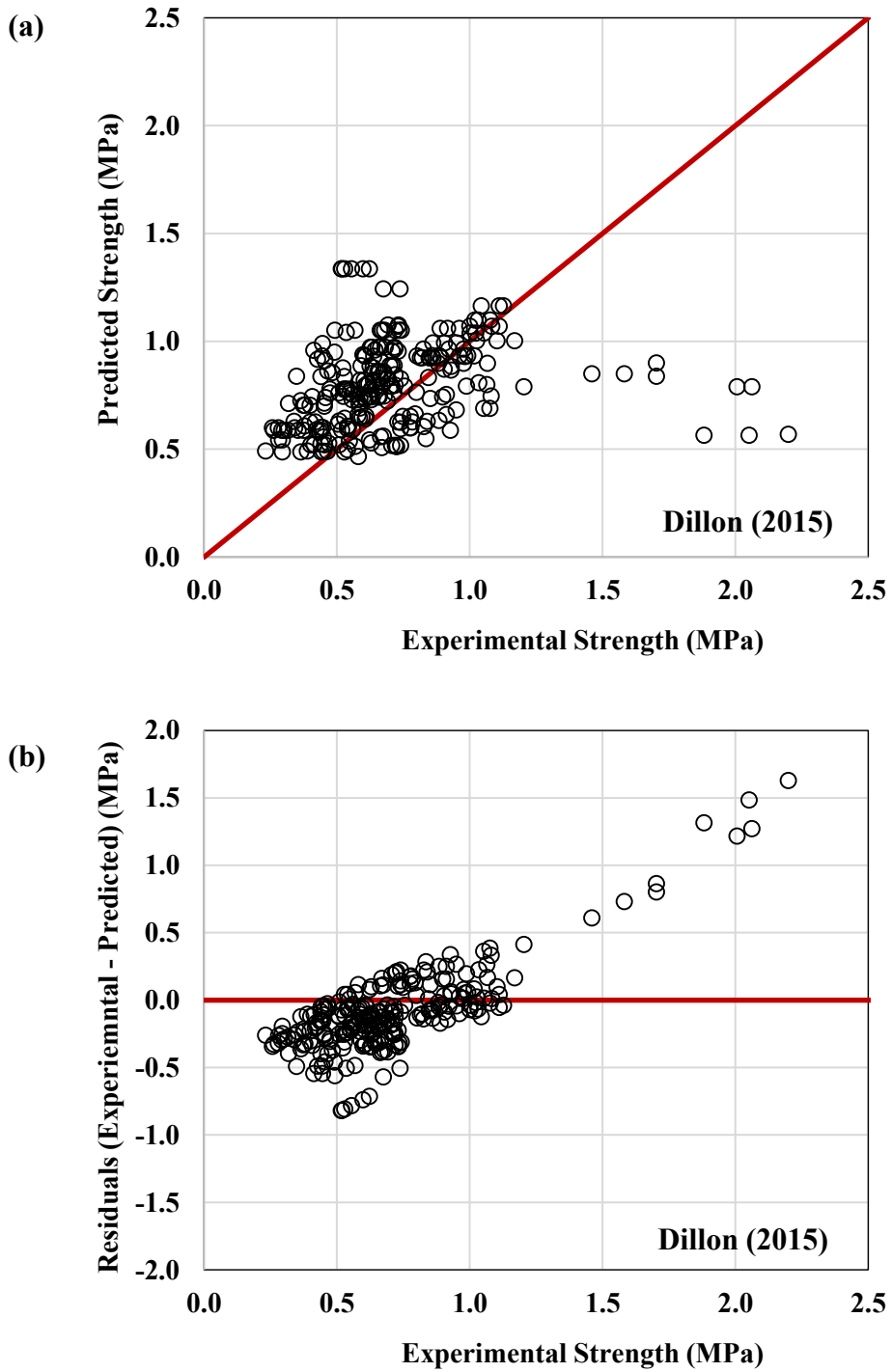


Figure 3.63 – Dillon (2015) model predictions; (a) Experimental strength vs. Predicted strength; (b) Experimental strength vs. Residuals

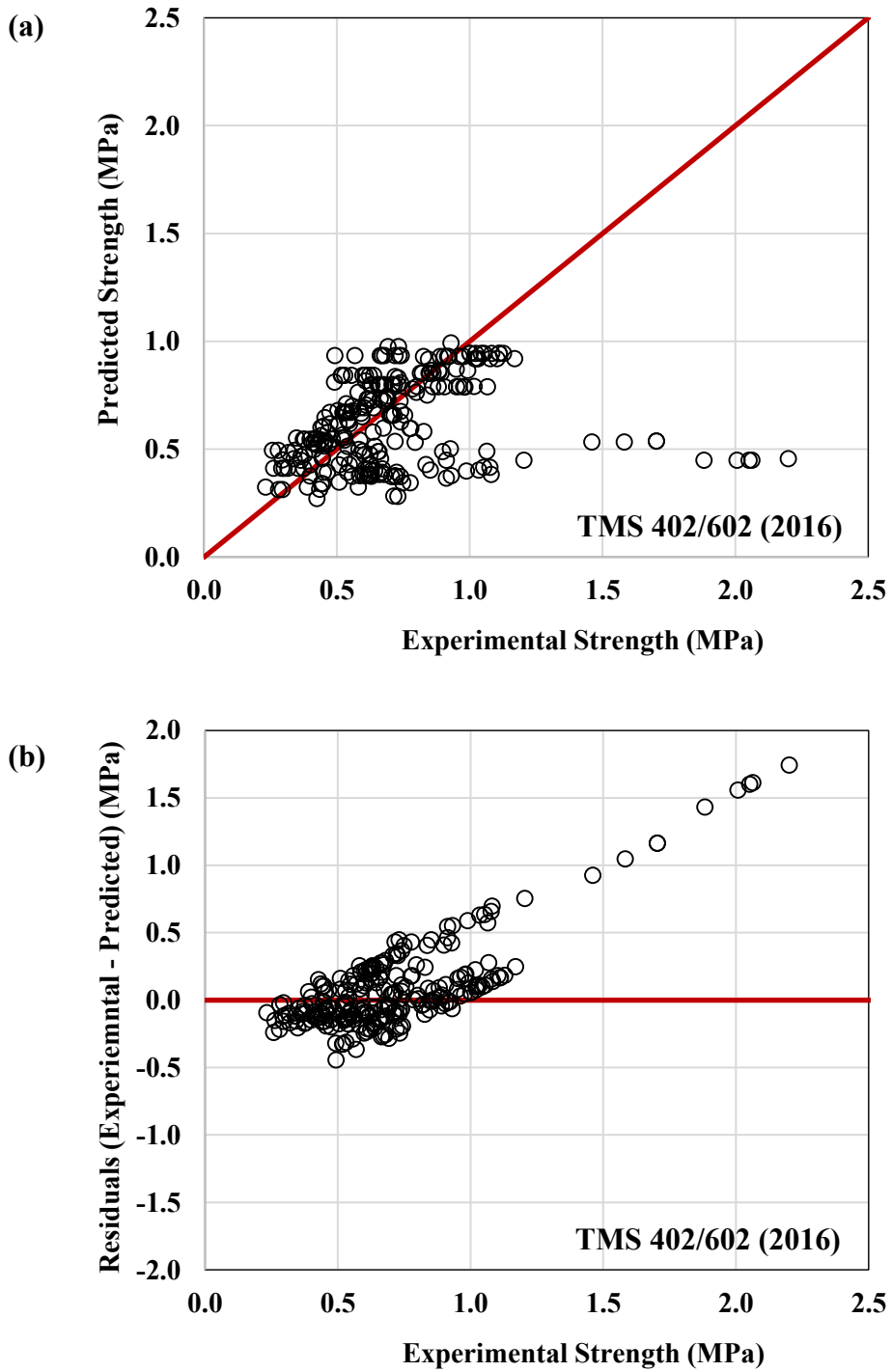


Figure 3.64 – TMS 402/602 (2016) model predictions; (a) Experimental strength vs. Predicted strength; (b) Experimental strength vs. Residuals

4 ARTIFICIAL NEURAL NETWORK INVESTIGATION & RESULTS

4.1 Artificial Neural Network Fundamentals

4.1.1 Introduction

The following description of ANNs in this thesis offers only elementary components of neural networks essential to the research conducted; it can be considered a mere introduction to the fundamentals of neural networks. The descriptions provided are sufficient for understanding how it can be used as a tool, as well as the advantages and limitations of neural networks. Readers interested in more detailed explanations of ANNs may refer to Haykin (1994), Tu (1996), Basheer and Hajmeer (2000), and Svozil et al. (1997).

ANNs are a powerful tool to process large datasets of information and recognize underlying patterns that may exist in the data. It is especially useful for identifying any nonlinear relationships among variables. Through a process of “learning,” an ANN mimics its biological counterpart by adapting synaptic weights with each new piece of information it receives.

Feedforward backpropagation (FFBP) neural networks are a type of multilayer perceptron network that is commonly used for engineering applications. FFBP neural networks are favorable due to its use of non-linear transformations for function approximations (El-Chabib and Nehdi 2005). A simplified schematic of an FFBP neural network is illustrated by Fig. 4.1.

A “neural network” is best described as numerous neurons highly interconnected to one another. The FFBP as previously described consists of three layers of neurons: an input layer, a hidden layer, and an output layer. The number of input parameters that are fed into the network determines the number of neurons in the input layer. The input layer itself does not process the input value but serves as a link that propagates the values into the neurons in the hidden layer. Hidden neurons process the input values by linearly combining them based on a matrix of weights plus a bias. Then, a transfer function is

applied to the linear combination computed. The transfer function is typically a non-linear transformation such as the sigmoid function, $g(x) = \frac{1}{1+e^{-x}}$. The output neuron then processes the values input from the hidden layer in a similar manner, computing a single predicted output by the ANN (Adhikary and Mutsuyoshi 2006; Aguilar et al. 2016; El-Chabib and Nehdi 2005; Elbahy et al. 2010; Garzón-Roca et al. 2013; Haykin 1994). A single neuron process is illustrated in Fig. 4.2.

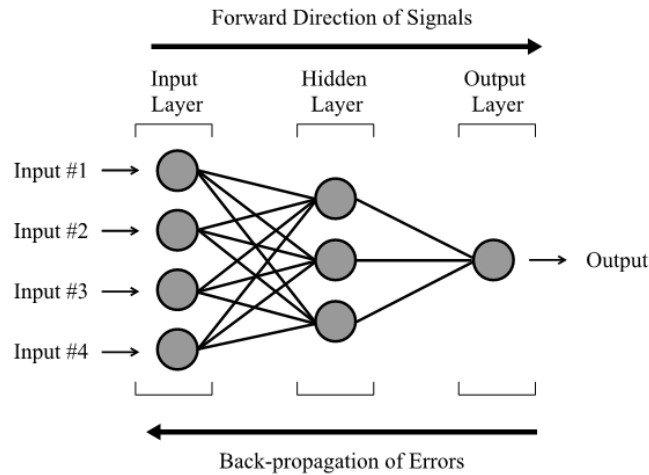


Figure 4.1 – Feedforward backpropagation neural network architecture (Adapted from Plevris and Asteris 2014)

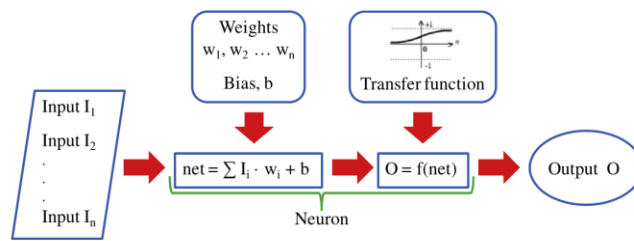


Figure 4.2 – Single neuron work (Garzón-Roca et al. 2013)

The matrix of weights and biases of a neural network are initially randomized; the neural network is incapable of accurate predictions without training. With each data point fed into the network, the expected output (experimental value) is compared with the network's predicted output, and its error is propagated backwards through the network to adjust and fine-tune the weights and biases. In this way, the ANN's capability to predict the output is incrementally improved.

The ability of an ANN to be successfully trained is highly dependent on the number of known sets of inputs and outputs that is processed by the network. Furthermore, the ability of a trained ANN to make predictions is limited within the range of input variables that was used for training. (El-Chabib and Nehdi 2005; Garzón-Roca et al. 2013; Haykin 1994; Rumelhart et al. 1986).

4.1.2 Hidden Layer and Hidden Neurons

Despite several guidelines developed to determine the optimal number of hidden neurons in the hidden layer of an ANN, no guideline or formula has been universally agreed upon (Karsoliya 2012; Sheela and Deepa 2013; Stathakis 2009). The number of hidden neurons, however, has a significant effect on an ANN’s performance. While too few hidden neurons will hinder its capacity for pattern recognition, too many hidden neurons in the ANN can lead to an overpowered neural network that tends to overfit the data, rendering it incapable of generalizing predictions (Haykin 1994; Tien Bui et al. 2012). A plot comparing the influence of hidden neurons on an ANN’s ability to generalize is illustrated in Fig. 4.3.

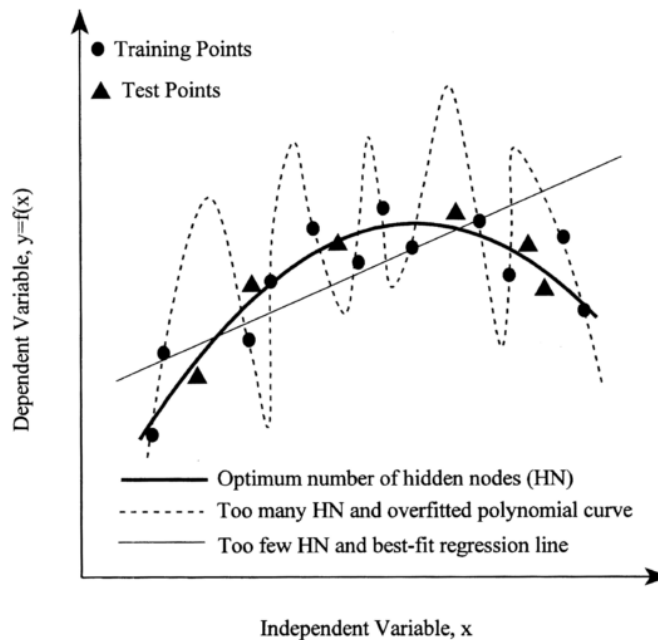


Figure 4.3 – Effect of hidden layer size on network generalization (Basheer and Hajmeer 2000)

4.1.3 Network Training, Validation and Testing

The dataset used to develop a ANN model can be divided into three subsets: a training set, a validation set, and a testing set. Typically, the percentage ratio of training-validation-testing is approximately 70-15-15, with no data point used in more than one set (Haykin 1994; MathWorks 2017; Naik and Kute 2013).

4.1.3.1 Training set

The training set is utilized by the ANN to “learn” and fit the model to the data. It is characteristically the largest of the three subsets to maximize the number of training vectors used for adjusting the network weights and biases.

During training, the ANN will undergo iterations or “epochs” of using all the training vectors to adjust its weights and biases. Each additional epoch increases the “fit” of the network predictions to the training data, decreasing the mean-squared error (MSE) of the model. While too few epochs result in underfitting and a high MSE, too many epochs result in overtraining the network and overfitting the data points. However, observing the MSE of the training data by itself does not provide a clear indication of whether the ANN model has been underfit, optimized, or overfit. Instead, a validation set is used to determine the optimum number of training epochs and prevent overfitting (Elbahy et al. 2010; Svozil et al. 1997; Tetko et al. 1995).

4.1.3.2 Validation set

An ANN capable of generalizing predictions exhibits low MSE for both the training set and the validation set. Conversely, when an ANN is overfitting the training data, the MSE for the training set may be virtually zero but exhibit large errors for the validation set. Fig. 4.4 compares how validation error can be used to identify a generalized model vs. an overfitted model. Therefore, network training is stopped at the point where the validation set has reached its minimum MSE (Haykin 1994). This concept is known as the early-stopping rule and is illustrated in Fig. 4.5.

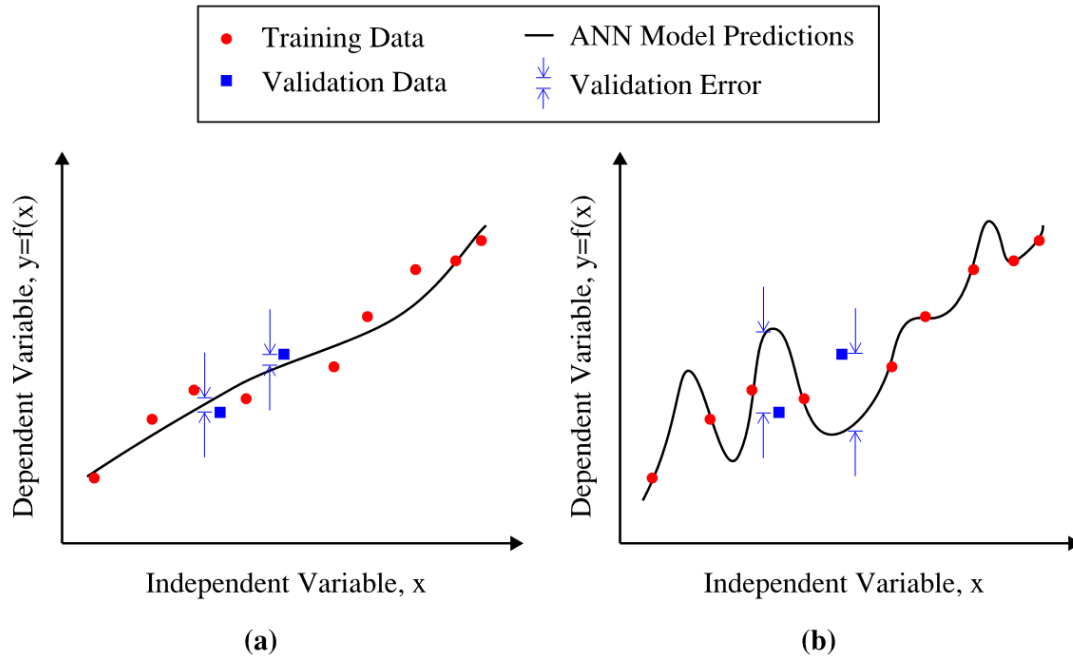


Figure 4.4 – (a) An ANN predicting validation data with small errors is an indication of generalization; (b) an ANN predicting validation data with large errors is an indication of overfitting

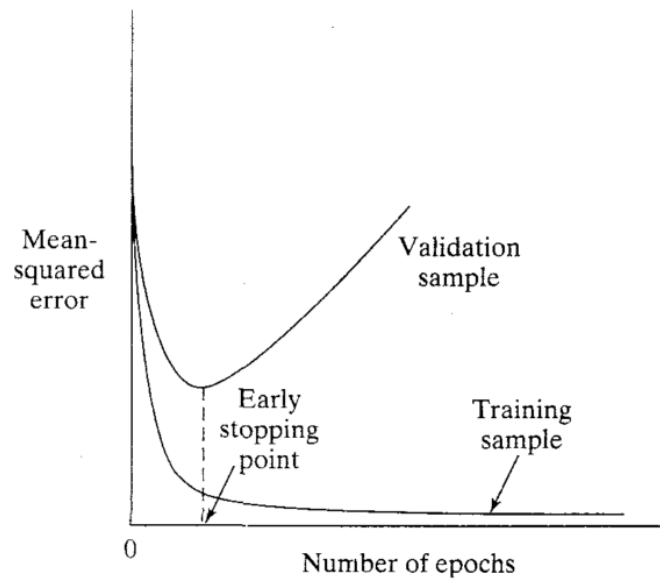


Figure 4.5 – Illustration of the early-stopping rule based on cross-validation (Haykin 1994)

4.1.3.3 Testing set

While the training set is used for adjusting weights and the validation set is used to select the optimal stopping point for training, the testing set is an isolated set of data that is used for neither training nor optimizing. Instead, the testing set provides a final measure of performance for the ANN; similar to the validation set, an ANN predicting the testing set with low errors is indicative of a network capable of generalization (Haykin 1994; Svozil et al. 1997).

4.1.4 Iterative Approach to ANNs

Each time a neural network training is initiated in MATLAB's Neural Network Toolbox, several network parameters are randomized: the set in which each data point is assigned (training, validation, or testing), the order in which each data point is fed into the neural network, and the matrix of layer weights and biases. Therefore, each initialization of a neural network in MATLAB results in a uniquely trained ANN (MathWorks 2016).

If an infinitely large dataset is available for training an ANN, then, in theory, it will eventually develop into a successfully trained neural network by adjusting the layer weight matrix with each new data point. However, the availability of large amounts of data is not typical in many structural engineering applications, often due to the logistical challenges involved with testing thousands of specimens. Since there is a limited number of experimental results available for this study, the randomized initial layer weight matrix becomes a critical factor in the ANN's ability to converge and train successfully. Therefore, one option to improve the prediction of the model is to reinitialize the ANN training several times to achieve an optimum ANN performance. The trained ANN with the best performance is then used for predicting the in-plane shear strength of PG walls.

4.1.5 ANN Performance Metrics and Model Selection

The performance of existing equations was evaluated in Section 3.7.6 using several metrics: the mean squared error, standard deviation, and 5th percentile of the V_{exp}/V_n . The same performance metrics are also useful for comparing neural network performance

with other neural networks, as well as with comparing neural networks with existing predictive models.

The determination coefficient (R^2) between experimental and predicted values can also be used as a measurement of neural network performance. R^2 is a statistical measurement of how well the variation in the predicted (model) values describe the variation in the actual (experimental) values. R^2 ranges in value between [0, 1], with an $R^2 = 1$ to indicate a model with perfect fit to the data. No threshold for R^2 exists to classify whether a predictive model—whether it is formulated by a neural network, regression analysis, or otherwise—is “suitable.” Rather, a spectrum exists when examining the performance of predictive models, and multiple statistical measurements should be considered concurrently to provide relative comparisons of performance among models (i.e. the mean squared error, standard deviation, 5th percentile, and sensitivity analysis should be examined and compared in conjunction with R^2). This is consistent with the study by Garzón-Roca et al. (2013), where a high determination coefficient along with a low mean squared error value was used as an indicator for ANN performance.

Finally, it is necessary to conduct a sensitivity analysis of trained ANN models to select the optimum model (Shirzad et al. 2014). The sensitivity analysis can be used to determine whether an ANN model is overfitting the data or if it has developed unrealistic relationships among variables. Further explanation of the sensitivity analysis performed in this study is outlined in Section 4.5.

4.1.6 Structural Applications of Neural Networks

Artificial neural networks have been used as a research tool in the field of structural engineering in the last two decades, with satisfactory results regarding determining reasonable correspondence between input and output data. Selected applications will be discussed next.

Goh (1995) demonstrated the use of neural networks as a design-support tool for complex engineering systems. Using a dataset of 45 data points, a neural network with 3 input nodes, 3 hidden nodes, and 1 output node was trained to predict the deflection of a

cantilevered beam with a point load at its tip. The neural network predicted with a mean squared error of less than 0.0005 when compared with the deflection based on Euler Bernoulli beam theory (i.e. $y = \frac{PL^3}{3EI}$).

Mukherjee and Deshpande (1995) trained a neural network to predict the initial design of reinforced concrete rectangular single span beams. Specifically, neural network can predict the optimal area of tensile reinforcement, width, depth, cost per meter, and the moment capacity of the beam, illustrating the potential for utilizing neural networks in structural design.

Taha et al. (2003) developed a neural network to predict the creep of structural masonry. Using a dataset of 47 specimens drawn from 14 testing groups, the trained neural network with 4 input nodes and 6 hidden nodes could predict creep more accurately than the conventional methods available.

Plevris and Asteris (2014) were successful in training a back-propagation neural network with two hidden layers (each with 8 hidden neurons), one input layer, and one output layer to predict masonry failure surfaces under biaxial compressive stress.

4.2 Previous Research Performed on PG Walls using Neural Networks

ANNs have been successfully developed to address highly complex problems for a wide spectrum of structural engineering applications. The inadequacy of current design expressions as discussed in Section 3.7 to consistently predict the in-plane shear strength of PG walls has prompted research with ANN-based analysis.

In a study conducted by Aguilar et al. (2016), ANNs were developed to predict the in-plane shear strength of both FG and PG walls. The ANNs were trained with an experimental dataset of 96 fully grouted concrete block walls, 95 partially grouted concrete block walls, 37 fully grouted ceramic block walls and 57 partially grouted ceramic brick walls. The determination coefficient (R^2) of the correlation between experimental values and predicted values, the mean squared-error (MSE), and the mean and standard deviation of experimental to predicted values (V_{exp}/V_n) for each trained

ANN by Aguilar et al. (2016) are summarized in Table 4.1. It is seen that the trained ANN for partially grouted concrete block walls did not perform as well as the ANN for the other three typologies. An insufficient dataset size, as well as gaps of information in the range of data used for training were given as possible reasons for the inability of the ANN to predict the in-plane shear strength of concrete block PG walls (Aguilar et al. 2016).

Table 4.1 – ANN results from study performed by Aguilar et al. (2016)

Wall Type	R ²	MSE	Mean $\frac{V_{exp}}{V_n}$	Std. Dev. $\frac{V_{exp}}{V_n}$
Fully Grouted Concrete Block	0.931	0.039	0.997	0.151
Partially Grouted Concrete Block	0.750	0.007	1.013	0.155
Fully Grouted Ceramic Block	0.952	0.024	0.985	0.089
Partially Grouted Ceramic Brick	0.848	0.007	1.005	0.152

The network architecture used by Aguilar et al. (2016) was a feedforward backpropagation multilayer perceptron network. A sigmoid transfer function was used for the hidden layer, and a linear (“*purelin*”) transfer function was used for the output layer. The Levenberg-Marquardt algorithm is used to adjust the weights and biases during backpropagation. 70% of the data was used to train, while 15% of the data was used to validate, and 15% used to test the neural network. MATLAB’s Neural Network Toolbox was used to generate and train the neural network.

The inputs in the study performed by Aguilar et al. (2016) combined design parameters to closely parallel terms in design expressions which they found to be reliable. Ten unique design variables were combined into 5 input variables in Aguilar’s study. It is worth noting, however, that Adhikary and Mutsuyoshi (2006) found that an ANN with more input neurons allowed it to achieve better training, suggesting that it may be beneficial to use uncombined variables as neural network inputs where possible.

4.3 Neural Network Test Matrix

In the current study, neural networks with 5 input neurons and 7 input neurons were trained. Each neural network will be given a unique identification tag, providing information on the dataset used for training, the number of input neurons, hidden neurons, and output neurons, as shown in Fig. 4.6.

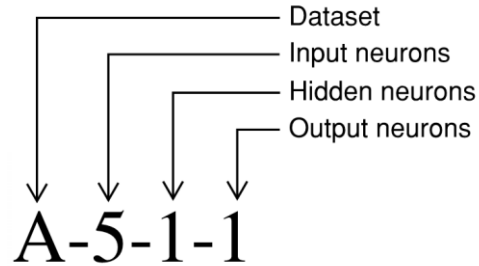


Figure 4.6 – Identification tag for neural networks used in this study

The 5-input (x -5- n -1) ANNs use the same input parameters as Aguilar et al. (2016) and thus can be used a direct comparison of performance with the results obtained in that study. The 7-input (x -7- n -1) ANNs use seven input parameters to investigate whether there is an improvement in performance when the neural network has more input neurons. The number of hidden neurons (n) for each set of networks will be varied from 1 to 5 to observe the effect of the number of hidden neurons on network performance. The network architecture used in both 5-input and 7-input ANNs in this study applies the exact same ANN architecture used by Aguilar et al. (2016) as described in the previous section.

The six dataset variations (datasets “A” to “F”) described in Section 3.5 are used for training. As outlined in Chapter 3, the six subsets possess generally increasing levels of data scrutinization and synthesization. The purpose of generating different datasets for neural network training is to achieve a balance between having a sufficiently large dataset, but also that the dataset contains only specimens that are appropriate and relevant for neural network training. The test matrix used in this study is summarized in Table 4.2.

Table 4.2 – Neural network test matrix used in this study

Dataset	Number of Specimens	5-input ANNs ($x-5-n-1$)	7-input ANNs ($x-7-n-1$)
Complete	292	n/a	n/a
A	255	A-5-n-1	A-7-n-1
B	150	B-5-n-1	B-7-n-1
C	150	C-5-n-1	C-7-n-1
D	120	D-5-n-1	D-7-n-1
E	120	E-5-n-1	E-7-n-1
F	120	F-5-n-1	F-7-n-1

The inputs and output for the ($x-5-n-1$) networks and the range of each variable for each dataset is summarized in Table 4.3. The inputs and output for the ($x-7-n-1$) networks and the range of each variable for each dataset is summarized in Table 4.4. As mentioned previously, the ability of a trained ANN to make predictions is limited within the range of input variables that was used for training.

Table 4.3 – Range of input and output parameters developed by Aguilar et al. (2016) for ($x-5-n-1$) ANN analysis

Parameter		Range of parameter in each dataset						
		Aguilar et al. (2016)	A	B	C	D	E	F
P1	$\sqrt{f'_m} \times \left(\frac{M}{VL}\right)^{-1}$ [MPa]	2.20-14.48	1.06-15.41					
P2	$\rho_h f_{yh}$ [MPa]	0.00-1.29	0.00-1.29					
P3	$\rho_v \sqrt{f_j f_{yv}}$ [MPa]	0.00-0.56	0.00-1.18				0-0.84	
P4	$\gamma \delta \sqrt{\rho_h f_{yh} f'_m}$ [MPa]	0.00-2.69	0.00-3.08					
P5	σ [MPa]	0.00-1.47	0.00-2.78	0.00-2.40		0.00-1.72		
Output (Target)	v_n [MPa]	0.25-0.95	0.23-2.20	0.23-1.70		0.23-1.08		

Table 4.4 – Range of input and output parameters for (x-7-n-1) ANN analysis

Parameter		Range of parameter in each dataset					
		A	B	C	D	E	F
Input 1	A_{scaled} [m ²]	0.66-19.42					
Input 2	M/VL [unitless]	0.250-2.295					
Input 3	A_{net}/A_{gross} [unitless]	0.356-0.808	0.405-0.808				
Input 4	$f'_{m,eff,corrected}$ [MPa]	4.25-22.29					
Input 5	$\rho_v f_{yv}$ [MPa]	0-4.84					0-3.25
Input 6	$\rho_h f_{yh}$ [MPa]	0-1.29					
Input 7	σ_{gross} [MPa]	0-2.78	0-2.00	0-1.72			
Output (Target)	$v_{max,gross}$ [MPa]	0.23-2.20	0.23-1.08				

4.4 Results

First, the determination coefficients are examined to compare neural networks against one another; higher values of R^2 are often associated with better performance. Then, the mean squared error, mean V_{exp}/V_n ratio, standard deviation V_{exp}/V_n ratio, and fifth percentile V_{exp}/V_n ratio are examined to compare neural networks with one another as well as against the performance of each existing predictive model analysed in Section 3.7.2. By considering each performance metric, the dataset and ANN architecture combination(s) can be identified for further analysis. Table 4.5 summarizes the highest values of R^2 for each network type, including the results obtained by Aguilar et al. (2016) for comparison. Several observations can be made from these results:

- In general, the (x-7-n-1) ANNs exhibited higher values of R^2 compared to the (x-5-n-1) ANNs, suggesting better performance in the trained (x-7-n-1) ANNs. This is consistent with Adhikary and Mutsuyoshi (2006)'s study which found their ANN models with 5 input neurons achieved better performance than those with 4 input neurons.

- In general, an increased number of hidden neurons results in higher R^2 values. This is expected, as increasing the number of hidden neurons increases its capacity for pattern recognition (although the risk of overfitting also increases).
- The ANNs trained using dataset “A” had the highest R^2 values out of all the other datasets. This is likely due to dataset “A” containing a significantly greater number of specimens; while dataset “A” has 255 specimens, datasets “B” and “C” have 150, and datasets “D”, “E”, and “F” have only 120. However, it should be noted that dataset “A” is the only dataset in this study which includes monotonic specimens. As mentioned previously, cyclic testing is advantageous because it allows for the quantification of strength degradation that occurs during cyclic, repeated loading, which cannot be observed through monotonic loading. Therefore, if the objective is to train an ANN model to predict the shear strength of PG walls subject to cyclic (seismic) loading, dataset “A” contains walls which are not suitable for training.
- The highest R^2 from Aguilar et al. (2016)’s study on PG walls was 0.750, obtained from their 5-3-1 network. Aguilar et al.’s study did not train any ANNs with greater than 3 hidden neurons. Compared against the other (x -5-3-1) ANNs in this study, only the “A-5-3-1” ANN has a higher R^2 of 0.812. To obtain comparable values of R^2 close to or exceeding 0.750, neural networks using datasets “B”, “C”, “D”, “E” and “F” must be trained using at least 5 hidden neurons (i.e. (x -5-5-1) ANNs).
- The R^2 values for datasets “B” and “C” are quite comparable, which is expected when considering the vast similarity between the two datasets. As discussed previously, dataset “C” is a variant of dataset “B”, where the horizontal reinforcement considered for analysis is modified based on the assumption that any bond beams at the bottom course do not provide additional shear resistance. The horizontal reinforcement modification was applied to only 9 of 150 walls in dataset “C”. The same observation also applies to comparing R^2 values for datasets “D” and “E,” where the horizontal modification was applied to only 9 of 120 walls in dataset “E”.
- While dataset “A” has significantly higher values of R^2 out of the 5 datasets in the (x -5- n -1) ANNs, the results for dataset “A” and “F” are quite comparable in the (x -7- n -1) ANNs. This is evident especially when comparing “A-7-5-1” and “F-7-5-1”

networks, which have R^2 values of 0.909 and 0.850, respectively, suggesting that dataset “F” is as viable of a dataset for training as dataset “A,” despite having significantly fewer specimens.

- Notably, the datasets “D”, “E” and “F” performed better than datasets “B” and “C” for both the $(x-5-n-1)$ and $(x-7-n-1)$ networks. In other words, the ANN models appear to have a better predictive capacity when specimens using the ESECMaSE test setup are removed from the overall dataset. This suggests that even though datasets “B” and “C” contain more specimens than datasets “D”, “E”, and “F”, the shortcomings of the ESECMaSE test setup as explained in Section 3.3.3 may be limiting the ANN from pattern recognition and/or drawing conclusions from its results.

Table 4.6 and Table 4.7 summarize the mean squared error, mean V_{exp}/V_n ratio, standard deviation V_{exp}/V_n ratio, and fifth percentile V_{exp}/V_n ratio for each network type, including the performance of each existing predictive model. Several observations can be made from these results:

- In general, both $(x-5-n-1)$ and $(x-7-n-1)$ networks have a mean V_{exp}/V_n ratio of approximately 1, and have comparable values for MSE, standard deviation V_{exp}/V_n ratios, and higher fifth percentile V_{exp}/V_n ratios.
- In general, an increased number of hidden neurons results in lower MSE values, lower standard deviation V_{exp}/V_n ratios, and higher fifth percentile V_{exp}/V_n ratios. As mentioned, this is expected, as increasing the number of hidden neurons increases its capacity for pattern recognition.
- Despite low R^2 values for ANNs with 1 hidden neuron, they exhibit lower MSE values, lower standard deviation V_{exp}/V_n ratios, and similar or higher fifth percentile V_{exp}/V_n ratios when compared with the existing predictive models, suggesting ANNs to be viable models for predicting the shear strength of PG walls.

Based on the observations made from the performance metrics, the following networks are chosen for further analysis:

- Although dataset “F” contains the least number of specimens, its performance metrics are comparable with dataset “A.” Therefore, dataset “F” is selected for further analysis, since it excludes specimens tested under monotonic loading, excludes specimens tested using the ESECMaSE test setup, the horizontal reinforcement considered for analysis is modified based on the assumption that any bond beams at the bottom course do not provide additional shear resistance, and only the interior vertical reinforcement is considered. This appears to have a sound basis when the mechanics of force transmission in the wall is considered.
- Despite the $(x-5-n-1)$ networks in this study having inferior performance metrics compared with the $(x-7-n-1)$ networks, “F-5-5-1” is chosen for comparison purposes with the “5- n -1” ANNs obtained in the study by Aguilar et al. (2016).
- Finally, “F-7-5-1” is chosen, investigating the network with the dataset that contains the most representative experimental testing data and an optimal ANN architecture.

Table 4.5 – ANN (x-5-n-1) and (x-7-n-1) performance

ANN Type	Aguilar et al. (2016)	R ²	ANN	R ²	ANN	R ²	ANN	R ²	ANN	R ²	ANN	R ²	ANN	R ²	
(x-5-n-1)	5-1-1	0.504	A-5-1-1	0.540	B-5-1-1	0.330	C-5-1-1	0.330	D-5-1-1	0.386	E-5-1-1	0.381	F-5-1-1	0.403	
	5-2-1	0.646	A-5-2-1	0.742	B-5-2-1	0.478	C-5-2-1	0.464	D-5-2-1	0.503	E-5-2-1	0.514	F-5-2-1	0.609	
	5-3-1	0.750	A-5-3-1	0.812	B-5-3-1	0.640	C-5-3-1	0.647	D-5-3-1	0.641	E-5-3-1	0.692	F-5-3-1	0.717	
	n/a	A-5-4-1	0.870	B-5-4-1	0.719	C-5-4-1	0.697	D-5-4-1	0.742	E-5-4-1	0.732	F-5-4-1	0.763		
		A-5-5-1	0.880	B-5-5-1	0.755	C-5-5-1	0.735	D-5-5-1	0.790	E-5-5-1	0.783	F-5-5-1	0.805		
(x-7-n-1)	n/a	A-7-1-1	0.533	B-7-1-1	0.420	C-7-1-1	0.406	D-7-1-1	0.481	E-7-1-1	0.481	F-7-1-1	0.568		
		A-7-2-1	0.797	B-7-2-1	0.651	C-7-2-1	0.646	D-7-2-1	0.707	E-7-2-1	0.716	F-7-2-1	0.767		
		A-7-3-1	0.859	B-7-3-1	0.774	C-7-3-1	0.766	D-7-3-1	0.806	E-7-3-1	0.801	F-7-3-1	0.816		
		A-7-4-1	0.889	B-7-4-1	0.814	C-7-4-1	0.805	D-7-4-1	0.846	E-7-4-1	0.845	F-7-4-1	0.842		
		A-7-5-1	0.909	B-7-5-1	0.839	C-7-5-1	0.838	D-7-5-1	0.872	E-7-5-1	0.880	F-7-5-1	0.850		
R² = 0.000												R² = 1.000			

Table 4.6 – (x-5-n-1) ANN models compared with existing models’ performance

PG Wall Shear Strength Model		MSE (MPa)	Mean V_{exp}/V_n	Std Dev V_{exp}/V_n	Fifth Percentile V_{exp}/V_n	Heatmap Legend	
Existing Models	Matsumura (1987)	0.163	2.263	1.855	0.369		
	AIJ (1987)	0.242	1.299	1.32	0.325		
	Shing et al. (1990)	0.199	0.916	0.489	0.334		
	Anderson and Priestley (1992)	0.139	0.782	0.316	0.469		
	Fattal (1993)	0.181	0.993	0.776	0.162		
	NEHRP (1997)	0.168	0.921	0.524	0.419		
	UBC (1997)	0.114	1.051	0.526	0.505		
	NZS-4230 (2004)	0.45	1.917	1.077	0.375		
	Eurocode 6 (2005)	1.218	0.972	0.896	0.191		
	Voon (2007)	0.113	1.073	0.531	0.527		
	IMNC (2010)	0.090	1.164	0.561	0.617		
	CSA-S304.14 (2014)	0.17	1.338	0.666	0.453		
	Dillon (2015)	0.11	1.505	0.684	0.793		
TMS 402/602 (2016)	0.111	1.223	0.691	0.678			
Dataset A	A-5-1-1	0.043	1.007	0.278	0.580		
	A-5-2-1	0.024	1.017	0.223	0.659		
	A-5-3-1	0.018	0.997	0.202	0.693		
	A-5-4-1	0.012	0.998	0.169	0.737		
	A-5-5-1	0.011	1.000	0.159	0.769		
Dataset B	B-5-1-1	0.019	1.006	0.232	0.666		
	B-5-2-1	0.015	1.017	0.210	0.700		
	B-5-3-1	0.010	1.014	0.179	0.756		
	B-5-4-1	0.008	1.014	0.159	0.766		
	B-5-5-1	0.007	1.010	0.157	0.803		
Dataset C	C-5-1-1	0.019	0.975	0.224	0.636		
	C-5-2-1	0.015	0.995	0.213	0.696		
	C-5-3-1	0.010	1.021	0.182	0.768		
	C-5-4-1	0.008	1.015	0.170	0.745		
	C-5-5-1	0.007	1.015	0.152	0.808		
Dataset D	D-5-1-1	0.018	0.995	0.234	0.605		
	D-5-2-1	0.015	1.003	0.211	0.660		
	D-5-3-1	0.011	1.008	0.184	0.692		
	D-5-4-1	0.008	1.009	0.175	0.793		
	D-5-5-1	0.006	0.994	0.132	0.796		
Dataset E	E-5-1-1	0.018	0.981	0.232	0.589		
	E-5-2-1	0.015	0.978	0.198	0.640		
	E-5-3-1	0.009	1.010	0.176	0.766		
	E-5-4-1	0.008	1.006	0.164	0.771		
	E-5-5-1	0.006	0.994	0.145	0.804		
Dataset F	F-5-1-1	0.018	1.003	0.242	0.626		
	F-5-2-1	0.015	0.998	0.210	0.674		
	F-5-3-1	0.011	1.004	0.167	0.725		
	F-5-4-1	0.009	1.003	0.174	0.772		
	F-5-5-1	0.007	0.988	0.147	0.780		

Table 4.7 – (x-7-n-1) ANN models compared with existing models’ performance

PG Wall Shear Strength Model		MSE (MPa)	Mean V_{exp}/V_n	Std Dev V_{exp}/V_n	Fifth Percentile V_{exp}/V_n	Heatmap Legend
Existing Models	Matsumura (1987)	0.163	2.263	1.855	0.369	
	AIJ (1987)	0.242	1.299	1.32	0.325	
	Shing et al. (1990)	0.199	0.916	0.489	0.334	
	Anderson and Priestley (1992)	0.139	0.782	0.316	0.469	
	Fattal (1993)	0.181	0.993	0.776	0.162	
	NEHRP (1997)	0.168	0.921	0.524	0.419	
	UBC (1997)	0.114	1.051	0.526	0.505	
	NZS-4230 (2004)	0.45	1.917	1.077	0.375	
	Eurocode 6 (2005)	1.218	0.972	0.896	0.191	
	Voon (2007)	0.113	1.073	0.531	0.527	
	IMNC (2010)	0.090	1.164	0.561	0.617	
	CSA-S304.14 (2014)	0.17	1.338	0.666	0.453	
	Dillon (2015)	0.11	1.505	0.684	0.793	
TMS 402/602 (2016)	0.111	1.223	0.691	0.678		
Dataset A	A-7-1-1	0.044	1.009	0.281	0.590	
	A-7-2-1	0.019	0.992	0.219	0.592	
	A-7-3-1	0.013	0.997	0.179	0.697	
	A-7-4-1	0.010	1.003	0.151	0.773	
	A-7-5-1	0.008	1.008	0.143	0.804	
Dataset B	B-7-1-1	0.016	1.007	0.212	0.676	
	B-7-2-1	0.010	1.005	0.161	0.733	
	B-7-3-1	0.006	0.995	0.139	0.775	
	B-7-4-1	0.005	0.998	0.148	0.798	
	B-7-5-1	0.005	1.008	0.123	0.834	
Dataset C	C-7-1-1	0.017	1.002	0.210	0.690	
	C-7-2-1	0.010	0.996	0.162	0.742	
	C-7-3-1	0.007	0.992	0.144	0.781	
	C-7-4-1	0.005	1.004	0.125	0.832	
	C-7-5-1	0.005	0.998	0.117	0.807	
Dataset D	D-7-1-1	0.015	1.012	0.227	0.651	
	D-7-2-1	0.009	1.001	0.166	0.727	
	D-7-3-1	0.006	0.992	0.138	0.782	
	D-7-4-1	0.005	1.006	0.122	0.817	
	D-7-5-1	0.004	0.994	0.106	0.873	
Dataset E	E-7-1-1	0.015	0.992	0.222	0.637	
	E-7-2-1	0.008	0.994	0.166	0.755	
	E-7-3-1	0.006	1.011	0.139	0.829	
	E-7-4-1	0.005	1.003	0.121	0.802	
	E-7-5-1	0.004	0.993	0.105	0.838	
Dataset F	F-7-1-1	0.013	0.984	0.196	0.645	
	F-7-2-1	0.007	1.002	0.152	0.770	
	F-7-3-1	0.005	1.007	0.133	0.801	
	F-7-4-1	0.005	0.998	0.126	0.772	
	F-7-5-1	0.004	1.013	0.129	0.839	

4.5 Sensitivity Analysis

The sensitivity analysis performed in this study parallels the analysis outlined by Aguilar et al. (2016). The in-plane shear strength of PG walls is predicted using a trained ANN by fixing all parameters to the medium value except one. The varied parameter is tested from the minimum value to the maximum value of that parameter found in the dataset. Then, a plot is generated based on the ratio of the network predicted value, v_n , to the shear strength predicted by fixing all parameters to the medium value, $v_{n_{\text{medium}}}$. The medium value is defined as the mid-point of the parameter between the minimum and maximum values, as calculated by Eq. (4.1):

$$x_{\text{medium}} = \frac{x_{\text{max}} + x_{\text{min}}}{2} \quad (4.1)$$

It is not uncommon for $v_{n_{\text{medium}}}$ to represent the shear strength of a hypothetical PG shear wall, although the hypothetical specimen must be verified as having realistic geometric and material properties.

As mentioned previously, a sensitivity analysis is necessary to select the optimum ANN model and eliminate ANN models which may have good performance metrics but output predictions that are contradictory to actual behaviour. An example of a sensitivity analysis revealing an ANN which predicts negative shear strengths is illustrated by Fig. 4.7, indicated by the negative values of $v_n/v_{n_{\text{medium}}}$. An example of a sensitivity analysis which suggests that the ANN model may be overfitting the data is illustrated by Fig. 4.8, based on the highly irregular and nonsensical prediction of how each input influences the shear strength of PG walls (note the many local minima and maxima that exist). Both ANNs demonstrate that performance metrics, by itself, are inadequate for model selection.

The optimum ANN model's sensitivity analysis for "F-5-5-1" and for "F-7-5-1" are presented and discussed in the next sections.

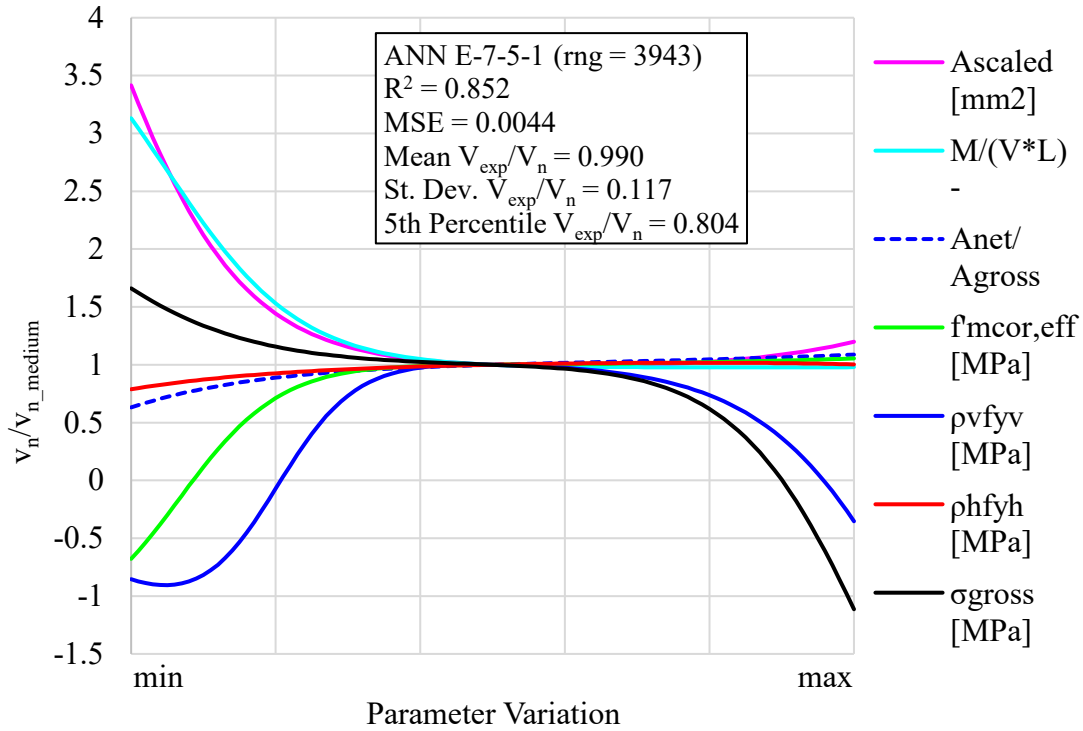


Figure 4.7 – Sensitivity analysis demonstrating an ANN model predicting negative values of peak shear strength

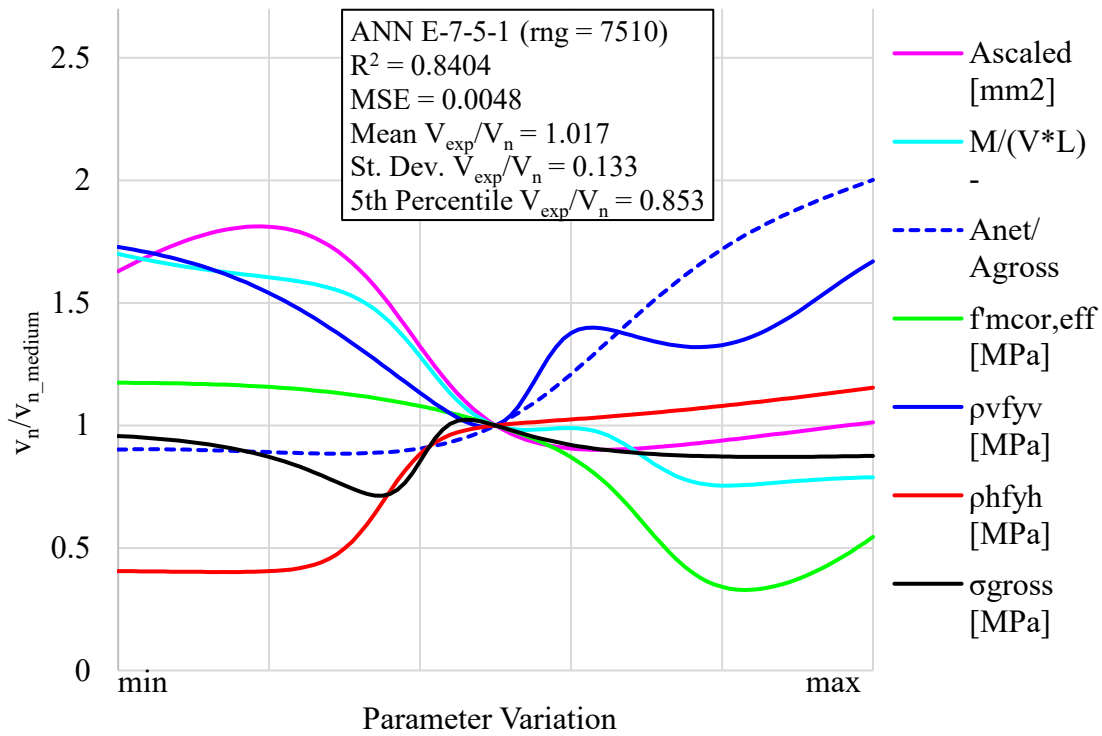


Figure 4.8 – Sensitivity analysis suggestive of an ANN model overfitting data

4.5.1 F-5-5-1 Neural Networks

As a point of reference, the sensitivity analyses for three typologies studied by Aguilar et al. (2016) [“CB-FG” (Concrete block, fully grouted), “BR FG” (Ceramic brick, fully grouted), and “BR PG” (Ceramic brick, partially grouted)] are presented in Fig. 4.9. A sensitivity analysis for PG walls made with concrete block was not conducted by Aguilar et al. (2016) due to the perceived low R^2 values obtained.

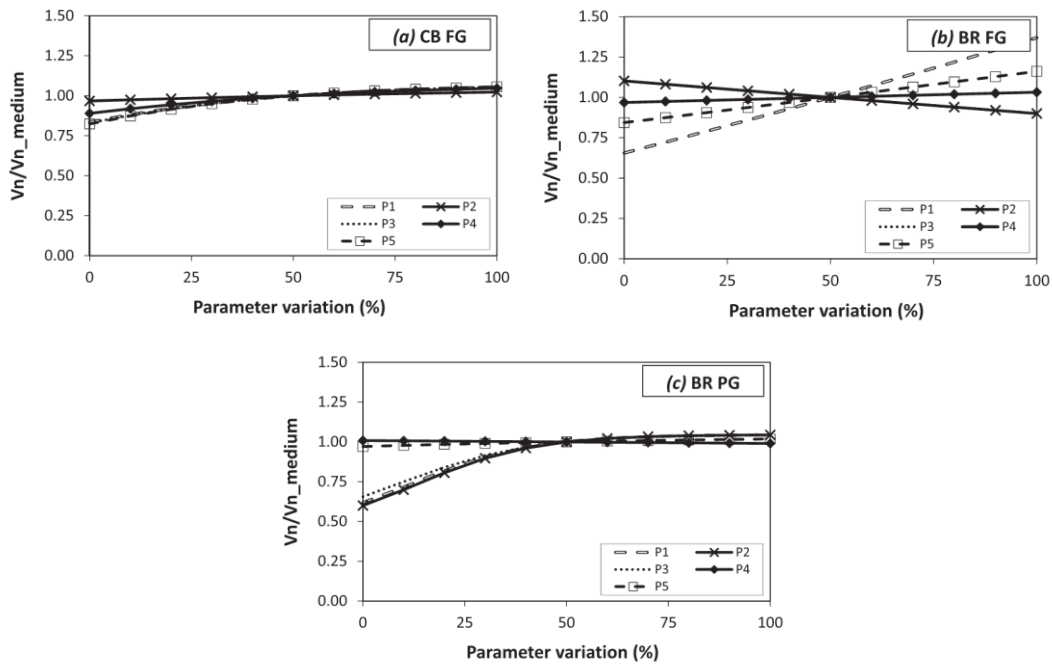


Figure 4.9 – Sensitivity analysis for equations developed by trained 5-n-1 neural networks in Aguilar et al. (2016): (a) Concrete block (fully grouted) walls; (b) Ceramic brick (fully grouted) walls; (c) Ceramic brick (partially grouted) walls (adapted from Aguilar et al. (2016))

The sensitivity analysis input variables for the “F-5-5-1” networks are summarized in Table 4.8.

Table 4.8 – Sensitivity analysis input variables for “F-5-5-1” networks

	Input Variable	Minimum value	Medium value	Maximum value
P1	$\sqrt{f'_m} \times \left(\frac{M}{VL}\right)^{-1}$ [MPa]	1.058	8.232	15.406
P2	$\rho_h f_{yh}$ [MPa]	0.000	0.645	1.290
P3	$\rho_v \sqrt{f_j f_{yv}}$ [MPa]	0.000	0.420	0.840
P4	$\gamma \delta \sqrt{\rho_h f_{yh} f'_m}$ [MPa]	0.000	1.540	3.080
P5	σ [MPa]	0.000	0.862	1.724

The sensitivity analysis for the optimum “F-5-5-1” network is given in Fig. 4.11. Based on the sensitivity analysis performed, several observations and comparisons can be made. Each of the parameters are commented on separately to outline the behaviour of the trained neural network in predicting the shear strength of hypothetical PG walls.

P1 $\left(\sqrt{f'_m} \times \left(\frac{M}{VL}\right)^{-1}\right)$ [√MPa]: P1 combines the influence of the compressive strength of masonry and the shear span ratio into one input parameter. Larger values of both f'_m and $(M/VL)^{-1}$ are expected to increase the shear strength of PG walls. However, the ANN predicts a *decrease* in shear strength as *PI* is increased, which is inconsistent with existing design expressions and conclusions by researchers.

However, supporting the relationship found by the ANN, a scatterplot of the compressive strength of masonry prism and the experimental shear strength reveals a slight negative correlation in the dataset, as illustrated by Fig. 4.10.

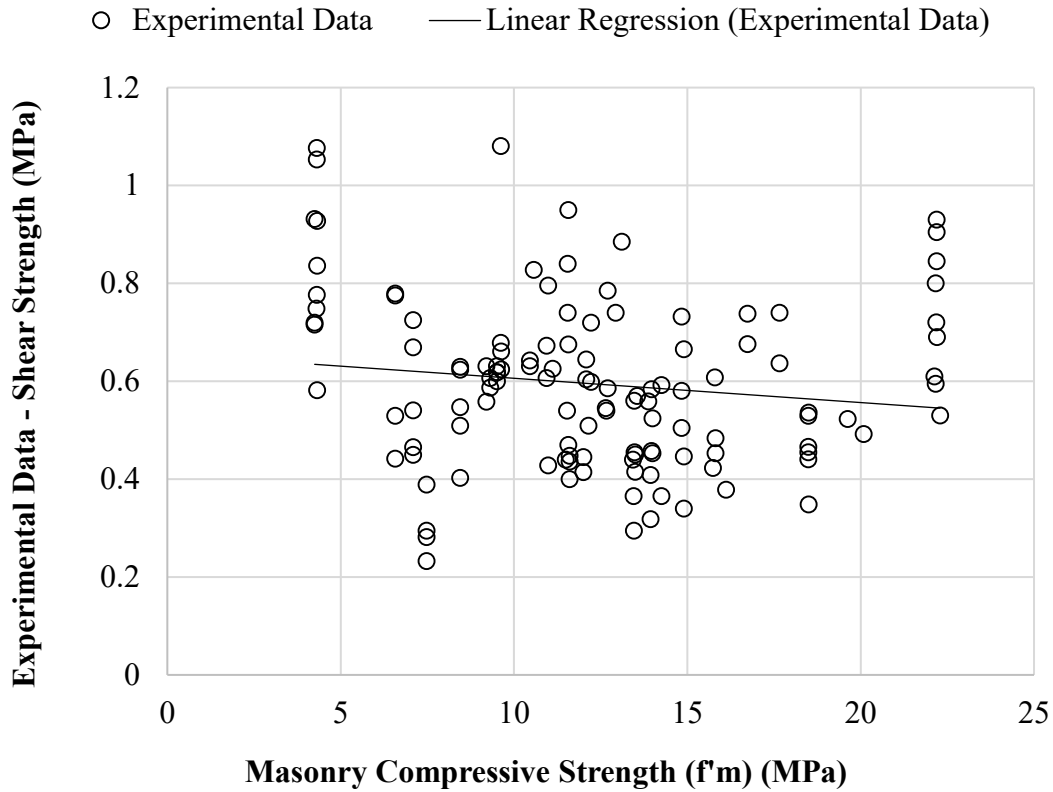


Figure 4.10 – Masonry compressive strength vs. experimental shear strength

As mentioned, larger values of $(M/VL)^{-1}$ are expected to be attributed to higher shear capacity, as a decrease in the height-to-length aspect ratio of a PG wall increases its shear strength (Matsumura 1988; Ramírez et al. 2015; Voon and Ingham 2006). However, since the ANN predicts a *decrease* in shear strength as PI is increased, the sensitivity analysis reveals that the ANN predicts the influence of the compressive strength of masonry to have a greater impact on the shear strength on PG walls than the influence of shear span ratio.

$P2$ ($\rho_h f_{yh}$) [MPa]: The ANN predicts an increase in shear strength as the horizontal reinforcement ratio and strength are increased. This is consistent with existing design expressions and conclusions by researchers. It has been reported by several authors that horizontal reinforcement ratios above 0.2% lead to a negligible increase in ultimate strength and deformation (Elmapruk 2010; Fattal 1993b; Haach et al. 2012; Hamid and Moon 2005; Shing et al. 1990b).

P3 ($\rho_v \sqrt{f_j f_{yv}}$) [MPa]: The ANN predicts an increase in shear strength as the vertical reinforcement ratio and strength are increased. The influence of *P3* is similar in magnitude to the influence of *P2*, a phenomenon that is supported by the model by Dillon (2015) which applies the same numerical coefficient applied to both horizontal and vertical (web) steel.

P4 ($\gamma \delta \sqrt{\rho_h f_{yh} f'_m}$) [MPa]: *P4* combines the influence of the horizontal reinforcement and the compressive strength of masonry into one input parameter. The ANN predicts a decrease in shear strength as *P4* is increased, contradicting existing design expression and conclusions by researchers; an increase in the horizontal reinforcement and compressive strength of masonry are both expected to increase the shear strength of PG walls. However, similar to the discussion on parameter *P1*, the scatterplot of the compressive strength of masonry prism and the experimental shear strength reveals a slight negative correlation which exists in the dataset. Therefore, the sensitivity analysis reveals that the ANN predicts the influence of the compressive strength of masonry to have a greater impact on the shear strength on PG walls than the influence of horizontal reinforcement.

P5 (σ) [MPa]: The ANN predicts an increase in shear strength as the axial loading, *P5*, on the wall is increased, which is consistent with the multiple studies which have found that an increase of axial load increases the ultimate shear resistance of PG shear walls (Haach 2009; Matsumura 1988; Ramírez et al. 2015; Voon and Ingham 2006).

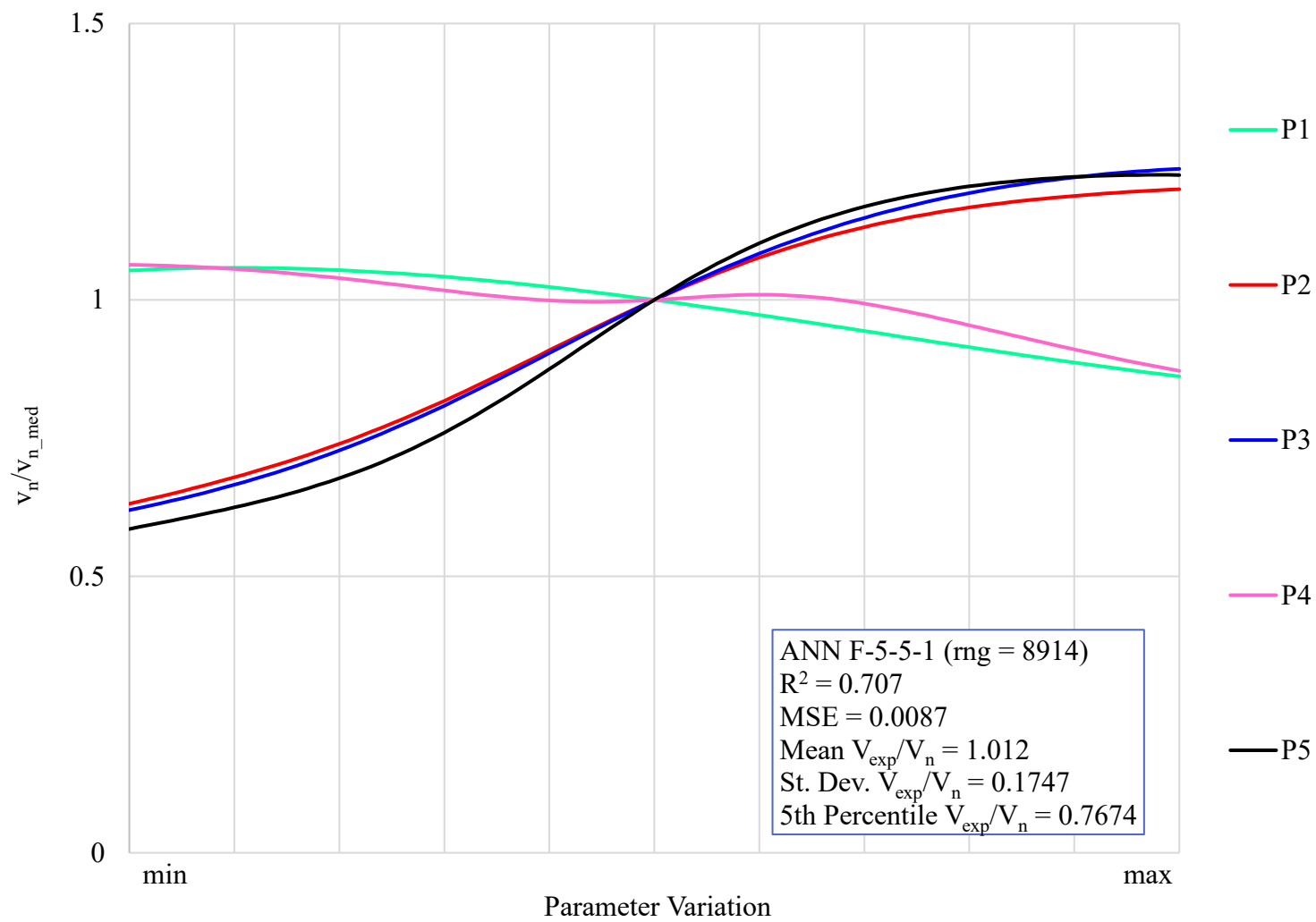


Figure 4.11 – Sensitivity Analysis, “F-5-5-1” Network

4.5.2 F-7-5-1 Neural Networks

The sensitivity analysis input variables for the “F-7-5-1” networks are summarized in Table 4.9.

Table 4.9 – Sensitivity analysis input variables for “F-7-5-1” networks

Input Variable		Minimum value	Medium value	Maximum value
Input 1	A_{scaled} [m ²]	0.66	10.04	19.43
Input 2	M/VL [unitless]	0.250	1.273	2.295
Input 3	A_{net}/A_{gross} [unitless]	0.405	0.607	0.808
Input 4	$f'_{m,eff,corrected}$ [MPa]	4.25	13.27	22.29
Input 5	$\rho_v f_{yv}$ [MPa]	0.000	1.625	3.249
Input 6	$\rho_h f_{yh}$ [MPa]	0.000	0.645	1.290
Input 7	σ_{gross} [MPa]	0.000	0.862	1.724

The sensitivity analysis for the optimum “F-7-5-1” ANN is illustrated by Fig. 4.12. Based on the sensitivity analysis performed, several observations can be made. Each of the parameters are commented on separately to outline the behaviour of the trained neural network in predicting the shear strength of hypothetical PG masonry walls.

A_{scaled} [m²]: The ANN predicts a *decrease* in shear strength as the A_{scaled} ($H \times L$) of the wall is increased. This suggests that the ANN recognizes a size effect on PG shear walls; smaller walls tend to resist lateral loading more effectively. The relative influence of this parameter appears to be less significant than other parameters.

Although there are currently no studies that have investigated the size effect of PG shear walls, a study by Sarhat and Sherwood (2015) on reinforced masonry beams found that crack spacing and crack width both increase as the effective depth of the beam is increased. As a result, smaller shear stress capacities and more brittle behaviour was observed in larger specimens. This is explained by the reduced ability of larger cracks to transfer shear due reduced aggregate interlocking. While the CSA S304.14 (2014) code accounts for size effects for masonry beam design, it does not apply any size effect factors

in masonry shear wall design. While there are currently no design expressions that account for size effects in masonry shear walls, Minaie et al. (2010) suggest that the area of the wall has a size effect on its in-plane shear strength.

M/VL [unitless]: The ANN predicts a *decrease* in shear strength as the shear span ratio of the wall is increased. This is consistent with both existing design expressions and experimental studies, which have found walls with a greater height-to-length ratio to lose shear capacity and are more likely to fail in flexure.

A_{net}/A_{gross} [unitless]: The ANN predicts a general increase in shear strength as the partial grouting ratio is increased, which is consistent with existing design expressions. According to a study by Voon and Ingham (2002), the influence of grouting on *net* shear strength is insignificant. Thus, the increase in *gross* shear strength should be linear with respect to the increase in the partial grouting ratio. The influence of grout spacing was also found to have a linear relationship with the compressive strength of PG masonry based on gross area by Hamid and Chandrakerthy (1992). However, the neural network is predicting a non-linear relationship between partial grouting ratio and shear strength, a phenomenon not observed in experimental studies.

$f'_{m,eff,corrected}$ [MPa]: Similar to the “F-5-5-1” ANN model, the “F-7-5-1” ANN predicts a *decrease* in shear strength as the compressive strength of masonry prism is increased, which is inconsistent with existing design expressions and conclusions by researchers. However, as mentioned, machine learning algorithms rely heavily on the training dataset to make predictions, and the negative correlation which exists in the dataset is the likely explanation for the ANN behaviour (refer to Fig. 4.10).

$\rho_v f_{yv}$ [MPa]: The ANN predicts a small increase in shear strength as the vertical reinforcement is increased, although the sensitivity analysis suggests that the influence of vertical reinforcement is less than the other variables. This is consistent with most design expressions which have excluded the contribution of vertical reinforcement on the shear strength of PG walls. However, vertical reinforcing steel is expected to provide shear resistance as cracking occurs through dowel action of the reinforcement (Haider 2007).

$\rho_h f_{yh}$ [MPa]: The ANN predicts an increase in shear strength as the horizontal reinforcement is increased. An increase in the horizontal reinforcement is expected to increase the shear strength of PG walls. Additionally, the model is predicting a very similar influence between $\rho_h f_{yh}$ and $\rho_v f_{yv}$ within the middle-range of parameter variation. This is consistent with the model proposed by Dillon (2015), with the same numerical coefficient applied to both horizontal and vertical (web) steel.

σ_{gross} [MPa]: The ANN predicts an increase in shear strength as the axial loading on the wall is increased, which is consistent with the multiple studies which have found that an increase of axial load increases the ultimate shear resistance of PG shear walls (Haach 2009; Matsumura 1988; Ramírez et al. 2015; Voon and Ingham 2006). Additionally, the model is predicting a greater influence of axial load in comparison to the vertical or horizontal reinforcements. This is consistent with the model proposed by Dillon (2015), with a higher coefficient applied to axial load at 0.15, in comparison to 0.12 for both the horizontal and vertical (web) steel reinforcements.

Overall, the sensitivity analysis reveals that the ANN predicts the relative influence of shear parameters consistent with experimental studies and design expressions. Despite both “F-5-5-1” and “F-7-5-1” ANN models predicting a decrease in shear strength as the compressive strength of masonry prism is increased, $f'_{m,eff,corrected}$ may not be an ideal parameter for predicting the shear strength of PG walls since it is dependent on the angle of the compression strut due to the anisotropy of masonry. Rather, the tensile strength of masonry may be more relevant than the compressive strength of a prism for studying the diagonal tension shear failure of PG walls.

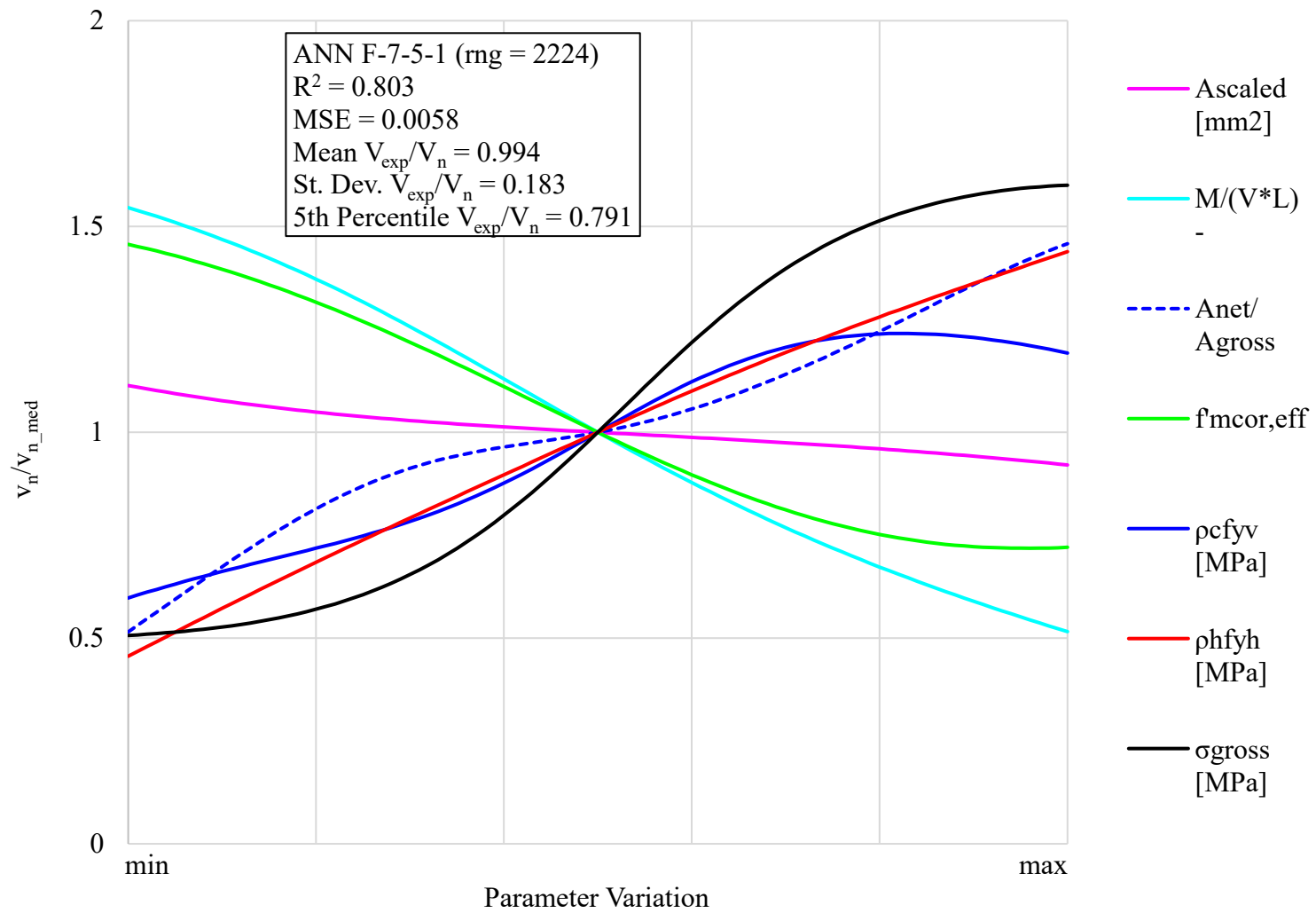


Figure 4.12 - Sensitivity Analysis, “F-7-5-1” Network

4.6 Summary of ANN Model Performance

The results of this thesis demonstrate the potential for utilizing ANNs to address the limitations of current design expressions to predict the in-plane shear strength of PG shear walls. A summary of the performance metrics comparing existing PG shear wall models with the two ANN models analysed in the sensitivity analysis is presented in Table 4.10. Overall, the mean squared error, mean V_{exp}/V_n ratio, standard deviation V_{exp}/V_n ratio, and fifth percentile V_{exp}/V_n ratio are all significantly improved in the ANN models.

Table 4.10 – Summary of ANN model performance in comparison with existing PG shear wall models

PG Wall Shear Strength Model		MSE (MPa)	Mean V_{exp}/V_n	Std Dev V_{exp}/V_n	Fifth Percentile V_{exp}/V_n
Existing Models	Matsumura (1987)	0.163	2.263	1.855	0.369
	AIJ (1987)	0.242	1.299	1.32	0.325
	Shing et al. (1990)	0.199	0.916	0.489	0.334
	Anderson and Priestley (1992)	0.139	0.782	0.316	0.469
	Fattal (1993)	0.181	0.993	0.776	0.162
	NEHRP (1997)	0.168	0.921	0.524	0.419
	UBC (1997)	0.114	1.051	0.526	0.505
	NZS-4230 (2004)	0.45	1.917	1.077	0.375
	Eurocode 6 (2005)	1.218	0.972	0.896	0.191
	Voon (2007)	0.113	1.073	0.531	0.527
	IMNC (2010)	0.091	1.169	0.562	0.617
	CSA-S304.14 (2014)	0.17	1.338	0.666	0.453
	Dillon (2015)	0.11	1.505	0.684	0.793
	TMS 402/602 (2016)	0.111	1.223	0.691	0.678
ANN	F-5-5-1 (rng = 8914)	0.009	1.012	0.175	0.767
	F-7-5-1 (rng = 2224)	0.006	0.994	0.183	0.791
Heatmap Legend			1.218	MSE	0.000
2.263	Mean V_{exp}/V_n		1.000	0.000	
1.855	Std Dev V_{exp}/V_n	0.000	0.000	Fifth Percentile V_{exp}/V_n	1.000

As previously explained, a plot of the residuals offers a visual representation of whether the model exhibits homoscedasticity; a homoscedastic plot will exhibit minimal variation in its residuals regardless of the magnitude of predicted value. The plot of residuals of ANN models “F-5-5-1” and “F-7-5-1” (Figs. 4.13(b) and 4.14(b), respectively) reveal that the models are exhibiting homoscedasticity. Compared existing PG wall shear strength models, this is vastly improved; each of the existing models in this study tended to overpredict stronger walls and under-predict weaker walls (thus exhibiting heteroscedasticity).

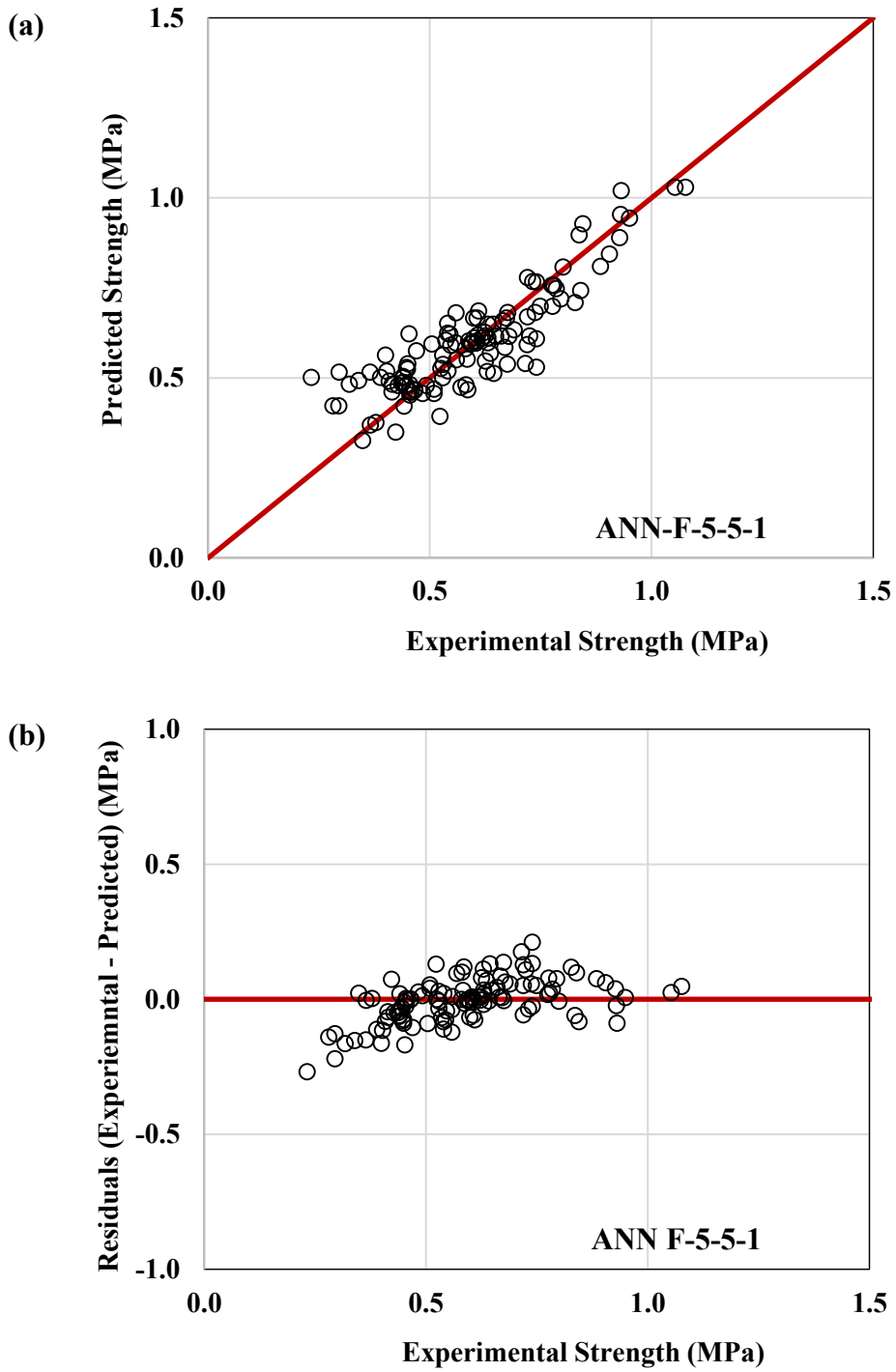


Figure 4.13 – ANN “F-5-5-1” model predictions; (a) Experimental strength vs. Predicted strength; (b) Experimental strength vs. Residuals

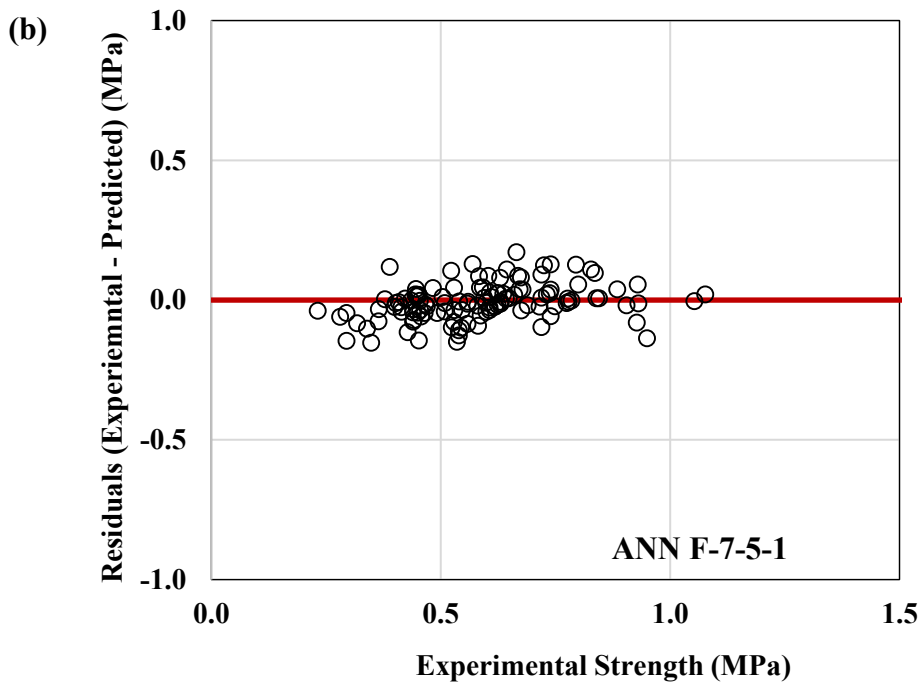
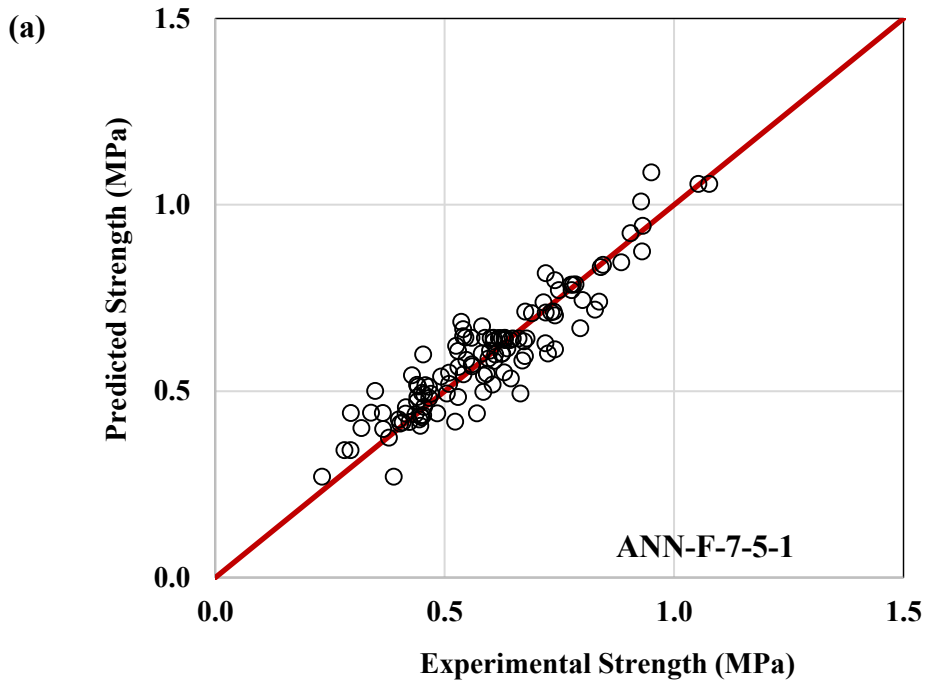


Figure 4.14 – ANN “F-7-5-1” model predictions; (a) Experimental strength vs. Predicted strength; (b) Experimental strength vs. Residuals

4.7 Shear Expressions Based on ANN

While it is possible to produce a formula based on the matrix of weights and biases described in Section 4.1, it is rarely practical in the sense of using it in hand calculations due to the complexity inherent to the use of sigmoid transfer functions and the inability to combine sigmoid terms with one another. Additionally, the interpretability of shear expressions based on ANNs are often difficult due to the sigmoid terms, and the relative influence of each parameter is not clearly represented by such formulas. For this reason, the Neural Network Toolbox in MATLAB offers a function to output a trained neural network as a MATLAB executable program, rather than a formula (refer to Appendix B). Nonetheless, the following section presents explicit formulations shear strength of PG walls for each of the ANN models developed in this study (“F-5-5-1” and “F-7-5-1”).

4.7.1 General Formula

An ANN model utilizes matrices of weights and biases to predict a normalized output value as a function of an input vector, as shown by the following formula:

$$y_{\text{norm}} = [LW] \cdot \tanh(b_1 + [IW]\{X_{\text{norm}}\}) + b_2 \quad (4.2)$$

where y_{norm} = normalized output prediction

LW = layer weight vector of size [1, # of inputs]

IW = input weight matrix of size [# of inputs, # of hidden neurons]

X_{norm} = normalized inputs vector of size [1, # of inputs]

= $\{x_{1\text{norm}}, x_{2\text{norm}}, x_{3\text{norm}}, \dots, x_{n\text{norm}}\}$

b_1 = hidden layer bias vector of size [# of inputs, 1]

b_2 = output layer bias vector of size [1,1]

To generate the normalized inputs vector, X_{norm} , each input variable, x_i , is scaled on a linear normalization function in the range of $[-1, +1]$ to obtain a normalized value of the input parameter by linear interpolation:

$$\frac{x_{i_{\min}} - x_{i_{\max}}}{(-1) - 1} = \frac{x_i - x_{i_{\max}}}{x_{i_{\text{norm}}} - 1} \quad (4.3)$$

where $x_{i_{\min}}$ = minimum value of input parameter in total dataset
 $x_{i_{\max}}$ = maximum value of input parameter in total dataset
 $x_{i_{\text{norm}}}$ = normalized input parameter for ANN training

Rearranged to solve for the normalized $x_{i_{\text{norm}}}$:

$$x_{i_{\text{norm}}} = \frac{(-2)(x_i - x_{i_{\max}})}{x_{i_{\min}} - x_{i_{\max}}} + 1 \quad (4.4)$$

The output data is also normalized, so the normalized output, y_{norm} must be unscaled by the same linear normalization function to obtain the “true” predicted output, y .

$$\frac{y_{\min} - y_{\max}}{(-1) - 1} = \frac{y - y_{\max}}{y_{\text{norm}} - 1} \quad (4.5)$$

where y_{\min} = minimum value of output (experimental) parameter in total dataset
 y_{\max} = maximum value of output (experimental) parameter in total dataset
 y_{norm} = normalized output (ANN predicted) parameter

Finally, rearranged to solve for the output y :

$$y = \frac{(y_{\min} - y_{\max})(y_{\text{norm}} - 1)}{-2} + y_{\max} \quad (4.6)$$

An application example will be given in Section 4.7.4.

4.7.2 F-5-5-1 Neural Network Model

The minimum and maximum values of input and output parameters used for normalization is given in the following table:

Table 4.11 – Input minimum and maximum values for linear normalization

Input Variable (x_i)		Minimum ($x_{i_{\min}}$)	Maximum ($x_{i_{\max}}$)
Input 1, x_1	$\sqrt{f'_m} \times \left(\frac{M}{VL}\right)^{-1}$ [MPa]	1.058	15.406
Input 2, x_2	$\rho_h f_{yh}$ [MPa]	0.000	1.290
Input 3, x_3	$\rho_v \sqrt{f_j f_{yv}}$ [MPa]	0.000	0.840
Input 4, x_4	$\gamma \delta \sqrt{\rho_h f_{yh} f'_m}$ [MPa]	0.000	3.080
Input 5, x_5	σ [MPa]	0.000	1.724
Output Variable (y)		Minimum (y_{\min})	Maximum (y_{\max})
Output	$v_{\max, gross}$ [MPa]	0.232	1.081

The matrices and biases used are given as follows:

$$IW = \begin{bmatrix} -0.5714 & 1.6221 & 2.6040 & 0.1556 & 1.1685 \\ -1.2179 & -1.1950 & 1.0211 & -0.8775 & 1.1548 \\ 0.6554 & 0.0098 & 0.6919 & 3.1815 & -0.5537 \\ 0.7644 & -1.5598 & -1.4824 & 1.0324 & -2.0312 \\ 0.3864 & 0.7971 & -2.1380 & -1.8096 & -2.4711 \end{bmatrix}$$

$$LW = [-1.6275 \quad -0.7684 \quad 0.2860 \quad -0.7706 \quad -0.4390]$$

$$b_1 = \begin{bmatrix} 5.9196 \\ -2.4419 \\ -0.2370 \\ -0.2831 \\ -3.8519 \end{bmatrix}$$

$$b_2 = 1.3944$$

4.7.3 F-7-5-1 Neural Network Model

The minimum and maximum values of input and output parameters used for normalization is given in the following table:

Table 4.12 – Input minimum and maximum values for linear normalization

Input Variable (x_i)		Minimum ($x_{i_{\min}}$)	Maximum ($x_{i_{\max}}$)
Input 1, x_1	A_{scaled} [m ²]	0.66	19.43
Input 2, x_2	M/VL [unitless]	0.250	2.295
Input 3, x_3	$A_{\text{net}}/A_{\text{gross}}$ [unitless]	0.405	0.808
Input 4, x_4	$f'_{\text{m,eff,corrected}}$ [MPa]	4.25	22.29
Input 5, x_5	$\rho_v f_{yv}$ [MPa]	0.000	4.842
Input 6, x_6	$\rho_h f_{yh}$ [MPa]	0.000	1.290
Input 7, x_7	σ_{gross} [MPa]	0.000	1.724
Output Variable (y)		Minimum (y_{\min})	Maximum (y_{\max})
Output	$v_{\text{max,gross}}$ [MPa]	0.232	1.081

The matrices and biases used are given as follows:

$$IW = \begin{bmatrix} -0.6183 & -0.6835 & 1.6011 & -0.3643 & 1.1593 & -0.0237 & 0.0430 \\ 1.3134 & 1.2532 & -2.1502 & -1.6223 & -0.0682 & -1.3960 & -1.7227 \\ 0.0637 & -1.3889 & -2.4748 & -0.9587 & -1.2993 & -0.8316 & 1.8284 \\ 0.0070 & -0.9053 & 1.0992 & -0.9918 & 1.9170 & 1.0863 & 1.9599 \\ 0.0206 & -0.6339 & 0.4812 & -0.4361 & 0.8425 & -1.2191 & 1.0364 \end{bmatrix}$$

$$LW = [0.8144 \quad -0.3618 \quad 0.3675 \quad 0.8712 \quad -0.8893]$$

$$b_1 = \begin{bmatrix} 1.5154 \\ 1.7618 \\ -0.4254 \\ -0.0269 \\ -1.3641 \end{bmatrix}$$

$$b_2 = -0.6123$$

4.7.4 Sample Calculation

The following section outlines a sample calculation using the shear expression based on the “F-7-5-1” ANN model. The sample calculation will predict the strength of specimen “PG254-48” from Elmapruk (2010)’s experimental study illustrated in Fig 4.15.

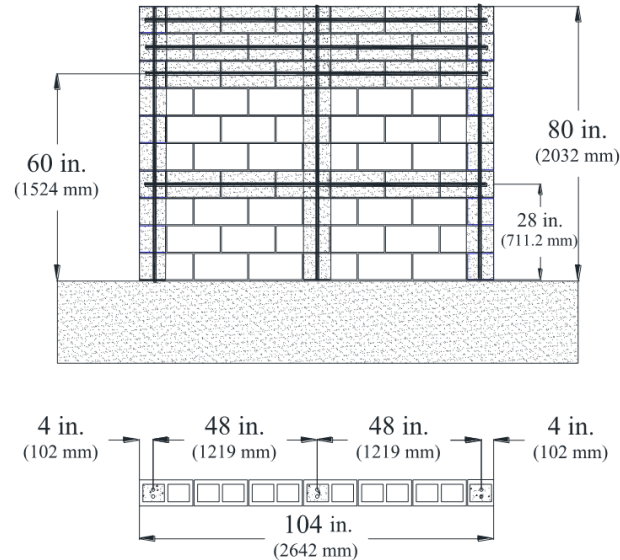


Figure 4.15 – PG wall specimen “PG254-48” (adapted from Elmapruk (2010))

The input parameters for the wall are summarized in Table 4.13, along with the associated normalized values mapped from $[-1, 1]$. The vector, $\{X_{norm}\}$, is comprised of the input values in the “Normalized” column.

Table 4.13 – Normalized input values for “PG254-48”

	Input Variable (x_i)	Min ($x_{i_{min}}$)	Max ($x_{i_{max}}$)	PG254-48 (x_i)	Normalized ($x_{i_{norm}}$)
Input 1, x_1	A_{scaled} [m ²]	0.66	19.43	4.03	-0.6413
Input 2, x_2	M/VL [unitless]	0.250	2.295	0.288	-0.9623
Input 3, x_3	A_{net}/A_{gross} [unitless]	0.405	0.808	0.450	-0.7756
Input 4, x_4	$f'_{m,eff,corrected}$ [MPa]	4.25	22.29	18.49	0.5792
Input 5, x_5	$\rho_v f_{yv}$ [MPa]	0.000	4.842	0.476	-0.7067
Input 6, x_6	$\rho_h f_{yh}$ [MPa]	0.000	1.290	0.614	-0.0478
Input 7, x_7	σ_{gross} [MPa]	0.000	1.724	0.096	-0.8888

Then, using the input matrix, $[IW]$, layer weight matrix, $[LW]$, and biases, b_1, b_2 for the “F-7-5-1” neural network model, a normalized prediction is calculated:

$$y_{\text{norm}} = [LW] \cdot \tanh(b_1 + [IW]\{X_{\text{norm}}\}) + b_2 \quad (4.7)$$

$$y_{\text{norm}} = [LW] \cdot \tanh \left(b_1 + [IW] \begin{pmatrix} -0.6413 \\ -0.9263 \\ -0.7756 \\ 0.5792 \\ -0.7067 \\ -0.0478 \\ -0.8888 \end{pmatrix} \right) + b_2 \quad (4.8)$$

In explicit form,

$$y_{\text{norm}} = [0.8144 \quad -0.3618 \quad -0.3675 \quad -0.8712 \quad -0.8893] \cdot \tanh \left(\begin{bmatrix} 1.5154 \\ 1.7618 \\ -0.4254 \\ -0.0269 \\ -1.3641 \end{bmatrix} + \begin{bmatrix} -0.6183 & -0.6835 & 1.6011 & -0.3643 & 1.1593 & -0.0237 & 0.0430 \\ 1.3134 & 1.2532 & -2.1502 & -1.6223 & -0.0682 & -1.3960 & -1.7227 \\ 0.0637 & -1.3889 & -2.4748 & -0.9587 & -1.2993 & -0.8316 & 1.8284 \\ 0.0070 & -0.9053 & 1.0992 & -0.9918 & 1.9170 & 1.0863 & 1.9599 \\ 0.0206 & -0.6339 & 0.4812 & -0.4361 & 0.8425 & -1.2191 & 1.0364 \end{bmatrix} \begin{bmatrix} -0.6413 \\ -0.9263 \\ -0.7756 \\ 0.5792 \\ -0.7067 \\ -0.0478 \\ -0.8888 \end{bmatrix} \right) - 0.6123 \quad (4.9)$$

$$y_{\text{norm}} = -0.4055 \quad (4.10)$$

Then, to obtain the predicted shear strength, y , the output, y_{norm} , must be unmapped using the minimum and maximum output values from Table 4.12.

$$y = \frac{(y_{\text{min}} - y_{\text{max}})(y_{\text{norm}} - 1)}{-2} + y_{\text{max}} \quad (4.11)$$

$$y = \frac{(0.232 - 1.081)(-0.4055 - 1)}{-2} + 1.081 \quad (4.12)$$

$$y = v_n = 0.4846 \text{ MPa} \quad (4.13)$$

In comparison to the experimental value, $v_{\text{exp}} = 0.529 \text{ MPa}$, the “F-7-5-1” neural network model outputs a $v_{\text{exp}}/v_n = 1.09$.

5 FINITE ELEMENT INVESTIGATION ON PARTIALLY GROUTED MASONRY SHEAR WALLS

5.1 Introduction

Although the results presented indicate that ANNs are a viable option to predict the in-plane shear strength of masonry walls, there are gaps in the design variables used as input in the dataset. Fig. 5.1 summarizes dataset “F,” highlighting the gaps which exist in variables such as the area of wall, vertical reinforcement ratio, and shear span ratio. It has also been mentioned previously that ANN based prediction models are dependable only within the range of parameters used for training and should not be relied upon for extrapolation. With the experimental strength of PG walls within dataset “F” only ranging from 0.232 to 1.081 MPa, the ANN model developed in this study may lose accuracy in predicting the shear strength of PG walls beyond 1.081 MPa. To address these gaps and expand the dataset beyond the current range of parameters for future ANN development, a FE analysis validated with experimental results can be used to generate hypothetical specimens.

It has been argued that accurate numerical modeling of masonry through the finite-element (FE) method can only be adequately addressed through micro-modelling of its individual components. Micro-modelling consists of representing units, mortar in the joints and grout as continuum elements whereas the unit-mortar interface is represented by discontinuous elements (Bolhassani et al. 2015). However, macro-modelling of masonry, in which all masonry components are considered to have smeared properties has also been used with varying success (Lourenço et al. 1995). In macro-modelling, the constitutive relationships for units, mortar, and unit-mortar interface are averaged in a homogeneous continuum (Lourenço 2002). Macro-models of masonry structure are more suited to estimate structural response at the global level but, predictably, are unable to capture local failure mechanisms (Lotfi and Shing 1991; Lourenço and Rots 1997).

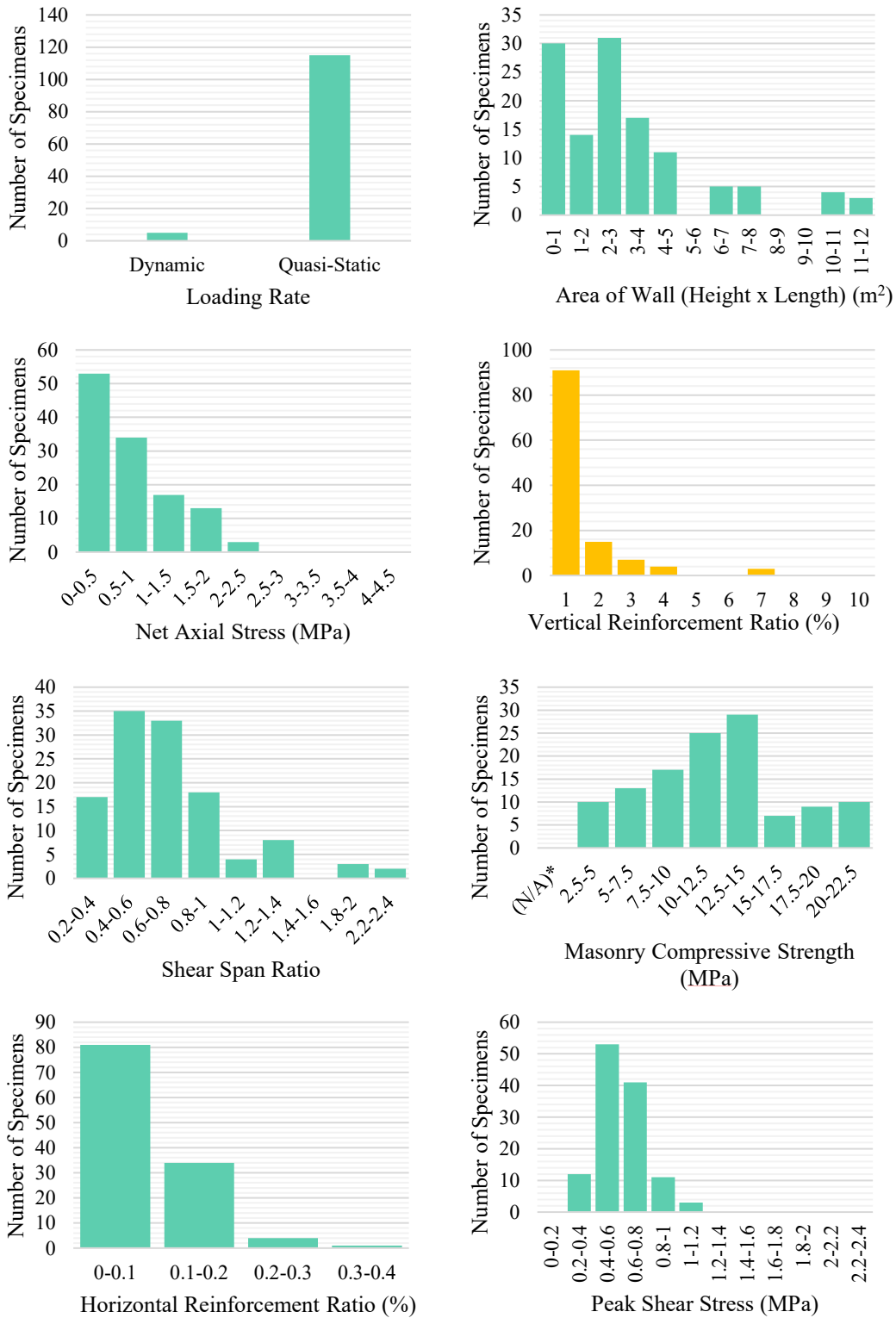


Figure 5.1 – Distribution of various parameters in dataset “F”

Formulations that combine the two approaches, such as the Disturbed Stress Field Model (DSFM) or the two-phase masonry model developed by Maleki (2008) have been shown to predict with satisfactory accuracy both the global and local responses of unreinforced masonry walls (Maleki 2008), reinforced masonry walls (Facconi et al. 2013) and partially grouted walls (Lotfi and Shing 1991). The DSFM, originally developed by Vecchio (2000, 2001) for reinforced concrete, can combine the average macroscopic representation of the masonry behavior with the local shear stress-slip response of mortar joints. The study by Seif EIDin and Galal (2016) demonstrated that the DSFM, originally used to model URM structures, can be also used to estimate the response of RM shear walls. A satisfactory prediction of peak strength, pre-peak and post-peak load-displacement response in fully grouted RM shear walls with a closely spaced vertical steel rebar arrangement (<400 mm) was reported. In walls with wider spacings (>800 mm), the DSFM approach led to a satisfactory estimation of peak shear strength only. These results indicate that the DSFM is a promising tool to investigate the peak shear behaviour of PG walls, the only output parameter needed in the development of an ANN analytical database.

5.2 VecTor2 Background

The program VecTor2 was chosen to conduct the FE analysis in this study. Developed at the University of Toronto in 1990, VecTor2 is a non-linear FE analysis program developed for analyzing two-dimensional reinforced concrete membrane structures modelled as an orthotropic material with smeared and rotating cracks. It is based on Modified Compression Field Theory (MCTF) developed by Vecchio and Collins (1986), and the Distributed Stress Field Model (DSFM) by Vecchio (2000, 2001) to predict strength, post-peak behavior, failure mode, deflections, and cracking. Readers interested in a more exhaustive description of the VecTor2 FE analysis program can refer to the VecTor2 and FormWorks Manual (Wong et al. 2013).

Although VecTor2 was originally intended for reinforced concrete structures, it also has built-in masonry settings for applying the FE analysis to reinforced masonry structures. Masonry can be modelled in VecTor2 as a continuum with average properties where joint

failures are smeared across the single element for sufficiently large masonry structures. The tensile behaviour of masonry is modelled as an isotropic linear elastic material and modelled as a continuum that may slip along the head and bed joints even when the material is uncracked (Wong et al. 2013).

5.3 VecTor2 Model Description

A PG wall specimen tested by Maleki (2008) was used to verify the performance of the FE analysis model. The wall chosen from Maleki (2008)'s study is "Wall 1." The specimen is illustrated by Fig. 5.2, and Fig. 5.3 is the experimental hysteresis loop and envelope obtained. The following section will outline the materials, boundary conditions, and loading conditions applied to Wall 1 in Maleki (2008)'s experimental study, as well as how it is modelled in VecTor2.

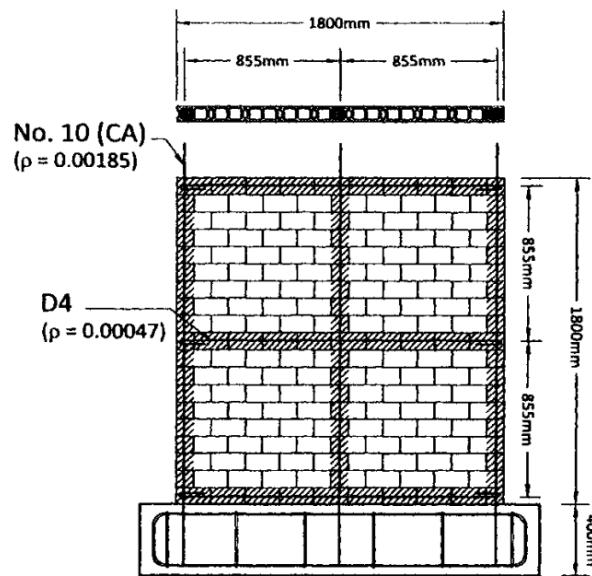


Figure 5.2 – Wall 1 (Maleki 2008)

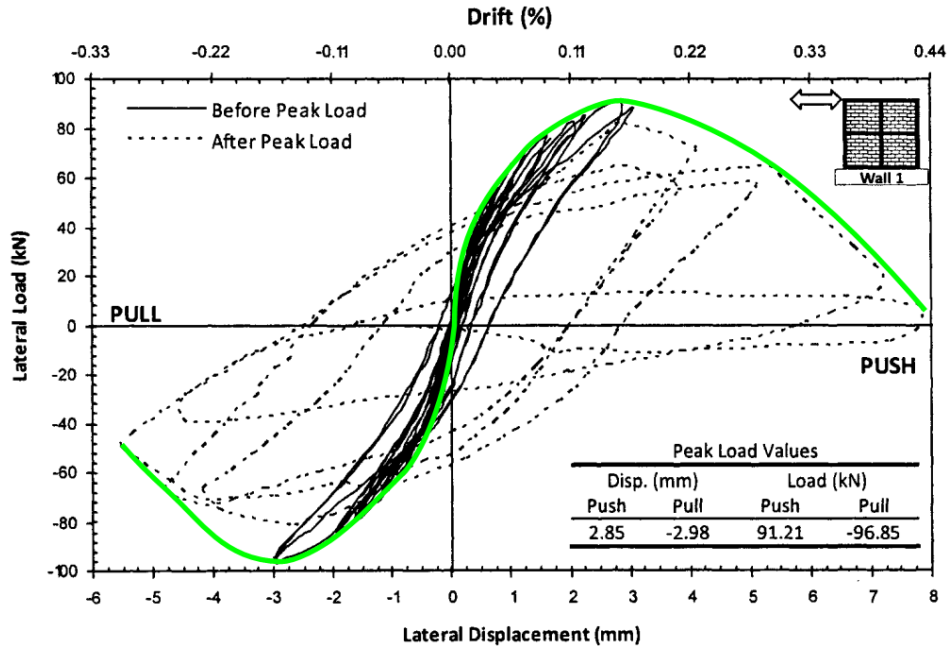


Figure 5.3 – Wall 1 hysteresis loop with envelope outlined in green (adapted from Maleki (2008))

5.3.1 Material Properties

Experimental Study: “Wall 1” is made of half-scale blocks and has dimensions of 1800mm x 1800mm x 90mm. Wall reinforcement consists of three horizontal D4 bars ($A_{bar} = 25.8 \text{ mm}^2$) and three vertical No. 10 bars ($A_{bar} = 100 \text{ mm}^2$).

VecTor2: Rectangular elements are used to model the grouted and hollow masonry, whilst truss elements are used to model the horizontal and vertical steel reinforcement. The height and length of each rectangular element measures 45 mm x 45 mm. The hollow masonry elements are modelled with a thickness equivalent to twice the face shell to account for the absence of grout (51.18 mm), while the grouted masonry elements are modelled with the thickness of the wall (90 mm). The material properties of the wall for VecTor2 input are summarized in Table 5.1, and the VecTor2 model of “Wall 1” is illustrated in Fig. 5.4.

Table 5.1 – VecTor2 model properties

GEOMETRIC PROPERTIES	LOADING CONDITIONS
$H = 1800$ mm $L = 1800$ mm $t = 90$ mm	Reverse Cyclic Loading Axial Load: 121.5 kN Axial Stress (Gross): 0.75 MPa
MATERIAL PROPERTIES	
<p>■ Grouted Masonry</p> $f'_m = 26.3$ MPa $\epsilon_m = 0.0013$ $f_{cr} = 2.65$ MPa $E_m = 20000$ MPa $N = 0.16$ <p>□ Hollow Masonry</p> $f'_m = 14.1$ MPa $\epsilon_m = 0.0014$ $f_{cr} = 1.4$ MPa $E_m = 20000$ MPa $N = 0.16$ <p>■ Concrete Beam*</p> $f'_c = 200$ MPa $f'_t = 200$ MPa <p>* Modelled to provide fixed support at top of wall (double curvature)</p>	<p>■ Horizontal Reinforcement</p> $A = 25.8$ mm ² (D4 Bars) $E_s = 198.2$ GPa $F_y = 690.7$ MPa $P = 0.05\%$ $F_u = 720$ MPa $\epsilon_{sh} = 3.5$ m ϵ $\epsilon_u = 12.54$ m ϵ <p>■ Vertical Reinforcement</p> $A = 100$ mm ² (No. 10 Bars) $E_s = 201.6$ GPa $F_y = 491.7$ MPa $P = 0.19\%$ $F_u = 620$ MPa $\epsilon_{sh} = 29.69$ m ϵ $\epsilon_u = 129.66$ m ϵ

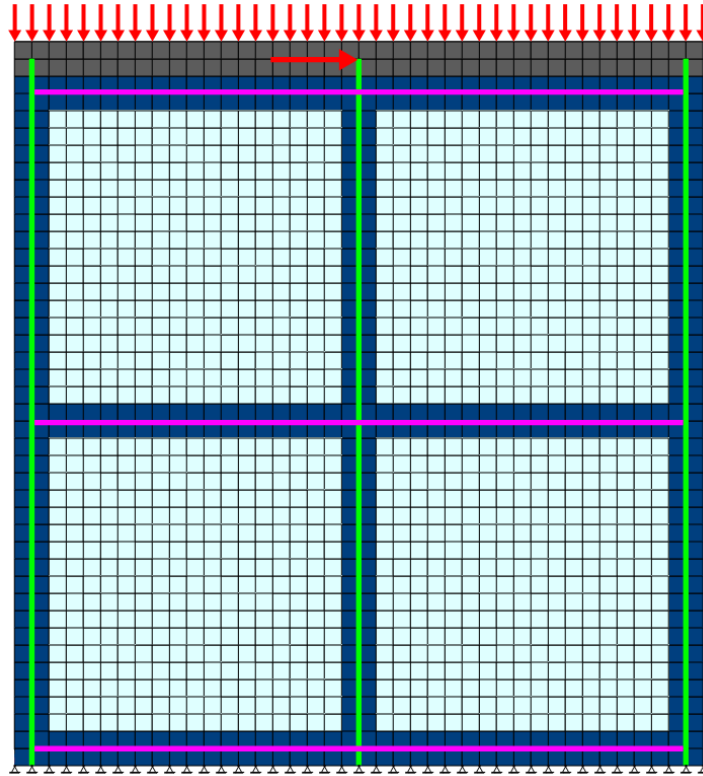


Figure 5.4 – VecTor2 model of Maleki (2008)’s PG specimen “Wall 1”

5.3.2 Boundary Conditions

Experimental Study: “Wall 1” is subject to double curvature boundary conditions. A 500 mm x 400 mm reinforced concrete base was built to simulate a fixed support at the bottom. A steel beam was attached to the top the wall to apply a uniform lateral load.

VecTor2: To simulate the boundary conditions in VecTor2, the joints at the base are restrained in the x and y directions with pinned supports, and a “concrete” loading beam with 200 MPa compressive and tensile strength is modelled at the top of the wall.

5.3.3 Loading Conditions

Experimental Study: The wall was subject to constant gravity load of 121.5 kN and a cyclic lateral displacement was applied up to 7.2 mm. Lateral load began with 0.01% storey drift, then increased by 1.3-1.5 times the previous loading, repeating each loading

cycle twice. The loading cycle used in Maleki (2008)'s study for Wall 1 is shown in Fig. 5.5.

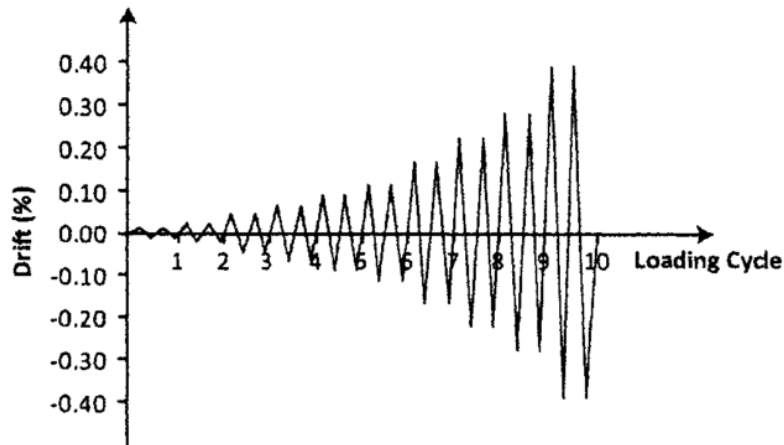


Figure 5.5 – Loading cycle used for “Wall 1” (Maleki 2008)

VecTor2: To simulate the gravity load, a single step, monotonic, force-controlled load case is applied by applying a gravity force of 2.9634 kN on each of the 41 nodes at the top of the wall, simulating a distributed load of 121.5 kN on the wall.

To simulate the lateral load, a reverse cyclic, displacement-controlled load case is activated in *VecTor2* with 2 repetitions per load cycle. An initial 0.18 mm displacement (equivalent to 0.01% storey drift) is applied with and a cyclic incremental factor of 0.72 mm. A total of 2,000 load stages are performed in *VecTor2*. The loading cycle used in *VecTor2* is illustrated in Fig. 5.6. It is recognized that the loading cycle simulated in *VecTor2* is not entirely identical to the experimental loading cycle, due to the experimental loading cycle using a varied cyclic incremental factor.

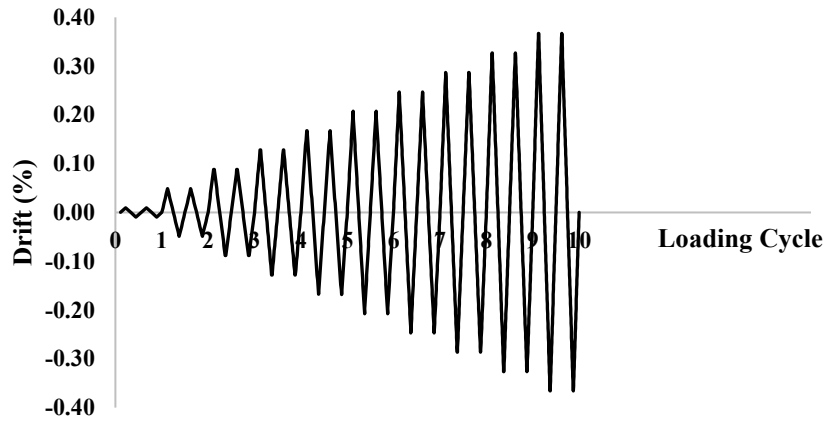


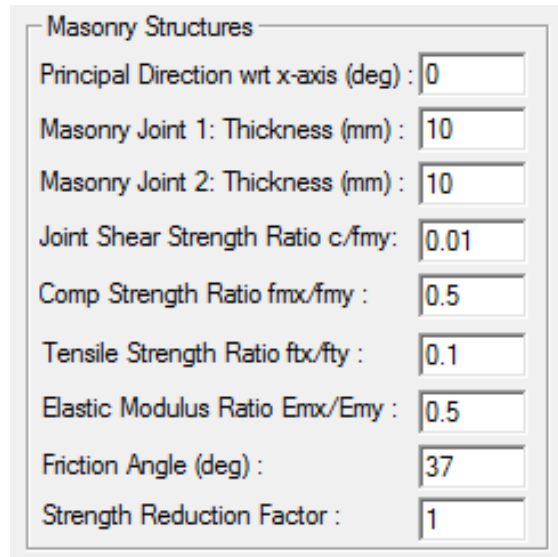
Figure 5.6 – Loading cycle used for “Wall 1” in VecTor2

The VecTor2 job description with both lateral and gravity loading cases (Case 1 and Case 2, respectively) is illustrated in Fig. 5.7.

Figure 5.7 – VecTor2 define job dialog

5.4 VecTor2 Results and Discussion

The material properties and ‘Masonry Structures’ settings were modified in various combinations to observe the response of the model. Further explanation of each of these settings can be found in the VecTor2 and FormWorks Manual (Wong et al. 2013). The default values in VecTor2 for masonry structures is shown in Fig. 5.8.



Masonry Structures	
Principal Direction wrt x-axis (deg) :	0
Masonry Joint 1: Thickness (mm) :	10
Masonry Joint 2: Thickness (mm) :	10
Joint Shear Strength Ratio c/f_{my} :	0.01
Comp Strength Ratio f_{mx}/f_{my} :	0.5
Tensile Strength Ratio f_{tx}/f_{ty} :	0.1
Elastic Modulus Ratio E_{mx}/E_{my} :	0.5
Friction Angle (deg) :	37
Strength Reduction Factor :	1

Figure 5.8 – VecTor2 masonry structures default settings

After conducting several parametric analyses, the ‘Joint Shear Strength Ratio’, the ratio between the shear strength of the joints and the maximum compressive strength of masonry, was observed to have the largest influence on the predicted response. The value for the ‘Joint Shear Strength Ratio’ that provided the best fit between experimental and analytical results was 0.03.

The relative error between measured and FE modelled peak strength is within 10%, as summarized in Table 5.2. This range of error is typical for FE models with materials similar to masonry, such as reinforced concrete and prestressed concrete structures.

Table 5.2 – Comparison of experimental vs VecTor2 model

Results		Experimental Wall 1	VecTor2 Model	% Error
Pull	Peak Load (kN)	96.9	93.4	3.61
	Displacement (mm)	3.06	3.016	1.44
Push	Peak Load (kN)	91.2	90.7	0.55
	Displacement (mm)	2.88	2.662	7.57

The VecTor2 model hysteresis loop with the hysteresis envelope outlined is illustrated in Fig. 5.9. The envelope from the VecTor2 model is then layered onto the experimental hysteresis loop and envelope for comparison in Fig. 5.10. The VecTor2 model wall exhibits greater stiffness than the experimental result. Also, the post-peak ductility of the VecTor2 model is comparable on the push cycle but exhibits greater ductility in the pull cycle than the experimental result.

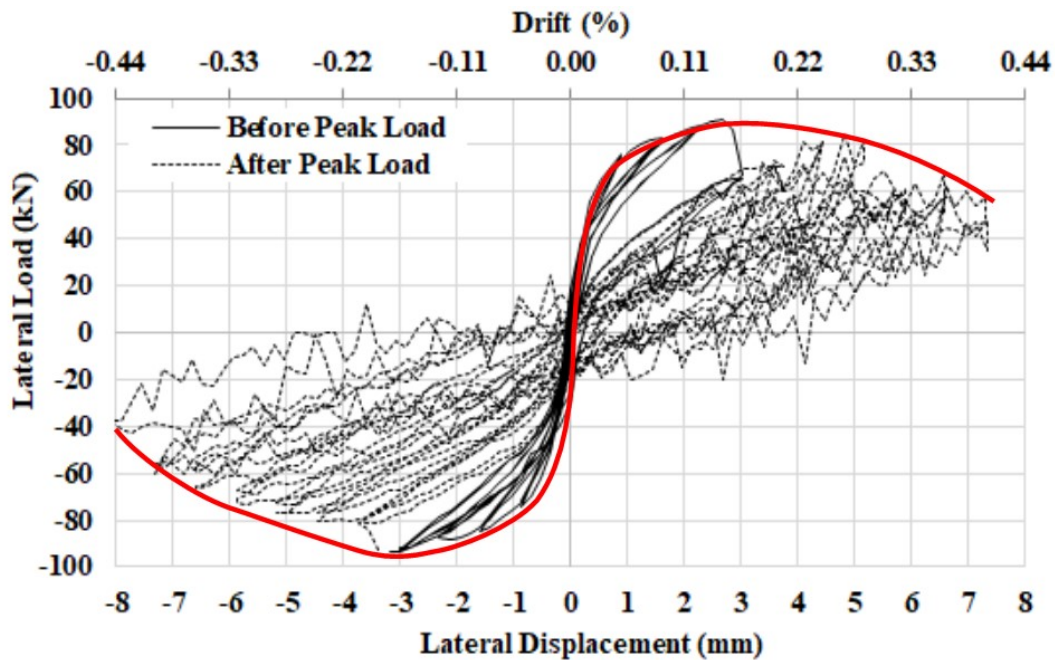


Figure 5.9 – Wall 1 VecTor2 model hysteresis loop with envelope outlined in red

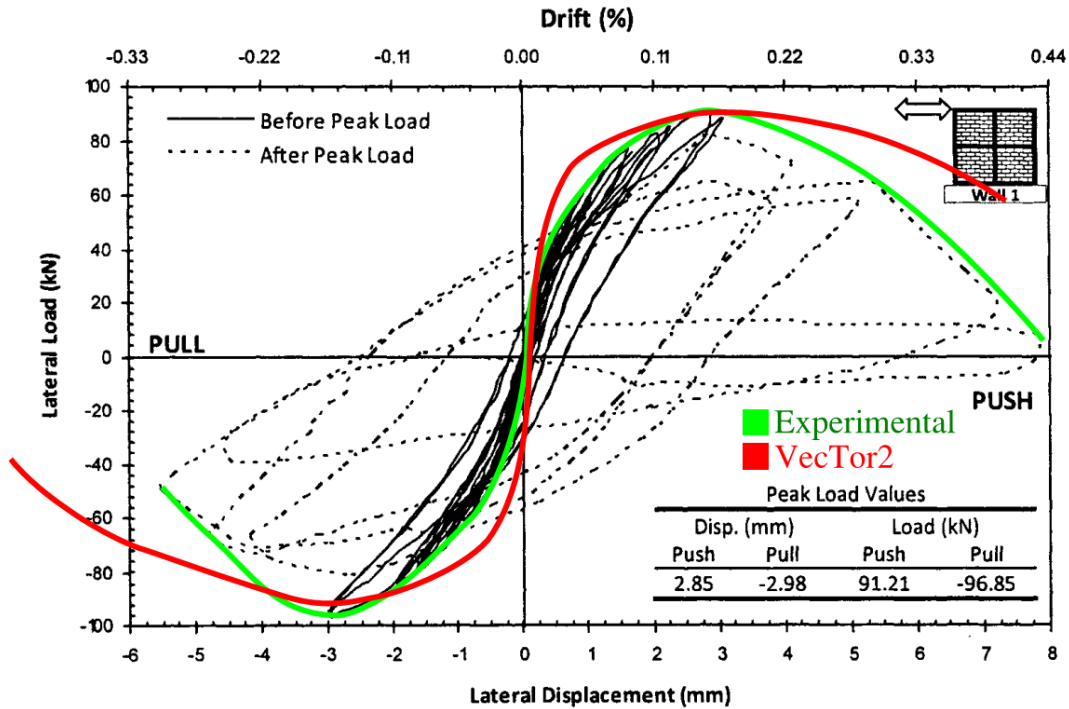


Figure 5.10 – Wall 1 experimental hysteresis loop envelope outlined in green with VecTor2 model hysteresis loop envelope outlined in red (adapted from Maleki (2008))

5.5 Summary

Overall, the results suggest that a FE analysis model is a practical option for generating additional input data for training the ANN. However, further work on the model is required to refine and validate the FE model prior to utilizing the model to simulate hypothetical PG walls and increase the number of specimens for developing an ANN model. Several improvements are suggested for further research:

- The reverse cyclic loading used in VecTor2 can be further refined to better simulate the actual loading used in Maleki (2008)'s experimental study. Since VecTor2 only allows users to specify a fixed value for the cyclic incremental factor, users must use seed files to store the strain and stress history of the structure, and then continue the analysis by loading the seed file back into VecTor2 with a different value for the cyclic incremental factor.

- Given that the FE model used in this study is a macroscale model, it would be expected that microscale models would be more accurate. A microscale model would require a program besides VecTor2.
- The FE model—whether microscale or macroscale—must be validated using walls from multiple studies. In particular, the wall tested by Maleki (2008) is a PG specimen built with a $\frac{1}{2}$ -scale factor. It is recommended that a FE model is built and validated using full scale PG specimens, such as the walls tested by Elmapruk (2010).
- A more robust FE model must also be capable of modelling joint reinforcement, which was not used in any of Maleki's walls.

6 CONCLUSIONS AND RECOMMENDATIONS

6.1 Summary

The objective of investigating the in-plane shear strength and behaviour of PG concrete block masonry walls governed by diagonal shear failure was achieved by the following:

1. A meta-analysis involving dataset assembly, scrutinization, and synthesization was performed:
 - 292 PG concrete block masonry walls exhibiting in-plane diagonal tension shear failure from 26 experimental studies was compiled
 - Six datasets (“A” to “F”) were developed with varying levels of scrutinization for ANN analysis.
 - Dataset “A”: 255 specimens; excludes studies in which the compressive strength of the masonry could not be determined or calculated
 - Dataset “B”: 150 specimens; dataset “A”, but also excludes specimens that were tested under monotonic loading
 - Datasets “C”: 150 specimens; dataset “B”, but the horizontal reinforcement considered for analysis is modified based on the assumption that any bond beams at the bottom course do not provide additional shear resistance
 - Dataset “D”: 120 specimens; dataset “C”, but also excludes also specimens tested using the ESECMaSE setup
 - Dataset “E”: 120 specimens; dataset “D”, but the horizontal reinforcement considered for analysis is modified based on the assumption that any bond beams at the bottom course do not provide additional shear resistance
 - Dataset “F”: 120 specimens; dataset “E”, but only the interior (web) reinforcement is considered as vertical reinforcement contributing to the shear strength of PG walls.
2. The performance of 14 currently available shear strength expressions from various researchers and design codes are evaluated to set a benchmark for ANN-based models

using several statistical measurements: mean squared error, mean V_{exp}/V_n ratio, standard deviation V_{exp}/V_n ratio, and fifth percentile V_{exp}/V_n ratio.

- The majority of the available design equations demonstrated a lack of consistency in predictions as indicated by high values of deviation for the V_{exp}/V_n ratio; the experimental-to-predicted ratio standard deviations for the CSA S304.1-04 (2004), TMS 402/602 (2016), and NZS 4230 (2004) equations were found to be 0.666, 0.691, and 1.077, respectively.
 - Currently available design equations were also found to predict non-conservative predictions as indicated by low values of fifth percentile for the V_{exp}/V_n ratio; the experimental-to-predicted ratio fifth percentiles for the CSA S304.1-04 (2004), TMS 402/602 (2016), and NZS 4230 (2004) equations were found to be 0.453, 0.678, and 0.375, respectively.
3. Various ANN models are investigated and compared against currently available design equations:
- 5-input ($x-5-n-1$) ANN models were generated using the following input parameters based on the ANN models developed by Aguilar et al. (2016): $\sqrt{f'_m} \times \left(\frac{M}{VL}\right)^{-1}$ [MPa], $\rho_h f_{yh}$ [MPa], $\rho_v \sqrt{f_j f_{yv}}$ [MPa], $\gamma \delta \sqrt{\rho_h f_{yh} f'_m}$ [MPa], σ [MPa].
 - 7-input ($x-7-n-1$) ANN models were generated using the following input parameters: A_{scaled} [m^2], M/VL [unitless], A_{net}/A_{gross} [unitless], $f'_{m,eff,corrected}$ [MPa], $\rho_v f_{yv}$ [MPa], $\rho_h f_{yh}$ [MPa], σ_{gross} [MPa].
 - The number of hidden neurons was varied from 1 to 5 for both ($x-5-n-1$) and ($x-7-n-1$) ANN models.
 - The performance of ANN models is evaluated for comparison against currently available design equations.
 - The experimental-to-predicted ratio standard deviations for the “F-5-5-1” and “F-7-5-1” ANN models were found to be 0.175 and 0.183, respectively.
 - The experimental-to-predicted ratio fifth percentiles for the “F-5-5-1” and “F-7-5-1” ANN models were found to be 0.767 and 0.791, respectively.

4. A sensitivity analysis is performed on “F-5-5-1” and “F-7-5-1” ANN models to gain further insight into the behaviour of PG walls.
 - The sensitivity analysis reveals a size effect in PG shear walls that is previously unaccounted for in currently available design equations
 - The sensitivity analysis reveals ANN models predicting a decrease in shear strength as the compressive strength of masonry prism is increased
 - The relative influence of each parameter is revealed through the sensitivity analysis
5. A preliminary finite-element (FE) model of a PG wall under in-plane shear loading was developed and validated in VecTor2
 - In general, the behaviour (i.e. peak shear load, displacement, stiffness and degradation) of the modelled PG wall under in-plane shear strength in VecTor2 was comparable with the experimental results.
 - The relative error between measured and FE modelled peak strength is within 10%, and the relative error for displacement is within 15%.

6.2 Conclusions

The results presented in this study demonstrate the potential for utilizing ANNs to address the limitations of current design expressions to predict the in-plane shear strength of PG shear walls. The following conclusions are made:

- Dataset “F” was found to be a viable dataset for training despite having the fewest number of specimens out of the datasets in this study, emphasizing the importance of data scrutinization and synthesization in meta-analysis. In comparison to dataset “A” containing 255 specimens, dataset “F” contains 120 specimens, and excludes specimens tested under monotonic loading, excludes specimens tested using the ESECMaSE test setup, the horizontal reinforcement considered for analysis is modified based on the assumption that any bond beams at the bottom course do not provide additional shear resistance, and only the interior vertical reinforcement is considered.

- ANN models were found to have a better predictive capacity when specimens using the ESECMaSE test setup are removed from the overall dataset, emphasizing the importance of an appropriate test setup for testing PG masonry shear walls and drawing conclusions from its results, whether by ANN analysis or otherwise.
- The 7-input models in this study performed better than the 5-input models. Additionally, an increased number of hidden neurons results in an improved predictive capacity ANN models, although the risk of overfitting also increases.
- Both “F-5-5-1” and “F-7-5-1” models exhibit significant improvements in all performance metrics in comparison with current design expressions; the mean squared error, mean V_{exp}/V_n ratio, standard deviation V_{exp}/V_n ratio, and fifth percentile V_{exp}/V_n ratio are all significantly improved in the ANN models. Additionally, the ANN models exhibit homoscedasticity in its predictions, whereas current design expressions tend to overpredict higher strength walls more severely than lower strength walls.
- The sensitivity analysis showed that the ANN models predicted an increase in gross shear strength as the shear span ratio (M/VL) is increased, as partial grouting ratio (A_{net}/A_{gross}) is increased, as the vertical reinforcement ratio and strength ($\rho_v f_{yv}$) is increased, as the horizontal reinforcement ratio and strength ($\rho_h f_{yh}$) is increased, and as gross axial load (σ_{gross}) is increased. Each of these observations are consistent with existing design expressions and conclusions by researchers.
- The sensitivity analysis revealed that the ANN models predict a decrease in shear strength as the compressive strength of masonry prism is increased, an observation that is inconsistent with existing design expressions. A possible explanation is that f'_m may not be an ideal parameter for predicting the shear strength of PG walls since it is dependent on the angle of the compression strut due to the anisotropy of masonry.
- The sensitivity analysis found horizontal reinforcement and interior vertical reinforcement to have a similar contribution to the shear strength of PG walls, consistent with the equation proposed by Dillon (2015).

- The sensitivity analysis revealed that the ANN models in this study recognize a size effect in PG masonry shear walls; larger walls (A_{scaled}) tend to exhibit less shear strength, a phenomenon currently unaccounted for in currently available design expressions.
- The FE model in VecTor2 demonstrates potential for generating additional data points for ANN analysis.

6.3 Recommendations & Future Research

The results presented in this study demonstrate the potential for utilizing ANNs to address the limitations of current design expressions to predict the in-plane shear strength of PG shear walls. The following points of further research are recommended:

- ANN based prediction models are dependable only within the range of parameters used for training and should not be relied upon for extrapolation. The range of gross shear strength in dataset “F” range from 0.232 MPa to 1.802 MPa. Further research is necessary to expand the range of ANN analysis and investigate how input variables affect walls stronger than 1.8 MPa.
- Experimental studies on size effect (influence of A_{scaled}) is necessary to investigate its effect on the shear strength of PG walls.
- The ANN models predict that an increase in f'_m leads to a decrease in PG wall shear strength. It is suggested that this is due to the trend which exists in the dataset, but not necessarily reflecting physical reality. Further studies may be required to increase the sample size and examine the effect of f'_m on shear strength.
- Further research is required to study whether the tensile strength of masonry may be more relevant than the compressive strength of masonry prisms for the predicting the diagonal tension shear failure of PG walls.
- The majority of available shear equations do not consider the interaction between variables. For example, axial loading has a greater influence on the shear strength of PG masonry walls as the aspect ratio decreases. On the other hand, the influence of horizontal reinforcement ratio tends to decrease when the aspect ratio decreases.

Further insight may be obtainable by ANN models by performing additional sensitivity analyses. The sensitivity analysis presented in this study fixes each input parameter at the medium value; performing sensitivity analysis at different fixed values may reveal subtleties in the interrelationships between variables.

- ANN models often produce equations that are challenging to distill; further research may involve generating simplified equations from ANN models using techniques such as numerical methods
- Further development and validation of a FE model is required to provide additional insight on the behaviour of PG walls and potentially increase the training dataset for ANN analysis.

REFERENCES

- Abrams, D. P., and Kreger, M. E. (1982). "Modeling of reinforced concrete members at small scales." *Proceedings of the Seventh World Conference on Earthquake Engineering*, Istanbul, Turkey.
- Adhikary, B. B., and Mutsuyoshi, H. (2006). "Prediction of shear strength of steel fiber RC beams using neural networks." *Construction and Building Materials*, 20(9), 801–811.
- Aguilar, V. (2013). "Estimation of shear strength of reinforced masonry walls. Comparative study and use of artificial neural networks." Universidad Austral de Chile.
- Aguilar, V., Sandoval, C., Adam, J. M., Garzón-Roca, J., and Valdebenito, G. (2016). "Prediction of the shear strength of reinforced masonry walls using a large experimental database and artificial neural networks." *Structure and Infrastructure Engineering*, 12(12), 1661–1674.
- Anderson, D., and Brzev, S. (2009). "Seismic design guide for masonry buildings." (April).
- Anderson, D. L., and Priestley, M. J. N. (1992). "In plane shear strength of masonry walls." *6th Canadian Masonry Symposium*, 223–234.
- Applied Technology Council. (2009). "FEMA P695: Quantification of building seismic performance factors." (June), 421.
- AS 3700. (2011). "Masonry Structures."
- Baenziger, G., and Porter, M. L. (2011). "Joint reinforcement for masonry shear walls." *11th North American Masonry Conference*.
- Basheer, I. A., and Hajmeer, M. (2000). "Artificial neural networks: Fundamentals, computing, design, and application." *Journal of Microbiological Methods*, 43(1), 3–31.
- Bažant, Z. P. (1997). "Scaling of quasibrittle fracture: asymptotic analysis." *International Journal of Fracture*, 83, 19–40.
- Bažant, Z. P., and Yu, Q. (2009). "Universal Size Effect Law and Effect of Crack Depth on Quasi-Brittle Structure Strength." *Journal of Engineering Mechanics*, 135(2), 78–84.
- Blomquist, N. S. (1980). "A Note on the Use of the Coefficient of Determination." *The Scandinavian Journal of Economics*, 82(3), 409–412.
- Blume, J. A., and Proulx, J. (1968). *Shear in grouted brick masonry wall elements*. San

Francisco.

- Bolhassani, M., Hamid, A. A., Johnson, C., and Schultz, A. E. (2016). "Shear strength expression for partially grouted masonry walls." *Engineering Structures*, 127, 475–494.
- Bolhassani, M., Hamid, A. A., Lau, A. C. W., and Moon, F. L. (2015). "Simplified micro modeling of partially grouted masonry assemblages." *Construction and Building Materials*, Elsevier Ltd, 83, 159–173.
- BS 5628. (2005). "Code of practice for the use of masonry."
- Casella, G. (1983). "Leverage and regression through origin." *The American Statistician*, 37(2), 147–152.
- Chatterjee, S., and Hadi, A. S. (2006). *Regression Analysis by Example*.
- Chen, S., Hidalgo, P. A., Mayes, R. L., Clough, R., and Mcniven, H. D. (1978). *Cyclic loading tests of masonry single piers, Volume 2. Height to width ratio of 1*. Berkeley, CA.
- CSA Standard S304.1. (2004). "Design of masonry structures."
- CSA Standard S304.14. (2014). "Design of masonry structures." Canadian Standards Association, Rexdale, ON.
- Dhanasekar, M. (2011). "Shear in reinforced and unreinforced masonry: response, design and construction." *Procedia Engineering*, 14, 2069–2076.
- Dhanasekar, M., and Haider, W. (2011). "Effect of spacing of reinforcement on the behaviour of partially grouted masonry shear walls." *Advances in Structural Engineering*, 14(2), 281–294.
- Dillon, P. (2015). "Shear strength prediction methods for grouted masonry shear walls." Brigham Young University.
- Dillon, P., and Fonseca, F. S. (2014a). "Preliminary Study into the Standardisation of Masonry Shear Wall Reporting Methods." *International Masonry Conference 2014*, 1–12.
- Dillon, P., and Fonseca, F. S. (2014b). "Analysing masonry research data in matrix form." *9th International Masonry Conference*, Guimaraes, Portugal.
- Dillon, P., and Fonseca, F. S. (2017). "Uncertainty in partially grouted masonry shear strength predictions." *13th Canadian Masonry Symposium*, Halifax.
- Drysdale, R. G., and Hamid, A. A. (2005). *Masonry structures: Behaviour and design*. Canadian Masonry Design Centre.

- Eisenhauer, J. G. (2003). "Regression through the Origin." *@BULLET Teaching Statistics*, 25(3).
- El-Chabib, H., and Nehdi, M. (2005). "Neural network modelling of properties of cement-based materials demystified." (3), 91–102.
- El-Dakhakhni, W. W., Banting, B. R., and Miller, S. C. (2013). "Seismic performance parameter quantification of shear-critical reinforced concrete masonry squat walls." *Journal of Structural Engineering*, 139(June), 957–973.
- Elbahy, Y. I., Nehdi, M., and Youssef, M. A. (2010). "Artificial neural network model for deflection analysis of superelastic shape memory alloy reinforced concrete beams." *Canadian Journal of Civil Engineering*, 37(6), 855–865.
- Elmapruk, J. H. (2010). "Shear strength of partially grouted squat masonry shear walls." Washington State University.
- Elmapruk, J. H., and Elgawady, M. A. (2009). "Evaluation of the MSJC 2008 shear strength equations for partially grouted masonry shear walls." *11th Canadian Masonry Symposium*.
- ESECMaSE, and Schermer, D. (2005). *Development of test methods for the determination of masonry properties under lateral loads in WP7, including test methods for European standardisation*. Munich, Germany.
- Faconi, L., Plizzari, G., and Vecchio, F. (2013). "Disturbed stress field model for unreinforced masonry." *Journal of Structural Engineering*, 140(4), 4013085.
- Fattal, S. G. (1993a). *Strength of partially-grouted masonry shear walls under lateral loads*. NISTIR 93-5147.
- Fattal, S. G. (1993b). *The effect of critical parameters on the behavior of partially-grouted masonry shear walls under lateral loads*. NISTIR 93-5147.
- Frost, J. (2012). "Why You Need to Check Your Residual Plots for Regression Analysis: Or, To Err is Human, To Err Randomly is Statistically Divine | Minitab." <<http://blog.minitab.com/blog/adventures-in-statistics-2/why-you-need-to-check-your-residual-plots-for-regression-analysis>> (Dec. 13, 2017).
- Garzón-Roca, J., Adam, J. M., Sandoval, C., and Roca, P. (2013). "Estimation of the axial behaviour of masonry walls based on artificial neural networks." *Computers and Structures*, 125, 145–152.
- Ghanem, G. M., Essawy, A. S., and Hamid, A. A. (1992). "Effect of steel distribution on the behavior of partially reinforced masonry shear walls." *6th Canadian Masonry Symposium*, 356–376.
- Ghanem, G. M., Salama, A. E., Shreif, E. A., and Hamid, A. A. (1993). "Effect of axial

- compression on the behavior of partially reinforced masonry shear walls.” *6th North American Masonry Conference*, 1145–1157.
- Goh, A. T. C. (1995). “Experiments with neural networks as a design-support tool for complex engineering systems.” *Civil Engineering Systems*, 12(4), 327–342.
- Gulec, C. K., and Whittaker, A. S. (2009). “MCEER-09-0010: Performance-Based Assessment and Design of Squat Reinforced Concrete Shear Walls by.”
- Haach, V. G. (2009). “Development of a design method for reinforced masonry subjected to in-plane loading based on experimental and numerical analysis.”
- Haach, V. G., Vasconcelos, G., and Lourenço, P. B. (2007). “Cyclic Behaviour of Truss Type Reinforced Concrete Masonry.” *7o Congresso de Sismologia e Engenharia Sísmica*, Universidade de Porto, Faculdade de Engenharia, Porto, Portugal, 1–12.
- Haach, V. G., Vasconcelos, G., and Lourenço, P. B. (2010). “Experimental Analysis of Reinforced Concrete Block Masonry Walls Subjected to In-Plane Cyclic Loading.” *Journal of Structural Engineering*, 136(April), 452–462.
- Haach, V. G., Vasconcelos, G., and Lourenço, P. B. (2012). “Proposal of a design model for masonry walls subjected to in-plane loading.” *Journal of Structural Engineering*, 139(April), 120814083328002.
- Haider, W. (2007). “Inplane response of wide spaced reinforced masonry shear walls.” Central Queensland University.
- Haidich, A. B. (2010). “Meta-analysis in medical research.” *Hippokratia*, 14(Suppl 1), 29–37.
- Hamedzadeh, A. (2013). “On the shear strength of partially grouted concrete masonry.” University of Calgary.
- Hamid, A. A., and Chandrakeerthy, S. (1992). “Compressive strength of partially grouted concrete masonry using small scale wall elements.” *TMS Journal*, 11(1), 75–85.
- Hamid, A. A., and Moon, F. L. (2005). “Seismic analysis of partially-grouted reinforced masonry walls constructed using masonry cement mortar.” (3), 55.
- Hassanli, R., and Elgawady, M. A. (2013). “The accuracy of in-plane shear strength of PGM walls in different international standards.” *12th Canadian Masonry Symposium*.
- Hassanli, R., Elgawady, M. A., and Mills, J. E. (2014). “An evaluation of design code expressions for in-plane shear strength of partially grouted masonry walls.” *Australian Journal of Structural Engineering*, 15(3), 299–320.
- Haykin, S. (1994). *Neural networks: A comprehensive foundation*. Macmillan College Publishing.

- Hoque, N. (2013). "In-Plane Cyclic Testing of Reinforced Concrete Masonry Walls to Assess the Effect of Varying Reinforcement Anchorage and Boundary Conditions."
- Janaraj, T., and Dhanasekar, M. (2016a). "Design expressions for the in-plane shear capacity of confined masonry shear walls containing squat panels." *Journal of Structural Engineering*, 142(2), 1–12.
- Janaraj, T., and Dhanasekar, M. (2016b). "Studies on the existing in-plane shear equations of partially grouted reinforced masonry." *Australian Journal of Structural Engineering*.
- Johal, P., and Anderson, E. (1988). "Shear Strength of Masonry Piers Under Cyclic Loading." *Masonry: Materials, Design, Construction, and Maintenance, ASTM STP 992*, 18–32.
- Karsoliya, S. (2012). "Approximating Number of Hidden layer neurons in Multiple Hidden Layer BPNN Architecture." *International Journal of Engineering Trends and Technology*, 3(6), 714–717.
- Kozak, A., and Kozak, R. A. (1995). "Notes on regression through the origin." *The Forestry Chronicle*, 71(3), 326–330.
- Lee Rodgers, J., and Alan Nicewander, W. (1988). "Thirteen Ways to Look at the Correlation Coefficient." *The American Statistician*, 42(1), 59–66.
- Lipsey, M., and Wilson, D. (2001). *Practical meta-analysis*. Thousand Oaks, CA: Sage.
- Lotfi, H. R., and Shing, P. B. (1991). "An appraisal of smeared crack models for masonry shear wall analysis." *Computers and Structures*, 41(3), 413–425.
- Lourenço, P. B. (2002). "Computations on historic masonry structures." *Prog. Struct. Engng Mater.*, 4(3), 301–319.
- Lourenço, P. B., and Rots, J. G. (1997). "Multisurface interface model for analysis of masonry structures." *Journal of Engineering Mechanics*, 123(7), 660–668.
- Lourenço, P. B., Rots, J. G., and Blaauwendraad, J. (1995). "Two approaches for the analysis of masonry structures: micro and macro-modeling." *HERON*, 40(4), 313–340.
- Maleki, M. (2008). "Behaviour of partially grouted masonry shear walls under cyclic reversed loading." McMaster University.
- Maleki, M., Drysdale, R. G., Hamid, A. A., and El-Damatty, A. A. (2009). "Behaviour of partially grouted reinforced masonry shear walls - experimental study." *11th Canadian Masonry Symposium*.
- Masonry Standard Joint Committee (MSJC). (2011). "Building code requirements and specifications for masonry structures."

- MathWorks. (2016). “Analyze Neural Network Performance After Training.” <<https://www.mathworks.com/help/nnet/ug/analyze-neural-network-performance-after-training.html>> (Nov. 13, 2016).
- MathWorks. (2017). “Divide Data for Optimal Neural Network Training.” <<https://www.mathworks.com/help/nnet/ug/divide-data-for-optimal-neural-network-training.html>> (Jun. 15, 2017).
- Matsumura, A. (1987). “Shear strength of reinforced hollow unit masonry walls.” *4th North American Masonry Conference*.
- Matsumura, A. (1988). “Shear strength of reinforced masonry walls.” *9th World Conference of Earthquake Engineering*.
- Mayes, R. L., Omote, Y., and Clough, R. W. (1976a). *Cyclic shear tests of masonry piers volume 1 - test results*.
- Mayes, R. L., Omote, Y., and Clough, R. W. (1976b). *Cyclic shear tests of masonry piers volume 2 - analysis of test results*.
- Meli, R., and Salgado, G. (1969). *Comportamiento de muros de mampostería sujetos a carga lateral, segundo informe*. Mexico City.
- Meli, R., Wolff, A. Z., and Esteve, L. (1968). “Comportamiento de muros de mampostería hueca ante carga lateral alternada.” *Revista ingeniera*, 38(3), 371–390.
- Minaie, E. (2009). “Behavior and vulnerability of reinforced masonry shear walls.” Drexel University.
- Minaie, E., Mota, M., Moon, F. L., and Hamid, A. A. (2010). “In-plane behavior of partially grouted reinforced concrete masonry shear walls.” *Journal of Structural Engineering*, 136(9), 1089–1097.
- Mongometry, D. C., Peck, E. A., and Vining, G. G. (2012). *Introduction to Linear Regression Analysis*.
- Morrison, S. C. (2013). “In-plane shear investigation on masonry walls.” University of Tennessee.
- MSJC. (2016). “TMS 402/602-16.”
- Mukherjee, B. A., and Deshpande, J. M. (1995). “Modeling Initial Design Process Using Artificial Neural Networks.” 9, 194–200.
- Naik, U., and Kute, S. Y. (2013). “Span-to-depth ratio effect on shear strength of steel fiber-reinforced high-strength concrete deep beams using ANN model.” *International Journal of Advanced Structural Engineering*, 5(29).
- NEHRP. (1997). “Recommended provisions for seismic regulations for new buildings

- and other structures, Part-1 provisions.” Building Seismic Safety Council, Washington, USA.
- Nolph, S. M. (2010). “In-plane shear performance of partially grouted masonry shear walls.” Washington State University.
- Nolph, S. M., and Elgawady, M. A. (2012). “Static cyclic response of partially grouted masonry shear walls.” *Journal of Structural Engineering*, 138(7), 864–879.
- NZS 4230-1990. (1990). “Code of practice for the design of masonry structures.”
- NZS 4230-2004. (2004). “Design of reinforced concrete masonry structures.”
- Oan, A. F. (2013). “Diagonal shear of partially grouted concrete masonry panels.” University of Calgary.
- Oesterle, R. G., Aristizabal-Ochoa, J. D., Shiu, K. N., and Corely, W. G. (1984). “Web Crushing of Reinforced Concrete Structural Walls.” *ACI journal Proceedings*, 81(3), 231–241.
- Okamoto, S., Tamazaki, Y., Kaminosono, T., Teshigawara, M., and Hirashi, H. (1987). “Seismic capacity of reinforced masonry walls and beams in wind and seismic effects.” *Proceedings of the 18th joint Meeting, U.S.-Japan Panel on Wind and Seismic Effects*, National Institute of Standards and Technology, Gaithersburg, MD.
- Page, A. W. (1989). “A parametric study of the behaviour of masonry.” *5th Canadian Masonry Symposium*, Vancouver, British Columbia, 341–352.
- Paliwal, M., and Kumar, U. A. (2009). “Neural networks and statistical techniques: A review of applications.” *Expert Systems with Applications*, Elsevier Ltd, 36(1), 2–17.
- Plevris, V., and Asteris, P. G. (2014). “Modeling of masonry failure surface under biaxial compressive stress using neural networks.” *Construction and Building Materials*, Elsevier Ltd, 55, 447–461.
- Priestley, M. J. N., Verma, R., and Xiao, Y. (1994). “Seismic shear strength of reinforced concrete columns.” *Journal of Structural Engineering*, 120(8), 2310–2329.
- Ramírez, P., Sandoval, C., and Almazán, J. L. (2015). “Experimental assessment of shear strength and displacement capacity of partially grouted reinforced concrete masonry shear walls.” *11th Canadian Conference on Earthquake Engineering*.
- Ramírez, P., Sandoval, C., and Almazán, J. L. (2016). “Experimental study on in-plane cyclic response of partially grouted reinforced concrete masonry shear walls.” *Engineering Structures*, 126, 598–617.
- Rizaei, S. (2015). “Assessing bond beam horizontal reinforcement efficacy with different end anchorage conditions in concrete block masonry shear walls.” University of

Calgary.

- Rumelhart, D. E., Hinton, G. E., and Williams, R. J. (1986). "Learning internal representations by error propagation." *Readings in Cognitive Science: A Perspective from Psychology and Artificial Intelligence*, 318–362.
- Sarhat, S. R., and Sherwood, E. G. (2015). "The Size Effect in Reinforced Masonry." *12th North American Masonry Conference*, Denver, Colorado.
- Schultz, A. E. (1994). *NIST research program on the seismic resistance of partially-grouted masonry shear walls (NISTIR 5481)*.
- Schultz, A. E. (1996). "Seismic performance of partially-grouted masonry shear walls." *Eleventh World Conference on Earthquake Engineering*.
- Schultz, A. E., Hutchinson, R. S., and Cheok, G. C. (1998). "Seismic performance of masonry walls with bed joint reinforcement." *Structural Engineers World Congress*, 18–23.
- Scrivener, J. C. (1967). "Static racking tests on concrete masonry walls." *International Conference on Masonry Structural Systems*, 185–191.
- Seif Eldin, H. M. (2016). "In-plane shear behaviour of fully grouted reinforced masonry shear walls." Concordia University.
- Seif Eldin, H. M., and Galal, K. (2016). "Effect of shear span to depth ratio on seismic performance of reinforced masonry shear walls." *Proceedings of the CSCE Conference London 2016*, STR-975-1-10.
- Sheela, K. G., and Deepa, S. N. (2013). "Review on methods to fix number of hidden neurons in neural networks." *Mathematical Problems in Engineering*, 2013.
- Shing, B. P. B., Member, A., Noland, J. L., Klamerus, E., and Spaeh, H. (1990a). "Inelastic behavior of concrete masonry shear walls." 115(9), 2204–2225.
- Shing, P. B., Schuller, M., and Hoskere, V. S. (1990b). "In-plane resistance of reinforced masonry shear walls." *Journal of Structural Engineering*, 116(3), 619–640.
- Shirzad, A., Tabesh, M., and Farmani, R. (2014). "A comparison between performance of support vector regression and artificial neural network in prediction of pipe burst rate in water distribution networks." *KSCE Journal of Civil Engineering*, 18(4), 941–948.
- Standards Australia. (2011). "AS 3700-2011 Masonry structures."
- Standards New Zealand. (2004). "NZS 4230:2004 Design of reinforced concrete masonry structures."
- Stathakis, D. (2009). "How many hidden layers and nodes?" *International Journal of*

- Remote Sensing*, 30(8), 2133–2147.
- Sveinsson, B. I., McNiven, H. D., and Sucuoglu, H. (1985). *Cyclic loading tests of masonry single piers - Volume 4: Additional tests with height to width ratio of 1*. Berkeley, CA.
- Svozil, D., Kvasnička, V., and Pospíchal, J. (1997). “Introduction to multi-layer feed-forward neural networks.” *Chemometrics and Intelligent Laboratory Systems*, 39(1), 43–62.
- Taha, M. . R., Noureldin, a, El-Sheimy, N., and Shrive, N. G. (2003). “Artificial neural networks for predicting creep with an example application to structural masonry.” *Canadian Journal of Civil Engineering*, 30(3), 523–532.
- Tetko, I. V., Livingstone, D. J., and Luik, A. I. (1995). “Neural Network Studies. 1. Comparison of Overfitting and Overtraining.” *Journal of Chemical Information and Computer Sciences*, 35(5), 826–833.
- Thurston, S. J., and Hutchinson, D. L. (1982). “Reinforced masonry shear walls: Cyclic load tests in contraflexure.” *Bulletin of the New Zealand Society for Earthquake Engineering*, 15(1), 27–45.
- Tien Bui, D., Pradhan, B., Lofman, O., Revhaug, I., and Dick, O. B. (2012). “Landslide susceptibility assessment in the Hoa Binh province of Vietnam: A comparison of the Levenberg-Marquardt and Bayesian regularized neural networks.” *Geomorphology*, 171–172(September 2016), 12–29.
- Tomažević, M. (1997). “Seismic design of masonry structures.” *Progress in Structural Engineering and Materials*, 1(1), 88–95.
- Tomazevic, M., and Lutman, M. (1996). “Seismic behavior of masonry walls: Modeling of hysteretic rules.” *Journal of Structural Engineering*, 122(9), 1048–1053.
- Tomažević, M., and Lutman, M. (1988). “Seismic resistance of reinforced masonry walls.” *9th World Conference on Earthquake Engineering*.
- Tomažević, M., Lutman, M., and Petkovic, L. (1996). “Seismic Behavior of Masonry Walls: Experimental Simulation.” *Journal of Structural Engineering*, 122(9), 1040–1047.
- Tomažević, M., and Velechovsky, T. (1992). “Some aspects of testing small-scale masonry building models on simple earthquake simulators.” *Earthquake Engineering & Structural Dynamics*, 21(11), 945–963.
- Tu, J. V. (1996). “Advantages and disadvantages of using artificial neural networks versus logistic regression for predicting medical outcomes.” *Journal of Clinical Epidemiology*, 49(11), 1225–1231.

- UBC. (1997). "International conference of building officials." Uniform Building Code, Whittier, CA.
- Vecchio, F. (2000). "Distributed stress field model for reinforced concrete: Formulation." *Journal of Structural Engineering*, 126(9), 1070–1077.
- Vecchio, F. J., and Collins, M. P. (1986). "The Modified Compression-Field Theory for Reinforced Concrete Elements Subjected to Shear." *ACI Journal Proceedings*, 8(22), 219–231.
- Voon, K. C. (2007). "In-plane seismic design of concrete masonry structures." University of Auckland.
- Voon, K. C., and Ingham, J. M. (2001). "Towards suitable shear strength provisions for inclusion in the New Zealand design standard." *6th Australasian Masonry Conference*, Adelaide, Australia, 393–402.
- Voon, K. C., and Ingham, J. M. (2002). *Shear strength of masonry walls*. New Zealand.
- Voon, K. C., and Ingham, J. M. (2006). "Experimental in-plane shear strength investigation of reinforced concrete masonry walls." *Journal of Structural Engineering*, 132(3), 400–408.
- Voon, K. C., and Ingham, J. M. (2007). "Design expression for the in-plane shear strength of reinforced concrete masonry." *Journal of Structural Engineering*, 133(5), 706–713.
- Williams, D. (1971). "Seismic behaviour of reinforced masonry shear walls." University of Canterbury.
- Wong, P. S., Vecchio, F. J., and Trommels, H. (2013). "VecTor2 and Formworks Manual." University of Toronto.
- Yancey, C. W. C., and Scribner, C. F. (1989). *Influence of horizontal reinforcement on shear resistance of concrete block masonry walls (NISTIR 4202)*.
- Young, P. H. (2000). "Generalized Coefficient of Determination." *The Journal of Cost Analysis & Management*, 2(1), 59–68.

APPENDIX A: FULL DATASET

This Appendix contains tables of the full dataset used in this study. The principles of meta-analysis and dataset assembly, including data compilation, scrutinization and synthesization, are outlined in Chapter 3. Several values were not found or not explicitly stated in the original source and are identified using the colour scheme outlined in Table A.1.

Table A.1 – Legend for colour scheme used in data tables

Orange	Values that were not found in the paper and were assumed based on the context and outside sources
Red	Values that were not explicitly stated in the paper but were calculated based on other provided data

Wall #	Experimental Study	Wall ID	Test Setup	Scale	LOADING CONDITION		BOUNDARY CONDITION
					Loading Type	Loading Rate	Support Type
1	Scrivener (1967)	C1	Other	1	Monotonic	Quasi-Static	Cantilever
2	Scrivener (1967)	D2	Other	1	Monotonic	Quasi-Static	Cantilever
3	Scrivener (1967)	C10	Other	1	Monotonic	Quasi-Static	Cantilever
4	Scrivener (1967)	C7	Other	1	Monotonic	Quasi-Static	Cantilever
5	Scrivener (1967)	C8	Other	1	Monotonic	Quasi-Static	Cantilever
6	Scrivener (1967)	C9	Other	1	Monotonic	Quasi-Static	Cantilever
7	Scrivener (1967)	D11	Other	1	Monotonic	Quasi-Static	Cantilever
8	Scrivener (1967)	C3	Other	1	Monotonic	Quasi-Static	Cantilever
9	Scrivener (1967)	D12	Other	1	Monotonic	Quasi-Static	Cantilever
10	Scrivener (1967)	D4	Other	1	Monotonic	Quasi-Static	Cantilever
11	Scrivener (1967)	D13	Other	1	Monotonic	Quasi-Static	Cantilever
12	Scrivener (1967)	D14	Other	1	Monotonic	Quasi-Static	Cantilever
13	Meli et al. (1968)	Muro 309	Other	1	Reverse Cyclic	Quasi-Static	Cantilever
14	Meli et al. (1968)	Muro 310	Other	1	Reverse Cyclic	Quasi-Static	Cantilever
15	Meli et al. (1968)	Muro 311	Other	1	Reverse Cyclic	Quasi-Static	Cantilever
16	Meli et al. (1968)	Muro 312	Other	1	Reverse Cyclic	Quasi-Static	Cantilever
17	Meli et al. (1968)	Muro 313	Other	1	Reverse Cyclic	Quasi-Static	Cantilever
18	Meli et al. (1968)	Muro 314	Other	1	Reverse Cyclic	Quasi-Static	Cantilever
19	Meli et al. (1968)	Muro 315	Other	1	Reverse Cyclic	Quasi-Static	Cantilever
20	Meli et al. (1968)	Muro 316	Other	1	Reverse Cyclic	Quasi-Static	Cantilever
21	Meli et al. (1968)	Muro 317	Other	1	Reverse Cyclic	Quasi-Static	Cantilever
22	Meli et al. (1968)	Muro 318	Other	1	Reverse Cyclic	Quasi-Static	Cantilever
23	Meli et al. (1969)	Muro 501	Other	1	Monotonic	Quasi-Static	Cantilever
24	Meli et al. (1969)	Muro 504	Other	1	Monotonic	Quasi-Static	Cantilever
25	Meli et al. (1969)	Muro 505	Other	1	Monotonic	Quasi-Static	Cantilever
26	Meli et al. (1969)	Muro 506	Other	1	Monotonic	Quasi-Static	Cantilever
27	Meli et al. (1969)	Muro 507	Other	1	Monotonic	Quasi-Static	Cantilever
28	Meli et al. (1969)	Muro 508	Other	1	Monotonic	Quasi-Static	Cantilever
29	Meli et al. (1969)	Muro 509	Other	1	Monotonic	Quasi-Static	Cantilever
30	Meli et al. (1969)	Muro 510	Other	1	Monotonic	Quasi-Static	Cantilever
31	Meli et al. (1969)	Muro 511	Other	1	Monotonic	Quasi-Static	Cantilever
32	Meli et al. (1969)	Muro 514	Other	1	Monotonic	Quasi-Static	Cantilever
33	Meli et al. (1969)	Muro 519	Other	1	Monotonic	Quasi-Static	Cantilever

Wall #	Experimental Study	Wall ID	Test Setup	Scale	LOADING CONDITION		BOUNDARY CONDITION
					Loading Type	Loading Rate	Support Type
34	Mayes et al. (1976)	HCBL-21-11	Other	1	Reverse Cyclic	Quasi-Static	Double Curvature
35	Mayes et al. (1976)	HCBL-21-12	Other	1	Reverse Cyclic	Quasi-Static	Double Curvature
36	Chen et al. (1978) / Hidalgo (1978)	HCBL-11-2	Other	1	Reverse Cyclic	Dynamic	Double Curvature
37	Chen et al. (1978) / Hidalgo (1978)	HCBL-11-5	Other	1	Reverse Cyclic	Dynamic	Double Curvature
38	Chen et al. (1978) / Hidalgo (1978)	HCBL-11-8	Other	1	Reverse Cyclic	Dynamic	Double Curvature
39	Chen et al. (1978) / Hidalgo (1978)	HCBL-11-10	Other	1	Reverse Cyclic	Dynamic	Double Curvature
40	Thurston and Hutchison (1982)	UNIT NO. 2	Other	1	Reverse Cyclic	Quasi-Static	Double Curvature
41	Thurston and Hutchison (1982)	UNIT NO. 4	Other	1	Reverse Cyclic	Quasi-Static	Double Curvature
42	Thurston and Hutchison (1982)	UNIT NO. 5	Other	1	Reverse Cyclic	Quasi-Static	Double Curvature
43	Matsumura (1987)	CW4-1-1	Other	1	Reverse Cyclic	Quasi-Static	Double Curvature
44	Matsumura (1987)	CW4-1-2	Other	1	Reverse Cyclic	Quasi-Static	Double Curvature
45	Matsumura (1987)	CW3-1-1	Other	1	Reverse Cyclic	Quasi-Static	Double Curvature
46	Matsumura (1987)	CW3-1-2	Other	1	Reverse Cyclic	Quasi-Static	Double Curvature
47	Matsumura (1987)	CW2-1-1	Other	1	Reverse Cyclic	Quasi-Static	Double Curvature
48	Matsumura (1987)	CW2-1-2	Other	1	Reverse Cyclic	Quasi-Static	Double Curvature
49	Matsumura (1987)	CW3-0-1	Other	1	Reverse Cyclic	Quasi-Static	Double Curvature
50	Matsumura (1987)	CW3-0-2	Other	1	Reverse Cyclic	Quasi-Static	Double Curvature
51	Matsumura (1987)	CW3-1'	Other	1	Reverse Cyclic	Quasi-Static	Double Curvature
52	Matsumura (1987)	CW3-2	Other	1	Reverse Cyclic	Quasi-Static	Double Curvature
53	Matsumura (1987)	CW3-3	Other	1	Reverse Cyclic	Quasi-Static	Double Curvature
54	Matsumura (1987)	CW3-1-A2	Other	1	Reverse Cyclic	Quasi-Static	Double Curvature
55	Matsumura (1987)	CW3-1-A3	Other	1	Reverse Cyclic	Quasi-Static	Double Curvature
56	Matsumura (1987)	CW3-1-A4	Other	1	Reverse Cyclic	Quasi-Static	Double Curvature
57	Matsumura (1987)	CW3-0-A2	Other	1	Reverse Cyclic	Quasi-Static	Double Curvature
58	Matsumura (1987)	CW3-2-A2	Other	1	Reverse Cyclic	Quasi-Static	Double Curvature
59	Matsumura (1987)	CW3-3-A2	Other	1	Reverse Cyclic	Quasi-Static	Double Curvature
60	Matsumura (1987)	CW3-4-A2	Other	1	Reverse Cyclic	Quasi-Static	Double Curvature
61	Matsumura (1987)	CWB3-1'-A2	Other	1	Reverse Cyclic	Quasi-Static	Double Curvature
62	Matsumura (1987)	CW3-0-A3	Other	1	Reverse Cyclic	Quasi-Static	Double Curvature
63	Matsumura (1987)	CW3-0'-A3	Other	1	Reverse Cyclic	Quasi-Static	Double Curvature
64	Matsumura (1987)	CW3-2-A3	Other	1	Reverse Cyclic	Quasi-Static	Double Curvature
65	Matsumura (1987)	CW3-3-A3	Other	1	Reverse Cyclic	Quasi-Static	Double Curvature
66	Matsumura (1987)	CW5-2'-A2-1	Other	1	Reverse Cyclic	Quasi-Static	Double Curvature

Wall #	Experimental Study	Wall ID	Test Setup	Scale	LOADING CONDITION		BOUNDARY CONDITION
					Loading Type	Loading Rate	Support Type
67	Matsumura (1987)	CW5-2'-A2-2	Other	1	Reverse Cyclic	Quasi-Static	Double Curvature
68	Matsumura (1987)	CW4-2'-A2	Other	1	Reverse Cyclic	Quasi-Static	Double Curvature
69	Matsumura (1987)	CW3-2'-A2	Other	1	Reverse Cyclic	Quasi-Static	Double Curvature
70	Matsumura (1987)	CW2-2'-A2-1	Other	1	Reverse Cyclic	Quasi-Static	Double Curvature
71	Matsumura (1987)	CW2-2'-A2-2	Other	1	Reverse Cyclic	Quasi-Static	Double Curvature
72	Tomaževic and Lutman (1988)	CN-0	Other	0.5	Reverse Cyclic	Quasi-Static	Cantilever
73	Tomaževic and Lutman (1988)	CN-14	Other	0.5	Reverse Cyclic	Quasi-Static	Cantilever
74	Tomaževic and Lutman (1988)	CN-28	Other	0.5	Reverse Cyclic	Quasi-Static	Cantilever
75	Tomaževic and Lutman (1988)	CN-50	Other	0.5	Reverse Cyclic	Quasi-Static	Cantilever
76	Tomaževic and Lutman (1988)	CV-0	Other	0.5	Reverse Cyclic	Quasi-Static	Cantilever
77	Tomaževic and Lutman (1988)	DN-0	Other	0.5	Reverse Cyclic	Quasi-Static	Cantilever
78	Tomaževic and Lutman (1988)	DN-14	Other	0.5	Reverse Cyclic	Quasi-Static	Cantilever
79	Tomaževic and Lutman (1988)	DN-28	Other	0.5	Reverse Cyclic	Quasi-Static	Cantilever
80	Tomaževic and Lutman (1988)	DN-50	Other	0.5	Reverse Cyclic	Quasi-Static	Cantilever
81	Tomaževic and Lutman (1988)	DV-0	Other	0.5	Reverse Cyclic	Quasi-Static	Cantilever
82	Johal and Anderson (1988)	DM1	Other	1	Reverse Cyclic	Quasi-Static	Double Curvature
83	Johal and Anderson (1988)	DM2	Other	1	Reverse Cyclic	Quasi-Static	Double Curvature
84	Johal and Anderson (1988)	DM3	Other	1	Reverse Cyclic	Quasi-Static	Double Curvature
85	Johal and Anderson (1988)	DM4	Other	1	Reverse Cyclic	Quasi-Static	Double Curvature
86	Johal and Anderson (1988)	DM5	Other	1	Reverse Cyclic	Quasi-Static	Double Curvature
87	Johal and Anderson (1988)	DM6	Other	1	Reverse Cyclic	Quasi-Static	Double Curvature
88	Johal and Anderson (1988)	DP1	Other	1	Reverse Cyclic	Quasi-Static	Double Curvature
89	Johal and Anderson (1988)	DP2	Other	1	Reverse Cyclic	Quasi-Static	Double Curvature
90	Johal and Anderson (1988)	DS1	Other	1	Reverse Cyclic	Quasi-Static	Double Curvature
91	Johal and Anderson (1988)	DS2	Other	1	Reverse Cyclic	Quasi-Static	Double Curvature
92	Johal and Anderson (1988)	DS3	Other	1	Reverse Cyclic	Quasi-Static	Double Curvature
93	Johal and Anderson (1988)	DS4	Other	1	Reverse Cyclic	Quasi-Static	Double Curvature
94	Johal and Anderson (1988)	DS5	Other	1	Reverse Cyclic	Quasi-Static	Double Curvature
95	Johal and Anderson (1988)	DS6	Other	1	Reverse Cyclic	Quasi-Static	Double Curvature
96	Johal and Anderson (1988)	DP3	Other	1	Reverse Cyclic	Quasi-Static	Double Curvature
97	Johal and Anderson (1988)	DP4	Other	1	Reverse Cyclic	Quasi-Static	Double Curvature
98	Yancey and Scribner (1989)	R1	Other	1	Reverse Cyclic	Quasi-Static	Double Curvature
99	Yancey and Scribner (1989)	R2	Other	1	Reverse Cyclic	Quasi-Static	Double Curvature

Wall #	Experimental Study	Wall ID	Test Setup	Scale	LOADING CONDITION		BOUNDARY CONDITION
					Loading Type	Loading Rate	Support Type
100	Yancey and Scribner (1989)	R4	Other	1	Reverse Cyclic	Quasi-Static	Double Curvature
101	Yancey and Scribner (1989)	R5	Other	1	Reverse Cyclic	Quasi-Static	Double Curvature
102	Yancey and Scribner (1989)	R6	Other	1	Reverse Cyclic	Quasi-Static	Double Curvature
103	Yancey and Scribner (1989)	R7	Other	1	Reverse Cyclic	Quasi-Static	Double Curvature
104	Yancey and Scribner (1989)	R8	Other	1	Reverse Cyclic	Quasi-Static	Double Curvature
105	Yancey and Scribner (1989)	R9	Other	1	Reverse Cyclic	Quasi-Static	Double Curvature
106	Yancey and Scribner (1989)	R10	Other	1	Reverse Cyclic	Quasi-Static	Double Curvature
107	Yancey and Scribner (1989)	R11	Other	1	Reverse Cyclic	Quasi-Static	Double Curvature
108	Ghanem et al (1992)	SWA	Other	0.33	Monotonic	Quasi-Static	Cantilever
109	Ghanem et al (1992)	SWB	Other	0.33	Monotonic	Quasi-Static	Cantilever
110	Ghanem et al (1993)	SWA-2	Other	0.33	Monotonic	Quasi-Static	Cantilever
111	Ghanem et al (1993)	SWA-3	Other	0.33	Monotonic	Quasi-Static	Cantilever
112	Tomazevic et al. (1996)	V2-BS	Other	0.5	Reverse Cyclic	Quasi-Static	Cantilever
113	Tomazevic et al. (1996)	V2-BD	Other	0.5	Reverse Cyclic	Dynamic	Cantilever
114	Tomazevic et al. (1996)	V2-CS	Other	0.5	Phased-Sequential	Quasi-Static	Cantilever
115	Tomazevic et al. (1996)	V2-CD	Other	0.5	Phased-Sequential	Dynamic	Cantilever
116	Tomazevic et al. (1996)	V2-DS	Other	0.5	Simulated Seismic	Quasi-Static	Cantilever
117	Tomazevic et al. (1996)	V2-DD	Other	0.5	Simulated Seismic	Dynamic	Cantilever
118	Schultz (1996)	1	Other	1	Phased-Sequential	Quasi-Static	Double Curvature
119	Schultz (1996)	3	Other	1	Phased-Sequential	Quasi-Static	Double Curvature
120	Schultz (1996)	5	Other	1	Phased-Sequential	Quasi-Static	Double Curvature
121	Schultz (1996)	7	Other	1	Phased-Sequential	Quasi-Static	Double Curvature
122	Schultz (1996)	9	Other	1	Phased-Sequential	Quasi-Static	Double Curvature
123	Schultz (1996)	11	Other	1	Phased-Sequential	Quasi-Static	Double Curvature
124	Schultz et al. (1998)	2	Other	1	Phased-Sequential	Quasi-Static	Double Curvature
125	Schultz et al. (1998)	4	Other	1	Phased-Sequential	Quasi-Static	Double Curvature
126	Schultz et al. (1998)	6	Other	1	Phased-Sequential	Quasi-Static	Double Curvature
127	Schultz et al. (1998)	8	Other	1	Phased-Sequential	Quasi-Static	Double Curvature
128	Schultz et al. (1998)	10	Other	1	Phased-Sequential	Quasi-Static	Double Curvature
129	Schultz et al. (1998)	12	Other	1	Phased-Sequential	Quasi-Static	Double Curvature
130	Voon and Ingham (2006)	5	Other	1	Reverse Cyclic	Quasi-Static	Cantilever
131	Voon and Ingham (2006)	6	Other	1	Reverse Cyclic	Quasi-Static	Cantilever
132	Haach et al. (2007)	N60-B1	Other	0.5	Reverse Cyclic	Quasi-Static	Cantilever

Wall #	Experimental Study	Wall ID	Test Setup	Scale	LOADING CONDITION		BOUNDARY CONDITION
					Loading Type	Loading Rate	Support Type
133	Haach et al. (2007)	N60-B2	Other	0.5	Reverse Cyclic	Quasi-Static	Cantilever
134	Haach et al. (2007)	N150-B1	Other	0.5	Reverse Cyclic	Quasi-Static	Cantilever
135	Haach et al. (2007)	N150-B2	Other	0.5	Reverse Cyclic	Quasi-Static	Cantilever
136	Maleki et al. (2009)	Wall #1	Other	0.5	Reverse Cyclic	Quasi-Static	Double Curvature
137	Maleki et al. (2009)	Wall #2	Other	0.5	Reverse Cyclic	Quasi-Static	Double Curvature
138	Maleki et al. (2009)	Wall #3	Other	0.5	Reverse Cyclic	Quasi-Static	Double Curvature
139	Maleki et al. (2009)	Wall #4	Other	0.5	Reverse Cyclic	Quasi-Static	Double Curvature
140	Maleki et al. (2009)	Wall #5	Other	0.5	Reverse Cyclic	Quasi-Static	Double Curvature
141	Elmapruk (2010)	PG127-48	Other	1	Reverse Cyclic	Quasi-Static	Double Curvature
142	Elmapruk (2010)	PG127-48I	Other	1	Reverse Cyclic	Quasi-Static	Double Curvature
143	Elmapruk (2010)	PG180-48	Other	1	Reverse Cyclic	Quasi-Static	Double Curvature
144	Elmapruk (2010)	PG254-48	Other	1	Reverse Cyclic	Quasi-Static	Double Curvature
145	Elmapruk (2010)	PG127-32	Other	1	Reverse Cyclic	Quasi-Static	Double Curvature
146	Elmapruk (2010)	PG127-24	Other	1	Reverse Cyclic	Quasi-Static	Double Curvature
147	Minaie et al. (2010)	PCL 1	Other	1	Reverse Cyclic	Quasi-Static	Cantilever
148	Minaie et al. (2010)	MC 1	Other	1	Reverse Cyclic	Quasi-Static	Cantilever
149	Minaie et al. (2010)	PCL 2	Other	1	Reverse Cyclic	Quasi-Static	Double Curvature
150	Minaie et al. (2010)	MC 2	Other	1	Reverse Cyclic	Quasi-Static	Double Curvature
151	Baenziger & Porter (2011)	A-1 (DR)	Other	1	Reverse Cyclic	Quasi-Static	Cantilever
152	Baenziger & Porter (2011)	A-2 (JR)	Other	1	Reverse Cyclic	Quasi-Static	Cantilever
153	Baenziger & Porter (2011)	A-6 (JR _{x2})	Other	1	Reverse Cyclic	Quasi-Static	Cantilever
154	Baenziger & Porter (2011)	B-7 (DR)	Other	1	Reverse Cyclic	Quasi-Static	Cantilever
155	Baenziger & Porter (2011)	B-5 (JR)	Other	1	Reverse Cyclic	Quasi-Static	Cantilever
156	Baenziger & Porter (2011)	D-3 (DR)	Other	1	Reverse Cyclic	Quasi-Static	Cantilever
157	Baenziger & Porter (2011)	D-4 (JR)	Other	1	Reverse Cyclic	Quasi-Static	Cantilever
158	Baenziger & Porter (2011)	D-8 (JR _{x2})	Other	1	Reverse Cyclic	Quasi-Static	Cantilever
159	Nolph et al. (2012)	PG085-48	Other	1	Reverse Cyclic	Quasi-Static	Cantilever
160	Nolph et al. (2012)	PG120-48	Other	1	Reverse Cyclic	Quasi-Static	Cantilever
161	Nolph et al. (2012)	PG169-48	Other	1	Reverse Cyclic	Quasi-Static	Cantilever
162	Nolph et al. (2012)	PG085-32	Other	1	Reverse Cyclic	Quasi-Static	Cantilever
163	Nolph et al. (2012)	PG085-24	Other	1	Reverse Cyclic	Quasi-Static	Cantilever
164	Oan (2013)	1	ESECMaSE	1	Monotonic	Quasi-Static	Cantilever
165	Oan (2013)	2	ESECMaSE	1	Monotonic	Quasi-Static	Cantilever

Wall #	Experimental Study	Wall ID	Test Setup	Scale	LOADING CONDITION		BOUNDARY CONDITION
					Loading Type	Loading Rate	Support Type
166	Oan (2013)	3	ESECMaSE	1	Monotonic	Quasi-Static	Cantilever
167	Oan (2013)	4	ESECMaSE	1	Monotonic	Quasi-Static	Cantilever
168	Oan (2013)	5	ESECMaSE	1	Monotonic	Quasi-Static	Cantilever
169	Oan (2013)	6	ESECMaSE	1	Monotonic	Quasi-Static	Cantilever
170	Oan (2013)	7	ESECMaSE	1	Monotonic	Quasi-Static	Cantilever
171	Oan (2013)	8	ESECMaSE	1	Monotonic	Quasi-Static	Cantilever
172	Oan (2013)	9	ESECMaSE	1	Monotonic	Quasi-Static	Cantilever
173	Oan (2013)	10	ESECMaSE	1	Monotonic	Quasi-Static	Cantilever
174	Oan (2013)	11	ESECMaSE	1	Monotonic	Quasi-Static	Cantilever
175	Oan (2013)	12	ESECMaSE	1	Monotonic	Quasi-Static	Cantilever
176	Oan (2013)	13	ESECMaSE	1	Monotonic	Quasi-Static	Cantilever
177	Oan (2013)	14	ESECMaSE	1	Monotonic	Quasi-Static	Cantilever
178	Oan (2013)	15	ESECMaSE	1	Monotonic	Quasi-Static	Cantilever
179	Oan (2013)	16	ESECMaSE	1	Monotonic	Quasi-Static	Cantilever
180	Oan (2013)	17	ESECMaSE	1	Monotonic	Quasi-Static	Cantilever
181	Oan (2013)	18	ESECMaSE	1	Monotonic	Quasi-Static	Cantilever
182	Oan (2013)	19	ESECMaSE	1	Monotonic	Quasi-Static	Cantilever
183	Oan (2013)	20	ESECMaSE	1	Monotonic	Quasi-Static	Cantilever
184	Oan (2013)	21	ESECMaSE	1	Monotonic	Quasi-Static	Cantilever
185	Oan (2013)	22	ESECMaSE	1	Monotonic	Quasi-Static	Cantilever
186	Oan (2013)	23	ESECMaSE	1	Monotonic	Quasi-Static	Cantilever
187	Oan (2013)	24	ESECMaSE	1	Monotonic	Quasi-Static	Cantilever
188	Oan (2013)	25	ESECMaSE	1	Monotonic	Quasi-Static	Cantilever
189	Oan (2013)	26	ESECMaSE	1	Monotonic	Quasi-Static	Cantilever
190	Oan (2013)	27	ESECMaSE	1	Monotonic	Quasi-Static	Cantilever
191	Oan (2013)	28	ESECMaSE	1	Monotonic	Quasi-Static	Cantilever
192	Oan (2013)	29	ESECMaSE	1	Monotonic	Quasi-Static	Cantilever
193	Oan (2013)	30	ESECMaSE	1	Monotonic	Quasi-Static	Cantilever
194	Oan (2013)	31	ESECMaSE	1	Monotonic	Quasi-Static	Cantilever
195	Oan (2013)	32	ESECMaSE	1	Monotonic	Quasi-Static	Cantilever
196	Oan (2013)	33	ESECMaSE	1	Monotonic	Quasi-Static	Cantilever
197	Oan (2013)	34	ESECMaSE	1	Monotonic	Quasi-Static	Cantilever
198	Oan (2013)	35	ESECMaSE	1	Monotonic	Quasi-Static	Cantilever

Wall #	Experimental Study	Wall ID	Test Setup	Scale	LOADING CONDITION		BOUNDARY CONDITION
					Loading Type	Loading Rate	Support Type
199	Oan (2013)	36	ESECMaSE	1	Monotonic	Quasi-Static	Cantilever
200	Oan (2013)	37	ESECMaSE	1	Monotonic	Quasi-Static	Cantilever
201	Oan (2013)	38	ESECMaSE	1	Monotonic	Quasi-Static	Cantilever
202	Oan (2013)	39	ESECMaSE	1	Monotonic	Quasi-Static	Cantilever
203	Oan (2013)	40	ESECMaSE	1	Monotonic	Quasi-Static	Cantilever
204	Oan (2013)	41	ESECMaSE	1	Monotonic	Quasi-Static	Cantilever
205	Oan (2013)	42	ESECMaSE	1	Monotonic	Quasi-Static	Cantilever
206	Oan (2013)	43	ESECMaSE	1	Monotonic	Quasi-Static	Cantilever
207	Oan (2013)	44	ESECMaSE	1	Monotonic	Quasi-Static	Cantilever
208	Oan (2013)	45	ESECMaSE	1	Monotonic	Quasi-Static	Cantilever
209	Oan (2013)	46	ESECMaSE	1	Monotonic	Quasi-Static	Cantilever
210	Oan (2013)	47	ESECMaSE	1	Monotonic	Quasi-Static	Cantilever
211	Oan (2013)	48	ESECMaSE	1	Monotonic	Quasi-Static	Cantilever
212	Oan (2013)	49	ESECMaSE	1	Monotonic	Quasi-Static	Cantilever
213	Oan (2013)	50	ESECMaSE	1	Monotonic	Quasi-Static	Cantilever
214	Oan (2013)	51	ESECMaSE	1	Monotonic	Quasi-Static	Cantilever
215	Oan (2013)	52	ESECMaSE	1	Monotonic	Quasi-Static	Cantilever
216	Oan (2013)	53	ESECMaSE	1	Monotonic	Quasi-Static	Cantilever
217	Oan (2013)	54	ESECMaSE	1	Monotonic	Quasi-Static	Cantilever
218	Oan (2013)	55	ESECMaSE	1	Monotonic	Quasi-Static	Cantilever
219	Oan (2013)	56	ESECMaSE	1	Monotonic	Quasi-Static	Cantilever
220	Oan (2013)	57	ESECMaSE	1	Monotonic	Quasi-Static	Cantilever
221	Oan (2013)	58	ESECMaSE	1	Monotonic	Quasi-Static	Cantilever
222	Oan (2013)	59	ESECMaSE	1	Monotonic	Quasi-Static	Cantilever
223	Oan (2013)	60	ESECMaSE	1	Monotonic	Quasi-Static	Cantilever
224	Oan (2013)	61	ESECMaSE	1	Monotonic	Quasi-Static	Cantilever
225	Oan (2013)	62	ESECMaSE	1	Monotonic	Quasi-Static	Cantilever
226	Oan (2013)	63	ESECMaSE	1	Monotonic	Quasi-Static	Cantilever
227	Oan (2013)	64	ESECMaSE	1	Monotonic	Quasi-Static	Cantilever
228	Oan (2013)	65	ESECMaSE	1	Monotonic	Quasi-Static	Cantilever
229	Oan (2013)	66	ESECMaSE	1	Monotonic	Quasi-Static	Cantilever
230	Hoque (2013)	1A	ESECMaSE	1	Reverse Cyclic	Quasi-Static	Double Curvature
231	Hoque (2013)	1B	ESECMaSE	1	Reverse Cyclic	Quasi-Static	Double Curvature

Wall #	Experimental Study	Wall ID	Test Setup	Scale	LOADING CONDITION		BOUNDARY CONDITION
					Loading Type	Loading Rate	Support Type
232	Hoque (2013)	2A	ESECMaSE	1	Reverse Cyclic	Quasi-Static	Double Curvature
233	Hoque (2013)	2B	ESECMaSE	1	Reverse Cyclic	Quasi-Static	Double Curvature
234	Hoque (2013)	3A	ESECMaSE	1	Reverse Cyclic	Quasi-Static	Double Curvature
235	Hoque (2013)	3B	ESECMaSE	1	Reverse Cyclic	Quasi-Static	Double Curvature
236	Hoque (2013)	3C	ESECMaSE	1	Reverse Cyclic	Quasi-Static	Double Curvature
237	Hoque (2013)	4A	ESECMaSE	1	Reverse Cyclic	Quasi-Static	Double Curvature
238	Hoque (2013)	4B	ESECMaSE	1	Reverse Cyclic	Quasi-Static	Double Curvature
239	Hoque (2013)	4C	ESECMaSE	1	Reverse Cyclic	Quasi-Static	Double Curvature
240	Hoque (2013)	5A	ESECMaSE	1	Reverse Cyclic	Quasi-Static	Double Curvature
241	Hoque (2013)	5B	ESECMaSE	1	Reverse Cyclic	Quasi-Static	Double Curvature
242	Hoque (2013)	6A	ESECMaSE	1	Reverse Cyclic	Quasi-Static	Double Curvature
243	Hoque (2013)	6B	ESECMaSE	1	Reverse Cyclic	Quasi-Static	Double Curvature
244	Hoque (2013)	7A	ESECMaSE	1	Reverse Cyclic	Quasi-Static	Double Curvature
245	Hoque (2013)	7B	ESECMaSE	1	Reverse Cyclic	Quasi-Static	Double Curvature
246	Hoque (2013)	8A	ESECMaSE	1	Monotonic	Quasi-Static	Double Curvature
247	Hoque (2013)	8B	ESECMaSE	1	Monotonic	Quasi-Static	Double Curvature
248	Hamedzadeh (2013)	1A (Type A)	ESECMaSE	0.5	Monotonic	Quasi-Static	Double Curvature
249	Hamedzadeh (2013)	1B (Type A)	ESECMaSE	0.5	Monotonic	Quasi-Static	Double Curvature
250	Hamedzadeh (2013)	2A (Type A)	ESECMaSE	0.5	Monotonic	Quasi-Static	Double Curvature
251	Hamedzadeh (2013)	2B (Type A)	ESECMaSE	0.5	Monotonic	Quasi-Static	Double Curvature
252	Hamedzadeh (2013)	3A (Type A)	ESECMaSE	0.5	Monotonic	Quasi-Static	Double Curvature
253	Hamedzadeh (2013)	3B (Type A)	ESECMaSE	0.5	Monotonic	Quasi-Static	Double Curvature
254	Hamedzadeh (2013)	4A (Type B)	ESECMaSE	0.5	Monotonic	Quasi-Static	Double Curvature
255	Hamedzadeh (2013)	4B (Type B)	ESECMaSE	0.5	Monotonic	Quasi-Static	Double Curvature
256	Hamedzadeh (2013)	4C (Type B)	ESECMaSE	0.5	Monotonic	Quasi-Static	Double Curvature
257	Hamedzadeh (2013)	5A (Type B)	ESECMaSE	0.5	Monotonic	Quasi-Static	Double Curvature
258	Hamedzadeh (2013)	5B (Type B)	ESECMaSE	0.5	Monotonic	Quasi-Static	Double Curvature
259	Hamedzadeh (2013)	5C (Type B)	ESECMaSE	0.5	Monotonic	Quasi-Static	Double Curvature
260	Hamedzadeh (2013)	6A (Type C)	ESECMaSE	0.5	Monotonic	Quasi-Static	Double Curvature
261	Hamedzadeh (2013)	6B (Type C)	ESECMaSE	0.5	Monotonic	Quasi-Static	Double Curvature
262	Hamedzadeh (2013)	6C (Type C)	ESECMaSE	0.5	Monotonic	Quasi-Static	Double Curvature
263	Hamedzadeh (2013)	7A (Type C)	ESECMaSE	0.5	Monotonic	Quasi-Static	Double Curvature
264	Hamedzadeh (2013)	7B (Type C)	ESECMaSE	0.5	Monotonic	Quasi-Static	Double Curvature

Wall #	Experimental Study	Wall ID	Test Setup	Scale	LOADING CONDITION		BOUNDARY CONDITION
					Loading Type	Loading Rate	Support Type
265	Hamedzadeh (2013)	7C (Type C)	ESECMaSE	0.5	Monotonic	Quasi-Static	Double Curvature
266	Hamedzadeh (2013)	8A (Type D)	ESECMaSE	0.5	Monotonic	Quasi-Static	Double Curvature
267	Hamedzadeh (2013)	8B (Type D)	ESECMaSE	0.5	Monotonic	Quasi-Static	Double Curvature
268	Hamedzadeh (2013)	8C (Type D)	ESECMaSE	0.5	Monotonic	Quasi-Static	Double Curvature
269	Rizae (2015)	Wall 1-A	ESECMaSE	1	Reverse Cyclic	Quasi-Static	Double Curvature
270	Rizae (2015)	Wall 2-A	ESECMaSE	1	Reverse Cyclic	Quasi-Static	Double Curvature
271	Rizae (2015)	Wall 3-B	ESECMaSE	1	Reverse Cyclic	Quasi-Static	Double Curvature
272	Rizae (2015)	Wall 4-B	ESECMaSE	1	Reverse Cyclic	Quasi-Static	Double Curvature
273	Rizae (2015)	Wall 5-C	ESECMaSE	1	Reverse Cyclic	Quasi-Static	Double Curvature
274	Rizae (2015)	Wall 6-C	ESECMaSE	1	Reverse Cyclic	Quasi-Static	Double Curvature
275	Rizae (2015)	Wall 7-D	ESECMaSE	1	Reverse Cyclic	Quasi-Static	Double Curvature
276	Rizae (2015)	Wall 8-D	ESECMaSE	1	Reverse Cyclic	Quasi-Static	Double Curvature
277	Rizae (2015)	Wall 9-E	ESECMaSE	1	Reverse Cyclic	Quasi-Static	Double Curvature
278	Rizae (2015)	Wall 10-E	ESECMaSE	1	Reverse Cyclic	Quasi-Static	Double Curvature
279	Rizae (2015)	Wall 11-F	ESECMaSE	1	Reverse Cyclic	Quasi-Static	Double Curvature
280	Rizae (2015)	Wall 12-F	ESECMaSE	1	Reverse Cyclic	Quasi-Static	Double Curvature
281	Rizae (2015)	Wall 13-G	ESECMaSE	1	Reverse Cyclic	Quasi-Static	Double Curvature
282	Rizae (2015)	Wall 14-G	ESECMaSE	1	Reverse Cyclic	Quasi-Static	Double Curvature
283	Ramirez et al. (2016)	M1	Other	1	Reverse Cyclic	Quasi-Static	Cantilever
284	Ramirez et al. (2016)	M2	Other	1	Reverse Cyclic	Quasi-Static	Cantilever
285	Ramirez et al. (2016)	M3	Other	1	Reverse Cyclic	Quasi-Static	Cantilever
286	Ramirez et al. (2016)	M4	Other	1	Reverse Cyclic	Quasi-Static	Cantilever
287	Ramirez et al. (2016)	M5	Other	1	Reverse Cyclic	Quasi-Static	Cantilever
288	Ramirez et al. (2016)	M6	Other	1	Reverse Cyclic	Quasi-Static	Cantilever
289	Ramirez et al. (2016)	M7	Other	1	Reverse Cyclic	Quasi-Static	Cantilever
290	Ramirez et al. (2016)	M8	Other	1	Reverse Cyclic	Quasi-Static	Cantilever
291	Ramirez et al. (2016)	M9	Other	1	Reverse Cyclic	Quasi-Static	Cantilever
292	Ramirez et al. (2016)	M10	Other	1	Reverse Cyclic	Quasi-Static	Cantilever

Wall #	WALL GEOMETRY											PARTIAL GROUTING				
	H [mm]	L [mm]	A [mm ²]	t [mm]	H _{scaled} [mm]	L _{scaled} [mm]	A _{scaled} [mm ²]	t _{scaled} [mm]	d _{v,scaled} [mm]	H/L -	M/(VL) -	A _{net} [mm]	A _{gross} [mm]	A _{net} / A _{gross}	Vertical Grout Spacing [mm]	Hor. Grout Spacing [mm]
1	2642	2438	6441277	143	2642	2438	6441277	143	1951	1.08	1.08	123871	348386	0.36	2438	2642
2	2642	2438	6441277	143	2642	2438	6441277	143	1951	1.08	1.08	159780	348386	0.46	2238	2642
3	2642	2438	6441277	143	2642	2438	6441277	143	1951	1.08	1.08	123871	348386	0.36	2438	1321
4	2642	2438	6441277	143	2642	2438	6441277	143	1951	1.08	1.08	159780	348386	0.46	2238	1321
5	2642	2438	6441277	143	2642	2438	6441277	143	1951	1.08	1.08	177735	348386	0.51	1119	2642
6	2642	2438	6441277	143	2642	2438	6441277	143	1951	1.08	1.08	195689	348386	0.56	746	2642
7	2642	2438	6441277	143	2642	2438	6441277	143	1951	1.08	1.08	159780	348386	0.46	2238	2642
8	2642	2438	6441277	143	2642	2438	6441277	143	1951	1.08	1.08	213644	348386	0.61	560	2642
9	2642	2438	6441277	143	2642	2438	6441277	143	1951	1.08	1.08	213644	348386	0.61	560	1321
10	2642	2438	6441277	143	2642	2438	6441277	143	1951	1.08	1.08	213644	348386	0.61	560	660
11	2642	2438	6441277	143	2642	2438	6441277	143	1951	1.08	1.08	213644	348386	0.61	560	881
12	2642	2438	6441277	143	2642	2438	6441277	143	1951	1.08	1.08	213644	348386	0.61	560	660
13	2650	3200	8480000	150	2650	3200	8480000	150	2560	0.83	0.83	327218	480000	0.68	800	2650
14	2650	3200	8480000	150	2650	3200	8480000	150	2560	0.83	0.83	327218	480000	0.68	800	2650
15	2650	3200	8480000	150	2650	3200	8480000	150	2560	0.83	0.83	327218	480000	0.68	800	2650
16	2650	3200	8480000	150	2650	3200	8480000	150	2560	0.83	0.83	347030	480000	0.72	1400	2650
17	2650	3200	8480000	150	2650	3200	8480000	150	2560	0.83	0.83	347030	480000	0.72	1400	2650
18	2650	3200	8480000	150	2650	3200	8480000	150	2560	0.83	0.83	327218	480000	0.68	800	2650
19	2650	3200	8480000	150	2650	3200	8480000	150	2560	0.83	0.83	347030	480000	0.72	1400	2650
20	2650	3200	8480000	150	2650	3200	8480000	150	2560	0.83	0.83	327218	480000	0.68	800	2650
21	2650	3200	8480000	150	2650	3200	8480000	150	2560	0.83	0.83	327218	480000	0.68	800	2650
22	2650	3200	8480000	150	2650	3200	8480000	150	2560	0.83	0.83	327218	480000	0.68	800	2650
23	2000	2000	4000000	150	2000	2000	4000000	150	1600	1.00	1.00	140288	300000	0.47	1800	2000
24	2000	2000	4000000	150	2000	2000	4000000	150	1600	1.00	1.00	140288	300000	0.47	1800	2000
25	2000	2000	4000000	150	2000	2000	4000000	150	1600	1.00	1.00	140288	300000	0.47	1800	2000
26	2000	2000	4000000	150	2000	2000	4000000	150	1600	1.00	1.00	140288	300000	0.47	1800	2000
27	2000	2000	4000000	150	2000	2000	4000000	150	1600	1.00	1.00	140288	300000	0.47	1800	2000
28	2000	2000	4000000	150	2000	2000	4000000	150	1600	1.00	1.00	178976	300000	0.60	900	2000
29	2000	2000	4000000	150	2000	2000	4000000	150	1600	1.00	1.00	140288	300000	0.47	1800	2000
30	2000	2000	4000000	150	2000	2000	4000000	150	1600	1.00	1.00	178976	300000	0.60	900	2000
31	2000	2000	4000000	150	2000	2000	4000000	150	1600	1.00	1.00	140288	300000	0.47	1800	2000
32	2000	2000	4000000	150	2000	2000	4000000	150	1600	1.00	1.00	140288	300000	0.47	1800	2000
33	2000	2000	4000000	150	2000	2000	4000000	150	1600	1.00	1.00	140288	300000	0.47	1800	2000

Wall #	WALL GEOMETRY											PARTIAL GROUTING				
	H [mm]	L [mm]	A [mm ²]	t [mm]	H _{scaled} [mm]	L _{scaled} [mm]	A _{scaled} [mm ²]	t _{scaled} [mm]	d _{v,scaled} [mm]	H/L -	M/(VL) -	A _{net} [mm]	A _{gross} [mm]	A _{net} / A _{gross}	Vertical Grout Spacing [mm]	Hor. Grout Spacing [mm]
34	1626	813	1321288	143	1626	813	1321288	143	650	2.00	1.00	83045	116129	0.72	613	1626
35	1626	813	1321288	143	1626	813	1321288	143	650	2.00	1.00	83045	116129	0.72	613	1626
36	1422	1219	1734190	193	1422	1219	1734190	193	975	1.17	0.58	141935	235549	0.60	1019	1422
37	1422	1219	1734190	193	1422	1219	1734190	193	975	1.17	0.58	141935	235549	0.60	1019	711
38	1422	1219	1734190	193	1422	1219	1734190	193	975	1.17	0.58	141935	235549	0.60	1019	1422
39	1422	1219	1734190	193	1422	1219	1734190	193	975	1.17	0.58	141935	235549	0.60	1019	474
40	2400	1600	3840000	140	2400	1600	3840000	140	1280	1.50	0.75	158400	224000	0.71	400	1000
41	2400	1600	3840000	140	2400	1600	3840000	140	1280	1.50	0.75	158400	224000	0.71	400	2400
42	2400	1600	3840000	140	2400	1600	3840000	140	1280	1.50	0.75	158400	224000	0.71	400	600
43	1800	1720	3096000	150	1800	1720	3096000	150	1655	1.05	0.52	180190	258000	0.70	360	400
44	1800	1720	3096000	150	1800	1720	3096000	150	1655	1.05	0.52	180897	258000	0.70	360	400
45	1800	1320	2376000	150	1800	1320	2376000	150	1255	1.36	0.68	139674	198000	0.71	450	400
46	1800	1320	2376000	150	1800	1320	2376000	150	1255	1.36	0.68	139420	198000	0.70	450	400
47	1800	920	1656000	150	1800	920	1656000	150	855	1.96	0.98	98943	138000	0.72	600	400
48	1800	920	1656000	150	1800	920	1656000	150	855	1.96	0.98	98838	138000	0.72	600	400
49	1800	1320	2376000	150	1800	1320	2376000	150	1255	1.36	0.68	139071	198000	0.70	450	400
50	1800	1320	2376000	150	1800	1320	2376000	150	1255	1.36	0.68	138981	198000	0.70	450	400
51	1800	1320	2376000	150	1800	1320	2376000	150	1255	1.36	0.68	140462	198000	0.71	450	400
52	1800	1320	2376000	150	1800	1320	2376000	150	1255	1.36	0.68	140315	198000	0.71	450	400
53	1800	1320	2376000	150	1800	1320	2376000	150	1255	1.36	0.68	139472	198000	0.70	450	400
54	1800	1320	2376000	150	1800	1320	2376000	150	1255	1.36	0.68	140123	198000	0.71	450	400
55	1800	1320	2376000	150	1800	1320	2376000	150	1255	1.36	0.68	139765	198000	0.71	450	400
56	1800	1320	2376000	150	1800	1320	2376000	150	1255	1.36	0.68	139992	198000	0.71	450	400
57	1800	1370	2466000	150	1800	1370	2466000	150	1293	1.31	0.66	147458	205500	0.72	450	400
58	1800	1370	2466000	150	1800	1370	2466000	150	1293	1.31	0.66	146928	205500	0.71	450	400
59	1800	1370	2466000	150	1800	1370	2466000	150	1293	1.31	0.66	146911	205500	0.71	450	400
60	1800	1370	2466000	150	1800	1370	2466000	150	1293	1.31	0.66	147340	205500	0.72	450	400
61	1800	1370	2466000	150	1800	1370	2466000	150	1293	1.31	0.66	147566	205500	0.72	450	400
62	1800	1320	2376000	150	1800	1320	2376000	150	1255	1.36	0.68	139559	198000	0.70	450	400
63	1800	1320	2376000	150	1800	1320	2376000	150	1255	1.36	0.68	139392	198000	0.70	450	400
64	1800	1320	2376000	150	1800	1320	2376000	150	1255	1.36	0.68	140008	198000	0.71	450	400
65	1800	1320	2376000	150	1800	1320	2376000	150	1255	1.36	0.68	140030	198000	0.71	450	400
66	1800	1970	3546000	150	1800	1970	3546000	150	1880	0.91	0.46	238829	295500	0.81	300	400

Wall #	WALL GEOMETRY											PARTIAL GROUTING				
	H [mm]	L [mm]	A [mm ²]	t [mm]	H _{scaled} [mm]	L _{scaled} [mm]	A _{scaled} [mm ²]	t _{scaled} [mm]	d _{v,scaled} [mm]	H/L -	M/(VL) -	A _{net} [mm]	A _{gross} [mm]	A _{net} / A _{gross}	Vertical Grout Spacing [mm]	Hor. Grout Spacing [mm]
67	1800	1970	3546000	150	1800	1970	3546000	150	1880	0.91	0.46	218837	295500	0.74	300	400
68	1800	1770	3186000	150	1800	1770	3186000	150	1680	1.02	0.51	206811	265500	0.78	360	400
69	1800	1370	2466000	150	1800	1370	2466000	150	1280	1.31	0.66	112091	205500	0.55	450	400
70	1800	970	1746000	150	1800	970	1746000	150	880	1.86	0.93	106898	145500	0.73	600	400
71	1800	970	1746000	150	1800	970	1746000	150	880	1.86	0.93	106440	145500	0.73	600	400
72	760	610	463600	100	1520	1220	1854400	200	976	1.25	1.25	36400	61000	0.60	510	760
73	760	610	463600	100	1520	1220	1854400	200	976	1.25	1.25	36400	61000	0.60	510	760
74	760	610	463600	100	1520	1220	1854400	200	976	1.25	1.25	36400	61000	0.60	510	760
75	760	610	463600	100	1520	1220	1854400	200	976	1.25	1.25	36400	61000	0.60	510	760
76	1400	610	854000	100	2800	1220	3416000	200	976	2.30	2.30	36400	61000	0.60	510	1400
77	760	610	463600	100	1520	1220	1854400	200	976	1.25	1.25	36400	61000	0.60	510	760
78	760	610	463600	100	1520	1220	1854400	200	976	1.25	1.25	36400	61000	0.60	510	760
79	760	610	463600	100	1520	1220	1854400	200	976	1.25	1.25	36400	61000	0.60	510	760
80	760	610	463600	100	1520	1220	1854400	200	976	1.25	1.25	36400	61000	0.60	510	760
81	1400	610	854000	100	2800	1220	3416000	200	976	2.30	2.30	36400	61000	0.60	510	1400
82	813	813	660644	200	813	813	660644	200	650	1.00	0.50	103368	162560	0.64	400	813
83	813	813	660644	200	813	813	660644	200	650	1.00	0.50	103368	162560	0.64	400	813
84	813	813	660644	200	813	813	660644	200	650	1.00	0.50	103368	162560	0.64	400	813
85	813	813	660644	200	813	813	660644	200	650	1.00	0.50	103368	162560	0.64	400	813
86	813	813	660644	200	813	813	660644	200	650	1.00	0.50	103368	162560	0.64	400	813
87	813	813	660644	200	813	813	660644	200	650	1.00	0.50	103368	162560	0.64	400	813
88	813	813	660644	200	813	813	660644	200	650	1.00	0.50	103368	162560	0.64	400	813
89	813	813	660644	200	813	813	660644	200	650	1.00	0.50	103368	162560	0.64	400	813
90	813	813	660644	200	813	813	660644	200	650	1.00	0.50	103368	162560	0.64	400	813
91	813	813	660644	200	813	813	660644	200	650	1.00	0.50	103368	162560	0.64	400	813
92	813	813	660644	200	813	813	660644	200	650	1.00	0.50	103368	162560	0.64	400	813
93	813	813	660644	200	813	813	660644	200	650	1.00	0.50	103368	162560	0.64	400	813
94	813	813	660644	200	813	813	660644	200	650	1.00	0.50	103368	162560	0.64	400	813
95	813	813	660644	200	813	813	660644	200	650	1.00	0.50	103368	162560	0.64	400	813
96	813	813	660644	200	813	813	660644	200	650	1.00	0.50	103368	162560	0.64	400	813
97	813	813	660644	200	813	813	660644	200	650	1.00	0.50	103368	162560	0.64	400	813
98	1422	1219	1734190	194	1422	1219	1734190	194	975	1.17	0.58	126774	236129	0.54	1219	1422
99	1422	1219	1734190	194	1422	1219	1734190	194	975	1.17	0.58	126774	236129	0.54	1219	1422

Wall #	WALL GEOMETRY											PARTIAL GROUTING				
	H [mm]	L [mm]	A [mm ²]	t [mm]	H _{scaled} [mm]	L _{scaled} [mm]	A _{scaled} [mm ²]	t _{scaled} [mm]	d _{v,scaled} [mm]	H/L -	M/(VL) -	A _{net} [mm]	A _{gross} [mm]	A _{net} / A _{gross}	Vertical Grout Spacing [mm]	Hor. Grout Spacing [mm]
100	1422	1219	1734190	194	1422	1219	1734190	194	975	1.17	0.58	126774	236129	0.54	1219	1422
101	1422	1219	1734190	194	1422	1219	1734190	194	975	1.17	0.58	126774	236129	0.54	1219	711
102	1422	1219	1734190	194	1422	1219	1734190	194	975	1.17	0.58	126774	236129	0.54	1219	711
103	1422	1219	1734190	194	1422	1219	1734190	194	975	1.17	0.58	126774	236129	0.54	1219	800
104	1422	1219	1734190	194	1422	1219	1734190	194	975	1.17	0.58	126774	236129	0.54	1219	711
105	1422	1219	1734190	194	1422	1219	1734190	194	975	1.17	0.58	126774	236129	0.54	1219	711
106	1422	1219	1734190	194	1422	1219	1734190	194	975	1.17	0.58	126774	236129	0.54	1219	711
107	1422	1219	1734190	194	1422	1219	1734190	194	975	1.17	0.58	126774	236129	0.54	1219	800
108	920	939	864147	48	2761	2816	7777322	143	2253	0.98	0.98	24429	44829	0.54	940	871
109	920	939	864147	48	2761	2816	7777322	143	2253	0.98	0.98	24429	44829	0.54	470	436
110	940	940	883224	48	2819	2819	7949016	143	2256	1.00	1.00	24452	44877	0.54	470	436
111	940	940	883224	48	2819	2819	7949016	143	2256	1.00	1.00	24452	44877	0.54	470	436
112	760	610	463600	100	1520	1220	1854400	200	976	1.25	1.25	42300	61000	0.69	510	760
113	760	610	463600	100	1520	1220	1854400	200	976	1.25	1.25	42300	61000	0.69	510	760
114	760	610	463600	100	1520	1220	1854400	200	976	1.25	1.25	42300	61000	0.69	510	760
115	760	610	463600	100	1520	1220	1854400	200	976	1.25	1.25	42300	61000	0.69	510	760
116	760	610	463600	100	1520	1220	1854400	200	976	1.25	1.25	42300	61000	0.69	510	760
117	760	610	463600	100	1520	1220	1854400	200	976	1.25	1.25	42300	61000	0.69	510	760
118	1422	2845	4045590	195	1422	2845	4045590	195	2276	0.50	0.25	242283	554775	0.44	2645	700
119	1422	2032	2889504	195	1422	2032	2889504	195	1626	0.70	0.35	187486	396240	0.47	1832	700
120	1422	1422	2022084	195	1422	1422	2022084	195	1138	1.00	0.50	146372	277290	0.53	1222	700
121	1422	2845	4045590	195	1422	2845	4045590	195	2276	0.50	0.25	242283	554775	0.44	2645	700
122	1422	2032	2889504	195	1422	2032	2889504	195	1626	0.70	0.35	187486	396240	0.47	1832	700
123	1422	1422	2022084	195	1422	1422	2022084	195	1138	1.00	0.50	146372	277290	0.53	1222	700
124	1422	2845	4045590	195	1422	2845	4045590	195	2276	0.50	0.25	242283	554775	0.44	2645	1422
125	1422	2032	2889504	195	1422	2032	2889504	195	1626	0.70	0.35	187486	396240	0.47	1832	1422
126	1422	1422	2022084	195	1422	1422	2022084	195	1138	1.00	0.50	146372	277290	0.53	1222	1422
127	1422	2845	4045590	195	1422	2845	4045590	195	2276	0.50	0.25	242283	554775	0.44	2645	1422
128	1422	2032	2889504	195	1422	2032	2889504	195	1626	0.70	0.35	187486	396240	0.47	1832	1422
129	1422	1422	2022084	195	1422	1422	2022084	195	1138	1.00	0.50	146372	277290	0.53	1222	1422
130	1800	1800	3240000	140	1800	1800	3240000	140	1440	1.00	1.00	186000	252000	0.74	400	1800
131	1800	1800	3240000	140	1800	1800	3240000	140	1440	1.00	1.00	186000	252000	0.74	800	1800
132	808	1200	969600	100	1616	2400	3878400	200	1920	0.67	0.67	57000	120000	0.48	800	1200

Wall #	WALL GEOMETRY											PARTIAL GROUTING				
	H [mm]	L [mm]	A [mm ²]	t [mm]	H _{scaled} [mm]	L _{scaled} [mm]	A _{scaled} [mm ²]	t _{scaled} [mm]	d _{v,scaled} [mm]	H/L -	M/(VL) -	A _{net} [mm]	A _{gross} [mm]	A _{net} / A _{gross}	Vertical Grout Spacing [mm]	Hor. Grout Spacing [mm]
133	808	1200	969600	100	1616	2400	3878400	200	1920	0.67	0.67	84000	120000	0.70	800	1200
134	808	1200	969600	100	1616	2400	3878400	200	1920	0.67	0.67	84000	120000	0.70	800	1200
135	808	1200	969600	100	1616	2400	3878400	200	1920	0.67	0.67	84000	120000	0.70	800	1200
136	1800	1800	3240000	90	3600	3600	12960000	180	2880	1.00	0.50	114372	162000	0.71	850	800
137	1800	1800	3240000	90	3600	3600	12960000	180	2880	1.00	0.50	122016	162000	0.75	567	567
138	1800	1800	3240000	90	3600	3600	12960000	180	2880	1.00	0.50	106728	162000	0.66	1700	1700
139	900	1800	1620000	90	1800	3600	6480000	180	2880	0.50	0.25	114372	162000	0.71	1700	1700
140	2698	1800	4856400	90	5396	3600	19425600	180	2880	1.50	0.75	114372	162000	0.71	850	867
141	1524	2642	4025798	193	1524	2642	4025798	193	2634	0.58	0.29	229677	510357	0.45	1219	711.2
142	1524	2642	4025798	193	1524	2642	4025798	193	2634	0.58	0.29	229677	510357	0.45	1219	711.2
143	1524	2642	4025798	193	1524	2642	4025798	193	2634	0.58	0.29	229677	510357	0.45	1219	711.2
144	1524	2642	4025798	193	1524	2642	4025798	193	2634	0.58	0.29	229677	510357	0.45	1219	711.2
145	1524	2642	4025798	193	1524	2642	4025798	193	2634	0.58	0.29	250322	510357	0.49	610	711.2
146	1524	2642	4025798	193	1524	2642	4025798	193	2634	0.58	0.29	271612	510357	0.53	610	711.2
147	2640	3860	10190400	200	2640	3860	10190400	200	3088	0.68	0.68	312464	772000	0.40	1219	1200
148	2640	3860	10190400	200	2640	3860	10190400	200	3088	0.68	0.68	312464	772000	0.40	1219	1200
149	2640	3860	10190400	200	2640	3860	10190400	200	3088	0.68	0.34	312464	772000	0.40	1219	1200
150	2640	3860	10190400	200	2640	3860	10190400	200	3088	0.68	0.34	312464	772000	0.40	1219	1200
151	2640	2850	7524000	193	2640	2850	7524000	193	2280	0.93	0.93	335806	550050	0.61	1219	1320
152	2640	2850	7524000	193	2640	2850	7524000	193	2280	0.93	0.93	335806	550050	0.61	1219	2640
153	2640	2850	7524000	193	2640	2850	7524000	193	2280	0.93	0.93	378838	550050	0.69	1219	2640
154	2640	2850	7524000	193	2640	2850	7524000	193	2280	0.93	0.93	378838	550050	0.69	1219	1320
155	2640	2850	7524000	193	2640	2850	7524000	193	2280	0.93	0.93	378838	550050	0.69	1219	2640
156	2640	4270	11272800	193	2640	4270	11272800	193	3416	0.62	0.62	503612	824110	0.61	1219	1320
157	2640	4270	11272800	193	2640	4270	11272800	193	3416	0.62	0.62	546773	824110	0.66	1219	2640
158	2640	4270	11272800	193	2640	4270	11272800	193	3416	0.62	0.62	546773	824110	0.66	1219	2640
159	2337	2631	6148647	194	2337	2631	6148647	194	2631	0.89	0.89	229677	510414	0.45	1219	1219
160	2337	2631	6148647	194	2337	2631	6148647	194	2631	0.89	0.89	229677	510414	0.45	1219	1219
161	2337	2631	6148647	194	2337	2631	6148647	194	2631	0.89	0.89	229677	510414	0.45	1219	1219
162	2337	2631	6148647	194	2337	2631	6148647	194	2631	0.89	0.89	250322	510414	0.49	813	1219
163	2337	2631	6148647	194	2337	2631	6148647	194	2631	0.89	0.89	271612	510414	0.53	610	1219
164	1200	1590	1908000	190	1200	1590	1908000	190	1272	0.75	0.75	204900	302100	0.68	1200	1200
165	1200	1590	1908000	190	1200	1590	1908000	190	1272	0.75	0.75	204900	302100	0.68	1200	1200

Wall #	WALL GEOMETRY											PARTIAL GROUTING				
	H [mm]	L [mm]	A [mm ²]	t [mm]	H _{scaled} [mm]	L _{scaled} [mm]	A _{scaled} [mm ²]	t _{scaled} [mm]	d _{v,scaled} [mm]	H/L -	M/(VL) -	A _{net} [mm]	A _{gross} [mm]	A _{net} / A _{gross}	Vertical Grout Spacing [mm]	Hor. Grout Spacing [mm]
166	1200	1590	1908000	190	1200	1590	1908000	190	1272	0.75	0.75	204900	302100	0.68	1200	1200
167	1200	1590	1908000	190	1200	1590	1908000	190	1272	0.75	0.75	204900	302100	0.68	1200	1200
168	1200	1590	1908000	190	1200	1590	1908000	190	1272	0.75	0.75	204900	302100	0.68	1200	1200
169	1200	1590	1908000	190	1200	1590	1908000	190	1272	0.75	0.75	204900	302100	0.68	1200	1200
170	1200	1590	1908000	190	1200	1590	1908000	190	1272	0.75	0.75	204900	302100	0.68	1200	1200
171	1200	1590	1908000	190	1200	1590	1908000	190	1272	0.75	0.75	204900	302100	0.68	1200	1200
172	1200	1590	1908000	190	1200	1590	1908000	190	1272	0.75	0.75	204900	302100	0.68	1200	1200
173	1200	1590	1908000	190	1200	1590	1908000	190	1272	0.75	0.75	204900	302100	0.68	600	1200
174	1200	1590	1908000	190	1200	1590	1908000	190	1272	0.75	0.75	204900	302100	0.68	600	1200
175	1200	1590	1908000	190	1200	1590	1908000	190	1272	0.75	0.75	204900	302100	0.68	600	1200
176	1200	1590	1908000	190	1200	1590	1908000	190	1272	0.75	0.75	204900	302100	0.68	600	1200
177	1200	1590	1908000	190	1200	1590	1908000	190	1272	0.75	0.75	204900	302100	0.68	600	1200
178	1200	1590	1908000	190	1200	1590	1908000	190	1272	0.75	0.75	204900	302100	0.68	600	1200
179	1200	1590	1908000	190	1200	1590	1908000	190	1272	0.75	0.75	204900	302100	0.68	1200	1200
180	1200	1590	1908000	190	1200	1590	1908000	190	1272	0.75	0.75	204900	302100	0.68	1200	1200
181	1200	1590	1908000	190	1200	1590	1908000	190	1272	0.75	0.75	204900	302100	0.68	1200	1200
182	1200	1590	1908000	190	1200	1590	1908000	190	1272	0.75	0.75	204900	302100	0.68	1200	1200
183	1200	1590	1908000	190	1200	1590	1908000	190	1272	0.75	0.75	204900	302100	0.68	1200	1200
184	1200	1590	1908000	190	1200	1590	1908000	190	1272	0.75	0.75	204900	302100	0.68	1200	1200
185	1200	1590	1908000	190	1200	1590	1908000	190	1272	0.75	0.75	204900	302100	0.68	1200	1200
186	1200	1590	1908000	190	1200	1590	1908000	190	1272	0.75	0.75	204900	302100	0.68	1200	1200
187	1200	1590	1908000	190	1200	1590	1908000	190	1272	0.75	0.75	204900	302100	0.68	1200	1200
188	1200	1590	1908000	190	1200	1590	1908000	190	1272	0.75	0.75	204900	302100	0.68	1200	1200
189	1200	1590	1908000	190	1200	1590	1908000	190	1272	0.75	0.75	204900	302100	0.68	1200	1200
190	1200	1590	1908000	190	1200	1590	1908000	190	1272	0.75	0.75	204900	302100	0.68	1200	1200
191	1200	1590	1908000	190	1200	1590	1908000	190	1272	0.75	0.75	204900	302100	0.68	600	1200
192	1200	1590	1908000	190	1200	1590	1908000	190	1272	0.75	0.75	204900	302100	0.68	600	1200
193	1200	1590	1908000	190	1200	1590	1908000	190	1272	0.75	0.75	204900	302100	0.68	600	1200
194	1200	1590	1908000	190	1200	1590	1908000	190	1272	0.75	0.75	204900	302100	0.68	600	1200
195	1200	1590	1908000	190	1200	1590	1908000	190	1272	0.75	0.75	204900	302100	0.68	600	1200
196	1200	1590	1908000	190	1200	1590	1908000	190	1272	0.75	0.75	204900	302100	0.68	600	1200
197	1200	1590	1908000	190	1200	1590	1908000	190	1272	0.75	0.75	204900	302100	0.68	1200	1200
198	1200	1590	1908000	190	1200	1590	1908000	190	1272	0.75	0.75	204900	302100	0.68	1200	1200

Wall #	WALL GEOMETRY											PARTIAL GROUTING				
	H [mm]	L [mm]	A [mm ²]	t [mm]	H _{scaled} [mm]	L _{scaled} [mm]	A _{scaled} [mm ²]	t _{scaled} [mm]	d _{v,scaled} [mm]	H/L -	M/(VL) -	A _{net} [mm]	A _{gross} [mm]	A _{net} / A _{gross}	Vertical Grout Spacing [mm]	Hor. Grout Spacing [mm]
199	1200	1590	1908000	190	1200	1590	1908000	190	1272	0.75	0.75	204900	302100	0.68	1200	1200
200	1200	1590	1908000	190	1200	1590	1908000	190	1272	0.75	0.75	204900	302100	0.68	1200	1200
201	1200	1590	1908000	190	1200	1590	1908000	190	1272	0.75	0.75	204900	302100	0.68	1200	1200
202	1200	1590	1908000	190	1200	1590	1908000	190	1272	0.75	0.75	204900	302100	0.68	1200	1200
203	1200	1590	1908000	190	1200	1590	1908000	190	1272	0.75	0.75	204900	302100	0.68	1200	1200
204	1200	1590	1908000	190	1200	1590	1908000	190	1272	0.75	0.75	204900	302100	0.68	1200	1200
205	1200	1590	1908000	190	1200	1590	1908000	190	1272	0.75	0.75	204900	302100	0.68	1200	1200
206	1200	1590	1908000	190	1200	1590	1908000	190	1272	0.75	0.75	204900	302100	0.68	1200	1200
207	1200	1590	1908000	190	1200	1590	1908000	190	1272	0.75	0.75	204900	302100	0.68	1200	1200
208	1200	1590	1908000	190	1200	1590	1908000	190	1272	0.75	0.75	204900	302100	0.68	1200	1200
209	1200	1590	1908000	190	1200	1590	1908000	190	1272	0.75	0.75	204900	302100	0.68	600	1200
210	1200	1590	1908000	190	1200	1590	1908000	190	1272	0.75	0.75	204900	302100	0.68	600	1200
211	1200	1590	1908000	190	1200	1590	1908000	190	1272	0.75	0.75	204900	302100	0.68	600	1200
212	1200	1590	1908000	190	1200	1590	1908000	190	1272	0.75	0.75	204900	302100	0.68	600	1200
213	1200	1590	1908000	190	1200	1590	1908000	190	1272	0.75	0.75	204900	302100	0.68	600	1200
214	1200	1590	1908000	190	1200	1590	1908000	190	1272	0.75	0.75	204900	302100	0.68	600	1200
215	1200	1590	1908000	190	1200	1590	1908000	190	1272	0.75	0.75	204900	302100	0.68	1200	1200
216	1200	1590	1908000	190	1200	1590	1908000	190	1272	0.75	0.75	204900	302100	0.68	1200	1200
217	1200	1590	1908000	190	1200	1590	1908000	190	1272	0.75	0.75	204900	302100	0.68	1200	1200
218	1200	1590	1908000	190	1200	1590	1908000	190	1272	0.75	0.75	204900	302100	0.68	1200	1200
219	1200	1590	1908000	190	1200	1590	1908000	190	1272	0.75	0.75	204900	302100	0.68	1200	1200
220	1200	1590	1908000	190	1200	1590	1908000	190	1272	0.75	0.75	204900	302100	0.68	1200	1200
221	1200	1590	1908000	190	1200	1590	1908000	190	1272	0.75	0.75	204900	302100	0.68	1200	1200
222	1200	1590	1908000	190	1200	1590	1908000	190	1272	0.75	0.75	204900	302100	0.68	1200	1200
223	1200	1590	1908000	190	1200	1590	1908000	190	1280	0.75	0.75	204900	302100	0.68	1200	1200
224	1200	1590	1908000	190	1200	1590	1908000	190	1272	0.75	0.75	204900	302100	0.68	1200	1200
225	1200	1590	1908000	190	1200	1590	1908000	190	1272	0.75	0.75	204900	302100	0.68	1200	1200
226	1200	1590	1908000	190	1200	1590	1908000	190	1272	0.75	0.75	204900	302100	0.68	1200	1200
227	1200	1590	1908000	190	1200	1590	1908000	190	1272	0.75	0.75	204900	302100	0.68	1200	1200
228	1200	1590	1908000	190	1200	1590	1908000	190	1272	0.75	0.75	204900	302100	0.68	1200	1200
229	1200	1590	1908000	190	1200	1590	1908000	190	1272	0.75	0.75	204900	302100	0.68	1200	1200
230	1800	1800	3240000	190	1800	1800	3240000	190	1440	1.00	0.50	188910	342000	0.55	800	800
231	1800	1800	3240000	190	1800	1800	3240000	190	1440	1.00	0.50	188910	342000	0.55	800	800

Wall #	WALL GEOMETRY											PARTIAL GROUTING				
	H [mm]	L [mm]	A [mm ²]	t [mm]	H _{scaled} [mm]	L _{scaled} [mm]	A _{scaled} [mm ²]	t _{scaled} [mm]	d _{v,scaled} [mm]	H/L -	M/(VL) -	A _{net} [mm]	A _{gross} [mm]	A _{net} / A _{gross}	Vertical Grout Spacing [mm]	Hor. Grout Spacing [mm]
232	1800	1800	3240000	190	1800	1800	3240000	190	1440	1.00	0.50	188910	342000	0.55	800	800
233	1800	1800	3240000	190	1800	1800	3240000	190	1440	1.00	0.50	188910	342000	0.55	800	800
234	1800	1800	3240000	190	1800	1800	3240000	190	1440	1.00	0.50	188910	342000	0.55	800	800
235	1800	1800	3240000	190	1800	1800	3240000	190	1440	1.00	0.50	188910	342000	0.55	800	800
236	1800	1800	3240000	190	1800	1800	3240000	190	1440	1.00	0.50	188910	342000	0.55	800	800
237	1800	1800	3240000	190	1800	1800	3240000	190	1440	1.00	0.50	188910	342000	0.55	800	800
238	1800	1800	3240000	190	1800	1800	3240000	190	1440	1.00	0.50	188910	342000	0.55	800	800
239	1800	1800	3240000	190	1800	1800	3240000	190	1440	1.00	0.50	188910	342000	0.55	800	800
240	1800	1800	3240000	190	1800	1800	3240000	190	1440	1.00	0.50	188910	342000	0.55	800	600
241	1800	1800	3240000	190	1800	1800	3240000	190	1440	1.00	0.50	188910	342000	0.55	800	600
242	1800	1800	3240000	190	1800	1800	3240000	190	1440	1.00	0.50	188910	342000	0.55	800	1800
243	1800	1800	3240000	190	1800	1800	3240000	190	1440	1.00	0.50	188910	342000	0.55	800	1800
244	1800	1800	3240000	190	1800	1800	3240000	190	1440	1.00	0.50	188910	342000	0.55	800	1800
245	1800	1800	3240000	190	1800	1800	3240000	190	1440	1.00	0.50	188910	342000	0.55	800	1800
246	1800	1800	3240000	190	1800	1800	3240000	190	1440	1.00	0.50	188910	342000	0.55	800	1800
247	1800	1800	3240000	190	1800	1800	3240000	190	1440	1.00	0.50	188910	342000	0.55	800	1800
248	1233	1235	1522755	91	2466	2470	6091020	181.4	1976	1.00	0.50	51073	112015	0.46	1233	1235
249	1233	1235	1522755	91	2466	2470	6091020	181.4	1976	1.00	0.50	51073	112015	0.46	1233	1235
250	1233	1235	1522755	91	2466	2470	6091020	181.4	1976	1.00	0.50	51073	112015	0.46	1233	1235
251	1233	1235	1522755	91	2466	2470	6091020	181.4	1976	1.00	0.50	51073	112015	0.46	1233	1235
252	1233	1235	1522755	91	2466	2470	6091020	181.4	1976	1.00	0.50	51073	112015	0.46	1233	1235
253	1233	1235	1522755	91	2466	2470	6091020	181.4	1976	1.00	0.50	51073	112015	0.46	1233	1235
254	2372	1235	2929420	91	4744	2470	11717680	181.4	1976	1.92	0.96	56480	112015	0.50	1233	1235
255	2372	1235	2929420	91	4744	2470	11717680	181.4	1976	1.92	0.96	56480	112015	0.50	1233	1235
256	2372	1235	2929420	91	4744	2470	11717680	181.4	1976	1.92	0.96	56480	112015	0.50	1233	1235
257	2372	1235	2929420	91	4744	2470	11717680	181.4	1976	1.92	0.96	56480	112015	0.50	1233	1235
258	2372	1235	2929420	91	4744	2470	11717680	181.4	1976	1.92	0.96	56480	112015	0.50	1233	1235
259	2372	1235	2929420	91	4744	2470	11717680	181.4	1976	1.92	0.96	56480	112015	0.50	1233	1235
260	2372	760	1802720	91	4744	1520	7210880	181.4	1216	3.12	1.56	46401	68932	0.67	1233	760
261	2372	760	1802720	91	4744	1520	7210880	181.4	1216	3.12	1.56	46401	68932	0.67	1233	760
262	2372	760	1802720	91	4744	1520	7210880	181.4	1216	3.12	1.56	46401	68932	0.67	1233	760
263	2372	760	1802720	91	4744	1520	7210880	181.4	1216	3.12	1.56	46401	68932	0.67	1233	760
264	2372	760	1802720	91	4744	1520	7210880	181.4	1216	3.12	1.56	46401	68932	0.67	1233	760

Wall #	WALL GEOMETRY											PARTIAL GROUTING				
	H [mm]	L [mm]	A [mm ²]	t [mm]	H _{scaled} [mm]	L _{scaled} [mm]	A _{scaled} [mm ²]	t _{scaled} [mm]	d _{v,scaled} [mm]	H/L -	M/(VL) -	A _{net} [mm]	A _{gross} [mm]	A _{net} / A _{gross}	Vertical Grout Spacing [mm]	Hor. Grout Spacing [mm]
265	2372	760	1802720	91	4744	1520	7210880	181.4	1216	3.12	1.56	46401	68932	0.67	1233	760
266	853	760	648280	91	1706	1520	2593120	181.4	1216	1.12	0.56	35588	68932	0.52	1233	760
267	853	760	648280	91	1706	1520	2593120	181.4	1216	1.12	0.56	35588	68932	0.52	1233	760
268	853	760	648280	91	1706	1520	2593120	181.4	1216	1.12	0.56	35588	68932	0.52	1233	760
269	1790	1790	3204100	190	1790	1790	3204100	190	1432	1.00	0.50	163700	340100	0.48	780	760
270	1790	1790	3204100	190	1790	1790	3204100	190	1432	1.00	0.50	163700	340100	0.48	780	760
271	1790	1790	3204100	190	1790	1790	3204100	190	1432	1.00	0.50	163700	340100	0.48	780	760
272	1790	1790	3204100	190	1790	1790	3204100	190	1432	1.00	0.50	163700	340100	0.48	780	760
273	1790	1790	3204100	190	1790	1790	3204100	190	1432	1.00	0.50	163700	340100	0.48	780	760
274	1790	1790	3204100	190	1790	1790	3204100	190	1432	1.00	0.50	163700	340100	0.48	780	760
275	1790	1790	3204100	190	1790	1790	3204100	190	1432	1.00	0.50	163700	340100	0.48	780	760
276	1790	1790	3204100	190	1790	1790	3204100	190	1432	1.00	0.50	163700	340100	0.48	780	760
277	1790	1790	3204100	190	1790	1790	3204100	190	1432	1.00	0.50	163700	340100	0.48	780	760
278	1790	1790	3204100	190	1790	1790	3204100	190	1432	1.00	0.50	163700	340100	0.48	780	760
279	1790	1790	3204100	190	1790	1790	3204100	190	1432	1.00	0.50	163700	340100	0.48	780	570
280	1790	1790	3204100	190	1790	1790	3204100	190	1432	1.00	0.50	163700	340100	0.48	780	570
281	1790	1790	3204100	190	1790	1790	3204100	190	1432	1.00	0.50	163700	340100	0.48	780	760
282	1790	1790	3204100	190	1790	1790	3204100	190	1432	1.00	0.50	163700	340100	0.48	780	760
283	1930	1990	3840700	140	1930	1990	3840700	140	1592	0.97	0.97	170668	278600	0.61	618	1930
284	1930	1990	3840700	140	1930	1990	3840700	140	1592	0.97	0.97	170668	278600	0.61	618	1930
285	1930	1990	3840700	140	1930	1990	3840700	140	1592	0.97	0.97	170668	278600	0.61	618	1930
286	1930	1990	3840700	140	1930	1990	3840700	140	1592	0.97	0.97	170668	278600	0.61	618	1930
287	1130	2590	2926700	140	1130	2590	2926700	140	2072	0.44	0.44	218542	362600	0.60	607	1130
288	1130	2590	2926700	140	1130	2590	2926700	140	2072	0.44	0.44	218542	362600	0.60	607	1130
289	1130	2590	2926700	140	1130	2590	2926700	140	2072	0.44	0.44	218542	362600	0.60	607	1130
290	1930	990	1910700	140	1930	990	1910700	140	792	1.95	1.95	102474	138600	0.74	400	1930
291	1930	990	1910700	140	1930	990	1910700	140	792	1.95	1.95	102474	138600	0.74	400	1930
292	1930	990	1910700	140	1930	990	1910700	140	792	1.95	1.95	102474	138600	0.74	400	1930

Wall #	MASONRY MATERIALS												
	f _{block} [MPa]	f _{mortar} [MPa]	f _{grout} [MPa]	v	f _{m(grouded)} [MPa]	f _{m(ungrouded)} [MPa]	# of courses in prism	h/t prism	# of tests	Dillon Correction Factor k	f _{mcor(grouded)} [MPa]	f _{mcor(ungrouded)} [MPa]	f _{mcor,eff} [MPa]
1	14.4	19.9	31.5	46%	12.0	9.9	-	-	-	1.000	12.0	9.9	10.2
2	20.1	21.9	36.1	46%	13.6	12.4	-	-	-	1.000	13.6	12.4	12.6
3	14.4	19.9	31.5	46%	12.0	9.9	-	-	-	1.000	12.0	9.9	10.2
4	20.1	21.9	31.5	46%	13.3	9.9	-	-	-	1.000	13.3	9.9	10.4
5	14.4	19.9	31.5	46%	12.0	9.9	-	-	-	1.000	12.0	9.9	10.2
6	20.1	21.9	31.5	46%	13.3	9.9	-	-	-	1.000	13.3	9.9	10.4
7	14.4	19.9	36.1	46%	12.3	12.4	-	-	-	1.000	12.3	12.4	12.4
8	20.1	21.9	31.5	46%	13.3	9.9	-	-	-	1.000	13.3	9.9	10.4
9	14.4	19.9	36.1	46%	12.3	12.4	-	-	-	1.000	12.3	12.4	12.4
10	20.1	21.9	36.1	46%	13.6	12.4	-	-	-	1.000	13.6	12.4	12.6
11	14.4	19.9	36.1	46%	12.3	12.4	-	-	-	1.000	12.3	12.4	12.4
12	20.1	21.9	36.1	46%	13.6	12.4	-	-	-	1.000	13.6	12.4	12.6
13	-	25.8	22.0	-	no info	10.3	3	3.93	-	0.938	no info	9.7	no info
14	-	23.8	21.0	-	no info	10.3	3	3.93	-	0.938	no info	9.7	no info
15	-	20.9	29.4	-	no info	10.3	3	3.93	-	0.938	no info	9.7	no info
16	-	15.7	14.8	-	no info	10.3	3	3.93	-	0.938	no info	9.7	no info
17	-	22.8	30.6	-	no info	10.3	3	3.93	-	0.938	no info	9.7	no info
18	-	21.4	24.3	-	no info	10.3	3	3.93	-	0.938	no info	9.7	no info
19	-	22.0	32.3	-	no info	10.3	3	3.93	-	0.938	no info	9.7	no info
20	-	16.1	21.0	-	no info	10.3	3	3.93	-	0.938	no info	9.7	no info
21	-	21.5	22.8	-	no info	10.3	3	3.93	-	0.938	no info	9.7	no info
22	-	21.7	30.4	-	no info	10.3	3	3.93	-	0.938	no info	9.7	no info
23	-	15.2	29.3	-	no info	10.3	3	3.93	-	0.938	no info	9.7	no info
24	-	20.4	33.1	-	no info	10.3	3	3.93	-	0.938	no info	9.7	no info
25	-	25.7	13.3	-	no info	14.4	3	3.93	-	0.938	no info	13.5	no info
26	-	23.1	15.9	-	no info	14.4	3	3.93	-	0.938	no info	13.5	no info
27	-	24.8	18.8	-	no info	14.4	3	3.93	-	0.938	no info	13.5	no info
28	-	20.4	10.6	-	no info	14.4	3	3.93	-	0.938	no info	13.5	no info
29	-	17.6	8.1	-	no info	14.4	3	3.93	-	0.938	no info	13.5	no info
30	-	17.5	11.9	-	no info	14.4	3	3.93	-	0.938	no info	13.5	no info
31	-	17.7	14.5	-	no info	14.4	3	3.93	-	0.938	no info	13.5	no info
32	-	24.1	23.2	-	no info	14.4	3	3.93	-	0.938	no info	13.5	no info
33	-	11.6	12.3	-	no info	14.4	3	3.93	-	0.938	no info	13.5	no info

Wall #	MASONRY MATERIALS												
	f _{block} [MPa]	f _{mortar} [MPa]	f _{grout} [MPa]	v	f _{m(gROUTED)} [MPa]	f _{m(UNROUTED)} [MPa]	# of courses in prism	h/t prism	# of tests	Dillon Correction Factor k	f _{mcOR(GROUTED)} [MPa]	f _{mcOR(UNROUTED)} [MPa]	f _{mcOR,eff} [MPa]
34	20.3	15.9	14.0	-	15.5	17.8	5	7.00	5	1.000	15.5	17.8	16.7
35	20.3	15.9	14.0	-	15.5	17.8	5	7.00	5	1.000	15.5	17.8	16.7
36	-	19.0	26.3	60%	11.8	10.6	5	5.00	3	1.000	11.8	10.6	11.0
37	-	19.0	26.3	60%	11.8	10.6	5	5.00	3	1.000	11.8	10.6	11.0
38	-	20.3	47.2	60%	11.8	10.8	5	5.00	3	1.000	11.8	10.8	11.1
39	-	16.0	47.5	60%	11.8	10.0	5	5.00	3	1.000	11.8	10.0	10.6
40	-	-	26.0	-	14.9	16.0	3	4.21	4	0.955	14.2	15.3	14.9
41	-	-	26.0	-	14.9	16.0	3	4.21	4	0.955	14.2	15.3	14.9
42	-	-	26.0	-	14.9	16.0	3	4.21	4	0.955	14.2	15.3	14.9
43	-	-	23.0	58%	16.4	9.5	3	3.93	-	0.938	15.4	8.9	13.4
44	-	-	23.0	58%	27.0	15.6	3	3.93	-	0.938	25.3	14.6	22.1
45	-	-	23.0	58%	16.4	9.5	3	3.93	-	0.938	15.4	8.9	13.5
46	-	-	23.0	58%	27.0	15.6	3	3.93	-	0.938	25.3	14.6	22.2
47	-	-	23.0	58%	16.4	9.5	3	3.93	-	0.938	15.4	8.9	13.5
48	-	-	23.0	58%	27.0	15.6	3	3.93	-	0.938	25.3	14.6	22.3
49	-	-	23.0	58%	16.4	9.5	3	3.93	-	0.938	15.4	8.9	13.5
50	-	-	23.0	58%	16.4	9.5	3	3.93	-	0.938	15.4	8.9	13.5
51	-	-	23.0	58%	16.4	9.5	3	3.93	-	0.938	15.4	8.9	13.5
52	-	-	23.0	58%	16.4	9.5	3	3.93	-	0.938	15.4	8.9	13.5
53	-	-	23.0	58%	16.4	9.5	3	3.93	-	0.938	15.4	8.9	13.5
54	-	-	23.0	58%	27.0	15.6	3	3.93	-	0.938	25.3	14.6	22.2
55	-	-	23.0	58%	27.0	15.6	3	3.93	-	0.938	25.3	14.6	22.2
56	-	-	23.0	58%	27.0	15.6	3	3.93	-	0.938	25.3	14.6	22.2
57	-	-	23.0	58%	14.0	8.1	3	3.93	-	0.938	13.1	7.6	11.6
58	-	-	23.0	58%	14.0	8.1	3	3.93	-	0.938	13.1	7.6	11.6
59	-	-	23.0	58%	14.0	8.1	3	3.93	-	0.938	13.1	7.6	11.6
60	-	-	23.0	58%	14.0	8.1	3	3.93	-	0.938	13.1	7.6	11.6
61	-	-	23.0	58%	14.0	8.1	3	3.93	-	0.938	13.1	7.6	11.6
62	-	-	23.0	58%	27.0	15.6	3	3.93	-	0.938	25.3	14.6	22.2
63	-	-	23.0	58%	14.0	8.1	3	3.93	-	0.938	13.1	7.6	11.5
64	-	-	23.0	58%	27.0	15.6	3	3.93	-	0.938	25.3	14.6	22.2
65	-	-	23.0	58%	27.0	15.6	3	3.93	-	0.938	25.3	14.6	22.2
66	-	-	23.0	58%	15.2	8.8	3	3.93	-	0.938	14.3	8.3	13.1

Wall #	MASONRY MATERIALS												
	f _{block} [MPa]	f _{mortar} [MPa]	f _{grout} [MPa]	v	f _{m(gROUTED)} [MPa]	f _{m(UNROUTED)} [MPa]	# of courses in prism	h/t prism	# of tests	Dillon Correction Factor k	f _{mcor(gROUTED)} [MPa]	f _{mcor(UNROUTED)} [MPa]	f _{mcor,eff} [MPa]
67	-	-	23.0	58%	15.2	8.8	3	3.93	-	0.938	14.3	8.3	12.7
68	-	-	23.0	58%	15.2	8.8	3	3.93	-	0.938	14.3	8.3	12.9
69	-	-	23.0	58%	15.2	8.8	3	3.93	-	0.938	14.3	8.3	11.5
70	-	-	23.0	58%	15.2	8.8	3	3.93	-	0.938	14.3	8.3	12.7
71	-	-	23.0	58%	15.2	8.8	3	3.93	-	0.938	14.3	8.3	12.6
72	17.4	9.3	9.3	53%	7.8	9.7	-	-	-	1.000	7.8	9.7	8.4
73	17.4	9.3	9.3	53%	7.8	9.7	-	-	-	1.000	7.8	9.7	8.4
74	17.4	9.3	9.3	53%	7.8	9.7	-	-	-	1.000	7.8	9.7	8.4
75	17.4	9.3	9.3	53%	7.8	9.7	-	-	-	1.000	7.8	9.7	8.4
76	17.4	9.3	9.3	53%	7.8	9.7	-	-	-	1.000	7.8	9.7	8.4
77	15.5	7.0	7.0	53%	6.5	8.1	-	-	-	1.000	6.5	8.1	7.1
78	15.5	7.0	7.0	53%	6.5	8.1	-	-	-	1.000	6.5	8.1	7.1
79	15.5	7.0	7.0	53%	6.5	8.1	-	-	-	1.000	6.5	8.1	7.1
80	15.5	7.0	7.0	53%	6.5	8.1	-	-	-	1.000	6.5	8.1	7.1
81	15.5	7.0	7.0	53%	6.5	8.1	-	-	-	1.000	6.5	8.1	7.1
82	19.3	15.8	21.2	53%	8.6	12.2	3	3.00	-	0.878	7.6	10.7	9.2
83	19.3	15.8	21.2	53%	8.6	12.2	3	3.00	-	0.878	7.6	10.7	9.2
84	19.3	17.2	21.2	53%	9.2	12.5	3	3.00	-	0.878	8.1	11.0	9.6
85	19.3	17.2	21.2	53%	9.2	12.5	3	3.00	-	0.878	8.1	11.0	9.6
86	19.3	19.6	21.2	53%	8.4	13.1	3	3.00	-	0.878	7.4	11.5	9.5
87	19.3	19.6	21.2	53%	8.4	13.1	3	3.00	-	0.878	7.4	11.5	9.5
88	19.3	22.3	21.2	53%	11.2	13.6	3	3.00	-	0.878	9.8	12.0	10.9
89	19.3	22.3	21.2	53%	11.2	13.6	3	3.00	-	0.878	9.8	12.0	10.9
90	19.3	17.3	21.2	53%	9.2	12.6	3	3.00	-	0.878	8.1	11.0	9.6
91	19.3	17.3	21.2	53%	9.2	12.6	3	3.00	-	0.878	8.1	11.0	9.6
92	19.3	18.1	21.2	53%	11.0	12.7	3	3.00	-	0.878	9.7	11.2	10.5
93	19.3	18.1	21.2	53%	11.0	12.7	3	3.00	-	0.878	9.7	11.2	10.5
94	19.3	19.6	21.2	53%	8.4	13.1	3	3.00	-	0.878	7.4	11.5	9.5
95	19.3	19.6	21.2	53%	8.4	13.1	3	3.00	-	0.878	7.4	11.5	9.5
96	19.3	17.9	21.2	53%	8.3	12.7	3	3.00	-	0.878	7.3	11.1	9.3
97	19.3	17.9	21.2	53%	8.3	12.7	3	3.00	-	0.878	7.3	11.1	9.3
98	12.5	-	10.7	52%	no info	no info	2	2.00	-	0.812	no info	no info	no info
99	12.5	-	10.7	52%	no info	no info	2	2.00	-	0.812	no info	no info	no info

Wall #	MASONRY MATERIALS												
	f _{block} [MPa]	f _{mortar} [MPa]	f _{grout} [MPa]	v	f _{m(grouted)} [MPa]	f _{m(ungrouded)} [MPa]	# of courses in prism	h/t prism	# of tests	Dillon Correction Factor k	f _{mcor(grouted)} [MPa]	f _{mcor(ungrouded)} [MPa]	f _{mcor,eff} [MPa]
100	12.5	-	10.7	52%	no info	no info	2	2.00	-	0.812	no info	no info	no info
101	12.5	-	10.7	52%	no info	no info	2	2.00	-	0.812	no info	no info	no info
102	12.5	-	10.7	52%	no info	no info	2	2.00	-	0.812	no info	no info	no info
103	12.5	-	10.7	52%	no info	no info	2	2.00	-	0.812	no info	no info	no info
104	12.5	-	10.7	52%	no info	no info	2	2.00	-	0.812	no info	no info	no info
105	12.5	-	10.7	52%	no info	no info	2	2.00	-	0.812	no info	no info	no info
106	12.5	-	10.7	52%	no info	no info	2	2.00	-	0.812	no info	no info	no info
107	12.5	-	10.7	52%	no info	no info	2	2.00	-	0.812	no info	no info	no info
108	19.3	15.5	31.0	-	20.0	15.9	3	4.45	6	0.969	19.4	15.4	15.9
109	19.3	15.5	31.0	-	20.0	15.9	3	4.45	6	0.969	19.4	15.4	16.2
110	19.3	15.5	31.0	-	20.0	15.9	3	4.45	6	0.969	19.4	15.4	16.2
111	19.3	15.5	31.0	-	20.0	15.9	3	4.45	6	0.969	19.4	15.4	16.2
112	-	-	-	-	no info	13.0	-	-	-	1.000	no info	13.0	no info
113	-	-	-	-	no info	13.0	-	-	-	1.000	no info	13.0	no info
114	-	-	-	-	no info	13.0	-	-	-	1.000	no info	13.0	no info
115	-	-	-	-	no info	13.0	-	-	-	1.000	no info	13.0	no info
116	-	-	-	-	no info	13.0	-	-	-	1.000	no info	13.0	no info
117	-	-	-	-	no info	13.0	-	-	-	1.000	no info	13.0	no info
118	-	21.7	29.6	-	17.6	17.1	2	2.00	-	0.812	14.3	13.9	13.9
119	-	21.7	29.6	-	17.6	17.1	2	2.00	-	0.812	14.3	13.9	14.0
120	-	21.7	29.6	-	17.6	17.1	2	2.00	-	0.812	14.3	13.9	14.0
121	-	21.7	29.6	-	17.6	17.1	2	2.00	-	0.812	14.3	13.9	13.9
122	-	21.7	29.6	-	17.6	17.1	2	2.00	-	0.812	14.3	13.9	14.0
123	-	21.7	29.6	-	17.6	17.1	2	2.00	-	0.812	14.3	13.9	14.0
124	23.3	22.2	28.2	-	16.5	14.5	2	2.00	-	0.812	13.4	11.8	12.0
125	23.3	22.2	28.2	-	16.5	14.5	2	2.00	-	0.812	13.4	11.8	12.1
126	23.3	22.2	28.2	-	16.5	14.5	2	2.00	-	0.812	13.4	11.8	12.2
127	23.3	22.2	28.2	-	16.5	14.5	2	2.00	-	0.812	13.4	11.8	12.0
128	23.3	22.2	28.2	-	16.5	14.5	2	2.00	-	0.812	13.4	11.8	12.1
129	23.3	22.2	28.2	-	16.5	14.5	2	2.00	-	0.812	13.4	11.8	12.2
130	-	-	-	-	-	-	3	4.21	-	0.955	-	-	18.5
131	-	-	-	-	-	-	3	4.21	-	0.955	-	-	18.5
132	11.4	10.0	-	54%	-	7.5	3	3.00	-	0.878	-	6.6	6.6

Wall #	MASONRY MATERIALS												
	f _{block} [MPa]	f _{mortar} [MPa]	f _{grout} [MPa]	v	f _{m(gROUTED)} [MPa]	f _{m(UNROUTED)} [MPa]	# of courses in prism	h/t prism	# of tests	Dillon Correction Factor k	f _{mcor(gROUTED)} [MPa]	f _{mcor(UNROUTED)} [MPa]	f _{mcor,eff} [MPa]
133	11.4	10.0	-	54%	-	7.5	3	3.00	-	0.878	-	6.6	6.6
134	11.4	10.0	-	54%	-	7.5	3	3.00	-	0.878	-	6.6	6.6
135	11.4	10.0	-	54%	-	7.5	3	3.00	-	0.878	-	6.6	6.6
136	-	23.8	40.7	-	21.6	12.4	4	4.33	6	0.962	20.8	12.0	14.8
137	-	23.8	40.7	-	21.6	12.4	4	4.33	6	0.962	20.8	12.0	15.8
138	-	23.8	40.7	-	21.6	12.4	4	4.33	6	0.962	20.8	12.0	13.9
139	-	23.8	40.7	-	21.6	12.4	4	4.33	6	0.962	20.8	12.0	14.8
140	-	23.8	40.7	-	21.6	12.4	4	4.33	6	0.962	20.8	12.0	14.8
141	-	14.9	35.9	-	17.4	24.4	2	1.95	5	0.809	14.1	19.7	18.5
142	-	14.9	35.9	-	17.4	24.4	2	1.95	5	0.809	14.1	19.7	18.5
143	-	14.9	35.9	-	17.4	24.4	2	1.95	5	0.809	14.1	19.7	18.5
144	-	14.9	35.9	-	17.4	24.4	2	1.95	5	0.809	14.1	19.7	18.5
145	-	14.9	35.9	-	17.4	24.4	2	1.95	5	0.809	14.1	19.7	17.7
146	-	14.9	35.9	-	17.4	24.4	2	1.95	5	0.809	14.1	19.7	17.7
147	14.0	13.8	22.0	53%	8.3	9.4	2	2.00	≥ 3	0.812	6.8	7.6	7.5
148	14.0	13.8	22.0	53%	8.3	9.4	2	2.00	≥ 3	0.812	6.8	7.6	7.5
149	14.0	13.8	22.0	53%	8.3	9.4	2	2.00	≥ 3	0.812	6.8	7.6	7.5
150	14.0	13.8	22.0	53%	8.3	9.4	2	2.00	≥ 3	0.812	6.8	7.6	7.5
151	-	9.9	28.6	-	21.2	19.5	2	2.00	≥ 3	0.812	17.2	15.8	16.1
152	-	9.9	28.6	-	17.0	17.7	2	2.00	≥ 3	0.812	13.8	14.4	14.3
153	-	9.9	28.6	-	17.0	17.7	2	2.00	≥ 3	0.812	13.8	14.4	14.3
154	-	9.9	28.6	-	20.5	19.2	2	2.00	≥ 3	0.812	16.6	15.6	15.8
155	-	9.9	28.6	-	20.5	19.2	2	2.00	≥ 3	0.812	16.6	15.6	15.8
156	-	9.9	28.6	-	20.5	19.2	2	2.00	≥ 3	0.812	16.6	15.6	15.7
157	-	9.9	28.6	-	24.6	24.1	2	2.00	≥ 3	0.812	20.0	19.6	19.6
158	-	9.9	28.6	-	20.5	25.4	2	2.00	≥ 3	0.812	16.6	20.6	20.1
159	18.1	-	29.2	-	19.7	11.3	3	3.04	4	0.881	17.4	9.9	11.6
160	18.1	-	29.2	-	19.7	11.3	3	3.04	4	0.881	17.4	9.9	11.6
161	18.1	-	29.2	-	19.7	11.3	3	3.04	4	0.881	17.4	9.9	11.6
162	18.1	-	29.2	-	19.7	11.3	3	3.04	4	0.881	17.4	9.9	12.2
163	18.1	-	29.2	-	19.7	11.3	3	3.04	4	0.881	17.4	9.9	12.7
164	18.4	6.7	21.8	-	9.8	18.2	3	3.11	10	0.885	8.7	16.1	12.5
165	18.4	6.8	25.7	-	9.8	18.2	3	3.11	10	0.885	8.7	16.1	12.5

Wall #	MASONRY MATERIALS												
	f_{block} [MPa]	f_{mortar} [MPa]	f_{grout} [MPa]	ν	$f_{\text{m(grouded)}}$ [MPa]	$f_{\text{m(ungrouded)}}$ [MPa]	# of courses in prism	h/t prism	# of tests	Dillon Correction Factor k	$f_{\text{mcor(grouded)}}$ [MPa]	$f_{\text{mcor(ungrouded)}}$ [MPa]	$f_{\text{mcor,eff}}$ [MPa]
166	18.4	6.8	25.7	-	9.8	18.2	3	3.11	10	0.885	8.7	16.1	12.5
167	18.4	6.5	21.0	-	9.8	18.2	3	3.11	10	0.885	8.7	16.1	12.5
168	18.4	4.3	20.0	-	9.8	18.2	3	3.11	10	0.885	8.7	16.1	12.5
169	18.4	4.3	20.0	-	9.8	18.2	3	3.11	10	0.885	8.7	16.1	12.5
170	18.4	6.5	21.0	-	9.8	18.2	3	3.11	10	0.885	8.7	16.1	12.5
171	18.4	6.5	21.0	-	9.8	18.2	3	3.11	10	0.885	8.7	16.1	12.5
172	18.4	4.3	20.0	-	9.8	18.2	3	3.11	10	0.885	8.7	16.1	12.5
173	18.4	6.5	23.7	-	9.8	18.2	3	3.11	10	0.885	8.7	16.1	12.5
174	18.4	7.3	25.1	-	9.8	18.2	3	3.11	10	0.885	8.7	16.1	12.5
175	18.4	7.5	21.9	-	9.8	18.2	3	3.11	10	0.885	8.7	16.1	12.5
176	18.4	6.5	23.7	-	9.8	18.2	3	3.11	10	0.885	8.7	16.1	12.5
177	18.4	7.3	25.1	-	9.8	18.2	3	3.11	10	0.885	8.7	16.1	12.5
178	18.4	7.5	21.9	-	9.8	18.2	3	3.11	10	0.885	8.7	16.1	12.5
179	18.4	6.5	23.7	-	9.8	18.2	3	3.11	10	0.885	8.7	16.1	12.5
180	18.4	7.3	25.1	-	9.8	18.2	3	3.11	10	0.885	8.7	16.1	12.5
181	18.4	7.5	21.9	-	9.8	18.2	3	3.11	10	0.885	8.7	16.1	12.5
182	18.4	4.6	24.7	-	9.8	18.2	3	3.11	10	0.885	8.7	16.1	12.5
183	18.4	4.6	24.7	-	9.8	18.2	3	3.11	10	0.885	8.7	16.1	12.5
184	18.4	10.1	22.9	-	9.8	18.2	3	3.11	10	0.885	8.7	16.1	12.5
185	18.4	7.8	23.2	-	9.8	18.2	3	3.11	10	0.885	8.7	16.1	12.5
186	18.4	7.8	23.2	-	9.8	18.2	3	3.11	10	0.885	8.7	16.1	12.5
187	18.4	10.1	22.9	-	9.8	18.2	3	3.11	10	0.885	8.7	16.1	12.5
188	18.4	7.8	23.2	-	9.8	18.2	3	3.11	10	0.885	8.7	16.1	12.5
189	18.4	4.6	24.7	-	9.8	18.2	3	3.11	10	0.885	8.7	16.1	12.5
190	18.4	10.1	22.9	-	9.8	18.2	3	3.11	10	0.885	8.7	16.1	12.5
191	18.4	7.2	26.3	-	9.8	18.2	3	3.11	10	0.885	8.7	16.1	12.5
192	18.4	5.0	25.2	-	9.8	18.2	3	3.11	10	0.885	8.7	16.1	12.5
193	18.4	6.2	22.8	-	9.8	18.2	3	3.11	10	0.885	8.7	16.1	12.5
194	18.4	7.8	23.0	-	9.8	18.2	3	3.11	10	0.885	8.7	16.1	12.5
195	18.4	6.2	22.8	-	9.8	18.2	3	3.11	10	0.885	8.7	16.1	12.5
196	18.4	5.0	25.2	-	9.8	18.2	3	3.11	10	0.885	8.7	16.1	12.5
197	18.4	7.5	21.4	-	9.8	18.2	3	3.11	10	0.885	8.7	16.1	12.5
198	18.4	6.2	22.8	-	9.8	18.2	3	3.11	10	0.885	8.7	16.1	12.5

Wall #	MASONRY MATERIALS												
	f_{block} [MPa]	f_{mortar} [MPa]	f_{grout} [MPa]	ν	$f_{\text{m(gROUTED)}}$ [MPa]	$f_{\text{m(ungROUTED)}}$ [MPa]	# of courses in prism	h/t prism	# of tests	Dillon Correction Factor k	$f_{\text{mcor(gROUTED)}}$ [MPa]	$f_{\text{mcor(ungROUTED)}}$ [MPa]	$f_{\text{mcor,eff}}$ [MPa]
199	18.4	5.0	25.2	-	9.8	18.2	3	3.11	10	0.885	8.7	16.1	12.5
200	18.4	7.2	26.3	-	9.8	18.2	3	3.11	10	0.885	8.7	16.1	12.5
201	18.4	6.7	23.8	-	9.8	18.2	3	3.11	10	0.885	8.7	16.1	12.5
202	18.4	7.8	23.0	-	9.8	18.2	3	3.11	10	0.885	8.7	16.1	12.5
203	18.4	7.5	21.4	-	9.8	18.2	3	3.11	10	0.885	8.7	16.1	12.5
204	18.4	7.8	23.0	-	9.8	18.2	3	3.11	10	0.885	8.7	16.1	12.5
205	18.4	6.8	25.7	-	9.8	18.2	3	3.11	10	0.885	8.7	16.1	12.5
206	18.4	7.2	26.3	-	9.8	18.2	3	3.11	10	0.885	8.7	16.1	12.5
207	18.4	6.7	23.8	-	9.8	18.2	3	3.11	10	0.885	8.7	16.1	12.5
208	18.4	7.8	23.0	-	9.8	18.2	3	3.11	10	0.885	8.7	16.1	12.5
209	18.4	6.4	-	-	9.8	18.2	3	3.11	10	0.885	8.7	16.1	12.5
210	18.4	7.8	-	-	9.8	18.2	3	3.11	10	0.885	8.7	16.1	12.5
211	18.4	5.5	-	-	9.8	18.2	3	3.11	10	0.885	8.7	16.1	12.5
212	18.4	6.1	-	-	9.8	18.2	3	3.11	10	0.885	8.7	16.1	12.5
213	18.4	6.7	-	-	9.8	18.2	3	3.11	10	0.885	8.7	16.1	12.5
214	18.4	7.8	-	-	9.8	18.2	3	3.11	10	0.885	8.7	16.1	12.5
215	18.4	6.4	-	-	9.8	18.2	3	3.11	10	0.885	8.7	16.1	12.5
216	18.4	7.8	-	-	9.8	18.2	3	3.11	10	0.885	8.7	16.1	12.5
217	18.4	5.5	-	-	9.8	18.2	3	3.11	10	0.885	8.7	16.1	12.5
218	18.4	12.8	-	-	9.8	18.2	3	3.11	10	0.885	8.7	16.1	12.5
219	18.4	13.2	-	-	9.8	18.2	3	3.11	10	0.885	8.7	16.1	12.5
220	18.4	15.0	-	-	9.8	18.2	3	3.11	10	0.885	8.7	16.1	12.5
221	18.4	12.5	-	-	9.8	18.2	3	3.11	10	0.885	8.7	16.1	12.5
222	18.4	13.2	-	-	9.8	18.2	3	3.11	10	0.885	8.7	16.1	12.5
223	18.4	15.0	-	-	9.8	18.2	3	3.11	10	0.885	8.7	16.1	12.5
224	18.4	13.7	11.3	-	9.8	18.2	3	3.11	10	0.885	8.7	16.1	12.5
225	18.4	15.3	11.1	-	9.8	18.2	3	3.11	10	0.885	8.7	16.1	12.5
226	18.4	13.0	15.4	-	9.8	18.2	3	3.11	10	0.885	8.7	16.1	12.5
227	18.4	15.3	11.5	-	9.8	18.2	3	3.11	10	0.885	8.7	16.1	12.5
228	18.4	13.7	11.3	-	9.8	18.2	3	3.11	10	0.885	8.7	16.1	12.5
229	18.4	13.0	15.4	-	9.8	18.2	3	3.11	10	0.885	8.7	16.1	12.5
230	16.5	5.7	30.1	-	8.5	20.4	5	5.21	5	1.000	8.5	20.4	16.5
231	16.5	5.7	31.1	-	8.5	20.4	5	5.21	5	1.000	8.5	20.4	16.5

Wall #	MASONRY MATERIALS												
	f_{block} [MPa]	f_{mortar} [MPa]	f_{grout} [MPa]	ν	$f_{\text{m(gROUTED)}}$ [MPa]	$f_{\text{m(ungROUTED)}}$ [MPa]	# of courses in prism	h/t prism	# of tests	Dillon Correction Factor k	$f_{\text{mcor(gROUTED)}}$ [MPa]	$f_{\text{mcor(ungROUTED)}}$ [MPa]	$f_{\text{mcor,eff}}$ [MPa]
232	16.5	5.7	32.1	-	8.5	20.4	5	5.21	5	1.000	8.5	20.4	16.5
233	16.5	5.7	33.1	-	8.5	20.4	5	5.21	5	1.000	8.5	20.4	16.5
234	16.5	5.7	34.1	-	8.5	20.4	5	5.21	5	1.000	8.5	20.4	16.5
235	16.5	5.7	35.1	-	8.5	20.4	5	5.21	5	1.000	8.5	20.4	16.5
236	16.5	5.7	35.1	-	8.5	20.4	5	5.21	5	1.000	8.5	20.4	16.5
237	16.5	5.7	36.1	-	8.5	20.4	5	5.21	5	1.000	8.5	20.4	16.5
238	16.5	5.7	37.1	-	8.5	20.4	5	5.21	5	1.000	8.5	20.4	16.5
239	16.5	5.7	35.1	-	8.5	20.4	5	5.21	5	1.000	8.5	20.4	16.5
240	16.5	5.7	38.1	-	8.5	20.4	5	5.21	5	1.000	8.5	20.4	16.5
241	16.5	5.7	39.1	-	8.5	20.4	5	5.21	5	1.000	8.5	20.4	16.5
242	16.5	5.7	40.1	-	8.5	20.4	5	5.21	5	1.000	8.5	20.4	16.5
243	16.5	5.7	41.1	-	8.5	20.4	5	5.21	5	1.000	8.5	20.4	16.5
244	16.5	5.7	42.1	-	8.5	20.4	5	5.21	5	1.000	8.5	20.4	16.5
245	16.5	5.7	43.1	-	8.5	20.4	5	5.21	5	1.000	8.5	20.4	16.5
246	16.5	5.7	44.1	-	8.5	20.4	5	5.21	5	1.000	8.5	20.4	16.5
247	16.5	5.7	45.1	-	8.5	20.4	5	5.21	5	1.000	8.5	20.4	16.5
248	26.9	4.5	11.1	-	8.1	8.9	3	3.22	10	0.893	7.2	7.9	7.8
249	26.9	4.5	11.1	-	8.1	8.9	3	3.22	10	0.893	7.2	7.9	7.8
250	26.9	4.5	11.1	-	8.1	8.9	3	3.22	10	0.893	7.2	7.9	7.8
251	26.9	4.5	11.1	-	8.1	8.9	3	3.22	10	0.893	7.2	7.9	7.8
252	26.9	4.5	11.1	-	8.1	8.9	3	3.22	10	0.893	7.2	7.9	7.8
253	26.9	4.5	11.1	-	8.1	8.9	3	3.22	10	0.893	7.2	7.9	7.8
254	26.9	4.5	11.1	-	8.1	8.9	3	3.22	10	0.893	7.2	7.9	7.7
255	26.9	4.5	11.1	-	8.1	8.9	3	3.22	10	0.893	7.2	7.9	7.7
256	26.9	4.5	11.1	-	8.1	8.9	3	3.22	10	0.893	7.2	7.9	7.7
257	26.9	4.5	11.1	-	8.1	8.9	3	3.22	10	0.893	7.2	7.9	7.7
258	26.9	4.5	11.1	-	8.1	8.9	3	3.22	10	0.893	7.2	7.9	7.7
259	26.9	4.5	11.1	-	8.1	8.9	3	3.22	10	0.893	7.2	7.9	7.7
260	26.9	4.9	11.5	-	8.2	9.1	3	3.22	10	0.893	7.3	8.1	7.5
261	26.9	4.9	11.5	-	8.2	9.1	3	3.22	10	0.893	7.3	8.1	7.3
262	26.9	4.9	11.5	-	8.2	9.1	3	3.22	10	0.893	7.3	8.1	7.3
263	26.9	4.9	11.5	-	8.2	9.1	3	3.22	10	0.893	7.3	8.1	7.3
264	26.9	4.9	11.5	-	8.2	9.1	3	3.22	10	0.893	7.3	8.1	7.3

Wall #	MASONRY MATERIALS												
	f_{block} [MPa]	f_{mortar} [MPa]	f_{grout} [MPa]	ν	$f_{\text{m(grouded)}}$ [MPa]	$f_{\text{m(ungrouded)}}$ [MPa]	# of courses in prism	h/t prism	# of tests	Dillon Correction Factor k	$f_{\text{mcor(grouded)}}$ [MPa]	$f_{\text{mcor(ungrouded)}}$ [MPa]	$f_{\text{mcor,eff}}$ [MPa]
265	26.9	4.9	11.5	-	8.2	9.1	3	3.22	10	0.893	7.3	8.1	7.3
266	26.9	4.9	11.5	-	8.2	9.1	3	3.22	10	0.893	7.3	8.1	7.9
267	26.9	4.9	11.5	-	8.2	9.1	3	3.22	10	0.893	7.3	8.1	7.9
268	26.9	4.9	11.5	-	8.2	9.1	3	3.22	10	0.893	7.3	8.1	7.9
269	35.7	22.1	25.7	-	10.5	18.6	3	3.11	5	0.885	9.3	16.5	14.9
270	35.7	22.1	25.7	-	10.5	18.6	3	3.11	5	0.885	9.3	16.5	14.9
271	35.7	22.1	25.7	-	10.5	18.6	3	3.11	5	0.885	9.3	16.5	14.9
272	35.7	22.1	21.7	-	9.5	18.6	3	3.11	5	0.885	8.4	16.5	14.7
273	29.3	9.5	25.2	-	12.7	22.3	3	3.11	5	0.885	11.2	19.7	17.9
274	29.3	9.5	25.2	-	12.7	22.3	3	3.11	5	0.885	11.2	19.7	17.9
275	29.3	11.5	31.7	-	12.7	22.3	3	3.11	5	0.885	11.2	19.7	17.9
276	29.3	11.5	31.7	-	12.7	22.3	3	3.11	5	0.885	11.2	19.7	17.9
277	29.3	11.0	31.8	-	12.7	22.3	3	3.11	5	0.885	11.2	19.7	17.9
278	29.3	11.0	31.8	-	12.7	22.3	3	3.11	5	0.885	11.2	19.7	17.9
279	20.1	9.3	24.7	-	8.8	14.7	3	3.11	5	0.885	7.8	13.0	11.9
280	20.1	9.3	24.7	-	8.8	14.7	3	3.11	5	0.885	7.8	13.0	11.9
281	20.1	11.6	29.3	-	8.8	14.7	3	3.11	5	0.885	7.8	13.0	11.9
282	20.1	11.6	29.3	-	8.8	14.7	3	3.11	5	0.885	7.8	13.0	11.9
283	6.4	18.0	31.7	53%	5.5	6.0	1	1.00	5	0.744	4.1	4.4	4.3
284	6.4	18.0	31.7	53%	5.5	6.0	1	1.00	5	0.744	4.1	4.4	4.3
285	6.4	18.0	31.7	53%	5.5	6.0	1	1.00	5	0.744	4.1	4.4	4.3
286	6.4	18.0	31.7	53%	5.5	6.0	1	1.00	5	0.744	4.1	4.4	4.3
287	6.4	18.0	31.7	53%	5.5	6.0	1	1.00	5	0.744	4.1	4.4	4.3
288	6.4	18.0	31.7	53%	5.5	6.0	1	1.00	5	0.744	4.1	4.4	4.3
289	6.4	18.0	31.7	53%	5.5	6.0	1	1.00	5	0.744	4.1	4.4	4.3
290	6.4	18.0	31.7	53%	5.5	6.0	1	1.00	5	0.744	4.1	4.4	4.3
291	6.4	18.0	31.7	53%	5.5	6.0	1	1.00	5	0.744	4.1	4.4	4.3
292	6.4	18.0	31.7	53%	5.5	6.0	1	1.00	5	0.744	4.1	4.4	4.3

Wall #	VERTICAL REINFORCEMENT											
	Vertical (Interior) Reinf	A _c [mm ²]	ρ _c [unitless]	Flexural Reinf	A _t [mm ²]	ρ _t [unitless]	A _{v, bar} [mm ²]	A _{v, total} [mm ²]	ρ _v [unitless]	f _{yv} [MPa]	ρ _v f _{yv} [MPa]	ρ _c f _{yv} [MPa]
1	-	0	0.00000	-	0	0.00000	0	0	0.00000	0	0.000	0.000
2	-	0	0.00000	(2)5/8"	396	0.00142	198	396	0.00142	285	0.405	0.000
3	-	0	0.00000	-	0	0.00000	0	0	0.00000	0	0.000	0.000
4	-	0	0.00000	(2)5/8"	396	0.00142	198	396	0.00142	285	0.405	0.000
5	(1)1/2"	127	0.00045	(2)5/8"	396	0.00142	127, 198	523	0.00187	231	0.434	0.105
6	(2)1/2"	253	0.00091	(2)5/8"	396	0.00142	127, 198	649	0.00233	233	0.543	0.212
7	-	0	0.00000	(2)5/8"+(2)1/2"	649	0.00233	127, 198	649	0.00233	236	0.549	0.000
8	(3)1/2"	380	0.00136	(2)5/8"	396	0.00142	127, 198	776	0.00278	235	0.653	0.320
9	(3)1/2"	380	0.00136	(2)5/8"	396	0.00142	127, 198	776	0.00278	237	0.659	0.323
10	(3)1/2"	380	0.00136	(2)5/8"	396	0.00142	127, 198	776	0.00278	237	0.659	0.323
11	(3)5/8"	594	0.00213	(2)5/8"	396	0.00142	198	990	0.00355	302	1.072	0.643
12	(3)5/8"	594	0.00213	(2)5/8"	396	0.00142	198	990	0.00355	302	1.072	0.643
13	(3)#3	213	0.00055	(2)2#4	1032	0.00269	71, 129	1245	0.00324	245	0.795	0.136
14	(3)#3	213	0.00055	(2)2#4	1032	0.00269	71, 129	1245	0.00324	245	0.795	0.136
15	(3)#3	213	0.00055	(2)2#4	1032	0.00269	71, 129	1245	0.00324	245	0.795	0.136
16	#3	213	0.00055	(2)#4	516	0.00134	71, 129	729	0.00190	245	0.466	0.136
17	#3	213	0.00055	(2)#4	516	0.00134	71, 129	729	0.00190	245	0.466	0.136
18	(3)#3	213	0.00055	(2)2#4	1032	0.00269	71, 129	1245	0.00324	245	0.795	0.136
19	#3	213	0.00055	(2)#4	516	0.00134	71, 129	729	0.00190	245	0.466	0.136
20	(3)#3	213	0.00055	(2)2#4	1032	0.00269	71, 129	1245	0.00324	245	0.795	0.136
21	(3)#3	213	0.00055	(2)4#4	1032	0.00269	71, 129	1245	0.00324	245	0.795	0.136
22	(3)#3	213	0.00055	(2)2#4	1032	0.00269	71, 129	1245	0.00324	245	0.795	0.136
23	-	0	0.00000	(2)2#5	800	0.00333	200	800	0.00333	392	1.307	0.000
24	-	0	0.00000	(2)2#5	800	0.00333	200	800	0.00333	392	1.307	0.000
25	-	0	0.00000	(2)2#5	800	0.00333	200	800	0.00333	392	1.307	0.000
26	-	0	0.00000	(2)2#5	800	0.00333	200	800	0.00333	392	1.307	0.000
27	-	0	0.00000	(2)2#5	800	0.00333	200	800	0.00333	392	1.307	0.000
28	(2)#4	258	0.00108	(2)2#5	800	0.00333	129, 200	1058	0.00441	392	1.728	0.421
29	-	0	0.00000	(2)2#4	516	0.00215	129	516	0.00215	392	0.843	0.000
30	(2)#4	258	0.00108	(2)2#5	800	0.00333	129, 200	1058	0.00441	392	1.728	0.421
31	-	0	0.00000	(2)2#5	800	0.00333	200	800	0.00333	392	1.307	0.000
32	-	0	0.00000	(2)#3	142	0.00059	71	142	0.00059	392	0.232	0.000
33	-	0	0.00000	(2)2#5	800	0.00333	200	800	0.00333	392	1.307	0.000

Wall #	VERTICAL REINFORCEMENT											
	Vertical (Interior) Reinf	A _c [mm ²]	ρ _c [unitless]	Flexural Reinf	A _t [mm ²]	ρ _t [unitless]	A _{v, bar} [mm ²]	A _{v, total} [mm ²]	ρ _v [unitless]	f _{yv} [MPa]	ρ _v f _{yv} [MPa]	ρ _c f _{yv} [MPa]
34	-	0	0.00000	2#6	568	0.00611	284	568	0.00611	516	3.153	0.000
35	-	0	0.00000	2#6	568	0.00611	284	568	0.00611	516	3.153	0.000
36	-	0	0.00000	-	0	0.00000	0	0	0.00000	0	0.000	0.000
37	-	0	0.00000	#5	400	0.00212	200	400	0.00212	488	1.036	0.000
38	-	0	0.00000	#8	1018	0.00540	509	1018	0.00540	477	2.578	0.000
39	-	0	0.00000	#8	1018	0.00540	509	1018	0.00540	477	2.578	0.000
40	D10	157	0.00088	D12	148	0.00082	78, 113	305	0.00170	353	0.600	0.309
41	D16	201	0.00112	D16	402	0.00224	201	603	0.00337	454	1.528	0.509
42	D16	201	0.00112	D16	402	0.00224	201	603	0.00337	454	1.528	0.509
43	(3)Ø9	191	0.00077	2D22	1549	0.00624	775	1740	0.00701	385	2.698	0.296
44	(3)Ø9	191	0.00077	D25&D22	1912	0.00770	956	2102	0.00847	385	3.260	0.296
45	(2)Ø9	127	0.00068	2D22	1547	0.00822	774	1675	0.00890	385	3.425	0.260
46	(2)Ø9	127	0.00068	D29	1412	0.00750	706	1539	0.00818	385	3.148	0.260
47	Ø9	64	0.00050	2D22	1549	0.01208	775	1613	0.01258	385	4.842	0.191
48	Ø9	64	0.00050	D25	1013	0.00790	507	1077	0.00840	385	3.232	0.191
49	(2)Ø9	127	0.00068	2D22	1547	0.00822	774	1675	0.00890	385	3.425	0.260
50	(2)Ø9	127	0.00068	2D22	1547	0.00822	774	1675	0.00890	385	3.425	0.260
51	(2)Ø9	127	0.00068	2D22	1547	0.00822	774	1675	0.00890	385	3.425	0.260
52	(2)Ø9	127	0.00068	(2)Ø9	1547	0.00822	774	1675	0.00890	385	3.425	0.260
53	(2)Ø9	127	0.00068	(3)Ø9	1547	0.00822	774	1675	0.00890	385	3.425	0.260
54	(2)Ø9	127	0.00068	2D22	1547	0.00822	774	1675	0.00890	385	3.425	0.260
55	(2)Ø9	127	0.00068	2D22	1547	0.00822	774	1675	0.00890	385	3.425	0.260
56	(2)Ø9	127	0.00068	2D22	1547	0.00822	774	1675	0.00890	385	3.425	0.260
57	(2)Ø9	127	0.00066	2D22	1548	0.00798	774	1675	0.00864	385	3.325	0.253
58	(2)Ø9	127	0.00066	2D22	1548	0.00798	774	1675	0.00864	385	3.325	0.253
59	(2)Ø9	127	0.00066	2D22	1548	0.00798	774	1675	0.00864	385	3.325	0.253
60	(2)Ø9	127	0.00066	2D22	1548	0.00798	774	1675	0.00864	385	3.325	0.253
61	(2)Ø9	127	0.00066	D19	574	0.00296	287	701	0.00362	385	1.392	0.253
62	(2)Ø9	127	0.00068	2D22	1547	0.00822	774	1675	0.00890	385	3.425	0.260
63	(2)Ø9	127	0.00068	2D22	1547	0.00822	774	1675	0.00890	385	3.425	0.260
64	(2)Ø9	127	0.00068	2D22	1547	0.00822	774	1675	0.00890	385	3.425	0.260
65	(2)Ø9	127	0.00068	2D22	1547	0.00822	774	1675	0.00890	385	3.425	0.260
66	(4)Ø9	254	0.00090	2D22	1545	0.00548	773	1800	0.00638	385	2.457	0.347

Wall #	VERTICAL REINFORCEMENT											
	Vertical (Interior) Reinf	A _c [mm ²]	ρ _c [unitless]	Flexural Reinf	A _t [mm ²]	ρ _t [unitless]	A _{v, bar} [mm ²]	A _{v, total} [mm ²]	ρ _v [unitless]	f _{yv} [MPa]	ρ _v f _{yv} [MPa]	ρ _c f _{yv} [MPa]
67	(4)Ø9	254	0.00090	2D22	1545	0.00548	773	1800	0.00638	385	2.457	0.347
68	(3)Ø9	191	0.00076	D29	1285	0.00510	643	1476	0.00586	385	2.255	0.292
69	(2)Ø9	127	0.00066	D25	1014	0.00528	507	1141	0.00594	385	2.288	0.255
70	Ø9	64	0.00048	D22	774	0.00586	387	837	0.00634	385	2.442	0.186
71	Ø9	64	0.00048	D22	774	0.00586	387	837	0.00634	385	2.442	0.186
72	-	0	0.00000	Ø10mm	157	0.00161	79	157	0.00161	522	0.840	0.000
73	-	0	0.00000	Ø10mm	157	0.00161	79	157	0.00161	522	0.840	0.000
74	-	0	0.00000	Ø10mm	157	0.00161	79	157	0.00161	522	0.840	0.000
75	-	0	0.00000	Ø10mm	157	0.00161	79	157	0.00161	522	0.840	0.000
76	-	0	0.00000	Ø10mm	157	0.00161	79	157	0.00161	522	0.840	0.000
77	-	0	0.00000	2Ø10mm	314	0.00322	79	314	0.00322	522	1.680	0.000
78	-	0	0.00000	2Ø10mm	314	0.00322	79	314	0.00322	522	1.680	0.000
79	-	0	0.00000	2Ø10mm	314	0.00322	79	314	0.00322	522	1.680	0.000
80	-	0	0.00000	2Ø10mm	314	0.00322	79	314	0.00322	522	1.680	0.000
81	-	0	0.00000	2Ø10mm	314	0.00322	79	314	0.00322	522	1.680	0.000
82	-	0	0.00000	#5	200	0.00154	200	200	0.00154	345	0.531	0.000
83	-	0	0.00000	#5	200	0.00154	200	200	0.00154	345	0.531	0.000
84	-	0	0.00000	#5	200	0.00154	200	200	0.00154	345	0.531	0.000
85	-	0	0.00000	#5	200	0.00154	200	200	0.00154	345	0.531	0.000
86	-	0	0.00000	#5	200	0.00154	200	200	0.00154	345	0.531	0.000
87	-	0	0.00000	#5	200	0.00154	200	200	0.00154	345	0.531	0.000
88	-	0	0.00000	#5	200	0.00154	200	200	0.00154	345	0.531	0.000
89	-	0	0.00000	#5	200	0.00154	200	200	0.00154	345	0.531	0.000
90	-	0	0.00000	#5	200	0.00154	200	200	0.00154	345	0.531	0.000
91	-	0	0.00000	#5	200	0.00154	200	200	0.00154	345	0.531	0.000
92	-	0	0.00000	#5	200	0.00154	200	200	0.00154	345	0.531	0.000
93	-	0	0.00000	#5	200	0.00154	200	200	0.00154	345	0.531	0.000
94	-	0	0.00000	#5	200	0.00154	200	200	0.00154	345	0.531	0.000
95	-	0	0.00000	#5	200	0.00154	200	200	0.00154	345	0.531	0.000
96	-	0	0.00000	#5	200	0.00154	200	200	0.00154	345	0.531	0.000
97	-	0	0.00000	#5	200	0.00154	200	200	0.00154	345	0.531	0.000
98	-	0	0.00000	-	0	0.00000	0	0	0.00000	0	0.000	0.000
99	-	0	0.00000	-	0	0.00000	0	0	0.00000	0	0.000	0.000

Wall #	VERTICAL REINFORCEMENT											
	Vertical (Interior) Reinf	A _c [mm ²]	ρ _c [unitless]	Flexural Reinf	A _t [mm ²]	ρ _t [unitless]	A _{v, bar} [mm ²]	A _{v, total} [mm ²]	ρ _v [unitless]	f _{yv} [MPa]	ρ _v f _{yv} [MPa]	ρ _c f _{yv} [MPa]
100	-	0	0.00000	-	0	0.00000	0	0	0.00000	0	0.000	0.000
101	-	0	0.00000	-	0	0.00000	0	0	0.00000	0	0.000	0.000
102	-	0	0.00000	-	0	0.00000	0	0	0.00000	0	0.000	0.000
103	-	0	0.00000	-	0	0.00000	0	0	0.00000	0	0.000	0.000
104	-	0	0.00000	-	0	0.00000	0	0	0.00000	0	0.000	0.000
105	-	0	0.00000	-	0	0.00000	0	0	0.00000	0	0.000	0.000
106	-	0	0.00000	-	0	0.00000	0	0	0.00000	0	0.000	0.000
107	-	0	0.00000	-	0	0.00000	0	0	0.00000	0	0.000	0.000
108	-	0	0.00000	2#4/3	53	0.00049	13.3	53	0.00049	443	0.219	0.000
109	#5/3	13	0.00012	#5/3	27	0.00025	13.3	40	0.00037	447	0.166	0.055
110	#5/3	13	0.00012	#5/3	27	0.00025	13.3	40	0.00037	447	0.165	0.055
111	#5/3	13	0.00012	#5/3	27	0.00025	13.3	40	0.00037	447	0.165	0.055
112	-	0	0.00000	D10	157	0.00161	78.5	157	0.00161	522	0.840	0.000
113	-	0	0.00000	D10	157	0.00161	78.5	157	0.00161	522	0.840	0.000
114	-	0	0.00000	D10	157	0.00161	78.5	157	0.00161	522	0.840	0.000
115	-	0	0.00000	D10	157	0.00161	78.5	157	0.00161	522	0.840	0.000
116	-	0	0.00000	D10	157	0.00161	78.5	157	0.00161	522	0.840	0.000
117	-	0	0.00000	D10	157	0.00161	78.5	157	0.00161	522	0.840	0.000
118	-	0	0.00000	2#6	1136	0.00256	568	1136	0.00256	400	1.024	0.000
119	-	0	0.00000	2#6	1136	0.00358	568	1136	0.00358	400	1.433	0.000
120	-	0	0.00000	2#6	1136	0.00512	568	1136	0.00512	400	2.048	0.000
121	-	0	0.00000	2#6	1136	0.00256	568	1136	0.00256	400	1.024	0.000
122	-	0	0.00000	2#6	1136	0.00358	568	1136	0.00358	400	1.433	0.000
123	-	0	0.00000	2#6	1136	0.00512	568	1136	0.00512	400	2.048	0.000
124	-	0	0.00000	2#6	1136	0.00256	568	1136	0.00256	400	1.024	0.000
125	-	0	0.00000	2#6	1136	0.00358	568	1136	0.00358	400	1.433	0.000
126	-	0	0.00000	2#6	1136	0.00512	568	1136	0.00512	400	2.048	0.000
127	-	0	0.00000	2#6	1136	0.00256	568	1136	0.00256	400	1.024	0.000
128	-	0	0.00000	2#6	1136	0.00358	568	1136	0.00358	400	1.433	0.000
129	-	0	0.00000	2#6	1136	0.00512	568	1136	0.00512	400	2.048	0.000
130	(3)D20	600	0.00298	D20	900	0.00446	300	1500	0.00744	320	2.381	0.952
131	D20	200	0.00099	D20	1300	0.00645	300	1500	0.00744	320	2.381	0.317
132	Ø5mm truss	39	0.00020	Ø5mm tr.	79	0.00041	39	118	0.00061	580	0.356	0.119

Wall #	VERTICAL REINFORCEMENT											
	Vertical (Interior) Reinf	A _c [mm ²]	ρ _c [unitless]	Flexural Reinf	A _t [mm ²]	ρ _t [unitless]	A _{v, bar} [mm ²]	A _{v, total} [mm ²]	ρ _v [unitless]	f _{yv} [MPa]	ρ _v f _{yv} [MPa]	ρ _c f _{yv} [MPa]
133	Ø5mm truss	39	0.00020	Ø5mm tr.	79	0.00041	39	118	0.00061	580	0.356	0.119
134	Ø5mm truss	39	0.00020	Ø5mm tr.	79	0.00041	39	118	0.00061	580	0.356	0.119
135	Ø5mm truss	39	0.00020	Ø5mm tr.	79	0.00041	39	118	0.00061	580	0.356	0.119
136	#10	100	0.00039	#10	200	0.00077	100	300	0.00116	492	0.569	0.190
137	2#3	142	0.00055	#3	142	0.00055	71	284	0.00110	503	0.551	0.276
138	-	0	0.00000	#4	252	0.00097	126	252	0.00097	565	0.549	0.000
139	#10	100	0.00039	#10	200	0.00077	100	300	0.00116	492	0.569	0.190
140	#10	100	0.00039	#10	200	0.00077	100	300	0.00116	492	0.569	0.190
141	2#6	568	0.00112	2#6	1135	0.00223	284	1703	0.00335	427	1.429	0.476
142	2#6	568	0.00112	2#6	1135	0.00223	284	1703	0.00335	427	1.429	0.476
143	2#6	568	0.00112	2#6	1135	0.00223	284	1703	0.00335	427	1.429	0.476
144	2#6	568	0.00112	2#6	1135	0.00223	284	1703	0.00335	427	1.429	0.476
145	(2)#6	1135	0.00223	2#6	568	0.00112	200, 284	1703	0.00335	427	1.429	0.953
146	(3)#5	600	0.00118	2#6	1135	0.00223	284	1735	0.00341	443	1.512	0.523
147	(2)#6	568	0.00092	#6	568	0.00092	284	1136	0.00184	414	0.762	0.381
148	(2)#6	568	0.00092	#6	568	0.00092	284	1136	0.00184	414	0.762	0.381
149	(2)#6	568	0.00092	#6	568	0.00092	284	1136	0.00184	414	0.762	0.381
150	(2)#6	568	0.00092	#6	568	0.00092	284	1136	0.00184	414	0.762	0.381
151	(2)#4	258	0.00059	2#6	1136	0.00258	129, 284	1394	0.00317	461	1.460	0.270
152	(2)#4	258	0.00059	2#6	1136	0.00258	129, 284	1394	0.00317	461	1.460	0.270
153	(8)#4	1032	0.00235	#6	568	0.00129	129, 284	1600	0.00364	461	1.676	1.081
154	(8)#4	1032	0.00235	#6	568	0.00129	129, 284	1600	0.00364	461	1.676	1.081
155	(8)#4	1032	0.00235	#6	568	0.00129	129, 284	1600	0.00364	461	1.676	1.081
156	(4)#4	258	0.00039	2#6	1394	0.00211	129, 284	1652	0.00251	461	1.155	0.180
157	(7)#4	903	0.00137	2#6	1136	0.00172	129, 284	2039	0.00309	461	1.426	0.631
158	(7)#4	903	0.00137	2#6	1136	0.00172	129, 284	2039	0.00309	461	1.426	0.631
159	2#7	774	0.00152	2#7	1548	0.00303	387	2322	0.00456	438	1.997	0.664
160	2#7	774	0.00152	2#7	1548	0.00303	387	2322	0.00456	438	1.997	0.664
161	2#7	774	0.00152	2#7	1548	0.00303	387	2322	0.00456	438	1.997	0.664
162	(2)2#6	1136	0.00223	2#6	1136	0.00223	284	2272	0.00446	438	1.953	0.975
163	(3)2#5	1200	0.00235	2#6	1640	0.00321	200,284	2840	0.00458	438	2.006	1.030
164	-	0	0.00000	-	0	0.00000	0	0	0.00000	0	0.000	0.000
165	-	0	0.00000	-	0	0.00000	0	0	0.00000	0	0.000	0.000

Wall #	VERTICAL REINFORCEMENT											
	Vertical (Interior) Reinf	A _c [mm ²]	ρ _c [unitless]	Flexural Reinf	A _t [mm ²]	ρ _t [unitless]	A _{v, bar} [mm ²]	A _{v, total} [mm ²]	ρ _v [unitless]	f _{yv} [MPa]	ρ _v f _{yv} [MPa]	ρ _c f _{yv} [MPa]
166	-	0	0.00000	-	0	0.00000	0	0	0.00000	0	0.000	0.000
167	-	0	0.00000	-	0	0.00000	0	0	0.00000	0	0.000	0.000
168	-	0	0.00000	-	0	0.00000	0	0	0.00000	0	0.000	0.000
169	-	0	0.00000	-	0	0.00000	0	0	0.00000	0	0.000	0.000
170	-	0	0.00000	-	0	0.00000	0	0	0.00000	0	0.000	0.000
171	-	0	0.00000	-	0	0.00000	0	0	0.00000	0	0.000	0.000
172	-	0	0.00000	-	0	0.00000	0	0	0.00000	0	0.000	0.000
173	2-15M	400	0.00166	15M	400	0.00166	200	800	0.00331	480	1.589	0.794
174	2-15M	400	0.00166	15M	400	0.00166	200	800	0.00331	480	1.589	0.794
175	2-15M	400	0.00166	15M	400	0.00166	200	800	0.00331	480	1.589	0.794
176	2-15M	400	0.00166	15M	400	0.00166	200	800	0.00331	480	1.589	0.794
177	2-15M	400	0.00166	15M	400	0.00166	200	800	0.00331	480	1.589	0.794
178	2-15M	400	0.00166	15M	400	0.00166	200	800	0.00331	480	1.589	0.794
179	-	0	0.00000	-	0	0.00000	0	0	0.00000	0	0.000	0.000
180	-	0	0.00000	-	0	0.00000	0	0	0.00000	0	0.000	0.000
181	-	0	0.00000	-	0	0.00000	0	0	0.00000	0	0.000	0.000
182	-	0	0.00000	-	0	0.00000	0	0	0.00000	0	0.000	0.000
183	-	0	0.00000	-	0	0.00000	0	0	0.00000	0	0.000	0.000
184	-	0	0.00000	-	0	0.00000	0	0	0.00000	0	0.000	0.000
185	-	0	0.00000	-	0	0.00000	0	0	0.00000	0	0.000	0.000
186	-	0	0.00000	-	0	0.00000	0	0	0.00000	0	0.000	0.000
187	-	0	0.00000	-	0	0.00000	0	0	0.00000	0	0.000	0.000
188	-	0	0.00000	-	0	0.00000	0	0	0.00000	0	0.000	0.000
189	-	0	0.00000	-	0	0.00000	0	0	0.00000	0	0.000	0.000
190	-	0	0.00000	-	0	0.00000	0	0	0.00000	0	0.000	0.000
191	2-15M	400	0.00166	15M	400	0.00166	200	800	0.00331	480	1.589	0.794
192	2-15M	400	0.00166	15M	400	0.00166	200	800	0.00331	480	1.589	0.794
193	2-15M	400	0.00166	15M	400	0.00166	200	800	0.00331	480	1.589	0.794
194	2-15M	400	0.00166	15M	400	0.00166	200	800	0.00331	480	1.589	0.794
195	2-15M	400	0.00166	15M	400	0.00166	200	800	0.00331	480	1.589	0.794
196	2-15M	400	0.00166	15M	400	0.00166	200	800	0.00331	480	1.589	0.794
197	-	0	0.00000	-	0	0.00000	0	0	0.00000	0	0.000	0.000
198	-	0	0.00000	-	0	0.00000	0	0	0.00000	0	0.000	0.000

Wall #	VERTICAL REINFORCEMENT											
	Vertical (Interior) Reinf	A _c [mm ²]	ρ _c [unitless]	Flexural Reinf	A _t [mm ²]	ρ _t [unitless]	A _{v, bar} [mm ²]	A _{v, total} [mm ²]	ρ _v [unitless]	f _{yv} [MPa]	ρ _v f _{yv} [MPa]	ρ _c f _{yv} [MPa]
199	-	0	0.00000	-	0	0.00000	0	0	0.00000	0	0.000	0.000
200	-	0	0.00000	-	0	0.00000	0	0	0.00000	0	0.000	0.000
201	-	0	0.00000	-	0	0.00000	0	0	0.00000	0	0.000	0.000
202	-	0	0.00000	-	0	0.00000	0	0	0.00000	0	0.000	0.000
203	-	0	0.00000	-	0	0.00000	0	0	0.00000	0	0.000	0.000
204	-	0	0.00000	-	0	0.00000	0	0	0.00000	0	0.000	0.000
205	-	0	0.00000	-	0	0.00000	0	0	0.00000	0	0.000	0.000
206	-	0	0.00000	-	0	0.00000	0	0	0.00000	0	0.000	0.000
207	-	0	0.00000	-	0	0.00000	0	0	0.00000	0	0.000	0.000
208	-	0	0.00000	-	0	0.00000	0	0	0.00000	0	0.000	0.000
209	2-15M	400	0.00166	15M	400	0.00166	200	800	0.00331	480	1.589	0.794
210	2-15M	400	0.00166	15M	400	0.00166	200	800	0.00331	480	1.589	0.794
211	2-15M	400	0.00166	15M	400	0.00166	200	800	0.00331	480	1.589	0.794
212	2-15M	400	0.00166	15M	400	0.00166	200	800	0.00331	480	1.589	0.794
213	2-15M	400	0.00166	15M	400	0.00166	200	800	0.00331	480	1.589	0.794
214	2-15M	400	0.00166	15M	400	0.00166	200	800	0.00331	480	1.589	0.794
215	-	0	0.00000	-	0	0.00000	0	0	0.00000	0	0.000	0.000
216	-	0	0.00000	-	0	0.00000	0	0	0.00000	0	0.000	0.000
217	-	0	0.00000	-	0	0.00000	0	0	0.00000	0	0.000	0.000
218	-	0	0.00000	-	0	0.00000	0	0	0.00000	0	0.000	0.000
219	-	0	0.00000	-	0	0.00000	0	0	0.00000	0	0.000	0.000
220	-	0	0.00000	-	0	0.00000	0	0	0.00000	0	0.000	0.000
221	-	0	0.00000	-	0	0.00000	0	0	0.00000	0	0.000	0.000
222	-	0	0.00000	-	0	0.00000	0	0	0.00000	0	0.000	0.000
223	-	0	0.00000	-	0	0.00000	0	0	0.00000	0	0.000	0.000
224	-	0	0.00000	-	0	0.00000	0	0	0.00000	0	0.000	0.000
225	-	0	0.00000	-	0	0.00000	0	0	0.00000	0	0.000	0.000
226	-	0	0.00000	-	0	0.00000	0	0	0.00000	0	0.000	0.000
227	-	0	0.00000	-	0	0.00000	0	0	0.00000	0	0.000	0.000
228	-	0	0.00000	-	0	0.00000	0	0	0.00000	0	0.000	0.000
229	-	0	0.00000	-	0	0.00000	0	0	0.00000	0	0.000	0.000
230	15M	200	0.00073	15M	400	0.00146	200	600	0.00219	450	0.987	0.329
231	15M	200	0.00073	15M	400	0.00146	200	600	0.00219	450	0.987	0.329

Wall #	VERTICAL REINFORCEMENT											
	Vertical (Interior) Reinf	A _c [mm ²]	ρ _c [unitless]	Flexural Reinf	A _t [mm ²]	ρ _t [unitless]	A _{v, bar} [mm ²]	A _{v, total} [mm ²]	ρ _v [unitless]	f _{yv} [MPa]	ρ _v f _{yv} [MPa]	ρ _c f _{yv} [MPa]
232	15M	200	0.00073	15M	400	0.00146	200	600	0.00219	450	0.987	0.329
233	15M	200	0.00073	15M	400	0.00146	200	600	0.00219	450	0.987	0.329
234	15M	200	0.00073	15M	400	0.00146	200	600	0.00219	450	0.987	0.329
235	15M	200	0.00073	15M	400	0.00146	200	600	0.00219	450	0.987	0.329
236	15M	200	0.00073	15M	400	0.00146	200	600	0.00219	450	0.987	0.329
237	15M	200	0.00073	15M	400	0.00146	200	600	0.00219	450	0.987	0.329
238	15M	200	0.00073	15M	400	0.00146	200	600	0.00219	450	0.987	0.329
239	15M	200	0.00073	15M	400	0.00146	200	600	0.00219	450	0.987	0.329
240	15M (no splice)	200	0.00073	15M (no splice)	400	0.00146	200	600	0.00219	450	0.987	0.329
241	15M (no splice)	200	0.00073	15M (no splice)	400	0.00146	200	600	0.00219	450	0.987	0.329
242	15M (top splice)	200	0.00073	15M (top splice)	400	0.00146	200	600	0.00219	450	0.987	0.329
243	15M (top splice)	200	0.00073	15M (top splice)	400	0.00146	200	600	0.00219	450	0.987	0.329
244	15M	200	0.00073	15M	400	0.00146	200	600	0.00219	450	0.987	0.329
245	15M	200	0.00073	15M	400	0.00146	200	600	0.00219	450	0.987	0.329
246	15M	200	0.00073	15M	400	0.00146	200	600	0.00219	450	0.987	0.329
247	15M	200	0.00073	15M	400	0.00146	200	600	0.00219	450	0.987	0.329
248	-	0	0.00000	10M	200	0.00112	100	200	0.00112	458	0.511	0.000
249	-	0	0.00000	10M	200	0.00112	100	200	0.00112	458	0.511	0.000
250	-	0	0.00000	10M	200	0.00112	100	200	0.00112	458	0.511	0.000
251	-	0	0.00000	10M	200	0.00112	100	200	0.00112	458	0.511	0.000
252	-	0	0.00000	10M	200	0.00112	100	200	0.00112	458	0.511	0.000
253	-	0	0.00000	10M	200	0.00112	100	200	0.00112	458	0.511	0.000
254	10M	100	0.00056	10M	200	0.00112	100	300	0.00167	458	0.767	0.256
255	10M	100	0.00056	10M	200	0.00112	100	300	0.00167	458	0.767	0.256
256	10M	100	0.00056	10M	200	0.00112	100	300	0.00167	458	0.767	0.256
257	10M	100	0.00056	10M	200	0.00112	100	300	0.00167	458	0.767	0.256
258	10M	100	0.00056	10M	200	0.00112	100	300	0.00167	458	0.767	0.256
259	10M	100	0.00056	10M	200	0.00112	100	300	0.00167	458	0.767	0.256
260	(2)10M	200	0.00181	10M	200	0.00181	100	400	0.00363	458	1.662	0.831
261	(2)10M	200	0.00181	10M	200	0.00181	100	400	0.00363	458	1.662	0.831
262	(2)10M	200	0.00181	10M	200	0.00181	100	400	0.00363	458	1.662	0.831
263	(2)10M	200	0.00181	10M	200	0.00181	100	400	0.00363	458	1.662	0.831
264	(2)10M	200	0.00181	10M	200	0.00181	100	400	0.00363	458	1.662	0.831

Wall #	VERTICAL REINFORCEMENT											
	Vertical (Interior) Reinf	A _c [mm ²]	ρ _c [unitless]	Flexural Reinf	A _t [mm ²]	ρ _t [unitless]	A _{v, bar} [mm ²]	A _{v, total} [mm ²]	ρ _v [unitless]	f _{yv} [MPa]	ρ _v f _{yv} [MPa]	ρ _c f _{yv} [MPa]
265	(2)10M	200	0.00181	10M	200	0.00181	100	400	0.00363	458	1.662	0.831
266	-	0	0.00000	10M	200	0.00181	100	200	0.00181	458	0.831	0.000
267	-	0	0.00000	10M	200	0.00181	100	200	0.00181	458	0.831	0.000
268	-	0	0.00000	10M	200	0.00181	100	200	0.00181	458	0.831	0.000
269	-	0	0.00000	15M	400	0.00147	200	400	0.00147	448	0.659	0.000
270	-	0	0.00000	15M	400	0.00147	200	400	0.00147	448	0.659	0.000
271	-	0	0.00000	15M	400	0.00147	200	400	0.00147	448	0.659	0.000
272	-	0	0.00000	15M	400	0.00147	200	400	0.00147	448	0.659	0.000
273	-	0	0.00000	15M	400	0.00147	200	400	0.00147	448	0.659	0.000
274	-	0	0.00000	15M	400	0.00147	200	400	0.00147	448	0.659	0.000
275	-	0	0.00000	15M	400	0.00147	200	400	0.00147	448	0.659	0.000
276	-	0	0.00000	15M	400	0.00147	200	400	0.00147	448	0.659	0.000
277	-	0	0.00000	15M	400	0.00147	200	400	0.00147	448	0.659	0.000
278	-	0	0.00000	15M	400	0.00147	200	400	0.00147	448	0.659	0.000
279	-	0	0.00000	15M	400	0.00147	200	400	0.00147	448	0.659	0.000
280	-	0	0.00000	15M	400	0.00147	200	400	0.00147	448	0.659	0.000
281	-	0	0.00000	15M	400	0.00147	200	400	0.00147	448	0.659	0.000
282	-	0	0.00000	15M	400	0.00147	200	400	0.00147	448	0.659	0.000
283	2Ø22mm	760	0.00341	2Ø10mm	157	0.00071	380, 79	917	0.00412	474	1.951	1.616
284	2Ø22mm	760	0.00341	2Ø10mm	157	0.00071	380, 79	917	0.00412	474	1.951	1.616
285	2Ø22mm	760	0.00341	2Ø10mm	157	0.00071	380, 79	917	0.00412	474	1.951	1.616
286	2Ø22mm	760	0.00341	2Ø10mm	157	0.00071	380, 79	917	0.00412	474	1.951	1.616
287	2Ø16mm	420	0.00145	3Ø10mm	218	0.00075	201, 79	638	0.00220	474	1.042	0.686
288	2Ø16mm	420	0.00145	3Ø10mm	218	0.00075	201, 79	638	0.00220	474	1.042	0.686
289	2Ø16mm	420	0.00145	3Ø10mm	218	0.00075	201, 79	638	0.00220	474	1.042	0.686
290	2Ø22mm	760	0.00685	1Ø10mm	79	0.00071	380, 79	839	0.00756	474	3.586	3.249
291	2Ø22mm	760	0.00685	1Ø10mm	79	0.00071	380, 79	839	0.00756	474	3.586	3.249
292	2Ø22mm	760	0.00685	1Ø10mm	79	0.00071	380, 79	839	0.00756	474	3.586	3.249

Wall #	HORIZONTAL (SHEAR) REINFORCEMENT										
	Bond Beam Reinf	A _h (Bond Beam) [mm ²]	A _{h,modified} (Bond Beam) [mm ²]	Joint Reinf	A _h (Joint) [mm ²]	A _{h, total} [mm ²]	A _{h, total, modified} [mm ²]	ρ _h [unitless]	ρ _{h,modified} [unitless]	f _{yh} [MPa]	ρ _h f _{yh} [MPa]
1	-	0	0	-	0	0	0	0.00000	0.00000	0	0.000
2	-	0	0	-	0	0	0	0.00000	0.00000	0	0.000
3	(2)5/8"+(2)1/2"	649	649	-	0	649	649	0.00172	0.00172	292	0.502
4	(2)1/2"	253	253	-	0	253	253	0.00067	0.00067	302	0.436
5	(1)1/2"	127	127	-	0	127	127	0.00034	0.00034	302	0.101
6	-	0	0	-	0	0	0	0.00000	0.00000	0	0.000
7	-	0	0	-	0	0	0	0.00000	0.00000	0	0.000
8	-	0	0	-	0	0	0	0.00000	0.00000	0	0.000
9	(2)1/2"	253	253	-	0	253	253	0.00067	0.00067	302	0.203
10	(4)1/2"	507	507	-	0	507	507	0.00134	0.00134	302	0.405
11	(3)5/8"	594	594	-	0	594	594	0.00157	0.00157	290	0.456
12	(4)5/8"	792	792	-	0	792	792	0.00210	0.00210	290	0.608
13	-	0	0	Ø2.5mm	10	10	10	0.00002	0.00002	245	0.006
14	-	0	0	Ø2.5mm	10	10	10	0.00002	0.00002	245	0.006
15	-	0	0	Ø2.5mm	10	10	10	0.00002	0.00002	245	0.006
16	-	0	0	Ø2.5mm	10	10	10	0.00002	0.00002	245	0.006
17	-	0	0	Ø2.5mm	10	10	10	0.00002	0.00002	245	0.006
18	-	0	0	-	0	0	0	0.00000	0.00000	245	0.000
19	-	0	0	-	0	0	0	0.00000	0.00000	245	0.000
20	-	0	0	Ø2.5mm	10	10	10	0.00002	0.00002	245	0.006
21	-	0	0	Ø2.5mm	10	10	10	0.00002	0.00002	245	0.006
22	-	0	0	Ø2.5mm	10	10	10	0.00002	0.00002	245	0.006
23	-	0	0	-	0	0	0	0.00000	0.00000	0	0.000
24	-	0	0	-	0	0	0	0.00000	0.00000	0	0.000
25	-	0	0	-	0	0	0	0.00000	0.00000	0	0.000
26	-	0	0	-	0	0	0	0.00000	0.00000	0	0.000
27	-	0	0	-	0	0	0	0.00000	0.00000	0	0.000
28	-	0	0	-	0	0	0	0.00000	0.00000	0	0.000
29	-	0	0	-	0	0	0	0.00000	0.00000	0	0.000
30	-	0	0	-	0	0	0	0.00000	0.00000	0	0.000
31	-	0	0	-	0	0	0	0.00000	0.00000	0	0.000
32	-	0	0	-	0	0	0	0.00000	0.00000	0	0.000
33	-	0	0	-	0	0	0	0.00000	0.00000	0	0.000

Wall #	HORIZONTAL (SHEAR) REINFORCEMENT										
	Bond Beam Reinf	A _h (Bond Beam) [mm ²]	A _{h,modified} (Bond Beam) [mm ²]	Joint Reinf	A _h (Joint) [mm ²]	A _{h,total} [mm ²]	A _{h,total,modified} [mm ²]	ρ _h [unitless]	ρ _{h,modified} [unitless]	f _{yh} [MPa]	ρ _h f _{yh} [MPa]
34	-	0	0	-	0	0	0	0.00000	0.00000	0	0.000
35	-	0	0	-	0	0	0	0.00000	0.00000	0	0.000
36	-	0	0	-	0	0	0	0.00000	0.00000	0	0.000
37	#5	200	200	-	0	200	200	0.00073	0.00073	330	0.240
38	-	0	0	-	0	0	0	0.00000	0.00000	0	0.000
39	(2)#5	400	400	-	0	400	400	0.00146	0.00146	330	0.481
40	(2)D12	226	226	-	0	226	226	0.00067	0.00067	353	0.000
41	-	0	0	-	0	0	0	0.00000	0.00000	0	0.000
42	(4)D12	452	452	-	0	452	452	0.00135	0.00135	454	0.000
43	-	192	192	-	0	192	192	0.00071	0.00071	385	0.273
44	-	192	192	-	0	192	192	0.00071	0.00071	385	0.273
45	-	192	192	-	0	192	192	0.00071	0.00071	385	0.273
46	-	192	192	-	0	192	192	0.00071	0.00071	385	0.273
47	-	192	192	-	0	192	192	0.00071	0.00071	385	0.273
48	-	192	192	-	0	192	192	0.00071	0.00071	385	0.273
49	-	0	0	-	0	0	0	0.00000	0.00000	0	0.000
50	-	0	0	-	0	0	0	0.00000	0.00000	0	0.000
51	-	192	192	-	0	192	192	0.00071	0.00071	385	0.273
52	-	400	400	-	0	400	400	0.00148	0.00148	385	0.570
53	-	599	599	-	0	599	599	0.00222	0.00222	385	0.855
54	-	192	192	-	0	192	192	0.00071	0.00071	385	0.273
55	-	192	192	-	0	192	192	0.00071	0.00071	385	0.273
56	-	192	192	-	0	192	192	0.00071	0.00071	385	0.273
57	-	0	0	-	0	0	0	0.00000	0.00000	0	0.000
58	-	400	400	-	0	400	400	0.00148	0.00148	385	0.570
59	-	599	599	-	0	599	599	0.00222	0.00222	385	0.855
60	-	905	905	-	0	905	905	0.00335	0.00335	385	1.290
61	-	192	192	-	0	192	192	0.00071	0.00071	385	0.273
62	-	0	0	-	0	0	0	0.00000	0.00000	0	0.000
63	-	0	0	-	0	0	0	0.00000	0.00000	0	0.000
64	-	400	400	-	0	400	400	0.00148	0.00148	385	0.570
65	-	599	599	-	0	599	599	0.00222	0.00222	385	0.855
66	-	400	400	-	0	400	400	0.00148	0.00148	385	0.570

Wall #	HORIZONTAL (SHEAR) REINFORCEMENT										
	Bond Beam Reinf	A _h (Bond Beam) [mm ²]	A _{h,modified} (Bond Beam) [mm ²]	Joint Reinf	A _h (Joint) [mm ²]	A _{h,total} [mm ²]	A _{h,total,modified} [mm ²]	ρ _h [unitless]	ρ _{h,modified} [unitless]	f _{yh} [MPa]	ρ _h f _{yh} [MPa]
67	-	400	400	-	0	400	400	0.00148	0.00148	385	0.570
68	-	400	400	-	0	400	400	0.00148	0.00148	385	0.570
69	-	400	400	-	0	400	400	0.00148	0.00148	385	0.570
70	-	400	400	-	0	400	400	0.00148	0.00148	385	0.570
71	-	400	400	-	0	400	400	0.00148	0.00148	385	0.570
72	-	0	0	-	0	0	0	0.00000	0.00000	0	0.000
73	-	0	0	2Ø3.1mm	15	15	15	0.00020	0.00020	323	0.064
74	-	0	0	2Ø4.2mm	28	28	28	0.00036	0.00036	391	0.143
75	-	0	0	2Ø6mm	57	57	57	0.00074	0.00074	253	0.188
76	-	0	0	-	0	0	0	0.00000	0.00000	0	0.000
77	-	0	0	-	0	0	0	0.00000	0.00000	0	0.000
78	-	0	0	2Ø3.1mm	15	15	15	0.00020	0.00020	323	0.064
79	-	0	0	2Ø4.2mm	28	28	28	0.00036	0.00036	391	0.143
80	-	0	0	2Ø6mm	57	57	57	0.00074	0.00074	253	0.188
81	-	0	0	-	0	0	0	0.00000	0.00000	0	0.000
82	-	0	0	-	0	0	0	0.00000	0.00000	0	0.000
83	-	0	0	-	0	0	0	0.00000	0.00000	0	0.000
84	-	0	0	-	0	0	0	0.00000	0.00000	0	0.000
85	-	0	0	-	0	0	0	0.00000	0.00000	0	0.000
86	-	0	0	-	0	0	0	0.00000	0.00000	0	0.000
87	-	0	0	-	0	0	0	0.00000	0.00000	0	0.000
88	-	0	0	-	0	0	0	0.00000	0.00000	0	0.000
89	-	0	0	-	0	0	0	0.00000	0.00000	0	0.000
90	-	0	0	-	0	0	0	0.00000	0.00000	0	0.000
91	-	0	0	-	0	0	0	0.00000	0.00000	0	0.000
92	-	0	0	-	0	0	0	0.00000	0.00000	0	0.000
93	-	0	0	-	0	0	0	0.00000	0.00000	0	0.000
94	-	0	0	-	0	0	0	0.00000	0.00000	0	0.000
95	-	0	0	-	0	0	0	0.00000	0.00000	0	0.000
96	-	0	0	-	0	0	0	0.00000	0.00000	0	0.000
97	-	0	0	-	0	0	0	0.00000	0.00000	0	0.000
98	-	0	0	-	0	0	0	0.00000	0.00000	0	0.000
99	-	0	0	9-ga Ladder	40	40	40	0.00024	0.00024	693	0.168

Wall #	HORIZONTAL (SHEAR) REINFORCEMENT										
	Bond Beam Reinf	A _h (Bond Beam) [mm ²]	A _{h,modified} (Bond Beam) [mm ²]	Joint Reinf	A _h (Joint) [mm ²]	A _{h,total} [mm ²]	A _{h,total,modified} [mm ²]	ρ _h [unitless]	ρ _{h,modified} [unitless]	f _{yh} [MPa]	ρ _h f _{yh} [MPa]
100	-	0	0	9-ga Ladder	40	40	40	0.00057	0.00057	693	0.392
101	(2)#4	258	258	-	0	258	258	0.00094	0.00094	336	0.315
102	(3)#5	600	600	-	0	600	600	0.00218	0.00218	437	0.953
103	(1)#5	200	200	-	0	200	200	0.00145	0.00145	385	0.558
104	(3)#5	600	600	-	0	600	600	0.00218	0.00218	374	0.814
105	(1)#3	71	71	9-ga Ladder	40	111	111	0.00076	0.00076	373	0.282
106	(2)#4, (1)#5	458	458	9-ga Ladder	40	498	498	0.00215	0.00215	341	0.734
107	(1)#5	200	200	-	0	200	200	0.00145	0.00145	373	0.540
108	(2)2#4/3	53	40	-	0	53	40	0.00121	0.00091	443	0.535
109	(3)#5/3	53	40	-	0	53	40	0.00121	0.00091	447	0.540
110	(3)#5/3	53	40	-	0	53	40	0.00118	0.00089	447	0.529
111	(3)#5/3	53	40	-	0	53	40	0.00118	0.00089	447	0.529
112	-	0	0	6mm Ladder	57	57	57	0.00074	0.00074	253	0.188
113	-	0	0	6mm Ladder	57	57	57	0.00074	0.00074	253	0.188
114	-	0	0	6mm Ladder	57	57	57	0.00074	0.00074	253	0.188
115	-	0	0	6mm Ladder	57	57	57	0.00074	0.00074	253	0.188
116	-	0	0	6mm Ladder	57	57	57	0.00074	0.00074	253	0.188
117	-	0	0	6mm Ladder	57	57	57	0.00074	0.00074	253	0.188
118	2#3	142	142	-	0	142	142	0.00051	0.00051	400	0.205
119	2#3	142	142	-	0	142	142	0.00051	0.00051	400	0.205
120	2#3	142	142	-	0	142	142	0.00051	0.00051	400	0.205
121	1#4, 1#5	329	329	-	0	329	329	0.00119	0.00119	400	0.475
122	1#4, 1#5	329	329	-	0	329	329	0.00119	0.00119	400	0.475
123	1#4, 1#5	329	329	-	0	329	329	0.00119	0.00119	400	0.475
124	-	0	0	9-ga Ladder	155	155	155	0.00056	0.00056	400	0.224
125	-	0	0	9-ga Ladder	155	155	155	0.00056	0.00056	400	0.224
126	-	0	0	9-ga Ladder	155	155	155	0.00056	0.00056	400	0.224
127	-	0	0	5-ga Ladder	305	305	305	0.00110	0.00110	400	0.440
128	-	0	0	5-ga Ladder	305	305	305	0.00110	0.00110	400	0.440
129	-	0	0	5-ga Ladder	305	305	305	0.00110	0.00110	400	0.440
130	-	0	0	-	0	0	0	0.00000	0.00000	0	0.000
131	-	0	0	-	0	0	0	0.00000	0.00000	0	0.000
132	-	0	0	Ø4mm truss	25	25	25	0.00031	0.00031	580	0.180

Wall #	HORIZONTAL (SHEAR) REINFORCEMENT										
	Bond Beam Reinf	A _h (Bond Beam) [mm ²]	A _{h,modified} (Bond Beam) [mm ²]	Joint Reinf	A _h (Joint) [mm ²]	A _{h,total} [mm ²]	A _{h,total,modified} [mm ²]	ρ _h [unitless]	ρ _{h,modified} [unitless]	f _{yh} [MPa]	ρ _h f _{yh} [MPa]
133	-	0	0	Ø4mm truss	25	25	25	0.00031	0.00031	580	0.180
134	-	0	0	Ø4mm truss	25	25	25	0.00031	0.00031	580	0.180
135	-	0	0	Ø4mm truss	25	25	25	0.00031	0.00031	580	0.180
136	(3)D4	77	52	-	0	77	52	0.00048	0.00032	744	0.355
137	(4)D3	78	58	-	0	78	58	0.00048	0.00036	691	0.331
138	(2)2D3	78	39	-	0	78	39	0.00048	0.00024	691	0.331
139	(2)D3	39	19	-	0	39	19	0.00048	0.00024	691	0.331
140	(4)D4	103	77	-	0	103	77	0.00043	0.00032	744	0.316
141	#5	400	400	-	0	400	400	0.00136	0.00136	452	0.614
142	#6	568	568	-	0	568	568	0.00193	0.00193	427	0.823
143	2#5	800	800	-	0	800	800	0.00272	0.00272	452	1.228
144	#5	400	400	-	0	400	400	0.00136	0.00136	452	0.614
145	#5	400	400	-	0	400	400	0.00136	0.00136	452	0.614
146	#5	400	400	-	0	400	400	0.00136	0.00136	452	0.614
147	(3)#6	852	568	-	0	852	568	0.00161	0.00108	321	0.518
148	(3)#6	852	568	-	0	852	568	0.00161	0.00108	321	0.518
149	(3)#6	852	568	-	0	852	568	0.00161	0.00108	321	0.518
150	(3)#6	852	568	-	0	852	568	0.00161	0.00108	321	0.518
151	(2)#4	258	258	-	0	258	258	0.00110	0.00110	445	0.490
152	-	0	0	(2)3/16"	470	470	470	0.00090	0.00090	606	0.546
153	-	0	0	(4)3/16"	941	941	941	0.00180	0.00180	606	1.092
154	(2)#4	258	258	-	0	258	258	0.00110	0.00110	445	0.490
155	-	0	0	(2)3/16"	470	470	470	0.00090	0.00090	606	0.546
156	(2)#4	258	258	-	0	258	258	0.00110	0.00110	445	0.490
157	-	0	0	(2)3/16"	470	470	470	0.00090	0.00090	606	0.546
158	-	0	0	(4)3/16"	941	941	941	0.00180	0.00180	606	1.092
159	#5	200	200	-	0	200	200	0.00085	0.00085	438	0.372
160	#6	284	284	-	0	284	284	0.00120	0.00120	438	0.526
161	2#5	400	400	-	0	400	400	0.00169	0.00169	438	0.740
162	#5	200	200	-	0	200	200	0.00085	0.00085	438	0.372
163	#5	200	200	-	0	200	200	0.00085	0.00085	438	0.372
164	-	0	0	-	0	0	0	0.00000	0.00000	0	0.000
165	-	0	0	-	0	0	0	0.00000	0.00000	0	0.000

Wall #	HORIZONTAL (SHEAR) REINFORCEMENT										
	Bond Beam Reinf	A _h (Bond Beam) [mm ²]	A _{h,modified} (Bond Beam) [mm ²]	Joint Reinf	A _h (Joint) [mm ²]	A _{h,total} [mm ²]	A _{h,total,modified} [mm ²]	ρ _h [unitless]	ρ _{h,modified} [unitless]	f _{yh} [MPa]	ρ _h f _{yh} [MPa]
166	-	0	0	-	0	0	0	0.00000	0.00000	0	0.000
167	-	0	0	Ø3.7mm	129	129	129	0.00057	0.00057	530	0.300
168	-	0	0	Ø3.7mm	129	129	129	0.00057	0.00057	530	0.300
169	-	0	0	Ø3.7mm	129	129	129	0.00057	0.00057	530	0.300
170	-	0	0	Ø4.9mm	226	226	226	0.00099	0.00099	560	0.556
171	-	0	0	Ø4.9mm	226	226	226	0.00099	0.00099	560	0.556
172	-	0	0	Ø4.9mm	226	226	226	0.00099	0.00099	560	0.556
173	-	0	0	-	0	0	0	0.00000	0.00000	0	0.000
174	-	0	0	-	0	0	0	0.00000	0.00000	0	0.000
175	-	0	0	-	0	0	0	0.00000	0.00000	0	0.000
176	-	0	0	Ø4.9mm	226	226	226	0.00099	0.00099	560	0.556
177	-	0	0	Ø4.9mm	226	226	226	0.00099	0.00099	560	0.556
178	-	0	0	Ø4.9mm	226	226	226	0.00099	0.00099	560	0.556
179	-	0	0	-	0	0	0	0.00000	0.00000	0	0.000
180	-	0	0	-	0	0	0	0.00000	0.00000	0	0.000
181	-	0	0	-	0	0	0	0.00000	0.00000	0	0.000
182	-	0	0	-	0	0	0	0.00000	0.00000	0	0.000
183	-	0	0	-	0	0	0	0.00000	0.00000	0	0.000
184	-	0	0	-	0	0	0	0.00000	0.00000	0	0.000
185	-	0	0	Ø3.7mm	129	129	129	0.00057	0.00057	530	0.300
186	-	0	0	Ø3.7mm	129	129	129	0.00057	0.00057	530	0.300
187	-	0	0	Ø3.7mm	129	129	129	0.00057	0.00057	530	0.300
188	-	0	0	Ø4.9mm	226	226	226	0.00099	0.00099	560	0.556
189	-	0	0	Ø4.9mm	226	226	226	0.00099	0.00099	560	0.556
190	-	0	0	Ø4.9mm	226	226	226	0.00099	0.00099	560	0.556
191	-	0	0	-	0	0	0	0.00000	0.00000	0	0.000
192	-	0	0	-	0	0	0	0.00000	0.00000	0	0.000
193	-	0	0	-	0	0	0	0.00000	0.00000	0	0.000
194	-	0	0	Ø4.9mm	226	226	226	0.00099	0.00099	560	0.556
195	-	0	0	Ø4.9mm	226	226	226	0.00099	0.00099	560	0.556
196	-	0	0	Ø4.9mm	226	226	226	0.00099	0.00099	560	0.556
197	-	0	0	-	0	0	0	0.00000	0.00000	0	0.000
198	-	0	0	-	0	0	0	0.00000	0.00000	0	0.000

Wall #	HORIZONTAL (SHEAR) REINFORCEMENT										
	Bond Beam Reinf	A _h (Bond Beam) [mm ²]	A _{h,modified} (Bond Beam) [mm ²]	Joint Reinf	A _h (Joint) [mm ²]	A _{h, total} [mm ²]	A _{h, total, modified} [mm ²]	ρ _h [unitless]	ρ _{h,modified} [unitless]	f _{yh} [MPa]	ρ _h f _{yh} [MPa]
199	-	0	0	-	0	0	0	0.00000	0.00000	0	0.000
200	-	0	0	-	0	0	0	0.00000	0.00000	0	0.000
201	-	0	0	-	0	0	0	0.00000	0.00000	0	0.000
202	-	0	0	-	0	0	0	0.00000	0.00000	0	0.000
203	-	0	0	Ø3.7mm	129	129	129	0.00057	0.00057	530	0.300
204	-	0	0	Ø3.7mm	129	129	129	0.00057	0.00057	530	0.300
205	-	0	0	Ø3.7mm	129	129	129	0.00057	0.00057	530	0.300
206	-	0	0	Ø4.9mm	226	226	226	0.00099	0.00099	560	0.556
207	-	0	0	Ø4.9mm	226	226	226	0.00099	0.00099	560	0.556
208	-	0	0	Ø4.9mm	226	226	226	0.00099	0.00099	560	0.556
209	-	0	0	-	0	0	0	0.00000	0.00000	0	0.000
210	-	0	0	-	0	0	0	0.00000	0.00000	0	0.000
211	-	0	0	-	0	0	0	0.00000	0.00000	0	0.000
212	-	0	0	Ø4.9mm	226	226	226	0.00099	0.00099	560	0.556
213	-	0	0	Ø4.9mm	226	226	226	0.00099	0.00099	560	0.556
214	-	0	0	Ø4.9mm	226	226	226	0.00099	0.00099	560	0.556
215	-	0	0	-	0	0	0	0.00000	0.00000	0	0.000
216	-	0	0	-	0	0	0	0.00000	0.00000	0	0.000
217	-	0	0	-	0	0	0	0.00000	0.00000	0	0.000
218	-	0	0	Ø3.7mm	129	129	129	0.00057	0.00057	530	0.300
219	-	0	0	Ø3.7mm	129	129	129	0.00057	0.00057	530	0.300
220	-	0	0	Ø3.7mm	129	129	129	0.00057	0.00057	530	0.300
221	-	0	0	Ø3.7mm	129	129	129	0.00057	0.00057	530	0.300
222	-	0	0	Ø3.7mm	129	129	129	0.00057	0.00057	530	0.300
223	-	0	0	Ø3.7mm	129	129	129	0.00057	0.00057	530	0.300
224	-	0	0	Ø3.7mm	129	129	129	0.00057	0.00057	530	0.300
225	-	0	0	Ø3.7mm	129	129	129	0.00057	0.00057	530	0.300
226	-	0	0	Ø3.7mm	129	129	129	0.00057	0.00057	530	0.300
227	-	0	0	Ø3.7mm	129	129	129	0.00057	0.00057	530	0.300
228	-	0	0	Ø3.7mm	129	129	129	0.00057	0.00057	530	0.300
229	-	0	0	Ø3.7mm	129	129	129	0.00057	0.00057	530	0.300
230	15M	600	1800	-	0	600	1800	0.00132	0.00132	450	0.592
231	15M	600	1800	-	0	600	1800	0.00132	0.00132	450	0.592

Wall #	HORIZONTAL (SHEAR) REINFORCEMENT										
	Bond Beam Reinf	A _h (Bond Beam) [mm ²]	A _{h,modified} (Bond Beam) [mm ²]	Joint Reinf	A _h (Joint) [mm ²]	A _{h,total} [mm ²]	A _{h,total,modified} [mm ²]	ρ _h [unitless]	ρ _{h,modified} [unitless]	f _{yh} [MPa]	ρ _h f _{yh} [MPa]
232	15M	600	1800	-	0	600	1800	0.00132	0.00132	450	0.592
233	15M	600	1800	-	0	600	1800	0.00132	0.00132	450	0.592
234	15M	600	1800	-	0	600	1800	0.00132	0.00132	450	0.592
235	15M	600	1800	-	0	600	1800	0.00132	0.00132	450	0.592
236	15M	600	1800	-	0	600	1800	0.00132	0.00132	450	0.592
237	15M	600	1800	-	0	600	1800	0.00175	0.00175	450	0.789
238	15M	600	1800	-	0	600	1800	0.00175	0.00175	450	0.789
239	15M	600	1800	-	0	600	1800	0.00132	0.00132	450	0.592
240	-	0	0	Ø3.665mm	86	86	86	0.00028	0.00028	521	0.147
241	-	0	0	Ø3.665mm	86	86	86	0.00028	0.00028	521	0.147
242	-	0	0	Ø3.665mm	86	86	86	0.00028	0.00028	521	0.147
243	-	0	0	Ø3.665mm	86	86	86	0.00028	0.00028	521	0.147
244	-	0	0	Ø3.665mm	86	86	86	0.00028	0.00028	521	0.147
245	-	0	0	Ø3.665mm	86	86	86	0.00028	0.00028	521	0.147
246	-	0	0	Ø3.665mm	86	86	86	0.00028	0.00028	521	0.147
247	-	0	0	Ø3.665mm	86	86	86	0.00028	0.00028	521	0.147
248	10M	100	100	-	0	100	100	0.00089	0.00089	458	0.409
249	10M	100	100	-	0	100	100	0.00089	0.00089	458	0.409
250	10M	100	100	-	0	100	100	0.00089	0.00089	458	0.409
251	10M	100	100	-	0	100	100	0.00089	0.00089	458	0.409
252	10M	100	100	-	0	100	100	0.00089	0.00089	458	0.409
253	10M	100	100	-	0	100	100	0.00089	0.00089	458	0.409
254	10M	100	100	-	0	100	100	0.00089	0.00089	458	0.409
255	10M	100	100	-	0	100	100	0.00089	0.00089	458	0.409
256	10M	100	100	-	0	100	100	0.00089	0.00089	458	0.409
257	10M	100	100	-	0	100	100	0.00089	0.00089	458	0.409
258	10M	100	100	-	0	100	100	0.00089	0.00089	458	0.409
259	10M	100	100	-	0	100	100	0.00089	0.00089	458	0.409
260	10M	100	100	-	0	100	100	0.00145	0.00145	458	0.665
261	10M	100	100	-	0	100	100	0.00145	0.00145	458	0.665
262	10M	100	100	-	0	100	100	0.00145	0.00145	458	0.665
263	10M	100	100	-	0	100	100	0.00145	0.00145	458	0.665
264	10M	100	100	-	0	100	100	0.00145	0.00145	458	0.665

Wall #	HORIZONTAL (SHEAR) REINFORCEMENT										
	Bond Beam Reinf	A _h (Bond Beam) [mm ²]	A _{h,modified} (Bond Beam) [mm ²]	Joint Reinf	A _h (Joint) [mm ²]	A _{h,total} [mm ²]	A _{h,total,modified} [mm ²]	ρ _h [unitless]	ρ _{h,modified} [unitless]	f _{yh} [MPa]	ρ _h f _{yh} [MPa]
265	10M	100	100	-	0	100	100	0.00145	0.00145	458	0.665
266	10M	100	100	-	0	100	100	0.00145	0.00145	458	0.665
267	10M	100	100	-	0	100	100	0.00145	0.00145	458	0.665
268	10M	100	100	-	0	100	100	0.00145	0.00145	458	0.665
269	15M	400	800	-	0	400	800	0.00067	0.00033	448	0.302
270	15M	400	800	-	0	400	800	0.00067	0.00033	448	0.302
271	15M	400	800	-	0	400	800	0.00067	0.00033	448	0.302
272	15M	400	800	-	0	400	800	0.00067	0.00033	448	0.302
273	10M	200	400	-	0	200	400	0.00034	0.00016	456	0.154
274	10M	200	400	-	0	200	400	0.00034	0.00016	456	0.154
275	10M	200	400	-	0	200	400	0.00034	0.00016	456	0.154
276	10M	200	400	-	0	200	400	0.00034	0.00016	456	0.154
277	10M	200	400	-	0	200	400	0.00034	0.00016	456	0.154
278	10M	200	400	-	0	200	400	0.00034	0.00016	456	0.154
279	10M	200	400	-	0	200	400	0.00045	0.00016	456	0.205
280	10M	200	400	-	0	200	400	0.00045	0.00016	456	0.205
281	10M	100	100	-	0	100	100	0.00034	0.00008	456	0.154
282	10M	100	100	-	0	100	100	0.00034	0.00008	456	0.154
283	-	0	0	4-2Ø4.2mm	111	111	111	0.00041	0.00041	610	0.250
284	-	0	0	4-2Ø4.2mm	111	111	111	0.00041	0.00041	610	0.250
285	-	0	0	9-2Ø4.2mm	249	249	249	0.00092	0.00092	610	0.563
286	-	0	0	9-2Ø4.2mm	249	249	249	0.00092	0.00092	610	0.563
287	-	0	0	3-2Ø4.2mm	83	83	83	0.00053	0.00053	610	0.321
288	-	0	0	6-2Ø4.2mm	166	166	166	0.00105	0.00105	610	0.641
289	-	0	0	3-2Ø4.2mm	83	83	83	0.00053	0.00053	610	0.321
290	-	0	0	4-2Ø4.2mm	111	111	111	0.00041	0.00041	610	0.250
291	-	0	0	9-2Ø4.2mm	249	249	249	0.00092	0.00092	610	0.563
292	-	0	0	4-2Ø4.2mm	111	111	111	0.00041	0.00041	610	0.250

Wall #	AXIAL STRESS				EXPERIMENTAL SHEAR CAPACITY								
	P [kN]	σ_{gross} [MPa]	σ_{gross}/f_m [MPa]	σ_{net} [MPa]	V_{min} [kN]	V_{max} [kN]	V_{avg} [kN]	k_{avg}	k_{mono}	k_{rate}	V_{cor} [kN]	$V_{max,gross}$ [MPa]	$V_{max,net}$ [MPa]
1	209	0.60	0.059	1.69	-	193.1	193.1	0.944	0.814	1	148.4	0.43	1.20
2	508	1.46	0.116	3.18	-	468.8	468.8	0.944	0.814	1	360.4	1.03	2.26
3	359	1.03	0.101	2.89	-	330.9	330.9	0.944	0.814	1	254.4	0.73	2.05
4	448	1.29	0.123	2.80	-	413.7	413.7	0.944	0.814	1	318.0	0.91	1.99
5	418	1.20	0.117	2.35	-	386.1	386.1	0.944	0.814	1	296.8	0.85	1.67
6	448	1.29	0.123	2.29	-	413.7	413.7	0.944	0.814	1	318.0	0.91	1.62
7	486	1.39	0.112	3.04	-	448.2	448.2	0.944	0.814	1	344.5	0.99	2.16
8	523	1.50	0.144	2.45	-	482.6	482.6	0.944	0.814	1	371.0	1.06	1.74
9	777	2.23	0.180	3.64	-	717.1	717.1	0.944	0.814	1	551.2	1.58	2.58
10	837	2.40	0.191	3.92	-	772.2	772.2	0.944	0.814	1	593.6	1.70	2.78
11	717	2.06	0.166	3.36	-	661.9	661.9	0.944	0.814	1	508.8	1.46	2.38
12	837	2.40	0.191	3.92	-	772.2	772.2	0.944	0.814	1	593.6	1.70	2.78
13	0	0.00	n/a	0.00	-	200.1	200.1	0.944	1	1	189.0	0.39	0.58
14	196	0.41	n/a	0.60	-	255.1	255.1	0.944	1	1	240.9	0.50	0.74
15	98	0.20	n/a	0.30	-	335.5	335.5	0.944	1	1	316.8	0.66	0.97
16	0	0.00	n/a	0.00	-	107.9	107.9	0.944	1	1	101.9	0.21	0.29
17	0	0.00	n/a	0.00	-	124.6	124.6	0.944	1	1	117.6	0.25	0.34
18	98	0.20	n/a	0.30	-	264.9	264.9	0.944	1	1	250.1	0.52	0.76
19	0	0.00	n/a	0.00	-	97.1	97.1	0.944	1	1	91.7	0.19	0.26
20	196	0.41	n/a	0.60	-	277.6	277.6	0.944	1	1	262.2	0.55	0.80
21	0	0.00	n/a	0.00	-	255.1	255.1	0.944	1	1	240.9	0.50	0.74
22	0	0.00	n/a	0.00	-	215.8	215.8	0.944	1	1	203.8	0.42	0.62
23	0	0.00	n/a	0.00	-	161.8	161.8	0.944	0.814	1	124.4	0.41	0.89
24	49	0.16	n/a	0.35	-	151.2	151.2	0.944	0.814	1	116.2	0.39	0.83
25	98	0.33	n/a	0.70	-	242.0	242.0	0.944	0.814	1	186.0	0.62	1.33
26	196	0.65	n/a	1.40	-	290.8	290.8	0.944	0.814	1	223.5	0.75	1.59
27	0	0.00	n/a	0.00	-	136.4	136.4	0.944	0.814	1	104.8	0.35	0.75
28	0	0.00	n/a	0.00	-	200.4	200.4	0.944	0.814	1	154.0	0.51	0.86
29	0	0.00	n/a	0.00	-	130.1	130.1	0.944	0.814	1	100.0	0.33	0.71
30	294	0.98	n/a	1.64	-	314.3	314.3	0.944	0.814	1	241.6	0.81	1.35
31	294	0.98	n/a	2.10	-	343.4	343.4	0.944	0.814	1	264.0	0.88	1.88
32	294	0.98	n/a	2.10	-	322.9	322.9	0.944	0.814	1	248.2	0.83	1.77
33	0	0.00	n/a	0.00	-	187.5	187.5	0.944	0.814	1	144.1	0.48	1.03

Wall #	AXIAL STRESS				EXPERIMENTAL SHEAR CAPACITY								
	P [kN]	σ_{gross} [MPa]	σ_{gross}/f'_m [MPa]	σ_{net} [MPa]	V_{min} [kN]	V_{max} [kN]	V_{avg} [kN]	k_{avg}	k_{mono}	k_{rate}	V_{cor} [kN]	$V_{max,gross}$ [MPa]	$V_{max,net}$ [MPa]
34	200	1.72	0.103	2.41	-	-	78.5	0.944	1	1	74.1	0.68	0.87
35	200	1.72	0.103	2.41	-	-	85.7	0.944	1	1	80.9	0.74	0.94
36	188	0.80	0.073	1.32	107.2	117.0	112.1	1	1	0.9	100.9	0.43	0.79
37	134	0.57	0.052	0.95	195.7	220.6	208.2	1	1	0.9	187.4	0.80	1.47
38	130	0.55	0.050	0.92	158.8	168.6	163.7	1	1	0.9	147.3	0.63	1.15
39	139	0.59	0.056	0.98	210.0	223.3	216.6	1	1	0.9	195.0	0.83	1.53
40	0	0.00	0.000	0.00	74.6	77.5	76.1	1	1	1	76.1	0.34	0.48
41	0	0.00	0.000	0.00	94.0	106.0	100.0	1	1	1	100.0	0.45	0.63
42	0	0.00	0.000	0.00	146.0	152.0	149.0	1	1	1	149.0	0.67	0.94
43	0	0.00	0.000	0.00	108.4	118.7	113.5	1	1	1	113.5	0.44	0.63
44	0	0.00	0.000	0.00	157.4	157.4	157.4	1	1	1	157.4	0.61	0.87
45	0	0.00	0.000	0.00	87.1	93.1	90.1	1	1	1	90.1	0.46	0.65
46	0	0.00	0.000	0.00	142.6	93.1	117.8	1	1	1	117.8	0.60	0.85
47	0	0.00	0.000	0.00	84.2	73.1	78.7	1	1	1	78.7	0.57	0.80
48	0	0.00	0.000	0.00	73.1	73.1	73.1	1	1	1	73.1	0.53	0.74
49	0	0.00	0.000	0.00	59.4	57.4	58.4	1	1	1	58.4	0.30	0.42
50	0	0.00	0.000	0.00	79.2	65.3	72.3	1	1	1	72.3	0.37	0.52
51	0	0.00	0.000	0.00	101.0	63.4	82.2	1	1	1	82.2	0.42	0.59
52	0	0.00	0.000	0.00	104.9	73.3	89.1	1	1	1	89.1	0.45	0.64
53	0	0.00	0.000	0.00	132.7	89.1	110.9	1	1	1	110.9	0.56	0.80
54	97	0.49	0.022	0.69	172.3	101.0	136.6	1	1	1	136.6	0.69	0.98
55	194	0.98	0.044	1.39	148.5	136.6	142.6	1	1	1	142.6	0.72	1.02
56	291	1.47	0.066	2.08	192.1	166.3	179.2	1	1	1	179.2	0.91	1.28
57	97	0.49	0.042	0.68	108.9	84.3	96.6	1	1	1	96.6	0.47	0.66
58	101	0.49	0.042	0.68	154.1	150.0	152.1	1	1	1	152.1	0.74	1.04
59	101	0.49	0.042	0.68	160.3	185.0	172.6	1	1	1	172.6	0.84	1.18
60	101	0.49	0.042	0.68	248.7	141.8	195.2	1	1	1	195.2	0.95	1.33
61	101	0.49	0.042	0.68	148.0	129.5	138.7	1	1	1	138.7	0.68	0.94
62	201	0.98	0.044	1.39	180.2	136.6	158.4	1	1	1	158.4	0.80	1.14
63	194	0.98	0.085	1.39	95.0	79.2	87.1	1	1	1	87.1	0.44	0.63
64	194	0.98	0.044	1.39	196.0	138.6	167.3	1	1	1	167.3	0.85	1.20
65	194	0.98	0.044	1.39	215.8	152.5	184.1	1	1	1	184.1	0.93	1.32
66	97	0.49	0.037	0.69	292.5	230.5	261.5	1	1	1	261.5	0.89	1.10

Wall #	AXIAL STRESS				EXPERIMENTAL SHEAR CAPACITY								
	P [kN]	σ_{gross} [MPa]	σ_{gross}/f_m [MPa]	σ_{net} [MPa]	V_{min} [kN]	V_{max} [kN]	V_{avg} [kN]	k_{avg}	k_{mono}	k_{rate}	V_{cor} [kN]	$V_{max,gross}$ [MPa]	$V_{max,net}$ [MPa]
67	145	0.49	0.039	0.69	239.4	224.6	232.0	1	1	1	232.0	0.79	1.06
68	145	0.49	0.038	0.68	212.4	180.5	196.5	1	1	1	196.5	0.74	0.95
69	130	0.49	0.043	0.67	123.3	98.6	111.0	1	1	1	111.0	0.54	0.99
70	101	0.49	0.039	0.67	87.3	69.8	78.6	1	1	1	78.6	0.54	0.74
71	71	0.49	0.039	0.67	90.2	68.4	79.3	1	1	1	79.3	0.55	0.75
72	60	0.98	0.117	1.65	-	32.9	32.9	0.944	1	1	31.1	0.51	0.85
73	60	0.98	0.117	1.65	-	40.7	40.7	0.944	1	1	38.4	0.63	1.06
74	60	0.98	0.117	1.65	-	35.3	35.3	0.944	1	1	33.4	0.55	0.92
75	60	0.98	0.117	1.65	-	40.3	40.3	0.944	1	1	38.0	0.62	1.04
76	60	0.98	0.117	1.65	-	26.0	26.0	0.944	1	1	24.6	0.40	0.67
77	60	0.98	0.139	1.65	-	30.1	30.1	0.944	1	1	28.4	0.47	0.78
78	60	0.98	0.139	1.65	-	34.9	34.9	0.944	1	1	33.0	0.54	0.91
79	60	0.98	0.139	1.65	-	43.2	43.2	0.944	1	1	40.8	0.67	1.12
80	60	0.98	0.139	1.65	-	46.8	46.8	0.944	1	1	44.2	0.73	1.22
81	60	0.98	0.139	1.65	-	29.1	29.1	0.944	1	1	27.4	0.45	0.75
82	0	0.00	0.000	0.00	-	96.1	96.1	0.944	1	1	90.8	0.56	0.93
83	0	0.00	0.000	0.00	-	108.5	108.5	0.944	1	1	102.5	0.63	1.05
84	0	0.00	0.000	0.00	-	116.8	116.8	0.944	1	1	110.3	0.68	1.13
85	0	0.00	0.000	0.00	-	186.1	186.1	0.944	1	1	175.7	1.08	1.80
86	0	0.00	0.000	0.00	-	103.3	103.3	0.944	1	1	97.5	0.60	1.00
87	0	0.00	0.000	0.00	-	106.5	106.5	0.944	1	1	100.5	0.62	1.03
88	0	0.00	0.000	0.00	-	115.8	115.8	0.944	1	1	109.3	0.67	1.12
89	0	0.00	0.000	0.00	-	104.4	104.4	0.944	1	1	98.6	0.61	1.01
90	0	0.00	0.000	0.00	-	113.7	113.7	0.944	1	1	107.4	0.66	1.10
91	0	0.00	0.000	0.00	-	107.5	107.5	0.944	1	1	101.5	0.62	1.04
92	0	0.00	0.000	0.00	-	110.6	110.6	0.944	1	1	104.4	0.64	1.07
93	0	0.00	0.000	0.00	-	108.5	108.5	0.944	1	1	102.5	0.63	1.05
94	0	0.00	0.000	0.00	-	108.5	108.5	0.944	1	1	102.5	0.63	1.05
95	0	0.00	0.000	0.00	-	106.5	106.5	0.944	1	1	100.5	0.62	1.03
96	0	0.00	0.000	0.00	-	104.4	104.4	0.944	1	1	98.6	0.61	1.01
97	0	0.00	0.000	0.00	-	101.1	101.1	0.944	1	1	95.5	0.59	0.98
98	175	0.74	n/a	1.38	105.9	122.3	114.1	1	1	1	114.1	0.48	0.90
99	175	0.74	n/a	1.38	128.6	156.1	142.3	1	1	1	142.3	0.60	1.12

Wall #	AXIAL STRESS				EXPERIMENTAL SHEAR CAPACITY								
	P [kN]	σ_{gross} [MPa]	σ_{gross}/f_m [MPa]	σ_{net} [MPa]	V_{min} [kN]	V_{max} [kN]	V_{avg} [kN]	k_{avg}	k_{mono}	k_{rate}	V_{cor} [kN]	$V_{max,gross}$ [MPa]	$V_{max,net}$ [MPa]
100	175	0.74	n/a	1.38	141.9	148.6	145.2	1	1	1	145.2	0.62	1.15
101	175	0.74	n/a	1.38	189.0	201.9	195.5	1	1	1	195.5	0.83	1.54
102	175	0.74	n/a	1.38	145.5	156.1	150.8	1	1	1	150.8	0.64	1.19
103	175	0.74	n/a	1.38	156.6	163.7	160.1	1	1	1	160.1	0.68	1.26
104	175	0.74	n/a	1.38	119.2	119.2	119.2	1	1	1	119.2	0.50	0.94
105	175	0.74	n/a	1.38	161.5	176.6	169.0	1	1	1	169.0	0.72	1.33
106	175	0.74	n/a	1.38	191.7	201.1	196.4	1	1	1	196.4	0.83	1.55
107	175	0.74	n/a	1.38	147.7	171.7	159.7	1	1	1	159.7	0.68	1.26
108	31	0.69	0.043	1.27	-	24.5	24.5	0.944	0.814	1	18.8	0.42	0.77
109	31	0.69	0.043	1.27	-	30.2	30.2	0.944	0.814	1	23.3	0.52	0.95
110	31	0.69	0.043	1.27	-	25.8	25.8	0.944	0.814	1	19.8	0.44	0.81
111	62	1.38	0.085	2.53	-	34.3	34.3	0.944	0.814	1	26.3	0.59	1.08
112	120	1.97	n/a	2.84	-	45.1	45.1	0.944	1	1	42.5	0.70	1.01
113	120	1.97	n/a	2.84	-	50.5	50.5	0.944	1	1	42.9	0.70	1.01
114	120	1.97	n/a	2.84	-	49.2	49.2	0.944	1	1	46.5	0.76	1.10
115	120	1.97	n/a	2.84	-	57.3	57.3	0.944	1	1	48.7	0.80	1.15
116	120	1.97	n/a	2.84	-	53.8	53.8	0.944	1	1	50.8	0.83	1.20
117	120	1.97	n/a	2.84	-	60.2	60.2	0.944	1	1	51.2	0.84	1.21
118	267	0.48	0.035	1.10	-	-	187.0	0.944	1	1	176.6	0.32	0.73
119	191	0.48	0.035	1.02	-	-	245.0	0.944	1	1	231.4	0.58	1.23
120	133	0.48	0.034	0.91	-	-	133.0	0.944	1	1	125.6	0.45	0.86
121	266	0.48	0.034	1.10	-	-	240.0	0.944	1	1	226.6	0.41	0.94
122	177	0.45	0.032	0.94	-	-	192.0	0.944	1	1	181.3	0.46	0.97
123	132	0.48	0.034	0.90	-	-	154.0	0.944	1	1	145.4	0.52	0.99
124	265	0.48	0.040	1.09	-	-	261.3	0.944	1	1	246.7	0.44	1.02
125	185	0.47	0.039	0.99	-	-	253.5	0.944	1	1	239.4	0.60	1.28
126	130	0.47	0.038	0.89	-	-	175.9	0.944	1	1	166.1	0.60	1.13
127	266	0.48	0.040	1.10	-	-	243.4	0.944	1	1	229.8	0.41	0.95
128	188	0.47	0.039	1.00	-	-	270.3	0.944	1	1	255.2	0.64	1.36
129	133	0.48	0.039	0.91	-	-	211.3	0.944	1	1	199.5	0.72	1.36
130	358	1.42	0.077	1.92	-	143.0	143.0	0.944	1	1	135.0	0.54	0.73
131	145	0.58	0.031	0.78	-	93.0	93.0	0.944	1	1	87.8	0.35	0.47
132	60	0.50	0.076	1.05	53.0	53.0	53.0	1	1	1	53.0	0.44	0.93

Wall #	AXIAL STRESS				EXPERIMENTAL SHEAR CAPACITY								
	P [kN]	σ_{gross} [MPa]	σ_{gross}/f'_m [MPa]	σ_{net} [MPa]	V_{min} [kN]	V_{max} [kN]	V_{avg} [kN]	k_{avg}	k_{mono}	k_{rate}	V_{cor} [kN]	$V_{max,gross}$ [MPa]	$V_{max,net}$ [MPa]
133	60	0.50	0.076	0.71	62.0	65.0	63.5	1	1	1	63.5	0.53	0.76
134	150	1.25	0.190	1.79	93.0	93.0	93.0	1	1	1	93.0	0.78	1.11
135	150	1.25	0.190	1.79	93.0	94.0	93.5	1	1	1	93.5	0.78	1.11
136	122	0.75	0.051	1.06	91.2	96.9	94.1	1	1	1	94.1	0.58	0.82
137	122	0.75	0.047	1.00	93.2	103.7	98.5	1	1	1	98.5	0.61	0.81
138	122	0.75	0.054	1.14	84.4	96.7	90.6	1	1	1	90.6	0.56	0.85
139	122	0.75	0.051	1.06	114.2	122.9	118.6	1	1	1	118.6	0.73	1.04
140	122	0.75	0.051	1.06	79.1	84.3	81.7	1	1	1	81.7	0.50	0.71
141	49	0.10	0.005	0.21	-	238.0	238.0	0.944	1	1	224.7	0.44	0.98
142	49	0.10	0.005	0.21	-	252.0	252.0	0.944	1	1	238.0	0.47	1.04
143	49	0.10	0.005	0.21	-	246.0	246.0	0.944	1	1	232.3	0.46	1.01
144	49	0.10	0.005	0.21	-	286.0	286.0	0.944	1	1	270.1	0.53	1.18
145	49	0.10	0.005	0.20	-	344.0	344.0	0.944	1	1	324.8	0.64	1.30
146	49	0.10	0.005	0.18	-	400.0	400.0	0.944	1	1	377.7	0.74	1.39
147	219	0.28	0.038	0.70	-	318.0	318.0	0.944	1	1	300.3	0.39	0.96
148	219	0.28	0.038	0.70	-	190.0	190.0	0.944	1	1	179.4	0.23	0.57
149	0	0.00	0.000	0.00	-	241.0	241.0	0.944	1	1	227.6	0.29	0.73
150	0	0.00	0.000	0.00	-	230.0	230.0	0.944	1	1	217.2	0.28	0.70
151	0	0.00	0.000	0.00	-	-	208.2	1	1	1	208.2	0.38	0.62
152	0	0.00	0.000	0.00	-	-	201.1	1	1	1	201.1	0.37	0.60
153	0	0.00	0.000	0.00	-	-	325.6	1	1	1	325.6	0.59	0.86
154	0	0.00	0.000	0.00	-	-	249.1	1	1	1	249.1	0.45	0.66
155	0	0.00	0.000	0.00	-	-	266.0	1	1	1	266.0	0.48	0.70
156	0	0.00	0.000	0.00	-	-	348.3	1	1	1	348.3	0.42	0.69
157	0	0.00	0.000	0.00	-	-	431.0	1	1	1	431.0	0.52	0.79
158	0	0.00	0.000	0.00	-	-	405.7	1	1	1	405.7	0.49	0.74
159	49	0.10	0.008	0.21	211.0	234.0	222.5	1	1	1	222.5	0.44	0.97
160	49	0.10	0.008	0.21	227.0	230.0	228.5	1	1	1	228.5	0.45	0.99
161	49	0.10	0.008	0.21	193.0	215.0	204.0	1	1	1	204.0	0.40	0.89
162	49	0.10	0.008	0.20	258.0	262.0	260.0	1	1	1	260.0	0.51	1.04
163	49	0.10	0.008	0.18	296.0	302.0	299.0	1	1	1	299.0	0.59	1.10
164	416	1.38	0.110	2.03	-	297.0	297.0	0.944	0.814	1	228.3	0.76	1.11
165	416	1.38	0.110	2.03	-	278.1	278.1	0.944	0.814	1	213.8	0.71	1.04

Wall #	AXIAL STRESS				EXPERIMENTAL SHEAR CAPACITY								
	P [kN]	σ_{gross} [MPa]	σ_{gross}/f'_m [MPa]	σ_{net} [MPa]	V_{min} [kN]	V_{max} [kN]	V_{avg} [kN]	k_{avg}	k_{mono}	k_{rate}	V_{cor} [kN]	$V_{max,gross}$ [MPa]	$V_{max,net}$ [MPa]
166	416	1.38	0.110	2.03	-	275.9	275.9	0.944	0.814	1	212.1	0.70	1.04
167	416	1.38	0.110	2.03	-	270.1	270.1	0.944	0.814	1	207.6	0.69	1.01
168	416	1.38	0.110	2.03	-	261.1	261.1	0.944	0.814	1	200.7	0.66	0.98
169	416	1.38	0.110	2.03	-	272.2	272.2	0.944	0.814	1	209.2	0.69	1.02
170	416	1.38	0.110	2.03	-	257.4	257.4	0.944	0.814	1	197.9	0.65	0.97
171	416	1.38	0.110	2.03	-	265.9	265.9	0.944	0.814	1	204.4	0.68	1.00
172	416	1.38	0.110	2.03	-	259.4	259.4	0.944	0.814	1	199.4	0.66	0.97
173	416	1.38	0.110	2.03	-	275.1	275.1	0.944	0.814	1	211.5	0.70	1.03
174	416	1.38	0.110	2.03	-	281.5	281.5	0.944	0.814	1	216.4	0.72	1.06
175	416	1.38	0.110	2.03	-	278.4	278.4	0.944	0.814	1	214.0	0.71	1.04
176	416	1.38	0.110	2.03	-	278.7	278.7	0.944	0.814	1	214.2	0.71	1.05
177	416	1.38	0.110	2.03	-	287.6	287.6	0.944	0.814	1	221.1	0.73	1.08
178	416	1.38	0.110	2.03	-	278.9	278.9	0.944	0.814	1	214.4	0.71	1.05
179	236	0.78	0.063	1.15	-	149.5	149.5	0.944	0.814	1	114.9	0.38	0.56
180	236	0.78	0.063	1.15	-	146.9	146.9	0.944	0.814	1	112.9	0.37	0.55
181	236	0.78	0.063	1.15	-	157.2	157.2	0.944	0.814	1	120.8	0.40	0.59
182	628	2.08	0.167	3.06	-	384.4	384.4	0.944	0.814	1	295.5	0.98	1.44
183	628	2.08	0.167	3.06	-	346.6	346.6	0.944	0.814	1	266.4	0.88	1.30
184	628	2.08	0.167	3.06	-	419.6	419.6	0.944	0.814	1	322.5	1.07	1.57
185	628	2.08	0.167	3.06	-	347.9	347.9	0.944	0.814	1	267.4	0.89	1.31
186	628	2.08	0.167	3.06	-	337.1	337.1	0.944	0.814	1	259.1	0.86	1.26
187	628	2.08	0.167	3.06	-	390.1	390.1	0.944	0.814	1	299.9	0.99	1.46
188	628	2.08	0.167	3.06	-	384.2	384.2	0.944	0.814	1	295.3	0.98	1.44
189	628	2.08	0.167	3.06	-	362.3	362.3	0.944	0.814	1	278.5	0.92	1.36
190	628	2.08	0.167	3.06	-	325.0	325.0	0.944	0.814	1	249.8	0.83	1.22
191	628	2.08	0.167	3.06	-	338.4	338.4	0.944	0.814	1	260.1	0.86	1.27
192	628	2.08	0.167	3.06	-	356.0	356.0	0.944	0.814	1	273.6	0.91	1.34
193	628	2.08	0.167	3.06	-	373.9	373.9	0.944	0.814	1	287.4	0.95	1.40
194	628	2.08	0.167	3.06	-	360.4	360.4	0.944	0.814	1	277.0	0.92	1.35
195	628	2.08	0.167	3.06	-	349.7	349.7	0.944	0.814	1	268.8	0.89	1.31
196	628	2.08	0.167	3.06	-	377.8	377.8	0.944	0.814	1	290.4	0.96	1.42
197	353	1.17	0.094	1.72	-	186.4	186.4	0.944	0.814	1	143.3	0.47	0.70
198	353	1.17	0.094	1.72	-	199.8	199.8	0.944	0.814	1	153.6	0.51	0.75

Wall #	AXIAL STRESS				EXPERIMENTAL SHEAR CAPACITY								
	P [kN]	σ_{gross} [MPa]	σ_{gross}/f'_m [MPa]	σ_{net} [MPa]	V_{min} [kN]	V_{max} [kN]	V_{avg} [kN]	k_{avg}	k_{mono}	k_{rate}	V_{cor} [kN]	$V_{max,gross}$ [MPa]	$V_{max,net}$ [MPa]
199	353	1.17	0.094	1.72	-	215.5	215.5	0.944	0.814	1	165.6	0.55	0.81
200	839	2.78	0.223	4.09	-	459.5	459.5	0.944	0.814	1	353.2	1.17	1.72
201	839	2.78	0.223	4.09	-	403.5	403.5	0.944	0.814	1	310.2	1.03	1.51
202	839	2.78	0.223	4.09	-	433.6	433.6	0.944	0.814	1	333.3	1.10	1.63
203	839	2.78	0.223	4.09	-	414.6	414.6	0.944	0.814	1	318.7	1.05	1.56
204	839	2.78	0.223	4.09	-	393.8	393.8	0.944	0.814	1	302.7	1.00	1.48
205	839	2.78	0.223	4.09	-	402.0	402.0	0.944	0.814	1	309.0	1.02	1.51
206	839	2.78	0.223	4.09	-	437.0	437.0	0.944	0.814	1	335.9	1.11	1.64
207	839	2.78	0.223	4.09	-	393.3	393.3	0.944	0.814	1	302.3	1.00	1.48
208	839	2.78	0.223	4.09	-	425.7	425.7	0.944	0.814	1	327.2	1.08	1.60
209	839	2.78	0.223	4.09	-	423.6	423.6	0.944	0.814	1	325.6	1.08	1.59
210	839	2.78	0.223	4.09	-	400.9	400.9	0.944	0.814	1	308.2	1.02	1.50
211	839	2.78	0.223	4.09	-	405.9	405.9	0.944	0.814	1	312.0	1.03	1.52
212	839	2.78	0.223	4.09	-	410.3	410.3	0.944	0.814	1	315.4	1.04	1.54
213	839	2.78	0.223	4.09	-	436.8	436.8	0.944	0.814	1	335.8	1.11	1.64
214	839	2.78	0.223	4.09	-	443.4	443.4	0.944	0.814	1	340.8	1.13	1.66
215	471	1.56	0.125	2.30	-	231.1	231.1	0.944	0.814	1	177.6	0.59	0.87
216	471	1.56	0.125	2.30	-	250.8	250.8	0.944	0.814	1	192.8	0.64	0.94
217	471	1.56	0.125	2.30	-	237.2	237.2	0.944	0.814	1	182.3	0.60	0.89
218	315	1.04	0.084	1.54	-	186.4	186.4	0.944	0.814	1	143.3	0.47	0.70
219	315	1.04	0.084	1.54	-	217.3	217.3	0.944	0.814	1	167.0	0.55	0.82
220	315	1.04	0.084	1.54	-	208.0	208.0	0.944	0.814	1	159.9	0.53	0.78
221	315	1.04	0.084	1.54	-	210.1	210.1	0.944	0.814	1	161.5	0.53	0.79
222	315	1.04	0.084	1.54	-	206.7	206.7	0.944	0.814	1	158.9	0.53	0.78
223	315	1.04	0.084	1.54	-	212.0	212.0	0.944	0.814	1	163.0	0.54	0.80
224	608	2.01	0.161	2.97	-	350.7	350.7	0.944	0.814	1	269.6	0.89	1.32
225	608	2.01	0.161	2.97	-	323.1	323.1	0.944	0.814	1	248.4	0.82	1.21
226	608	2.01	0.161	2.97	-	339.2	339.2	0.944	0.814	1	260.7	0.86	1.27
227	608	2.01	0.161	2.97	-	320.4	320.4	0.944	0.814	1	246.3	0.82	1.20
228	608	2.01	0.161	2.97	-	334.6	334.6	0.944	0.814	1	257.2	0.85	1.26
229	608	2.01	0.161	2.97	-	333.2	333.2	0.944	0.814	1	256.1	0.85	1.25
230	684	2.00	0.121	3.62	189.0	229.6	229.6	1	1	1	229.6	0.67	1.22
231	684	2.00	0.121	3.62	225.6	227.1	227.1	1	1	1	227.1	0.66	1.20

Wall #	AXIAL STRESS				EXPERIMENTAL SHEAR CAPACITY								
	P [kN]	σ_{gross} [MPa]	σ_{gross}/f'_m [MPa]	σ_{net} [MPa]	V_{min} [kN]	V_{max} [kN]	V_{avg} [kN]	k_{avg}	k_{mono}	k_{rate}	V_{cor} [kN]	$V_{max,gross}$ [MPa]	$V_{max,net}$ [MPa]
232	684	2.00	0.121	3.62	250.7	254.1	254.1	1	1	1	254.1	0.74	1.35
233	684	2.00	0.121	3.62	224.7	232.4	232.4	1	1	1	232.4	0.68	1.23
234	684	2.00	0.121	3.62	233.5	251.4	251.4	1	1	1	251.4	0.74	1.33
235	684	2.00	0.121	3.62	225.6	246.3	246.3	1	1	1	246.3	0.72	1.30
236	684	2.00	0.121	3.62	160.1	168.6	168.6	1	1	1	168.6	0.49	0.89
237	684	2.00	0.121	3.62	195.0	236.8	236.8	1	1	1	236.8	0.69	1.25
238	684	2.00	0.121	3.62	230.8	250.5	250.5	1	1	1	250.5	0.73	1.33
239	684	2.00	0.121	3.62	186.7	194.6	194.6	1	1	1	194.6	0.57	1.03
240	684	2.00	0.121	3.62	204.9	208.1	208.1	1	1	1	208.1	0.61	1.10
241	684	2.00	0.121	3.62	208.0	218.5	218.5	1	1	1	218.5	0.64	1.16
242	684	2.00	0.121	3.62	202.0	204.9	204.9	1	1	1	204.9	0.60	1.08
243	684	2.00	0.121	3.62	209.5	213.3	213.3	1	1	1	213.3	0.62	1.13
244	684	2.00	0.121	3.62	175.7	177.7	177.7	1	1	1	177.7	0.52	0.94
245	684	2.00	0.121	3.62	180.7	190.0	190.0	1	1	1	190.0	0.56	1.01
246	684	2.00	0.121	3.62	-	230.3	230.3	0.944	0.814	1	177.0	0.52	0.94
247	684	2.00	0.121	3.62	-	235.8	235.8	0.944	0.814	1	181.3	0.53	0.96
248	56	0.50	0.064	1.10	-	54.7	54.7	0.944	0.814	1	42.0	0.38	0.82
249	56	0.50	0.064	1.10	-	51.6	51.6	0.944	0.814	1	39.7	0.35	0.78
250	56	0.50	0.064	1.10	-	38.2	38.2	0.944	0.814	1	29.4	0.26	0.57
251	56	0.50	0.064	1.10	-	46.0	46.0	0.944	0.814	1	35.4	0.32	0.69
252	56	0.50	0.064	1.10	-	42.7	42.7	0.944	0.814	1	32.8	0.29	0.64
253	56	0.50	0.064	1.10	-	44.0	44.0	0.944	0.814	1	33.8	0.30	0.66
254	56	0.50	0.065	0.99	-	108.0	108.0	0.944	0.814	1	83.0	0.74	1.47
255	56	0.50	0.065	0.99	-	103.0	103.0	0.944	0.814	1	79.2	0.71	1.40
256	56	0.50	0.065	0.99	-	105.0	105.0	0.944	0.814	1	80.7	0.72	1.43
257	224	2.00	0.258	3.97	-	96.0	96.0	0.944	0.814	1	73.8	0.66	1.31
258	224	2.00	0.258	3.97	-	95.5	95.5	0.944	0.814	1	73.4	0.66	1.30
259	224	2.00	0.258	3.97	-	131.0	131.0	0.944	0.814	1	100.7	0.90	1.78
260	34	0.50	0.067	0.74	-	197.3	197.3	0.944	0.814	1	151.7	2.20	3.27
261	34	0.50	0.069	0.74	-	168.8	168.8	0.944	0.814	1	129.7	1.88	2.80
262	34	0.50	0.069	0.74	-	184.0	184.0	0.944	0.814	1	141.4	2.05	3.05
263	138	2.00	0.275	2.97	-	180.0	180.0	0.944	0.814	1	138.4	2.01	2.98
264	138	2.00	0.275	2.97	-	185.0	185.0	0.944	0.814	1	142.2	2.06	3.06

Wall #	AXIAL STRESS				EXPERIMENTAL SHEAR CAPACITY								
	P [kN]	σ_{gross} [MPa]	σ_{gross}/f_m [MPa]	σ_{net} [MPa]	V_{min} [kN]	V_{max} [kN]	V_{avg} [kN]	k_{avg}	k_{mono}	k_{rate}	V_{cor} [kN]	$V_{max,gross}$ [MPa]	$V_{max,net}$ [MPa]
265	138	2.00	0.275	2.97	-	108.0	108.0	0.944	0.814	1	83.0	1.20	1.79
266	34	0.50	0.063	0.97	-	25.1	25.1	0.944	0.814	1	19.3	0.28	0.54
267	34	0.50	0.063	0.97	-	23.1	23.1	0.944	0.814	1	17.8	0.26	0.50
268	34	0.50	0.063	0.97	-	30.6	30.6	0.944	0.814	1	23.5	0.34	0.66
269	680	2.00	0.134	4.16	232.0	273.0	273.0	1	1	1	273.0	0.80	1.67
270	680	2.00	0.134	4.16	276.0	327.0	327.0	1	1	1	327.0	0.96	2.00
271	680	2.00	0.134	4.16	276.0	346.0	346.0	1	1	1	346.0	1.02	2.11
272	680	2.00	0.136	4.16	282.0	334.0	334.0	1	1	1	334.0	0.98	2.04
273	680	2.00	0.112	4.16	216.0	232.0	232.0	1	1	1	232.0	0.68	1.42
274	680	2.00	0.112	4.16	191.0	215.0	215.0	1	1	1	215.0	0.63	1.31
275	680	2.00	0.112	4.16	208.0	244.0	244.0	1	1	1	244.0	0.72	1.49
276	680	2.00	0.112	4.16	217.0	223.0	223.0	1	1	1	223.0	0.66	1.36
277	680	2.00	0.112	4.16	214.0	226.0	226.0	1	1	1	226.0	0.66	1.38
278	680	2.00	0.112	4.16	184.0	213.0	213.0	1	1	1	213.0	0.63	1.30
279	680	2.00	0.168	4.16	180.0	211.0	211.0	1	1	1	211.0	0.62	1.29
280	680	2.00	0.168	4.16	206.0	209.0	209.0	1	1	1	209.0	0.61	1.28
281	680	2.00	0.168	4.16	175.0	215.0	215.0	1	1	1	215.0	0.63	1.31
282	680	2.00	0.168	4.16	206.0	230.0	230.0	1	1	1	230.0	0.68	1.41
283	156	0.56	0.130	0.91	211.7	221.1	216.4	1	1	1	216.4	0.78	1.27
284	156	0.56	0.130	0.91	196.3	220.9	208.6	1	1	1	208.6	0.75	1.22
285	156	0.56	0.130	0.91	283.6	303.1	293.4	1	1	1	293.4	1.05	1.72
286	156	0.56	0.130	0.91	291.6	308.3	299.9	1	1	1	299.9	1.08	1.76
287	203	0.56	0.130	0.93	290.1	316.4	303.2	1	1	1	303.2	0.84	1.39
288	203	0.56	0.130	0.93	330.4	342.4	336.4	1	1	1	336.4	0.93	1.54
289	0	0.00	0.000	0.00	199.9	221.8	210.8	1	1	1	210.8	0.58	0.96
290	78	0.56	0.132	0.76	99.2	100.3	99.8	1	1	1	99.8	0.72	0.97
291	78	0.56	0.132	0.76	116.5	141.7	129.1	1	1	1	129.1	0.93	1.26
292	0	0.00	0.000	0.00	98.4	99.9	99.2	1	1	1	99.2	0.72	0.97

APPENDIX B: MATLAB CODE

There are several MATLAB programs that have been used to perform the neural network analyses and sensitivity analyses. Appendix B will present all MATLAB programs and functions used, as well as brief explanations on how they have been used to perform neural network analysis.

MATLAB R2017a (Academic License) has been used for this study.

B.1 Neural Network MATLAB Function

Most of the MATLAB code remains unchanged throughout the entire study, with exception to slight modifications necessary to adjust the input dataset and number of hidden neurons. The code will be presented with highlighted portions where these modifications are made. The following program will perform the following:

1. Load the dataset “A” (`load('PG-A-7-n-1')`)
 - a. The file ‘PG-A-7-n-1.mat’ must contain two matrices: x and t .
 - b. x is the input matrix with size [Number of input variables x Number of specimens], where each column represents a single wall specimen, and each row represents an input variable.
 - c. t is the output (target) matrix with size [1 x Number of specimens], where each column represents a single wall specimen and its experimental shear strength.

Variables - x			
	1	2	3
1	6.4413e+06	6.4413e+06	6.4413
2	1.0833	1.0833	1.
3	0.3556	0.4586	0.
4	10.2315	12.5927	10.
5	0	0.4048	
6	0	0	0.
7	0.6003	1.4579	1.

Variables - t			
	1	2	3
1	0.4259	1.0344	0.73
2			

Figure B.1 – MATLAB input variables for NN analysis

2. Train 10,000 different “A-5-1-1” neural networks (`for i = 1:10000`)
 - a. Users may decide to train more than 10,000 neural networks by changing the number of iterations in the “for” loop
 - b. The MATLAB function `net=fitnet(hiddenSizes)` will initiate MATLAB’s Neural Network Toolbox and begin training a function fitting neural network when the code `train(net)` is run. More information on MATLAB’s Neural Network Toolbox can be found here: <https://www.mathworks.com/products/neural-network.html>.
 - c. The MATLAB function `rng(seed)` will seed the random number generator; doing so will allow users to replicate the neural network result by using the same value for seed prior to training the neural network. More information on the `rng` function can be found here: <https://www.mathworks.com/help/matlab/ref/rng.html>.
3. Save the performance metrics for each trained network in a .mat file (`save('PG-A-7-1-1_1-10000')`)
 - a. In this example, 10,000 neural networks are trained. The “A” matrix saved in the .m file will be a [10,000 x 7] matrix, with each row representing a single trained neural network, and each column representing a performance metric.
 - b. Users are encouraged to import this data into an Excel spreadsheet, where results can be sorted to select which networks will be used for further analysis.

	A	B	C	D	E	F	G
1	rng	R	R ²	mse	mear	std	5th
2	5632	0.888061	0.788652	0.006272	1.006225	0.154498	0.824187
3	4558	0.887208	0.787139	0.006332	0.993089	0.139291	0.766771
4	6627	0.879637	0.773761	0.00673	1.001221	0.165411	0.747682
5	1856	0.879042	0.772715	0.006759	1.010299	0.147422	0.76886
6	2641	0.878764	0.772277	0.006783	1.00557	0.147	0.778027

Figure B.2 – Excel spreadsheet with MATLAB output

```

function [A]=PG_A_7_1_1()

for i = 1:10000 % Run the network i times
[r, meansquarederror, meanvalue, rsquared, standarddev,
fifthp] = runnetwork(i);

j=i-0; % Record the index for "A" matrix
A(j,1)=i; % Record the rng
A(j,2)=r; % Record the correlation
coefficient
A(j,3)=rsquared; % Record the determination
coefficient
A(j,4)=meansquarederror; % Record the mean squared error
A(j,5)=meanvalue; % Record the mean of v_exp/v_n
A(j,6)=standarddev; % Record standard deviation
v_exp/v_n
A(j,7)=fifthp; % Record the fifth percentile of
v_exp/v_n

end

save('PG-A-7-1-1_1-10000') % Save all variables

end

function [r, meansquarederror, meanvalue, rsquared, standarddev,
fifthp] = runnetwork(i)

load('PG-A-7-n-1') % Load the input and
output(target) dataset

% Create network for curve fitting
hiddenLayerSize = 1; % Number of hidden neurons
net = fitnet(hiddenLayerSize); % Use MATLAB's NN Toolbox
WB = getwb(net);
rng(i); % Initialize the RNG so that
results can be duplicated

% Setting the sample size
net.divideFcn = 'dividerand'; % Split data randomly
net.divideMode = 'sample';
net.divideParam.trainRatio = 70/100; % 70-percent training
net.divideParam.valRatio = 15/100; % 15-percent validation
net.divideParam.testRatio = 15/100; % 15-percent testing

net = train(net,x,t); % Train the network
y = net(x); % Save the network

[m,b,r]=postreg(t,y); % Use "postreg" to output the
correlation coefficient
vexp = t; % Obtain the experimental values
of shear strength
vn = y; % Obtain the network predicted
values of shear strength

```

```

e = vexp-vn;           % Calculate the errors for each
                      % specimen
ratio = vexp./vn;     % Calculate the ratios for each
                      % specimen

meansquarederror = mse(e); % Calculate the mean squared error
meanvalue = mean(ratio); % Calculate the mean v_exp/v_n
ratio

rsquared = r^2;       % Calculate the determination
                      % coefficient
standarddev = std(ratio); % Calculate the standard deviation
                      % of the v_exp/v_n ratio
fifthp = prctile(ratio,5); % Calculate the fifth percentile
                      % of the v_exp/v_n

end

```

B.2 Generate MATLAB Neural Network Function

Once a neural network is trained, MATLAB has a built-in function to automatically generate a function for simulating a trained neural network, `genFunction(net, pathname)`. It will generate a .m program like the following:

```

>> genFunction(ans, 'ANN_A_7_5_1_1262')

MATLAB function generated: ANN_A_7_5_1_1262.m
To view generated function code: edit ANN A 7 5 1 1262
For examples of using function: help ANN A 7 5 1 1262

```

Figure B.3 – MATLAB `genFunction` Output

In the example above, the function output = `ANN_A_7_5_1_1262(input)` will take an input variable containing 7 parameters, and outputs the neural network prediction of shear strength.

To use the code, users must first define a matrix `rngs`, which should contain the `rng` values associated with the neural networks that they are interested in. They must be listed in a [`rngs` x 1] column matrix. Users can identify which `rng` values that they are interested in by sorting the Excel spreadsheet as shown in Section B.1.

Then, the following code will allow users to automatically generate as many trained neural network MATLAB programs as needed, which will then be used for sensitivity analysis. Users must change the number of hidden layers in the code, as well as the function name to correspond to the dataset and number of input variables.

```
function GenerateANNFunctions(rngs)

hiddenlayers = 5;
n = size(rngs,1);

for i = 1:n
    network = TEST_ANN_ONE(rngs(i),hiddenlayers);
    genFunction(network, strcat('ANN_A_7_', num2str(hiddenlayers), '_1_',
    num2str(rngs(i))))
end
```

Additionally, the function TEST_ANN_ONE must be in the same folder directory for the code to work. Users will have to ensure that the loaded dataset corresponds to the neural networks that they wish to train by modifying the highlighted line below.

```
function [net] = TEST_ANN_ONE(index,hiddenlayers)

load('PG-A-7-n-1')

hiddenLayerSize = hiddenlayers;
net = fitnet(hiddenLayerSize);
WB = getwb(net);

rng(index);

net.divideFcn = 'dividerand';
net.divideMode = 'sample';
net.divideParam.trainRatio = 70/100;
net.divideParam.valRatio = 15/100;
net.divideParam.testRatio = 15/100;

net = train(net,x,t);
```

MATLAB should then generate the following output:

```
>> GenerateANNFunctions(rngs)

MATLAB function generated: ANN_A_7_5_1_2053.m
To view generated function code: edit ANN\_A\_7\_5\_1\_2053
For examples of using function: help ANN\_A\_7\_5\_1\_2053

MATLAB function generated: ANN_A_7_5_1_5423.m
```

Figure B.4 – MATLAB inputs and output for `GenerateANNFunctions(rngs)`

The ANN functions should also appear in the ‘Current Folder’:

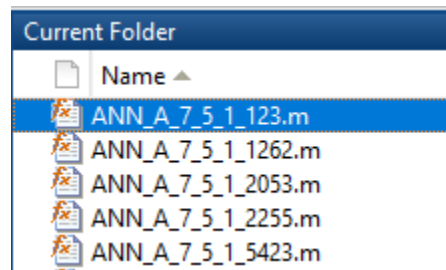


Figure B.5 – MATLAB ANN functions generated into the current folder

B.3 Sensitivity Analysis MATLAB Function

The code used for sensitivity analysis must be used in conjunction with Microsoft Excel. It also requires that MATLAB ANN functions are generated for the ANN that will undergo sensitivity analysis (see Section B.2). First, the MATLAB function is presented, followed by the Excel spreadsheet.

Most of the MATLAB code remains unchanged throughout the entire study, with exception to slight modifications necessary to adjust the input dataset and number of hidden neurons. The code will be presented with highlighted portions where these modifications are made. The following program will perform the following:

1. Load the dataset “A” (`load('PG-E-7-n-1.avg')`)
 - a. The file ‘PG-A-7-n-1.avg.mat’ must contain three matrices: `maxvec`, `minvec` and `avg`.
 - b. `maxvec` is a column matrix with size [Number of input variables x 1], where each row represents the input variable’s maximum value used for training.

- c. `minvec` is a column matrix with size [Number of input variables x 1], where each row represents the input variable's minimum value used for training.
- d. `medvec` is a column matrix with size [Number of input variables x 1], where each row represents the input variable's medium value used for training. (Recall: $\text{medium} = 0.5 * (\text{max} + \text{min})$)

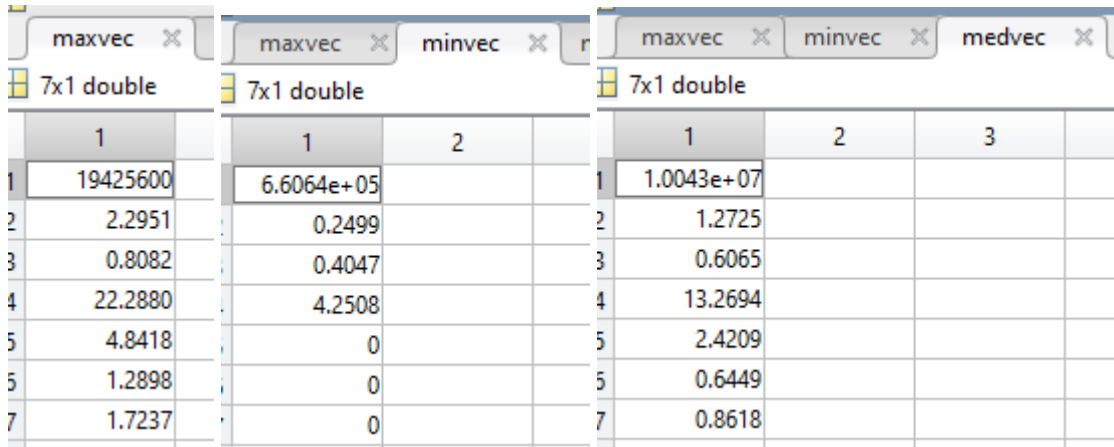


Figure B.6 – MATLAB input variables for sensitivity analysis

- e. In this example, the input variables for ANN “E-7-n-1” are used:

Table B.1 - Input variables used for sensitivity analysis

Input Variable		Minimum value	Medium value	Maximum value
Input 1	A_{scaled} [m ²]	0.66	10.04	19.43
Input 2	M/VL [unitless]	0.250	1.273	2.295
Input 3	A_{net}/A_{gross} [unitless]	0.405	0.607	0.808
Input 4	$f'_{m,eff,corrected}$ [MPa]	4.25	13.27	22.29
Input 5	$\rho_v f_{yv}$ [MPa]	0.000	2.421	4.842
Input 6	$\rho_h f_{yh}$ [MPa]	0.000	0.645	1.290
Input 7	σ_{gross} [MPa]	0.000	0.862	1.724

2. The code should run the same number of iterations as the number of inputs. In this example, the sensitivity analysis will be run on an “E-7-5-1” network, so 7 “for” loops must be run (`for i = 1:7`). Users may modify this as necessary.

- a. Users must specify which ANN they are interested in performing the sensitivity analysis. Each of the highlighted (“ANN_E_7_5_1_44662”) must be modified accordingly. (Ensure that the MATLAB generated function “ANN_E_7_5_1_44662.m” is in the current folder.)
 - b. First, the ANN function is used to predict the shear strength of the hypothetical PG wall where all input variables are fixed at its medium value, $v_{n_{medium}}$ (MPa).
 - c. With each iteration, a different input variable is selected for variation from its minimum value to its maximum value in 101 steps (0-100%, varied at 1% increments).
3. When run, the code will output a single matrix of with size [101 x (3)*(Number of input variables)]. This matrix will need to be

	1	2	3	4
1	6.6064e+05	0.8013	1.0070	0.2
2	8.4829e+05	0.8022	1.0081	0.2
3	1.0359e+06	0.8031	1.0092	0.2
4	1.2236e+06	0.8040	1.0103	0.3

Figure B.7 – MATLAB output matrix for sensitivity analysis

- a. The first column contains the first input variables’ variation from 0-100% at 1% increments. In this example, the medium values for each input variable are used except A_{scaled} , where $A_{scaled} = 0.66 \text{ m}^2$ to 19.43 m^2 .
- b. The second column contains the predicted shear strength, v_n (MPa) using the medium values for each input variable are used except A_{scaled} , where $A_{scaled} = 0.66 \text{ m}^2$ to 19.43 m^2 .
- c. The third column contains the ratio of $v_n/v_{n_{medium}}$.
- d. Columns 4-6 are similar to columns 1-3, but for the second variable (in this example M/VL). Columns 7-9 are similar to columns 1-3, but for the third variable, and so on.

4. Users can then import this data into an Excel spreadsheet, where results of the sensitivity analysis can be interpreted.
 - a. A scatterplot is generated in Excel, with the parameter variation on the x-axis, and the ratio of $v_n/v_{n_{medium}}$ for each variable on the y-axis.

%	Ascaled[mm2]	vmax	vn/vn_med
0	660643.84	0.801283	1.006974
1	848293.4016	0.802165	1.008082
2	1035942.963	0.803055	1.009201
3	1223592.525	0.803951	1.010320

Figure B.7 – MATLAB output matrix imported into Excel

```
function [A]=sensitivityanalysis()
close all
load('PG-E-7-n-1-avg.mat')
for i = 1:7
    j = 1;
    testvec=medvec;
    minvar=minvec(i);
    maxvar=maxvec(i);
    testvec(i)=minvar;
    vnmedium=ANN_E_7_5_1_44662(medvec);
    while testvec(i) <= 1.0001*maxvar
        k = 3*i;
        A(j,k-2) = testvec(i);
        A(j,k-1) = ANN_E_7_5_1_44662(testvec);
        A(j,k) = ANN_E_7_5_1_44662(testvec)/vnmedium;
        if A(j,k) < 0
            clc
            disp('error, negative prediction')
            %return
        end
        j = j + 1;
        testvec(i) = testvec(i)+0.01*(maxvar-minvar);
    end
end
end
```

APPENDIX C: NOTES ON LINEAR REGRESSION

C.1 Linear Regression

Simple linear regression uses an optimized linear function to model the relationship between a response variable and a single predictor variable.

$$Y = \beta_0 + \beta_1 X + \varepsilon \quad (\text{C.1})$$

where Y = response variable

β_i = model regression coefficients or parameters

X = predictor variable

ε = random disturbance or error

Multiple linear regression uses an optimized linear function to model the relationship between a response variable and multiple predictor variables

$$Y = \beta_0 + \beta_1 X_1 + \beta_2 X_2 + \cdots + \beta_p X_p + \varepsilon \quad (\text{C.2})$$

The β_i parameters are estimated using ordinary least squares, minimizing the sum of squares of the vertical distances from each point to the linear regression model. The coefficient of determination, R^2 , is a statistical measurement of the total variation in the predicted values are described by the variation in the actual values. The coefficient of determination has a range between $[0,1]$, and is often used to measure the goodness-of-fit of the model, where $R^2 = 1$ indicates a model with perfect fit to the data.

Although statisticians have defined the coefficient of determination in different ways over the past century, the most commonly used definition of R^2 is presented in Eq. (C.3) (Chatterjee and Hadi 2006; Lee Rodgers and Alan Nicewander 1988). The coefficient of determination formula is only valid for simple and multiple regressions when the fitted function is linear and the function is optimized by ordinary least squares (Blomquist 1980; Young 2000).

$$R^2 = \frac{SSR}{SST} = 1 - \frac{SSE}{SST} \quad (C.3)$$

where R^2 = coefficient of determination

SSR = regression sum of squares

$$= \sum(\hat{y}_i - \bar{y})^2$$

SST = total sum of squares

$$= \sum(y_i - \bar{y})^2$$

SSE = residual sum of squares

$$= \sum(y_i - \hat{y}_i)^2$$

This definition of R^2 is dependent on the following inequality:

$$SST = SSE + SSR \quad (C.4)$$

The inequality presented in Eq. (C.4) is derived by the following set of equations:

$$\sum_{i=1}^n (y_i - \bar{y})^2 = \sum_{i=1}^n [(y_i - \hat{y}_i) + (\hat{y}_i - \bar{y})]^2 \quad (C.5)$$

$$\sum_{i=1}^n (y_i - \bar{y})^2 = \sum_{i=1}^n (y_i - \hat{y}_i)^2 + 2 \sum_{i=1}^n (y_i - \hat{y}_i)(\hat{y}_i - \bar{y}) + \sum_{i=1}^n (\hat{y}_i - \bar{y})^2 \quad (C.6)$$

$$SST = SSE + 2 \sum_{i=1}^n (y_i - \hat{y}_i)(\hat{y}_i - \bar{y}) + SSR \quad (C.7)$$

However, when the linear regression model is optimized by ordinary least squares, the sum of the residuals must equal to zero. Consequently, the covariance between the residuals and the fitted values to equal to zero (Eisenhauer 2003).

$$\sum_{i=1}^n (y_i - \hat{y}_i)(\hat{y}_i - \bar{y}) = 0 \quad (\text{C.8})$$

C.2 Regression Through the Origin (RTO)

Regression through the origin (RTO) uses an optimized linear function to model the relationship between a response variable and a single predictor variable, setting the y-intercept (β_0) equal to zero.

$$Y = \beta_1 X + \varepsilon \quad (\text{C.9})$$

The coefficient of determination for RTO is calculated differently, due to the inequality given by Eq. (C.8) not equalling zero when there is no constant in the regression. Additionally, if Eq. (C.3) is used to calculate the coefficient of determination for RTO, negative values may result. Therefore, the formula used to calculate the coefficient of determination for RTO is given as follows:

$$R_0^2 = \frac{SSR_0}{SST_0} = 1 - \frac{SSE_0}{SST_0} \quad (\text{C.10})$$

where R_0^2 = coefficient of determination (regression through the origin)

SSR_0 = regression sum of squares

$$= \sum (\hat{y}_{i_0})^2$$

SST_0 = total sum of squares

$$= \sum (y_i)^2$$

SSE_0 = residual sum of squares

$$= \sum (y_i - \hat{y}_{i_0})^2$$

This definition of R_0^2 is dependent on the following inequality:

$$SST_0 = SSE_0 + SSR_0 \quad (\text{C.11})$$

The inequality presented in Eq. (C.11) is derived by the following set of equations:

$$\sum (y_i - 0)^2 = \sum_{i=1}^n [(y_i - \hat{y}_{i_0}) + (\hat{y}_{i_0} - 0)]^2 \quad (\text{C.12})$$

$$\sum_{i=1}^n (y_i)^2 = \sum_{i=1}^n (y_i - \hat{y}_{i_0})^2 + 2 \sum_{i=1}^n (y_i - \hat{y}_{i_0})(\hat{y}_{i_0} - 0) + \sum_{i=1}^n (\hat{y}_{i_0})^2 \quad (\text{C.13})$$

$$SST_0 = SSE_0 + 2 \sum_{i=1}^n (y_i - \hat{y}_{i_0})(\hat{y}_{i_0}) + SSR_0 \quad (\text{C.14})$$

However, when the regression through the origin model is optimized by ordinary least squares, the sum of the residuals must equal to zero. Consequently, the cross-product term equal to zero (Eisenhauer 2003):

$$\sum_{i=1}^n (y_i - \hat{y}_i)(\hat{y}_i) = 0 \quad (\text{C.15})$$